Shining light on radiation detection and energy transfer

Dijkstra, Peter

Shining light on radiation detection and energy transfer

Triazole ligands used for detection of radiation and lanthanide binding

Peter Dijkstra

The research presented in this thesis was carried out at INCAS³, Assen, The Netherlands and at the Stratingh Institute for Chemistry, according to the requirements of the Graduate School of Science (Faculty of Mathematics and Natural Sciences), University of Groningen, The Netherlands.


provincie Drenthe

Gemeente Assen

INCAS³ is made possible by the support of: The Northern Netherlands Provinces (SNN). This project is co-financed by the European Union, European Fund for Regional Development and the Ministry of Economic Affairs, Peaks in the Delta. The European Research Council (StG, no. 279549, WRB) and Funding from the Ministry of Education, Culture and Science (Gravity program 024.001.035, WRB) are acknowledged for financial support.

The printing of this thesis was financially supported by the University of Groningen

Cover design: Peter Dijkstra
Cover photo: Peter Dijkstra, Deborah Roffel Photography, INCAS³
Thesis design: Peter Dijkstra
Print: Ipskamp Drukkers

ISBN: 978-90-367-9290-5 (book)
ISBN: 978-90-367-9289-9 (e-book)

rijksuniversiteit
groningen

Shining light on radiation detection and energy transfer

Triazole ligands used for detection of radiation and lanthanide binding

Proefschrift

ter verkrijging van de graad van doctor aan de
Rijksuniversiteit Groningen
op gezag van de
rector magnificus prof. dr. E. Sterken
en volgens besluit van het College voor Promoties.

De openbare verdediging zal plaatsvinden op

vrijdag 25 november 2016 om 11.00 uur

door

Peter Dijkstra

geboren op 5 oktober 1978
te Assen

Promotores

Prof. dr. W.R. Browne

Prof. dr. H.J. Wörtche

Beoordelingscommissie

Prof. dr. B.L. Feringa

Prof. dr. J.G. Vos

Prof. dr. A. Buffler

Contents

Cosmic Gall

Neutrinos they are very small.
They have no charge and have no mass
And do not interact at all.
The earth is just a silly ball
To them, through which they simply pass,
Like dustmaids down a drafty hall
Or photons through a sheet of glass.
They snub the most exquisite gas,
Ignore the most substantial wall,
Cold-shoulder steel and sounding brass,
Insult the stallion in his stall,
And, scorning barriers of class,
Infiltrate you and me! Like tall
And painless guillotines, they fall
Down through our heads into the grass.
At night, they enter at Nepal
And pierce the lover and his lass
From underneath the bed – you call
It wonderful; I call it crass.

–John Updike

Chapter 1

ENERGY TRANSFER IN LIQUID ORGANIC SCINTILLATORS

The various aspects of liquid scintillation technology treated in this thesis are introduced in this chapter. The chapter is divided into 4 sections. The first part is an introduction aimed at chemists to the field of radiation detection. The second part is an introduction aimed at physicists to the field of fluorescence and energy transfer. The third part combines the fields of radiation detection and fluorescence by describing the use of fluorescent solutions (liquid scintillators) for radiation detection. This latter section provides a general introduction, discusses composition and energy transfer in scintillators. In the fourth section the challenges that lie ahead in designing new liquid scintillators are discussed.

1

1. Radiation detection

We are bombarded by radiation coming from many sources. For example radon gas in the air in granite containing regions, potassium-40 in bananas, cosmic radiation from the Sun and stars. Visible light itself is a form of electromagnetic radiation albeit much less harmful (ionising) than a burst of X-rays. In this thesis the focus will be on ionising radiation emanating from radioactive sources; including alpha, beta, and gamma radiation, and (indirect ionising) thermal neutrons.

In regard to nuclear radiation, a distinction can be drawn between radiation that ionises matter directly upon interaction and indirectly ionising radiation, which ionises via secondary mechanisms.[1] A special case in nuclear radiation is the neutrino, which has an exceptionally low probability of interacting with matter, but can still be used in radiation detection experiments as will be discussed below.

1.1.1. Direct ionising radiation

Ionising radiation are forms of radiation that possess sufficient energy upon interaction to result in expulsion of electrons from matter. Many forms of radiation are charged particles which can easily ionise the matter with which they interact. The most common cases and the ones which will be discussed in this thesis are alpha particles (He^{2+}) and beta particles (electrons or positrons). Other forms of ionising radiation are high energy electromagnetic waves (gamma rays) which possess sufficient energy to knock electrons from their core shells. In this thesis we will focus on gamma rays, which arise from nuclear decay processes.

1.1.2. Indirect ionising radiation

Neutrons are, as their name suggests, neutral particles, and when thermally equilibrated they therefore do not interact strongly with matter. However when neutrons have sufficient kinetic energy to be overcome the barrier to the nucleus of an atom, the new particle formed is unstable and will subsequently decay resulting in production of ionising radiation and / or ions thus resulting in indirect ionisation by radiation.

1.1.3. Neutrinos

In 1930 Wolfgang Pauli postulated the existence of the neutrino (scheme 1.1) to solve the problem of missing energy in beta decay.[2][*] It turned out to be an elusive particle, with almost no interaction with matter; the neutrino has a mean free pathlength in the order of a light year. Every second billions of neutrinos fly through a person and on average 1 will interact every 30 years.[3]

[*] Pauli was reluctant to postulate it, as, in his view, it would be essentially undetectable.

$$^{A}_{Z}X \rightarrow {}^{A}_{z+1}X' + e^{-} + \bar{\nu}$$

Scheme 1.1. General equation for beta minus decay. A proton of an atom is transformed into a neutron, to maintain zero charge an electron is emitted; energy is lost by emission of a neutrino.

$$\bar{\nu} + {}^{37}Cl \rightarrow {}^{37}Ar + e^{-}$$

Scheme 1.2. Capture of an antineutrino by a chlorine atom, resulting in a (radioactive) argon atom and electron.

Many nuclear reactions produce neutrinos i.e. nuclear power plants, thermonuclear explosions and stars. The first concrete idea to detect neutrinos was using a nuclear bomb as radiation source, however due to foreseen technical difficulties of measuring near an explosion this was never actually done. Reines and Cowan changed their plan and performed the first detection of neutrinos on site at a nuclear power reactor.[4] The first quantitative detection of neutrinos was performed by Davis and co-workers in the Homestake mine where a container with 600 tons of dry cleaning fluid (tetrachloroethylene, $Cl_2C{=}CCl_2$) was situated 1480 meters below the surface.[3] As scheme 1.2 shows, a neutrino hitting a ^{37}Cl atom produces a (radioactive) argon atom, at a rate of 1 event per day. The container was extracted with helium to obtain the argon produced, which would be counted.* Current methods are less laborious; one method used to detect neutrinos is in large liquid detectors (> 1 m³) where they interact with protons (hydrogen atoms from the solvent) and produce positrons and thermal neutrons both of which can be detected subsequently by the scintillation light they produce (scheme 1.3).[4, 5]

$$\bar{\nu} + p \rightarrow e^{+} + n$$

Scheme 1.3. Inverse beta decay: An electron antineutrino interacts with a free proton resulting in the formation of a positron and neutron. The positron encounters an electron and is annihilated almost directly. The thermal neutron is absorbed between 10-200 ms.

Neutrino physics remains an important subject with some of the largest detectors in the world currently deployed. SNO is a 1000 ton heavy water filled detector currently being upgraded to SNO+.[6, 7] Super Kamiokande is a detector filled with 50,000 tons of water to detect atmospheric and solar neutrinos and keeps a watch for neutrinos emanating from supernovae.[8] In the Antarctic ice sheet IceCube operates; a cubic kilometre neutrino telescope equipped with 5,000 10 inch photomultipliers.

Neutrino physics has led to the awarding of several Nobel prizes [9]; In 1988 Lederman, Schwartz and Steinberger won the Nobel prize for using a neutrino beam and discovering the

* Leading to a big discussion from the experimental chemist and theoretical physicist due to the lack of $^{1}/_{3}$ of the expected neutrinos. Continued research showed that this is due to mixing of one flavor (electron) of neutrino to other (muon and tau neutrinos), which cannot be detected by capture on a chlorine atom.

muon neutrino. Reines received the Nobel prize in 1995 for the detection of neutrinos.[*] In 2002 Davis and Koshiba (director of Super Kamiokande and its predecessors Kamiokande and Kamiokande II) received the Nobel prize "for pioneering contributions to astrophysics, in particular for the detection of cosmic neutrinos" and the discovery of neutrino oscillation resulted in a Nobel prize for McDonald (director of SNO) and Kajita (director of Super Kamiokande).

1.2. Reasons to detect radiation

The need to detect nuclear radiation arises from many sources. Safety is a major reason, as is scientific discovery but also increasing knowledge about the processes that occur within nuclear power reactors and radioactive waste. In terms of safety there are two primary regimes; personal and anti-terrorism. Personal safety refers to people working (or being treated) with radioactive materials in, for example, hospitals, and mining. Here dosimeters are mainly used, these are offline detectors; worn by people and read-out later to estimate the radiation exposure.[10] This only provides information about dosage, but does not identify the source of the radiation.

Fundamental scientific understanding of matter, nuclear reactions, inner workings of the sun, and many other processes requires the detection of radiation.[11, 12] Understanding of cosmic rays, neutrino mixing, detection of the Higgs boson, carbon-14 dating, are focused on determining radiation of one sort or another.

Medical interventions either require the use of radioactive materials or detection of those materials. For example in oncology tumours are irradiated and in PET scanners (positron emission tomography) imaging is achieved by means of measuring gamma rays emitted from positron sources introduced into a body.[13-15] In both cases, care is needed that the dosage is low enough not to cause harm (to unintended parts of the body).

Natural sources of radiation, at normal levels, are so low that the human body can cope with the radiation damage they cause.[16-18] Only high levels of radiation from sources such as a nuclear explosion and medical treatments are powerful enough to cause lasting damage and natural sources pose little risk.[†] Therefore there is not much need to measure levels, type and intensity of radiation for safety reasons on a constant basis. There are, however, other reasons to monitor radiation in detail.

1.2.1. Nuclear industry: waste and re-use of fuel rods

In the nuclear industry there are two primary motivations to monitor radiation, besides the need to directly monitor the reactor itself. When nuclear waste, either from reactors,

[*] Cowan had passed away in 1974 and could therefore not receive the Nobel Prize.

[†] The only real exception is radon gas (from granite and other stones), which is a significant source of lung cancer, and regions where radioactive rocks are near the surface such as thorium containing sand in southern India.[19, 20]

medical or scientific facilities, is stored, it has to be monitored for radiation output to ensure safety and protection of humans and the environment.[21] Research in the nuclear power plant industry to re-use the used fuel rods is a second motivation as understanding the composition of the spent fuel rods is the only way to successfully re-use them.[22] However the processes inside the reactor are not easily monitored (monitoring inside the reactor destroys the sensor due to high radiation fluxes and outside the reactor core there should be to little radiation to measure if the shielding is adequate). [23, 24] Therefore detailed knowledge of the specific isotopic contents of spent fuel rods is unavailable. In order to re-use these rods techniques should be employed which makes this possible, but the lack of information on their state prevents this at present.[25, 26]

However, the elusive neutrino is of interest in the case of unmeasurable radiation. Neutrinos are emitted by the nuclear processes inside the reactor and, travelling unaffected through the concrete safety structure, give information about the ongoing decay processes.[25, 26] With large enough detectors and enough statistics it is possible to gain information without being exposed to (dangerous and destructive) radiation.[27, 28]

1.2.2. Security

The possibility of malevolent use of nuclear material to produce a thermonuclear bomb is low, due to the technical difficulties in fabrication and deployment.[29, 30] A so called “dirty bomb” is considered a greater risk due to ease of fabrication and use. A dirty bomb is a normal high explosive bomb equipped with radioactive matter which can contaminate the blast site after detonation, without going critical. To secure against this low tech nuclear threat it is essential to prevent rogue nuclear material from leaving or entering a country.[31] For this reason many ports and border crossings are now equipped with radiation detectors. These detectors detect the small amounts of radioactive decay products in illicit transports. The problem here is to determine a sufficient positive/negative discrimination ratio and have good background suppression.

The IAEA (international atomic energy agency) inspects nuclear facilities worldwide to prevent the proliferation of nuclear weapons but is not welcome everywhere.[29, 32] Large scale neutrino detectors (> 10.000 m^3) could be able to detect rogue actions from outside the borders of non-cooperating nations. These systems would be fitted in oil carrier type ships and positioned near places of interest.[33, 34]

1.3. Historic development of radiation detectors

1.3.1. Earliest detectors

The first detectors for radiation were spectroscopes and photographic plates (for a comprehensive overview of the history of detectors see reference [35]). These methods only show the effect of bulk radiation, individual rays or particles could not be quantified or qualified. Crookes showed that individual alpha particles could be visualised on zinc sulfide screens.[36] However detection was difficult since actual monitoring had to be done in real-time by continuous visual inspection. With the invention of the Geiger Müller counter radioactive events could be quantified.[37] However the specific amount of energy of the

detected event was still unknown. The advantages of electronic counting above visual observation of scintillation meant that the former approach dominated quickly.

1.3.2. Detector types

Most early detectors are solid-state detectors but the introduction of ionisation counters and cloud chamber, which are gas based detectors, changed this.[35] The invention and improvement of photomultiplier tubes (PMT) allows low level scintillation to be converted into an electric signal thereby making scintillation light countable with electronic equipment.[38] The advantage of a scintillator over Geiger Müller counters is that they respond proportionally to the energy of the incoming particle, providing also qualitative information.[35] By their improved use and qualitative information scintillators became popular again with the increase in research into nuclear technologies during and after WWII and use of liquid scintillators took off in the 1960s.

1.3.3. Liquids

Liquid scintillator detectors come in two varieties, water based and organic solvent based. Water has the advantage that it is cheap and available in bulk quantities.[39-43] However photon emission from exited water molecules is negligible, and the only light emission in water based radiation detectors is from Cherenkov radiation.* Aromatic solvents can readily dissolve fluorescent compounds and transfer excitation energy to them, resulting in good characteristics for use in radiation detectors.[1]

1.4. Future challenges

Nuclear power reactors, nuclear waste and nuclear disasters bring with them the need to track nuclear material. Most nuclear materials are heavily guarded and their high radioactivity provides an inherent safety measure to deter malevolent intentions. Theft of radioactive materials due to (incorrect) assumption of value has happened in the past and smuggling material e.g. from the former Soviet Union, is also a realistic threat.[44, 45] Therefore when monitoring of radiation at check points, it is important to quantify radioactive material content.

1.4.1. ^{3}He depletion

One of the most deployed radiation detection technologies in border control are ^{3}He detectors.[46] These are detectors filled with ^{3}He gas; a by-product of tritium production. Tritium was used in nuclear bomb production and as these are no longer being produced there is also a halt in the production of ^{3}He. A shortage of ^{3}He has resulted in increased difficulty in finding enough ^{3}He for large scientific detectors.[47]

^{3}He is used in radiation detection because of its ability to function as a neutron capture agent (NCA, see paragraph 3.5.4), as one of the methods used to detect thermal neutrons is to

* Cherenkov radiation is caused by particles that travel close to the speed of light (c, in vacuum) through matter, e.g.water, as this is faster than is actually possible in water (0.75c) they cause a shockwave, akin to a sonic boom, which manifests as blue light.

employ neutron capture agents.[47] NCA are specific isotopes with a high neutron absorption cross section, enabling efficient capture of thermal neutrons. The NCA will undergo decay and emit an ionising photon or particle which can be detected easily. This process is used in radiation detectors (^{3}He) but also in so called neutron capture therapy where it is used as a highly localizable source for in vivo use i.e. irradiation of tumours through the release of alpha particles.[13, 48]

1.4.2. Gadolinium scarcity

Many liquid scintillators for thermal neutron detection use gadolinium as the neutron capture agent, as possesses the largest neutron capture cross section of all atoms. Currently there is no scarcity of gadolinium but, since this is one of the rare earth metals it is considered to be a strategic compound regarding production, and distribution.[49]

1.4.3. Increased deployment

Clean up at the Fukushima Daiichi plant, increased border security since 9/11, and an increase in non-proliferation inspections, are all factors which increase the global need for radiation detectors and the dwindling stocks of ^{3}He require that an alternative for ^{3}He detectors is found.[46]

1.5. Global thesis goal

As discussed the depletion of ^{3}He has prompted the search for other scintillator systems which should be designed with scarcity of materials in mind. Liquid organic scintillators can be produced from industrially used solvents and pose no problem. Other additives should possess no scarce or strategically important components such as gadolinium. The global goals of this thesis is the production of liquid organic scintillators and to investigate how the energy captured by the solvent is transferred in the scintillator and emitted as visible light. In the subsequent part of this chapter fluorescence and energy transfer will be introduced followed by an introduction on the specific properties of liquid organic scintillators.

2. Fluorescence and energy transfer

2.1. Energy states

Under ambient conditions molecules are in their electronic ground state; the state of lowest energy for the system.[50]* If a system takes up energy, for example by absorption of electromagnetic radiation, it goes from a ground state to an excited state. Depending on the energy of excitation this can have different effects. Energy in the infrared range will result in a vibrational excitation of one or more modes of the molecule and it will vibrate more energetically. Visible light, which has a higher energy, can excite an electron from its ground state to a higher excited state (S_1 or higher, **figure 1.1**) after which it can return to the ground

* For a detailed overview of fluorescence see reference [50]

state by emission of a photon. Still higher energy uptake by the molecule will cause an electron to gain sufficient energy to result in ionisation.

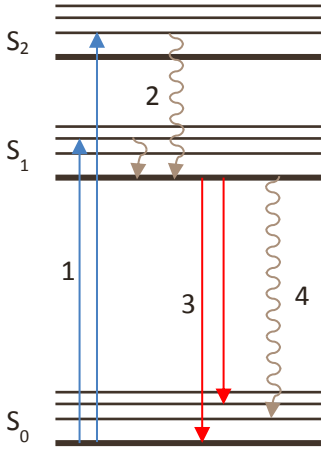

Figure 1.1. Schematic overview of energy levels upon excitation. Step 1: An electron is excited to an exited state (S_1 or higher) from the ground state (S_0). Step 2: Vibrational relaxation and internal conversion relax the molecule to the lowest thermally equilibrated excited state (Kasha's rule) after which it can emit fluorescent light (step 3) or be quenched by other means (step 4).

2.2. Excitation and relaxation

A molecule can reach an excited state via different pathways, and whether excitation energy is delivered by light or by other forms of radiation the end state is the same. After an electron is promoted to an excited state this is followed by quick (femtoseconds) relaxation to lower excited energy levels (figure 1.1). Regardless of the pathway taken (either nuclear radiation or UV/VIS light) and energy level occupied first, internal conversion will result in the identical final excited energy state (Kasha's rule).[*] The only difference between excitation by light and other mechanisms (electric, ionising) is that excitation of closed shell systems via visible light will result singlet excited states forming initially, while excitation by other means results in a mix of triplet and singlet states. This affects the amount of scintillation light produced but not the characteristics of the singlet light emitted. This enables the use of a simple method such as excitation by light instead of more cumbersome excitation by nuclear radiation pathways to model the behaviour of scintillators.

[*] Taking into account that only promotion to a higher energy level occurs, and photochemistry does not occur, i.e. electron expulsion.

2.3. Relaxation

Ultimately an excited molecule will relax to its ground state, via one of several pathways. The mechanism required in scintillator cocktails is that a molecule relaxes to the ground state via the emission of a photon, which can be detected subsequently by photodetectors.

2.3.1. Energy loss by radiationless energy transfer and quenching

When a molecule releases its energy via non radiative relaxation this energy is dissipated in the form of vibration or rotational energy. It can thus not be monitored by means of photodetectors and is lost to detection. Other molecules can also absorb the energy of the excited molecule and thus quench the excited state, for example oxygen is a well-known quencher of excited states. Singlet oxygen relaxes predominantly via radiationless pathways and NIR emission and the energy is thus again lost to detection. Hence, O_2 is excluded from fluorescent solutions, by means of thorough degassing.

2.4. Mechanisms of energy transfer

2.4.1. Trivial energy transfer

There are several possible pathways for radiative energy transfer from a donor molecule to an acceptor molecule. Emission and absorption happens when a photon is emitted by a donor and is absorbed by the acceptor molecule (scheme 1.4). This is a process which happens predominantly at high concentrations and makes use of the inner filter effect.

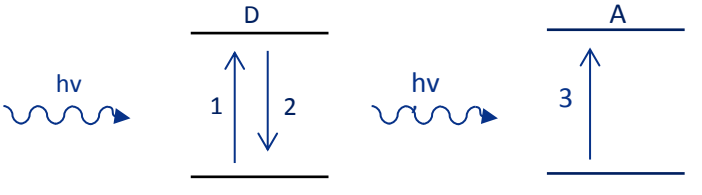

Scheme 1.4. Trivial energy transfer; A molecule (D) in the ground state accepts energy from a photon (step 1) and is excited. This donor molecule can transfer its energy by emission of a photon (step 2) which excites an acceptor molecule (A, step 3).

2.4.2. Förster energy transfer process

The Förster mechanism for energy transfer is the exchange of energy between a donor and acceptor via dipolar interactions and can occur, if the difference in excited state energy of the two compounds is minimal.[50] When in proximity (about 100 nm or less) the donor molecule can undergo radiationless relaxation with energy transfer to the acceptor molecule. The efficiency of this process is dictated by the extent of overlap between the donor emission and acceptor absorption spectrum (figure 1.2).

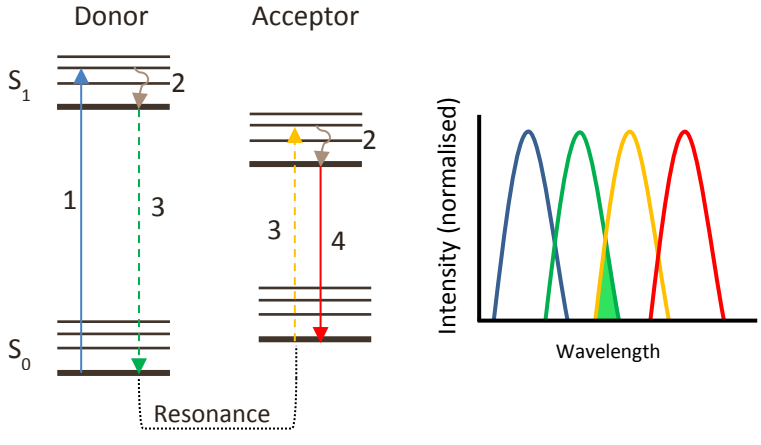

Figure 1.2. Left: Schematic representation of overlap between donor and acceptor energy levels; step 1 donor excitation, step 2 relaxation, step 3 resonance energy transfer between donor and acceptor, step 4 donor emission.Right: overlap between emission/absorption spectra of donor and acceptor molecule (light green area, colors of spectra correspond with left figure).

$$E = \frac{k_{ET}}{k_f + k_{ET} + \sum k_i}$$

Equation 1.1. Energy transfer, k_{ET} is rate of energy transfer, k_f is rate of fluorescence and k_i is rate of quenching.

$$E = \frac{1}{1 + (r/R_0)^6}$$

Equation 1.2. Energy transfer dependence on distance, r is the distance between donor and acceptor,
R_0 is the Förster distance (energy transfer efficiency is 50%).

The energy available for energy transfer is dependent on the rate of energy transfer (k_{ET}), the rate of loss by fluorescence (k_f) and the rate of quenching (k_i) (equation 1.1). The consequence of this is that Förster energy transfer can only take place in solutions where the rate of energy transfer is at least similar to the rate of fluorescence and quenching rates are low. As can be seen from equation 1.2 the energy is proportional to the inverse of the distance to the 6^{th} power. This means that energy transfer can only occur over short distances (up to 100 nm) and for effective use in radiation detection concentrations of donor and acceptor should be of the order of 10^{-5} M or higher.[50]

2.4.3. Dexter energy transfer process

A second mechanism for radiationless energy transfer is referred to as Dexter energy transfer; the transfer of energy via simultaneous double electron exchange between the donor and acceptor (scheme 1.5).[50] One of the most important characteristics of this mechanism is the overlap of the orbitals of donor and acceptor molecules to allow for the exchange of electrons, and hence they should be in proximity (< 3 nm) to allow for exchange (equation 1.3). As the rate of transfer shows an exponential dependence with distance, energy transfer can only be achieved at concentrations of ca. 10^{-2} M. Spectral overlap is of less importance.

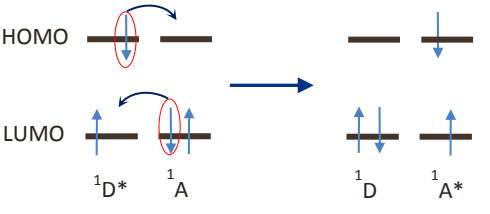

Scheme 1.5. Schematic representation Dexter energy transfer; simultaneous double electron exchange from the excited donor (^{1}D*) to the acceptor molecule (^{1}A).*

$$k_{ET} \propto Je^{-2r/L}$$

Equation 1.3. Rate constant of Dexter energy transfer. J is spectral overlap between donor and acceptor with r the distance between them. L is the sum of the Van der Waal Radius.

2.4.4. Triplet-triplet annihilation

A specific case of Dexter energy transfer is triplet-triplet annihilation. If two triplets encounter each other they can combine their total energy, resulting in one molecule to be in the ground state and the other in an excited singlet state (figure 1.3). These events occur if the combined energy of the two triplets is greater than the energy of the excited singlet state ($2\,\Delta T_1 > S_n$).

* The notation ^{1}D* depicts the spin state of a molecule. The number identifies a singlet (^{1}) or triplet (^{3}) state spin and the presence of the asterisk notes that the system is in the excited state.

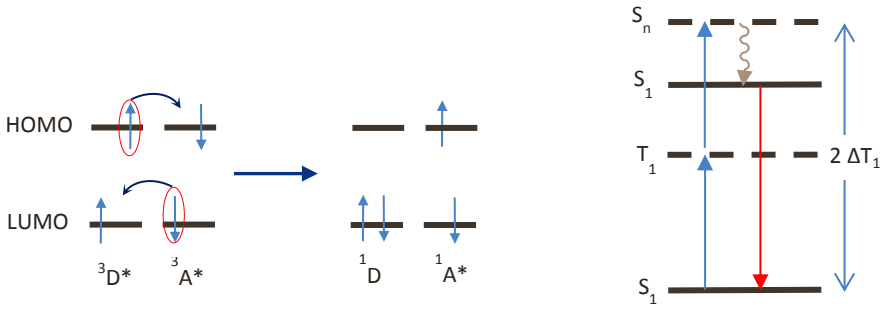

Figure 1.3. Left: triplet-triplet annihilation scheme; two triplet excited states (^{3}D* and ^{3}A*) exchange electrons resulting in one ground state (^{1}D) and one excited singlet state (^{1}A*). Right: Minimum energy of triplet state (ΔT_1) to enable population of S_n orbital to allow successful singlet generation ($2\ \Delta T_1 > S_n$).

2.4.5. Non-Markovian dynamics

When concentrations of fluorophores are even higher than under Dexter circumstances donor and acceptor molecules can get so close that their wavefunctions will overlap. Also when molecules start to form aggregate e.g. π-π stacking, strong coupling will occur resulting in wavelike energy transfer by means of the mixing of excited states.[51, 52] Due to the coherent nature of this energy transfer (in contrast to the non-coherent hopping of energy in Förster energy transfer) energy transfer is done via excitons which can be delocalised over more than one acceptor molecule.[53, 54] As consequence energy is transferred in a wavelike manner and the interactions of excitons need to be described exactly instead of perturbatively, casing non-Markovian effects e.g. memory effects.[55]

2.4.6. Time domain for energy transfer

Fluorescence in liquid media is a fast process, typically with emission lifetimes less than 10 nanoseconds, i.e. much faster than emission lifetimes of solid state materials which can reach up to milliseconds.[50] A form of slow emission, which is present in liquid media, is the aforementioned triplet-triplet annihilation; Since it takes time for two molecules with long-lived, excited triplet states to encounter each other this process will give rise to so-called delayed fluorescence. Absorption of energy and subsequent internal conversion in a fluorescent molecule occurs on an even faster timescale (less than picoseconds).

If a photon, after emission from the first fluorescent molecule, is re-absorbed by another fluorescent molecule it will undergo another cycle of absorption/internal conversion/emission which will extend the overall emission lifetime, leading to slower scintillator systems. If the concentration of fluorophore or the pathlength between initial absorption and detector is long this process can have a significant impact on the total emission lifetime of the system and hence the fundamental photochemistry and photophysics of scintillator components has a considerable impact on limitations faced in the design of detection systems.

3. Liquid organic scintillators; combining radiation detection and fluorescence

Liquid organic scintillators are a diverse group of liquids used in many forms of radiation detection.[56-60] They can be used to detect incoming radiation from the surroundings but also can be used as alpha counters wherein the radioactive material is introduced into the liquid itself. Liquid scintillators have to exhibit several distinct properties to work correctly.

3.1.1. Properties

A liquid organic scintillator (LOS) needs to be a substance in which the photon or particle can deposit its energy resulting in excitation of the scintillator cocktail.[60] For most purposes this does not put limitations on the material. As the solvent is the most abundant material in the scintillator cocktail most excited molecules will be of this type. In order for the solvent to achieve energy transfer it must have a stable excited state and be able to donate energy to another molecule. For this reason conjugated compounds are required as solvent. In most cases this means that the solvent will be an aromatic compound.

The next step is transferring the energy from the solvent to a compound, which can then re-emit that light at a longer wavelength; commonly known as a fluorophore. However most of the fluorophores, which accept the energy from the solvent efficiently, emit the light at a too short wavelength to be suited for detection by electronic means. Therefore a third compound is added, a wavelength shifter, to shift the wavelength of the emitted light from the UV to the visible range.[60]

Other components which may need to be added are NCA's to improve response to thermal neutrons, and solubilisers when using a LOS for liquid scintillation counting purposes and aqueous samples need to be introduced.

3.1.2. Characteristics

One of the advantages of liquid scintillators are their fast timing characteristics.[60] Pulse durations of several nanoseconds enable high count rates without pulse overlap. These pulses follow an exponential decay profile with several different timing components. The specific distribution of these timing components can give information about the type of ionising particle (see paragraph 3.3.1 pulse shape discrimination).

Since there has been a technological circular enhancement of PMTs for radiation detection and the emission wavelength of the LOSs, both are optimised for emission at 420 nm. Therefore, when designing new LOS cocktails focusing on this region of emission simplifies finding of off-the-shelf components for measurement systems.

3.1.3. Deployment

One of the major fields for use of liquid organic scintillation is determining the radioactivity of samples by means of liquid scintillation counting.[60] This technique is used for environmental samples, medical testing and radioactivity monitoring. A sample is dissolved in

the scintillator (~ 20 mL) and radioactivity is measured in a dedicated apparatus. Liquid organic scintillation counting is an offline method where the scintillator cocktail is disposed of after measurement.

Hermetically sealed liquid organic scintillator detectors on the other hand can be used continuously and in a real time mode. They come in various ranges depending on the source and type of radiation. For detection of neutrinos multi-ton detectors are used.[61-63]

3.2. Present status and usage

3.2.1. Examples of large scale scientific neutrino detectors

The Borexino detector is located in the Gran Sasso national laboratories, Italy, with 1400 meters of rock overhead. The detector is filled with 300 tons of pseudocumene and doped with PPO and POPOP (figure 1.4). Its main goal is solar neutrino physics but also geo-neutrino research is performed.[63]

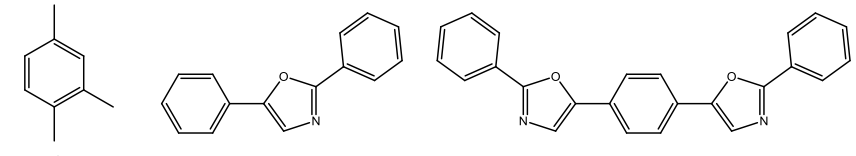

Figure 1.4 Components in the Borexino detector, pseudocumene, PPO and POPOP.

KamLAND is a detector in the Kamioka mine, Japan, with a 2700 meter water equivalent rock overburden. It is filled with 1000 tons of dodecane (80%) and pseudocumene (20%) and doped with PPO and POPOP. By measuring electron antineutrinos from nearby nuclear reactors it is able to establish the neutrino mixing angles. Further goals are measurement of geo- and solar neutrinos.[64, 65]

3.2.2. Border monitoring

Radiation portal monitors are used in the screening of vehicles at border crossings and containers in ports. Most of these detectors use ^{3}He as a detector medium but, as stated above, the stock of ^{3}He is dwindling and replacements are sought. Other techniques are being developed to take over the role of ^{3}He as detector medium and liquid organic scintillators are among them.[29, 46, 47, 66]

3.2.3. Nuclear power plants

Inside the containment area of a nuclear reactor the flux of ionising radiation is so high that semiconductors inside it will malfunction or be damaged.[24] Therefore continuous monitoring inside is almost impossible and hence reactor conditions are established from secondary means such as power output. This secondary information feed gives little insight into the nuclear processes in the reactor core.[32] As a consequence the precise composition of spent fuel rods is unknown. New reactor designs are being developed with the intention to

re-use spent fuel rods, however without precise knowledge of the composition of the rod this is a challenging goal.[22]

The power output of a reactor can be manipulated by the operator, enabling different nuclear fission processes to be employed. By specific actions it is possible to increase the amount of plutonium production in the fuel rods while maintaining an energy output associated will lower plutonium production. This can then be covertly extracted to be used for production of weapons grade plutonium.[32]

3.3. Advantages of liquid organic scintillators

Liquid organic scintillators have several benefits when compared to other detection methods. They are a proven technology which possesses fast response times and pulse shape discrimination (PSD), see paragraph 3.3.1. Since they are liquids which can be poured in any desired geometric container (sphere, cylinder even tetrahedron and micrometre thin reads) [64, 67, 68] and their size can range from millilitres to several hundreds of tons. For large detectors liquids are almost exclusively the preferred option since fabrication of > 1 kg of radiation detection crystals is almost impossible. As aromatic liquids are used in many processes and products they can be bought in bulk quantities reducing pricing (one of the commonly used solvents is LAB (linear alkyl benzene), which is a precursor for laundry detergents).[69]

3.3.1. Pulse shape discrimination

When an ionising particle interacts with matter it does so on a specific time scale and via specific interactions. An alpha particle loses its energy in a small volume ($\frac{dE}{dx}$ is high) this causes other processes compared with a gamma ray, which loses its energy in a more gradual manner. When energy is dissipated in a small volume there is more generation of triplet character in the excited state.* Excited states in the singlet state will lose their energy following exponential decay in nanoseconds. Relaxation of triplet states is spin forbidden so return to the ground state will take longer (the major route being aforementioned triplet-triplet annihilation, paragraph 2.4.4). From figure 1.5 it can be seen that decay profiles generated by gamma particles have a more prominent fast component, due to that their excited state is of mainly singlet character. Alpha particles have more triplet character in their excited state and therefore have a more pronounced long component in their decay profile.[70-74]

* The specific mechanism how a high $\frac{dE}{dx}$ fraction causes more triplet character in the excited state is still unclear. [1]

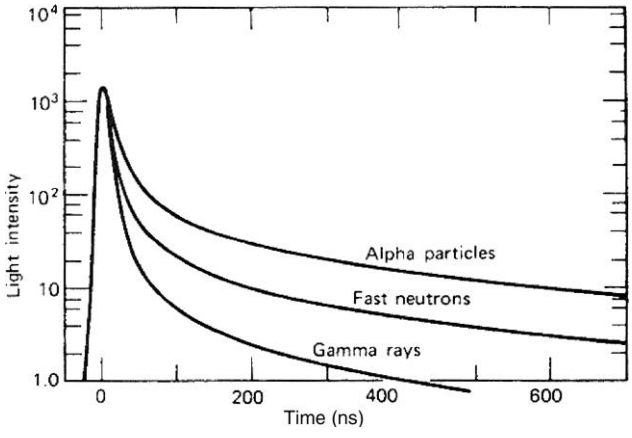

Figure 1.5 Decay profile of different sources of radiation. Gamma rays are characterised as short intense burst. The decay profile of an alpha particle is more gradual making distinction between the two possible (Reproduced from [75], © Oxford university press 2007).

By determining the ratio between the long component of the decay profile and the short component of the decay profile it is possible to label events to their specific type of radiation. When detecting neutrons and alpha particles pulse shape discrimination makes it possible to distinguish background events from the radiation source of interest. In most circumstances the background signal is composed of gamma rays and will be several orders of magnitude more intense than the signals under investigation. The use of background rejection by means of PSD significantly improves the signal to noise ratio in these cases.

3.4. Challenges in liquid organic scintillator technology

Besides the benefits they bring, liquid organic scintillators also pose some challenges. Safe handling is an issue with commonly used liquid organic scintillators.[76] These compounds are flammable liquids, most of them with low flash points and high volatility. Due to their toxicity benzene, toluene and pseudocumene which were used widely are being phased out.[77]

Liquid scintillators also pose specific problems, compared to solid detectors liquid scintillators have low resolution.[1] Moreover the density of liquids is significantly lower than crystal based detectors, and hence provide lower interaction potential with radiation.

Since the solvents used are not capable of emitting at readily detected wavelengths a multistep energy transfer process is required, and hence the need to add extra components to the scintillator.[76] Besides complexity and cost these extra compounds also lead to energy loss in the process.

The technique of liquid organic scintillation is nearly half a century old and is a well-established radiation detection technology.[1, 60, 76] It has adequate support by photodetectors, albeit in a narrow wavelength range, and can rely on good electronic read-out

systems. However the actual processes involved in energy transfer are not well understood, i.e. the technique works empirical but how it works is not clear which possess challenges to further development.[78-81]

3.5. Composition, requirements and challenges of liquid scintillators

A scintillator needs to be safe, respond quickly, possess a high resolution and have a high quantum yield. These demands provide a framework to define the specifications which a scintillator must fulfil. This involves the actual scintillator composition which should be made of at least 2 compounds: solvent and fluorophore but which can be extended with wavelength shifter, NCA and solubilisers if needed.

3.5.1. Solvent

The solvent used in a scintillator should be a conjugated compound thereby enabling absorption and emission of energy, in practice this will be an aromatic solvent. Due to the wide range of deployment this should be liquid over a wide range preferably from -20 to at least 80 °C.[32, 47] It should be stable to ensure prolonged deployment and should be safe to use, from environmental, fire hazard and toxicity standpoints. To be able to be used in anti-neutrino detection it should possess a certain amount of hydrogen atoms (>5%) to ensure capture of neutrinos on those “free protons”.

3.5.2. Fluorophore

The fluorophore should have a high quantum yield, enabling almost all absorbed photons to be emitted again and be photostable. To enable the absorption of as many photons as possible the molar absorption coefficient should be as high as possible. However to prevent re-absorption of emitted light the emission bands should overlap as little as possible with the absorption bands. This prevents self-absorption which reduces efficiency and increase time between initial absorption and detection.

From a synthesis perspective care should be taken to avoid introduction of radioactive materials, as ^{40}K, thus potassium salts and columns should be avoided and the fewer synthetic steps the better.

3.5.3. Wavelength shifter

If a wavelength shifter (WLS) is necessary the energy transfer of fluorophore to WLS should be optimal. Furthermore a WLS should hold the same characteristics and demands as the fluorophore with the addition of having its emission at 420 nm to match with the optimum efficiency of PMTs.

3.5.4. NCA

Thermal neutrons are not directly ionising and need to be captured by a suitable isotope to yield an unstable atom which will emit ionising radiation, either gamma rays or alpha particles. Neutron capture is possible with hydrogen atoms, but the cross section for this

process is a minor only 0.33 barns* (still better than oxygen with a neutron cross section of just 0.28 millibarn). In order to decrease the capture time of neutrons in organic solvents neutron capture agents are added to increase the chance of capturing thermal neutrons. NCAs used currently are specific boron, lithium and gadolinium isotopes. While gadolinium has a cross section of 55 kbarn stable unreactive incorporation in scintillator cocktails is problematic. Furthermore the supply of gadolinium is almost entirely from one country making this a possible strategic compound. Lithium and boron each have lower cross sections than gadolinium but are considered less strategically sensitive. Lithium has a low cross section and as for Gd, it produces gamma rays upon neutron capture. Boron has a higher cross section than lithium and emits alpha particles upon neutron capture. The emission of alpha particles is beneficial because these have a shorter free pathlength reducing losses through escape from the detector. Other atoms have higher cross sections than boron but are not as suited, due to toxicity; cadmium, or being radioactive themselves e.g. fermium. Therefore boron has a preference for being used as neutron capture agent.

3.6. Interaction of radiation with solvent

When a 1 MeV electron excites a scintillator several distinct processes can occur. The most important is the excitation of electrons to an excited state as this will produce fast scintillation emissions.[76] When there is so much energy deposited that a molecule is ionised it will undergo ion recombination yielding either excited singlet or triplet status. The amount of triplet character is a measure of which kind of radiation has excited the scintillator. By means of pulse shape discrimination techniques the various types of radiation can be distinguished from each other (see paragraph 3.3.1). Scintillation will only be the result if the π-π^* excitations are produced, excitation (or ionisation) of p or s electrons will not result in scintillation, and these states will dissipate their energy thermally.

3.7. Energy transfer in liquid scintillators

Energy transfer in liquid scintillators is carried out under quite different conditions when compared to “normal” fluorescence studies. This is due to involvement of the solvent in the process, high concentrations of fluorophores and multistep intermolecular energy transfer.

3.8. Difference between conventional fluorescence studies vs high concentration LOS studies

3.8.1. Solvent interaction

An important factor to note in scintillator technology is that the solvent is an active component of the detection mechanism and is used for initial absorption of the deposited

* A barn is a unit equal to 10^{-24} cm², about the size of a uranium nucleus, during neutron scattering experiments the apparent size of a uranium atom for neutron capture was apparently “as big as a barn”.[82]

energy. Thus the concentration of the first active component (the solvent) is around 5 to 10 M. This is staggeringly high compared to normal fluorescence studies, where concentrations are in the sub-millimolar concentration regime. It is important to note that the solvent is not UV-transparent and it cannot be ignored in the process of radiation detection. Since the emission and absorption bands of the solvent overlap there will be complete re-absorption of emitted light. The consequence of this is that with solvents alone all energy will be dissipated as heat.

To minimize re-absorption by the solvent it is therefore essential that energy is transferred as rapidly as possible from the solvent to a fluorophore, which emits at longer wavelength than the solvent. Whereas in standard systems energy is absorbed by a molecule and emitted as light which escape the cuvette, in scintillators the emitted light is transferred first to another (type of) compound.

In order to compete with the re-absorption by the solvent (inner filter effect), which is present at high concentrations, the fluorophore needs to be present at a high concentration also; concentrations of grams per litre are not unusual. These high concentrations of solute cause problems with solubility, and again cause problems, albeit less, with re-absorption, by the fluorophore itself. Wavelength shifters are added to overcome this limitation.

4. Challenges encountered in effect to improve scintillator design

An example of the challenges faced when improving new scintillators is given in the following thought experiment.

4.1. Using a new fluorophore for radiation detection; Bodipy

A new scintillator should possess favourable characteristics regarding photophysical properties. This means that a work-horse fluorescent compound could be a good candidate: i.e. Bodipy (figure 1.6)[83-85] Bodipy has a high quantum yield and high molar absorptivity; any photon entering the solution will be absorbed and re-emitted. It has a narrow emission band, thus a photodetector of the right sensitivity can efficiently absorb the emitted light. Furthermore as the name suggest **Bo**ron-**dipy**rromethene contains boron and thus can act as a nuclear capture agent. It thus seems that bodipy is the perfect candidate to use in scintillator cocktails, however; The high quantum yield of bodipy comes at the price of a low Stokes shift.[50] The difference between the wavelengths of absorbed light and emitted light is small (about 10 nm between the respective maxima). As a consequence there is an extensive overlap of the emission and absorption bands, thus enabling reabsorption of the light. This re-absorption is also known as the inner filter effect and reduces the efficiency and elongates the total emission times through delayed fluorescence.

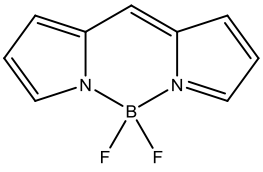

Bodipy
Boron-dipyrromethene

Figure 1.6 Structure of bodipy, a possible candidate for scintillator cocktails

PMTs and current scintillators have been developed to have maximum efficiency at 420 nm.[38] Although the emission band of bodipy is narrow it is not in this range (>500 nm), and consequently not optimal for detection by a traditional radiation detector PMT. For affordable large scale detectors off-the-shelf technology is a prerequisite therefore the emission of the scintillator has to be around 420 nm, making bodipy less suited for the task.

Although bodipy contains boron and can therefore function as NCA, its boron content is not high enough for efficient neutron capture. For successful neutron capture the NCA concentration needs to be 5% (w/w).[47] With the low amount of boron in a compound of 400 Da the amount of bodipy needed to achieve the 5% goal is around 2 kg per litre, which is not reasonable.

4.2. Other potential solutions and the problems they present

One of the issues with detection of alpha particles is their deposition of large amounts of energy within a small volume (high $\frac{dE}{dx}$ fraction).[1] This will be sufficiently high to destroy neighbouring molecules, rendering them inadequate for energy emission. The amount of energy lost in this way is around 90%, i.e. only 10% of the energy from a 1 MeeV alpha particle is detected compared to the energy detected from a 1 MeeV gamma ray. Making chemically more robust compounds would prevent destruction and thus generate more efficient energy output. Switching from aromatic solvents to more robust perfluoronated solvents would address this problem also but would make the solvent incapable of slowing down thermal neutrons or interacting with neutrinos. Furthermore the quantum yield of perfluoronated compounds tends to be significantly lower when compared to non-perfluoronated compounds.[86]

Methods of introducing sufficient amounts of boron containing compounds rely on addition of low molecular mass borates. These volatile compounds tend to be unstable or even corrosive hindering easy handling. Use of borosilicate glass might seem an option however introduction of fluorescent compounds into the glass would be troublesome. Furthermore borosilicate glass does not emit the radiation energy and hence require other dopants as well. Borosilicate sol-gels would allow for facile incorporation of fluorophores and

dopants. The advantage of forming a sol-gel in situ i.e. ease of fabrication, is limited by the danger of cracks emerging in the drying sol-gel, reducing the optical qualities of the material.

The conclusion there is no simple solution for improvements to scintillator compositions. Every change influences other components of the cocktail or hinders some of the needed physical processes.

5. Thesis overview

In this thesis the synthesis, characterisation and use of new scintillators for radiation detection is described. Energy transfer experiments are used to study model compounds and real scintillator cocktails to widen the knowledge of scintillator functionality.

In chapter 2 boron triazoles are prepared in order to use fewer components in a scintillator which absorbs UV radiation and emits in the visible range, preferably as blue light. This new class of compounds are characterised both chemically and photophysically. In chapter 3 the efficiency of this new scintillator will be compared to commercial scintillators with photophysical measurements and in chapter 4 nuclear radiation emitting sources will be used to test the scintillator under real world conditions.

In chapter 5 the energy transfer in scintillators will be investigated by using a model scintillator consisting of bodipy and a relevant solvent. This will be done to enhance understanding of energy transfer processes in scintillators.

In chapter 6 the use of triazole ligands with lanthanides instead of boron will be investigated.

6. References

[1] G. F. Knoll, *Radiation detection and measurement* (John Wiley & Sons USA, **1989**).
[2] L. M. Brown, Phys Today, *vol 31,* **1978**, pg 23.
[3] F. Close, *Neutrino* (Oxford University Press, **2010**).
[4] C. L. Cowan, F. Reines, F. B. Harrison, H. W. Kruse, and A. D. Mcguire, Science, *vol 124,* **1956**, pg 103.
[5] F. Reines and C. L. Cowan, Nature, *vol 178,* **1956**, pg 446.
[6] M. C. Chen, Nucl Phys B-Proc Sup, *vol 145,* **2005**, pg 65.
[7] S. Biller, arXiv:1405. 3401, **2014**
[8] S. Fukuda, Y. Fukuda, T. Hayakawa*, et al.*, Nucl Instrum Meth A, *vol 501,* **2003**, pg 418.
[9] www.nobelprize.org
[10] J. Seco, B. Clasie, and M. Partridge, Phys Med Biol, *vol 59,* **2014**, pg R303.
[11] K. Scholberg, Annu Rev Nucl Part Sci, **2012**
[12] M. Apollonio, A. Baldini, C. Bemporad*, et al.*, Phys Lett B, *vol 466,* **1999**, pg 415.
[13] R. Barth, J. Coderre, M. Vicente, and T. Blue, Clin Cancer Res, *vol 11,* **2005**, pg 3987.
[14] I. Tannock, J Clin Oncol, *vol 14,* **1996**, pg 3156.
[15] P. Zanzonico, Semin Nucl Med, *vol 34,* **2004**, pg 87.
[16] A. Mustapha, J. Patel, and I. Rathore, Radiat Prot Dosimet, *vol 82,* **1999**, pg 285.

[17] L. S. Quindos, P. L. Fernandez, and J. Soto, Nucl Tracks Rad Meas, *vol 21,* **1993**, pg 295.
[18] R. Grasty and J. LaMarre, Radiat Prot Dosimet, *vol 108,* **2004**, pg 215.
[19] *EPA Assessment of Risks from Radon in Homes* (EPA, **2003**).
[20] M. K. Nair, K. S. V. Nambi, N. S. Amma*, et al.*, Radiat Res, *vol 152,* **1999**, pg S145.
[21] *Monitoring and Surveillance of Radioactive Waste Disposal Facilities* (IAEA, **2014**).
[22] J. J. Carbajo, G. L. Yoder, S. G. Popov, and V. K. Ivanov, J Nucl Mater, *vol 299,* **2001**, pg 181.
[23] D. Bisello, A. Candelori, A. Kaminski*, et al.*, IEEE Trans Nucl Sci, *vol 49,* **2002**, pg 1027.
[24] A. Ruzin, G. Casse, M. Glaser, A. Zanet, F. Lemeilleur, and S. Watts, IEEE Trans Nucl Sci, *vol 46,* **1999**, pg 1310.
[25] D. Lhuillier, Nucl Phys B-Proc Sup, *vol 188,* **2009**, pg 112.
[26] M. Battaglieri, Proc Fron Detec Fron Phys, **2009**, pg 1.
[27] A. Bernstein, G. Baldwin, B. Boyer*, et al.*, arXiv:0908.4338v1, **2009**
[28] D. Reyna, Workshop Towards Neutrino Technologies, Italy, **2009**
[29] *Strengthening the Effectiveness and Improving the Efficiency of the Safeguards System Including Implementation of Additional Protocols* (IAEA, **2009**).
[30] *Combating nuclear smuggling challenges facing U.S. efforts to deploy radiation detection equipment in other countries and in the United States* (U.S. Government Accountability Office, **2006**).
[31] J. R. W. Merrick and L. A. McLay, Decis Anal, *vol 7,* **2010**, pg 155.
[32] *Final Report: Focused Workshop on antineutrino detection for safeguards applications* (IAEA, 2009)
[33] J. G. Learned, S. T. Dye, and S. Pakvasa, **2007**, pg 235.
[34] E. Guillian, Earth, Moon, and Planets, *vol 99,* **2006**, pg 309.
[35] F. N. Flakus, IAEA Bull, *vol 23,* **1981**, pg 31.
[36] W. Crookes, P R Soc London, *vol 71,* **1902**, pg 405.
[37] H. Geiger and W. Müller, Naturwissenschaften, *vol 16,* **1928**, pg 617.
[38] *Photomultiplier tubes - Basics and application* (Hamamatsu, **2007**).
[39] V. Aynutdinov, A. Avrorin, V. Balkanov*, et al.*, Nucl Instrum Meth A, *vol 604,* **2009**, pg S130.
[40] H. Watanabe, H. Zhang, K. Abe*, et al.*, Astropart Phys, *vol 31,* **2009**, pg 320.
[41] S. Dazeley, a. Bernstein, N. S. Bowden, and R. Svoboda, Nucl Instrum Meth A, *vol 607,* **2009**, pg 616.
[42] W. F. Coleman, thesis on "Testing of $GdCl_3$ Doping in Water Cherenkov Antineutrino Detectors" (Louisiana State University, **2009).**
[43] W. Coleman, A. Bernstein, S. Dazeley, and R. Svoboda, Nucl Instrum Meth A, *vol 595,* **2008**, pg 339.
[44] G. R. Moore and M. A. Pomper, B Atom Sci, **2013**
[45] W. C. Potter and E. Sokova, Nonprolif Rev, *vol 9.2,* **2002**, pg 112.
[46] J. Cartwright, Chem World-UK, **2012**
[47] *Neutron Detectors: Alternatives to Using Helium-3* (U. S. Government Accountability Office, **2011**), GAO-11-753.
[48] A. H. Soloway, W. Tjarks, B. A. Barnum*, et al.*, Chem Rev, *vol 98,* **1998**, pg 1515.
[49] *Risk list 2012* (British geological survey, 2012)
[50] J. R. Lakowicz, *Principles of Fluorescence Spectroscopy* (Springer US, **2006**).
[51] Y. Cheng and G. R. Fleming, Physical Chemistry, *vol 60,* **2009**
[52] G. S. Engel, T. R. Calhoun, E. L. Read*, et al.*, Nature, *vol 446,* **2007**, pg 782.
[53] V. May and O. Kühn, *Charge and energy transfer dynamics in molecular systems* (John Wiley & Sons, **2008**).
[54] V. Kenkre and R. Knox, Phys Rev B, *vol 9,* **1974**, pg 5279.
[55] G. D. Scholes and K. P. Ghiggino, J. Chem. Phys., *vol 103,* **1995**, pg 8873.
[56] J. A. B. Gibson and A. E. Lally, Analyst, *vol 96,* **1971**, pg 681.
[57] R. Vaninbro and I. Stanef, Nucl Instrum Meth, *vol 112,* **1973**, pg 111.

[58] M. J. Wood, R. G. C. Mcelroy, R. A. Surette, and R. M. Brown, Health Phys, *vol 65,* **1993**, pg 610.
[59] E. Rapkin, Int J Appl Radiat Isot, *vol 15,* **1964**, pg 69.
[60] D. L. Horrocks, *Application of Liquid scintillation counting* (Academic Press, Inc, **1974**).
[61] P. Lightfoot, V. Kudryavtsev, N. Spooner, I. Liubarsky, R. Luscher, and N. Smith, Nucl Instrum Meth A, *vol 522,* **2004**, pg 439.
[62] S. E. Quirk, thesis on "Purification of liquid scintillator and Monte Carlo simulations of relevant internal backgrounds in SNO" (Queen's University Kingston Ontario, Canada, **2008).**
[63] M. G. Giammarchi, Nucl Instrum Meth A, *vol 724,* **2014**, pg 250.
[64] KamLAND Collaboration, Phys Rev Lett, *vol 90,* **2003**, pg 021802.
[65] S. Enomoto, E. Ohtani, K. Inoue, and A. Suzuki, Earth Planet Sci Lett, *vol 258,* **2007**, pg 147.
[66] N. S. Bowden, J Phys: Conf Ser, *vol 136,* **2008**, pg 022008.
[67] R. J. De Meijer and W. Van Westrenen, S Afr J Sci, *vol 104,* **2008**, pg 111.
[68] G. Barbiellini, A. Martinis, R. Sangoi, and F. Scuri, Nucl Instrum Meth B, *vol 72,* **1992**, pg 481.
[69] M. Yeh, S. Hans, W. Beriguete*, et al.*, Nucl Instrum Meth A, *vol 660,* **2011**, pg 51.
[70] G. Ranucci, IEEE Nucl Sci Symp Conf Rec, *vol 2,* **2004**, pg 804.
[71] S. Normand, Nucl Instrum Meth A, *vol 484,* **2002**, pg 342.
[72] A. C. Kaplan, M. Flaska, A. Enqvist, J. L. Dolan, and S. A. Pozzi, Nucl Instrum Meth A, *vol 729,* **2013**, pg 463.
[73] Z. Cao and L. F. Miller, Nucl Instrum Meth A, *vol 416,* **1998**, pg 32.
[74] T. Szczesniak, M. Moszynski, A. Syntfeld-Kazuch*, et al.*, IEEE T Nucl Sci, *vol 57,* **2010**, pg 3846.
[75] L. F. Miller, J. Preston, S. Pozzi, M. Flaska, and J. Neal, Radiation Protection Dosimetry, *vol 126,* **2007**, pg 253.
[76] J. B. Birks, *The theory and practice of scintillation counting* (Macmillan, **1964**).
[77] F. Venema and De Meijer R. J., *antineutrino detectors* (PolyVation, Groningen, 2009)
[78] J. B. Birks, S. Georghio, and I. H. Munro, J Phys Pt B Atom M P, *vol 1,* **1968**, pg 266.
[79] J. B. Birks and K. N. Kuchela, Proc Phys Soc, *vol 77,* **1961**, pg 1083.
[80] J. B. Birks, S. Georghiou, and I. H. Munro, J Phys Pt B Atom M P, *vol 1,* **1968**, pg 266.
[81] A. Hallam and J. B. Birks, J Phys B, *vol 11,* **1978**, pg 3273.
[82] D. Wackeroth, FermiNews, *vol 19,* **1996**, pg 4.
[83] N. Boens, V. Leen, and W. Dehaen, Chem Soc Rev, *vol 41,* **2012**, pg 1130.
[84] R. Ziessel, G. Ulrich, and A. Harriman, New J Chem, *vol 31,* **2007**, pg 496.
[85] G. Ulrich, R. Ziessel, and A. Harriman, Angew Chem Int Ed, *vol 47,* **2008**, pg 1184.
[86] M. L. Renak, G. P. Bartholomew, S. Wang, P. J. Ricatto, R. J. Lachicotte, and G. C. Bazan, J Am Chem Soc, *vol 121,* **1999**, pg 7787.

Chapter 2

PYRIDYL-1,2,4-TRIAZOLE DIPHENYL BORON COMPLEXES AS EFFICIENT TUNEABLE BLUE EMITTERS

The detection of nuclear radiation necessitates the availability of new generations of tuneable blue emitting fluorophores with high emission quantum yields. Here we show that pyridyl-1,2,4-triazole based diphenyl boron complexes can provide for highly tuneable emission through facile modification of the C5 position of the 1,2,4-triazolato ring. The series of complexes prepared show a wide range of emission from near-UV to green enabling fine control over the spectral overlap with detectors used in scintillator technology.

Part of this work was published: P. Dijkstra, D. Angelone, E. Talnishnikh, H. J. Wörtche, E. Otten, and W. R. Browne, Dalton Trans., *43*, **2014**, 17740.

1. Introduction

As discussed in chapter 1, detection of nuclear radiation, specifically neutrons, represents a major technical challenge. One of the methods used to detect radiation are liquid scintillator cocktails (LSC),[1] they comprise of an aromatic solvent to capture radiation and transfer the energy released to a fluorophore and subsequently a wavelength shifter (WLS). Surprisingly the compositions used currently are largely unchanged from those developed in the 1950s despite the fantastic progress made in the development of novel fluorophores for applications as diverse as imaging, OLEDs, etc. A primary reason for this may lie in the requirement that the fluorophores used in LSC emit in the blue region of the visible spectrum in order to achieve optimum overlap with the range of maximum responsivity of the fluorescence detectors used, in particular with photomultiplier tubes (PMT) where responsivity is typically at a maximum at ca. 420 nm.[2] Furthermore they must be available in sufficient amounts for detector volumes in excess of 1 m^3. The recent surge in interest into blue emitters for OLED technologies has in large part focused on iridium based complexes, which are uneconomic in regard to large scale radiation detection.

Application of boron compounds in thermal neutron detection is of particular note due to the unusually large cross-section of the ^{10}B isotope towards thermal neutron capture, and boron is thus added to ensure efficient thermal neutron detection.[3, 4] Combining the neutron capture qualities of boron and the fact that boron containing fluorophores have attracted intensive interest over the last decades leads to our interest to use boron containing fluorophores as scintillator.[5, 6] One of the most investigated boron fluorophores has been the BODIPY class of complexes, tuning of the basic dipyrrole ligand structure enables tuning of the relatively narrow absorption and emission bands over a wide range of wavelengths. In addition to enhancing the quantum yield of fluorescence of the ligands, the BF_2 moiety imparts considerable chemical stability to the dipyrrole unit also enabling application in areas as diverse as materials, luminescent bioprobes, etc.[7-9]

However, as discussed in chapter 1 section 4, bodipy is not suited as “drop in” fluorophore in radiation detection because of mismatch between emission maximum and PMT efficiency, low absorption in the UV region and the boron content is too low to be meaningful for thermal neutron capture. [1, 10, 11] Nevertheless, other four-coordinate boron complexes might be suited for radiation detection purposes. Increasing interest in OLED applications in recent years, as highlighted in a recent reviews by Li et al. and Frath et al.,[12, 13] in particular, for applications where emission in the blue region of the spectrum is of interest. In 2003, Cheng et al. reported a pyridylpyrazolate boron complex with its lowest energy absorption band between 315 and 350 nm and emission at 375 to 460 nm.[14] More recently, Suresh et al. have reported iminopyrrolyl based BPh_2 complexes for application in OLEDSs with emission at ca. 450 to 520 nm.[15]

Surprisingly, 1,2,4-triazole based boron complexes have not yet been explored for emission purposes, despite that the properties of the 1,2,4-triazoles (figure 2.1) can be tuned

readily by substituents at the C5 position and the extensive application of 1,2,4-triazole complexes of Ru(II), Os(II)[16] and more recently Ir(III).[17] Furthermore the synthesis of substituted pyrid-2'-yl-1,2,4-triazoles can be carried out readily on large scale and these ligands are chemically robust. These attributes are essential in particular in their application as fluorophores in scintillation detectors, where detector volumes are typically of the order of m^3 and radiation induced degradation of fluorophores is a challenge.

In this chapter we report the synthesis, photophysical and electrochemical characterisation of a series of tetracoordinate $[LB(Ph)_2]$ complexes, where L is a substituted pyrid-2'-yl-1,2,4-triazoles (figure 2.1). The complexes formed show readily tuneable luminescence properties with emission showing a strong dependence on the nature of the substituent at the C5 position of the 1,2,4-triazole moiety and emission quantum yields of up to 0.7 at room temperature in solution. Furthermore, we demonstrate the potential of using these complexes as fluorophores in liquid organic scintillators for nuclear radiation detection.

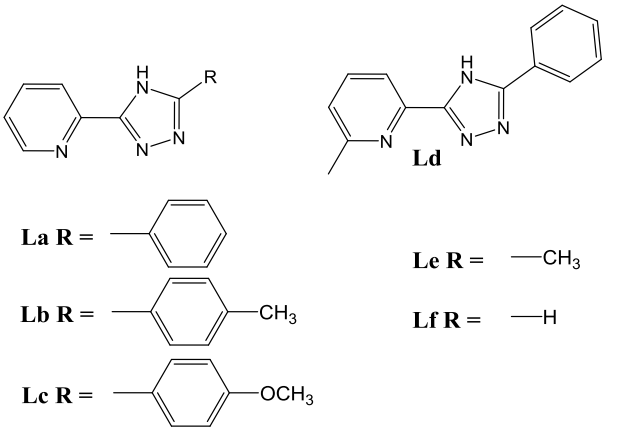

Figure 2.1. Structure of ligands **La-Lf**.

2. Results and discussion

The synthesis of the ligands **La**-**Lf** were carried out using methods reported elsewhere.[18] Initial attempts to prepare the corresponding boron complexes using $BF_3{\cdot}OEt_2$ were unsuccessful, however, reaction of the ligands with $B(Ph)_3$ at reflux in toluene, (or THF in the case of **Le**) provided complexes of the type $(L)B(Ph)_2$ in 25-40% isolated yields (figure 2.2). In the case of **Lf**, although an obvious increase in fluorescence intensity was apparent (i.e. an emission band at 535 nm) after heating with $B(Ph)_3$ at reflux in toluene, isolation of the corresponding boron complex by crystallisation or column chromatography was unsuccessful, most probably due to the acidity of the C(5)-H of the 1,2,4-triazole (pK_a ca. 10).[19] The boron complexes of ligands **La**-**Le** were characterised by elemental analysis, ^1H, ^{13}C and ^{11}B NMR

spectroscopy and mass spectrometry. In all cases only a single signal is observed by ^{11}B NMR spectroscopy.

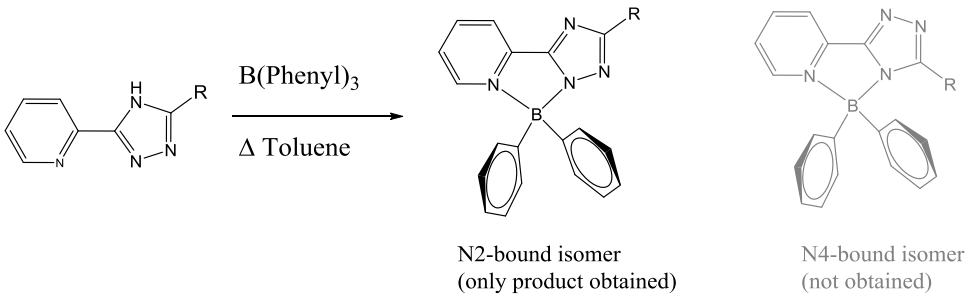

Figure 2.2. Synthesis of 5-R-(pyridine-2'-yl)-1,2,4-triazolato $B(Ph)_2$ complexes. The N2 and N4 (greyed out) coordination isomers are shown.

The FTIR and Raman spectra of ligands and complexes confirm deprotonation of the ligands by $B(Ph)_3$ to yield $LB(Ph)_2$ (figure 2.3). In particular, the pyridyl based mode at ca. 1594 cm^{-1} undergoes a shift of 30-40 cm^{-1} to higher wavenumbers upon complexation.

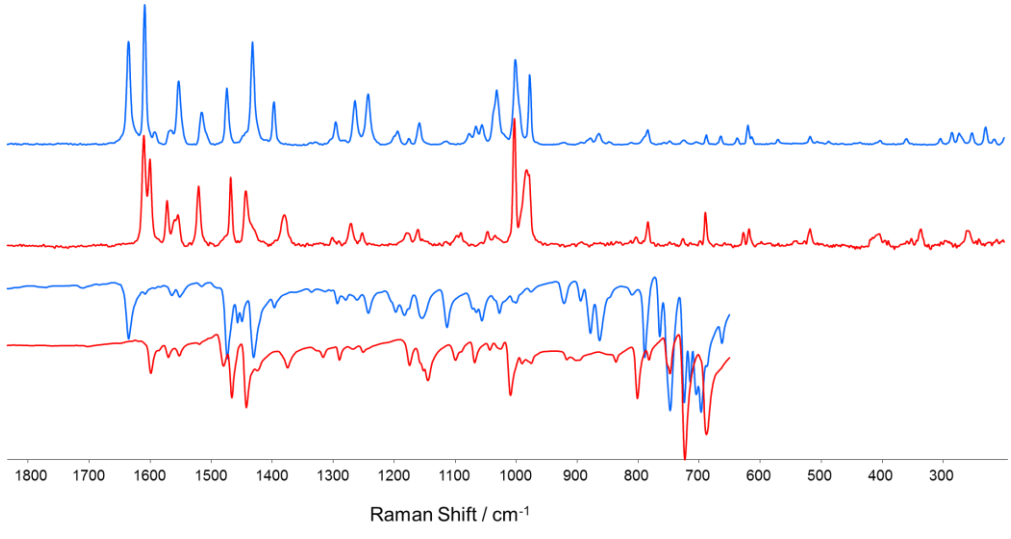

Figure 2.3. Raman spectra (λ_{ex}785 nm) and FTIR spectra of ligand **La** (red) and complex **1a** (blue).

Coordination of the 1,2,4-triazole moiety to the boron atom can, in principle be *via* either the N2 or N4 nitrogen (figure 2.2). The ^{1}H NMR spectra indicate that only a single coordination isomer is obtained, however definitive assignment cannot be made on the bases of the spectra alone. Nevertheless the presence of a substituent at the C5 position introduces steric interactions that disfavour coordination via the N4 nitrogen as found earlier for octahedral Ru(II),[20] Os(II)[21], La(III)[22] and Ir(III) complexes,[23] as well as tetrahedral square planar complexes.[24]

2.1. Single crystal X-ray crystallography of 1e

Single crystal X-ray structural analysis of **1e** confirmed the N2 coordination of the 1,2,4-triazolato moiety (figure 2.4) The boron atom binds to the triazolato ring via the nitrogen in the N2 position (B(1)-N(2) = 1.5652(16) Å) and to the pyridyl nitrogen (B(1)-N(1) = 1.6332(15) Å). The difference between the two B-N bond lengths is consistent with other tetrahedral $LBPh_2$ complexes.[14, 15] The tetrahedral coordination environment around the boron atom is completed by the two phenyl rings with bond lengths of 1.6053(17) (B(1)-C(1)) and 1.6081(17) Å (B(1)-C(7)). The phenyl rings are essentially orthogonal to the plane of the ligand (88.08(14)°, planes through B(1)-C(1)-C(7) and B(1)-N(1)-N(2)). The 5-methyl-(pyrid-2'-yl)-1,2,4-triazolato ligand deviates slightly from planarity with a dihedral angle of 3.27(13)° (N(1)-C(17)-C(18)-N(2)).

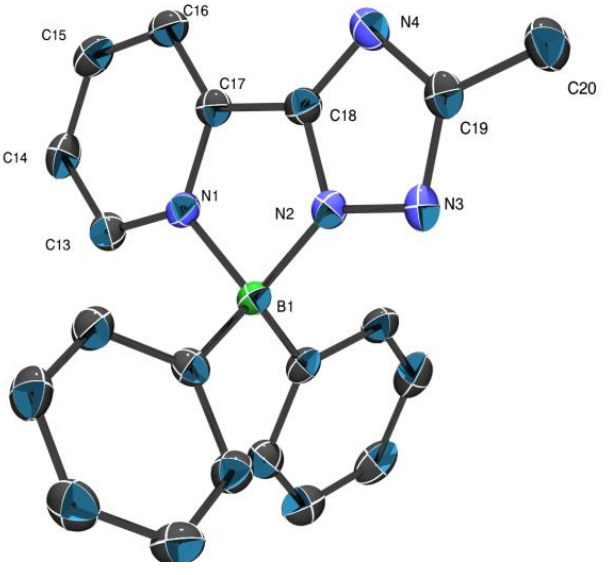

Figure 2.4: Ortep plot for **1e**. The ellipsoids are drawn at 50% probability level. H atoms are omitted for clarity. CCDC 1001413

2.2. UV/vis absorption spectra of ligands and complexes

The unbound ligands **La**-**Lf** show absorbance in the UV region of the UV/vis absorption spectrum at ca. 250 nm. Coordination of the ligand to diphenylborane results in the appearance of a new absorption band at ca. 350 nm for all complexes and an increase in molar absorptivity at 250 nm due to the additional contribution of absorption by the phenyl rings (table 1.1).

Table 1.1: Photophysical properties of complexes **1a-e** and ligands **La** and **Lb,** In CH_2Cl_2 at 20 °C
Φ is quantum yield and τ is fluorescence lifetime

	λ_{abs} (log ε) nm (M^{-1} cm^{-1})		λ_{em} nm	Φ	τ ns
1a	263 (4.38)	344 (3.86)	451	0.72	9.52
1b	267 (4.34)	351 (3.70)	461	0.71	10.7
1c	274 (4.38)	360 (3.73)	494	0.49	12.5
1d	265 (4.43)	345 (3.95)	441	0.75	7.77
1e	261 (4.01)	327 (3.74)	397	0.77	8.64
La	235 (4.24)		345	0.03	< 0.4
Lb	253		354	0.08	< 0.4

The UV/vis absorption spectra of **1a**-**e** are generally similar with absorption maxima at ca. 250 and 340 nm (figure 2.5). Complex **1e** shows the most blue shifted absorbance with a maximum at 325 nm. For the aryl substituted ligands **1a**-**c**, a 15 nm red shift (-H, -Me, -OMe) is observed, which is consistent with destabilisation of the largely triazole based HOMO orbital by electron donating groups (*vide infra*). Notably, the presence of a methyl group at the 6'-position of **1d**, which would be expected to cause steric hindrance and thereby affect the B-N(pyr) bonding has a negligible effect on the absorption spectrum.

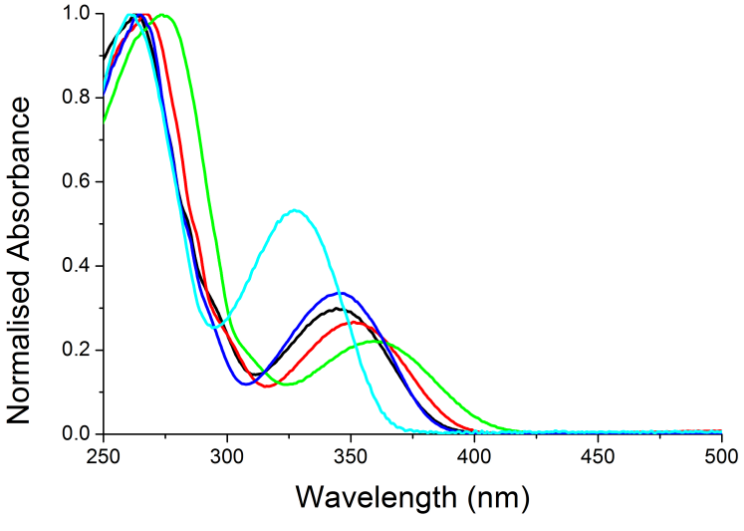

Figure 2.5. Normalised absorption spectra of complexes **1a** (black), **1b** (red), **1c** (green), **1d** (dark blue) and **1e** (light blue) in dichloromethane.

2.3. Emission and excitation spectroscopy

Variation of the substituent at the C5 position of the triazole affects the emission spectrum, quantum yield (Φ) and fluorescence lifetime (τ) also. Ligand **La** emits at 350 nm, which shifts bathochromically to 451 nm when complexed to $B(Ph)_2$, together with a substantial increase in emission quantum yield (table 1.1).

As for the UV/vis absorption spectra of complexes **1a**-**1e**, the emission spectra show a similar dependence on the substituent at the C5 position of the 1,2,4-triazole (figure 2.6). Complexes **1a**, **1b** and **1d** emit at ca. 450 nm and exhibit a small shoulder at the blue side of their spectra, which is most pronounced for **1d**. Introduction of the *para*-methoxy group in **1c** results in a considerable bathochromic shift in emission to 494 nm, which corresponds with the bathochromic shift of its lowest absorption band compared with **1a**. In the case of **1e**, which bears a methyl group at the C5 position of the triazole moiety, the emission is shifted hypsochromically to 397 nm. These data demonstrate the ease with which the emission spectrum of this class of boron complexes can be tuned by relatively minor peripheral variations in ligand structure. An important aspect with regard to application, however, is that such tuning should not impact negatively on the quantum yield of emission or emission lifetimes. In both regards, variation of the substituents on the ligand has a relatively minor effect, with the exception of complex **1c**, which shows a small decrease in emission quantum yield and an increase in emission lifetime compared with **1a**. The increase in emission lifetime and decrease in quantum yield, observed on going from **1a** to **1c** indicates that a decrease in the radiative decay rate occurs.

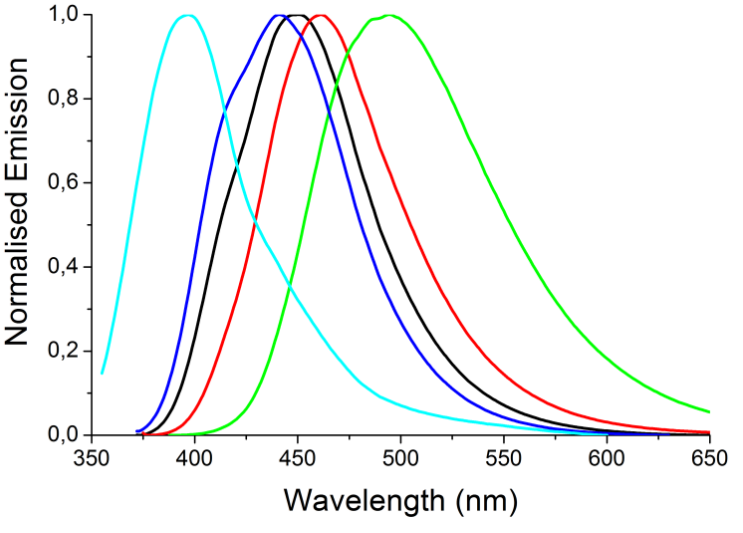

Figure 2.6. Normalised emission spectra of complexes **1a** (black), **1b** (red), **1c** (green), **1d** (dark blue) and **1e** (light blue) in dichloromethane.

2.4. Cyclic voltammetry

The redox properties of **1a**-**e** were determined by cyclic voltammetry in dichloromethane at room temperature (figure 2.7). For complexes **1a**, **1b** and **1c** the oxidation occurs at potentials close or at the onset potential for solvent oxidation (figure 2.8). Complex **1c** however shows an irreversible oxidation at $E_{p,a}$ +1.37 V, which is > 200 mV less positive than for the other complexes, indicating destabilisation of the HOMO orbital by the electron donating methoxy substituent. All complexes showed an irreversible reduction ($E_{p,c}$) at ca. -1.85 V vs SCE, with the exception of **1d**, which is reduced cat -1.92 V. The irreversibility for both oxidation and reduction is ascribed to chemical instability of the oxidised and reduced species, respectively. Indeed reduction results in the appearance of a new oxidation wave at ca. -0.5 V.

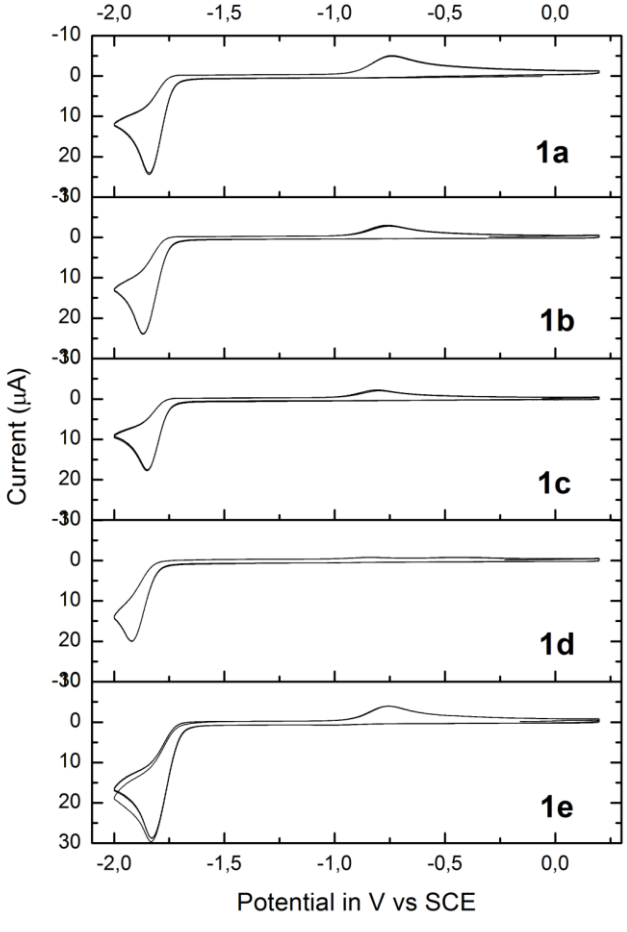

Figure 2.7. Cyclic voltammetry of complexes **1a-e** in CH_2Cl_2 with 0.1 mM $TBAPF_6$ at a GC electrode and platinum counter electrode. Scan rate 0.1 V s^{-1}.

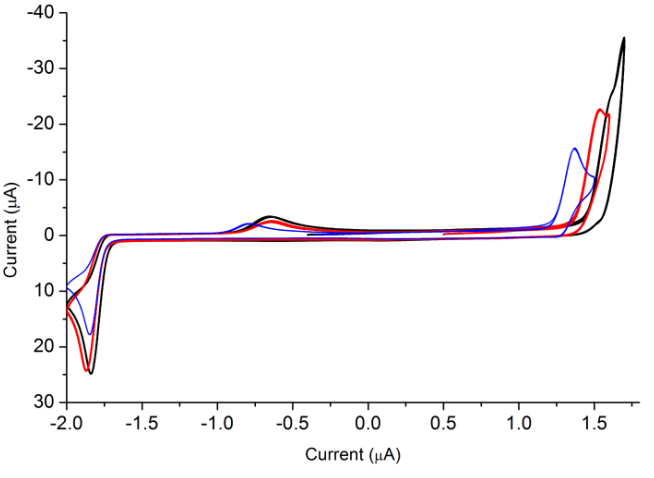

Figure 2.8. Cyclic voltammetry of complexes **1a** (black), **1b** (red) and **1c** (blue) in CH_2Cl_2 with 0.1 M $TBAPF_6$ at a GC electrode, 0.1 V s^{-1}.

1d bears an electron donating methyl group in the *ortho* position of the pyridyl ring and potentially introduces steric strain between the pyridine and the $B(Ph)_2$ unit. The localization of the LUMO on the pyridyl ring (*vide infra*) is consistent with the effect of a methyl substituent on the pyridyl ring in **1d** to shift the reduction potential negatively. Overall, however, the HOMO/LUMO gaps estimated from the difference in the oxidation and reduction potentials (3.1 to 3.3 eV) are consistent with the lowest energy absorption band (3.1 to 3.2 eV).

2.5. Density functional theory

Calculation of the frontier molecular orbitals of **1e** was carried out using DFT methods in order to rationalise the effect of substitution at the C5 position of the 1,2,4-triazole unit. The calculated length for the B(1)-N(2) bond is 1.564 (from X-ray analysis = 1.5652(16) Å) and B(1)-N(1) is 1.652 (from X-ray analysis = 1.6332(15) Å) and the calculated dihedral angle for (N(1)-C(17)-C(18)-N(2) is 1.067° (compared with 3.27(13)° as determined by X-ray structural analysis).

The HOMO to HOMO-5 orbitals are localised on the triazolato and $B(Ph)_2$ moieties with negligible electron density on the pyridyl rings (figure 2.9). The lowest virtual orbitals (LUMO to LUMO+2) are localised across the triazole-pyridyl ligand with no distribution of the orbitals on the phenyl rings until the LUMO+3 level. TDDFT was carried also (figure 2.10) and confirms the assignment of the electronic spectrum. Hence, the perturbation of the redox and electronic properties of the complexes by the C5 substitutions can be understood through inductive perturbation of electron density on the triazole ring.

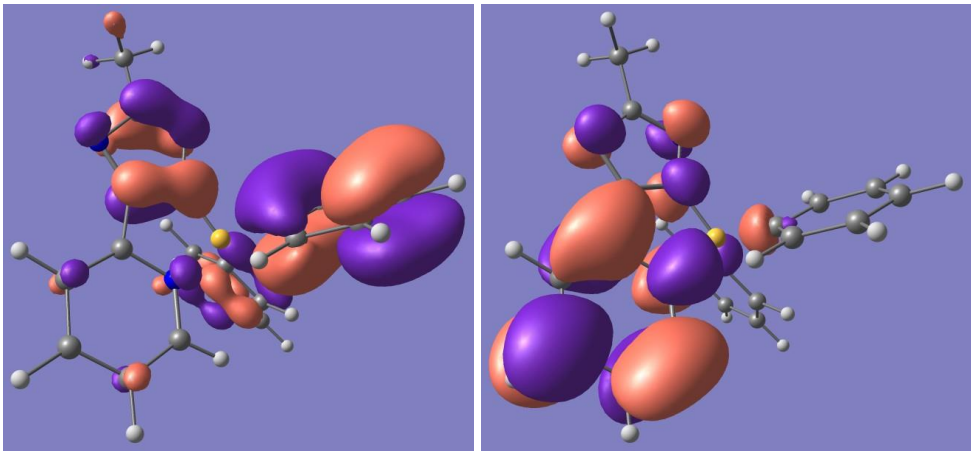

Figure 2.9. HOMO (left) and LUMO (right) orbitals calculated for complex **1e**.

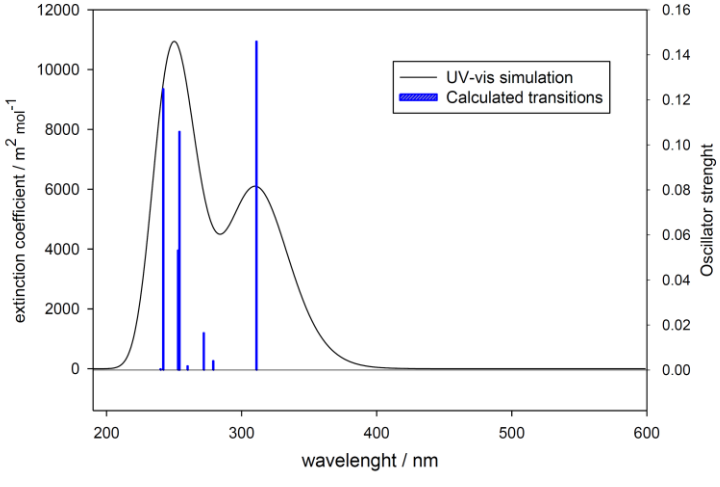

Figure 2.10. TDDFT calculated UV/vis absorption spectrum of complex **1e** (black line). The blue vertical lines correspond to the excitation transition calculated using TD-DFT/CAM-B3LYP/6-311++G(3d, 3p).

2.6. Application of complexes in liquid scintillation

To investigate the efficiency of boron triazole complexes in radiation detection, scintillation cocktails where made. Complex **1a** was dissolved in DIN (di-isopropylnaphthalene, a common scintillator solvent) to determine its efficiency in radiation detection using ^{133}Ba as a source of gamma radiation.* As the concentration of **1a** is increased, it approaches the

* Gamma radiation and fast neutrons are both detected in the scintillation systems employed here, with pulse shape discrimination used to distinguish the two radiation types. Gamma radiation detection is used for an initial assessment of the functionality of a detection system for practical reasons.

measured transformed Spectral Index of the External Standard (tSIE) value (the closer this tSIE value is to 1000 the better the fit to the theoretical ^{133}Ba energy spectrum). The best result is obtained at 8.7 mM above which concentration **1a** is not soluble (figure 2.11). The tSIE value of 632 indicates a detection efficiency of about 63%, while the control achieves 98% efficacy.

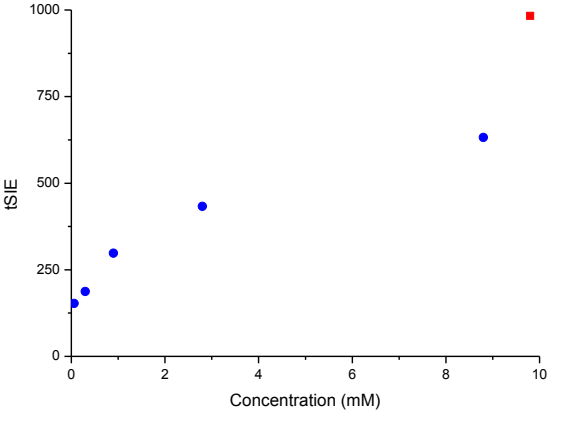

Figure 2.11. Transformed-Spectral Index of the External Standard (tSIE) versus concentration of **1a**. The molarity of the control is set arbitrarily at 10 mM (indicated by red square).

3. Conclusions

The drive for new fluorophores that show spectral overlap of their emission spectrum with the range of optimum responsivity of the detector technology used for liquid scintillators must face demands in regard to cost and the avoidance of scarce elements and non-scalable syntheses. In this contribution, we demonstrate that boron complexes of the well-known pyridyl-1,2,4-triazole based ligand system can allow for high quantum yield emission in the blue region of the spectrum with facile control over emission wavelength achieved by substitution at the C5 position of the triazole. The complexes described here hold further potential in other applications where blue emission is required, not least in OLEDs.

4. Experimental section

4.1. Materials and instrumentation

All reagents were commercially available and used without further purification unless stated otherwise. Dichloromethane, diethyl ether, THF, toluene were dried using a MBraun solvent purification system. Ligands **La-e** were prepared according to previously reported methods.

^{1}H (400 MHz) and ^{13}C (100 MHz) NMR spectra were recorded on a Varian Avance {400MHz} NMR spectrometer, ^{11}B NMR spectra were recorded on a Varian Avance NMR

spectrometer. Spectra were referenced to residual solvent peak.[25] FT-Infrared spectra were recorded as solids on a PerkinElmer Spectrum400 FTIR spectrometer equipped with an ATR accessory. UV/vis absorption spectra were recorded on a Specord600 UV/vis absorption spectrometer (AnalytikJena) in 1 cm pathlength quartz cuvettes. Fluorescence spectra were recorded using a JASCO FP7200 spectrofluorimeter, and were corrected for instrument response. Quantum yields were determined relative to a diphenylanthracene in ethanol.[26] Fluorescence decay lifetimes were measured using a PicoQuant 300 TCSPC. Melting points were determined using a BUCHI Melting Point B-545 apparatus with open glass capillaries. Mass spectra were recorded using a Xevo G2-S QTof equipped with Ion Sense DART SVP. Elemental analysis was determined using a EuroVector Euro EA. For details of single crystal X-ray diffraction, see ESI. Scintillator cocktails consisting of di-isopropylnaphthalene (DIN) and complex were made at concentrations ranging from 0.57 to 87 µM. The samples were introduced into a PerkinElmer Tricarb 2910 TR and measured with a ^{133}Ba source.

Complex 1a; 5-phenyl-(pyridine-2'-yl)-1,2,4-triazolato boron diphenyl

10 mL of toluene was added to a dried Schlenk tube containing 182 mg (0.75 mmol) Ph_3B and 167 mg (0.75 mmol) of **La** and heated at reflux overnight. Solvent was removed *in vacuo* and solids were dissolved in 5 mL of DCM and filtered. The filtrate was stored in a freezer and the resulting solid was filtered and washed with cold EtOH to yield a white crystalline powder, 117 mg, yield 40%. m.p. 257.3 - 257.7 °C. Elemental analysis: Calc. C 77.7, H 4.96, N 14.51 Found C 77.6, H 4.87, N 14.20. ^{1}H NMR (400 MHz, $CDCl_3$) δ 8.65 (d, J = 5.8, 1H), 8.31 (d, J = 7.7, 1H), 8.26 (m, 3H), 7.61 (t, 1H), 7.49 – 7.23 (m, 13H). ^{13}C NMR (50 MHz, $CDCl_3$) δ 169.1, 154.9, 144.6, 143.9, 142.7, 134.9, 132.9, 131.9, 129.2, 128.7, 128.1, 127.7, 126.9, 124.1, 119.4. ^{11}B NMR (128 MHz, CDCl3) δ 5.21. Mass spectrum (DART): M+H 386.16 Da (23.7%) and 387.15 Da (100%) and 388.15 Da (27.6%) Calculated: m/z: 386.18 Da (24.8%) and 387.18 Da (100%) and 388.18 Da (28.7%) Resp. ^{10}B, ^{11}B and ^{11}B with ^{13}C

Complex 1b; 5-tolyl-(pyridine-2'-yl)-1,2,4-triazolato boron diphenyl

15 mL of toluene was added to a dried Schlenk tube containing 500 mg (2.0 mmol) Ph_3B and 443 mg (1.9 mmol) of **Lb** and heated at reflux overnight. Solvent was removed *in vacuo* and solids were dissolved in 5 mL of EtOAc and filtered. The filtrate was stored in a freezer and the resulting solid was filtered and washed with cold EtOH to yield a white crystalline powder, 236 mg, yield 35%. m.p. 258.4 - 259 °C. Elemental analysis: Calc. C 78.01, H 5.29 , N 14.00 Found C 77.71, H 5.21, N 13.58. ^{1}H NMR (400 MHz, $CDCl_3$) δ 8.63 (d, J = 5.8 Hz, 1H), 8.28 (d, J = 8.0 Hz, 1H), 8.22 (td, J = 8.0, 1.2 Hz, 1H), 8.14 (d, J = 8.1 Hz, 2H), 7.57 (ddd, J = 7.2, 5.8, 1.2 Hz, 1H), 7.38 – 7.21 (m, 12H), 2.40 (s, 3H). ^{13}C NMR (101 MHz, $CDCl_3$) δ 169.2, 154.8, 144.6, 143.9, 142.7, 139.2, 132.9, 129.4, 129.2, 128.0, 127.6, 126.8, 124.1, 119.4, 21.6. DART MS spectrum: M+H 400.23 Da (27.7%) and 401.23 Da (100%) and 402.23 Da (29.00%) Calculated: m/z: 400.20 (24.8%), 401.19 (100.0%), 402.20 (29.3%) Resp ^{10}B, ^{11}B and ^{11}B with ^{13}C.

Complex 1c; 5-(para-methoxyphenyl)-(pyridine-2'-yl)-1,2,4-triazolato boron diphenyl

10 mL of toluene was added to a dried Schlenk tube containing 148 mg (0.6 mmol) Ph_3B and 350 mg (1.4 mmol) of **Lc** and heated at reflux overnight. Solvent was removed in vacuo and solids were dissolved in 5 mL of THF and filtered. The filtrate was stored in a freezer and

the resulting solid was filtered and washed with cold EtOH to yield a white crystalline powder, 160 mg, yield 27%. m.p. 236.3 - 237.4 °C. Elemental analysis: Calc. C 75.02, H 5.08, N 13.48 Found C 72.35, H 5.53, N 11.85 (note **Lc** · EtOH complex calc: C 72.74, 5.89, N 12.12) . ^{1}H NMR (400 MHz, $CDCl_3$) δ 8.61 (d, J = 5.6, 1H), 8.26 (d, J = 7.8, 1H), 8.19 (t, J = 7.9, 3H), 7.55 (t, J = 6.5, 1H), 7.40 – 7.16 (m, 10H), 6.97 (d, J = 8.6, 2H), 3.85 (s, 3H). ^{13}C NMR (101 MHz, $CDCl^3$) δ 169.0, 160.6, 154.7, 144.7, 143.9, 142.7, 134.9, 132.9, 131.2, 128.3, 128.0, 127.6, 124.8, 124.0, 119.3, 114.0, 55.5. ^{11}B NMR (128 MHz, $CDCl_3$) δ 5.21. Mass Spec. (DART): M+H 416.14 Da (14%) 417.16 Da (100%) and 418.17 Da (17%) Calculated: m/z: 416.19 (24.8%), 417.19 (100.0%), 418.19 (29.9%), Resp ^{10}B, ^{11}B and ^{11}B with ^{13}C.

Complex 1d; 5-phenyl-(3-methyl-pyridine-2'-yl)-1,2,4-triazolato boron diphenyl

15 mL of toluene was added to a dried Schlenk tube containing 205 mg (0.85 mmol) Ph_3B and 316 mg (0.85 mmol) **Ld** and the mixture heated at reflux overnight. Solvent was removed *in vacuo* and solids were dissolved in 5 mL of DCM and filtered. The filtrate was in a freezer. The solid obtained was recovered by filtration and washed with cold EtOH to yield a white crystalline powder, 123 mg, yield 30%, m.p. 278.0 -278.5 °C. Elemental analysis Calc :C 78.01, H 5.29, N 14.00. Found C 77.62, H 5.14, N 13.63. ^{1}H NMR (400 MHz, $CDCl_3$) δ 8.34 – 8.03 (m, 4H), 7.46 – 7.12 (m, 15H), 2.48 (s, 3H). ^{13}C NMR (50 MHz, $CDCl_3$) δ 168.8, 157.5, 145.2, 142.6, 134.9, 133.8, 132.0, 131.0, 129.0, 128.5, 128.0, 127.9, 127.5, 126.8, 126.6, 126.2, 116.9, 22.4. ^{11}B NMR (128 MHz, $CDCl_3$) δ 5.43 (s, 1B). DART-MS: M+H 400.17 Da (32.0%) and 401.16 Da (100%) and 402.17 Da (26.4%) Calculated: m/z: 400.20 (24.8%), 401.19 (100.0%), 402.20 (29.3%), Resp ^{10}B, ^{11}B and ^{11}B with ^{13}C.

Complex 1e; 5-methyl-(pyridine-2'-yl)-1,2,4-triazolato boron diphenyl

20 mL of dry THF was added to a dried Schlenk tube containing 0.69 g (4.3 mmol) of **Le** 1.06 g (4.4 mmol) Ph_3B was added, which resulted in the immediate appearance of a milky white solution. After stirring for 1 h at room temperature the solvent was removed *in vacuo*. All solids were dissolved in DCM and loaded on Celite. The sample was purified by column chromatography on silica with pentane/EtOAc (0-100%) as eluent. The blue fluorescent fraction was collected and recrystallized from EtOAc, yielding 360 mg of a white solid, yield 26%. M. P. 239.5 - 240.5 °C. Elemental analysis, calc: C 74.1, H 5.29, N 17.28 Measured: C 73.93, H 5.30, N 17.17. ^{1}H NMR (400 MHz, $CDCl_3$) δ 8.63 (d, J = 5.7, 1H), 8.22 (m, 2H), 7.59 (ddd, J = 7.3, 5.8, 1.5, 1H), 7.27 (m, 10H), 2.59 (s, 3H). ^{13}C NMR (101 MHz, $CDCl_3$) δ 167.6, 154.3, 144.6, 143.9, 142.7, 132.7, 128.0, 127.6, 124.0, 119.2, 14.8. ^{11}B NMR (128 MHz, $CDCl_3$) δ 4.93. Mass spec. (DART): M+H 324.14 Da (23.8%) and 325.14 Da (100%) and 326.14 Da (25.2%) Calculated: m/z: 324.17 (24.8%), 324.16 (100.0%), 326.17 (22.4%) Resp M+H for ^{10}B, ^{11}B and ^{11}B with ^{13}C.

X-ray crystallography.

A suitable crystals of 1a was mounted on a cryo-loop transferred into the cold nitrogen stream of a Bruker D8 Venture diffractometer. The final unit cell was obtained from the xyz centroids of 9705 reflections after integration. Intensity data were corrected for Lorentz and polarisation effects, scale variation, for decay and absorption: a multiscan absorption correction was applied, based on the intensities of symmetry-related reflections measured at

different angular settings (SADABS).[27] The structures were solved by direct methods using the program SHELXS.[28] The hydrogen atoms were generated by geometrical considerations and constrained to idealised geometries and allowed to ride on their carrier atoms with an isotropic displacement parameter related to the equivalent displacement parameter of their carrier atoms. Structure refinement was performed with the program package SHELXL.[28] Crystal data and details on data collection and refinement are presented in table 2. Full details of crystal structure in reference [29].

Table 2: Crystallographic data for **1e**

chem formula	$C_{20}H_{17}BN_4$	Temp (K)	100(2)
M_r	324.19	θ range (°)	2.9-27.15
Cryst syst	Orthorhombic	Data collected (h,k,l)	-11:11, -14:14, -20:20
Color, habit	Colourless, block	Min, max transm	0.9712, 0.9819
Size (mm)	0.37 x 0.23 x 0.23	rflns collected	42384
Space group	P212121	independt reflextions	3624
a (Å)	9.1229(9)	observed reflns $F_o \geq 2.0\ \sigma\ (F_o)$	3515
b (Å)	10.9815(11)	R(F) (%)	3.03
c (Å)	16.3366(17)	$wR(F^2)$ (%)	7.79
V ($Å^3$)	1636.7(3)	GooF	1.042
Z	4	weighting a,b	0.0431, 0.4723
P_{calc} ($g\ cm^{-3}$)	1.316	params refined	227
μ(Mo Kα) (mm^{-1})	0.080	min, max resid dens	-0.117, 0.257
F(000)	680		

DFT Calculations

DFT Calculations were carried out using the Gaussian09c[30] software package with geometry optimisation carried out by using DFT rb3lyp/6-311++g(2d,2p). The TD-DFT studies were performed in vacuo using Gaussian 09 c (DFT) CAM-B3LYP functional and 6-311++G(3d, 3p) basis set.[31, 32] Full details of DFT calculations in reference [29].

5. Acknowledgements

Perkin Elmer (Groningen NL) are acknowledged for providing DIN and assistance with scintillation measurements.

6. References

[1] J. B. Birks, *The theory and practice of scintillation counting* (Macmillan, **1964**).
[2] *Photomultipliers: data handbook. PC04* (Philips Components, **1990**).
[3] S. Wang, C. C. Hsu, R. W. S. Leung, *et al.*, Nucl Instrum Meth A, *vol 432,* **1999**, pg 111.
[4] *Neutron Detectors: Alternatives to Using Helium-3* (U. S. Government Accountability Office, **2011**), GAO-11-753.

[5] R. Ziessel, G. Ulrich, and A. Harriman, New J Chem, *vol 31,* **2007**, pg 496.
[6] G. Ulrich, R. Ziessel, and A. Harriman, Angew Chem Int Ed, *vol 47,* **2008**, pg 1184.
[7] A. Kamkaew, S. H. Lim, H. B. Lee, L. V. Kiew, L. Y. Chung, and K. Burgess, Chem Soc Rev, *vol 42,* **2013**, pg 77.
[8] N. Boens, V. Leen, and W. Dehaen, Chem Soc Rev, *vol 41,* **2012**, pg 1130.
[9] F. Cheng and F. Jaekle, Polym Chem, *vol 2,* **2011**, pg 2122.
[10] P. Dijkstra, H. J. Wortche, and W. R. Browne, AIP Conf Proc, *vol 1338,* **2011**, pg 221.
[11] C. Gomez-Duran, I. Garcia-Moreno, A. Costela*, et al.*, Chem Commun, *vol 46,* **2010**, pg 5103.
[12] D. Li, H. Zhang, and Y. Wang, Chem Soc Rev, *vol 42,* **2013**, pg 8416.
[13] D. Frath, A. Poirel, G. Ulrich, A. De Nicola, and R. Ziessel, Chem Commun, *vol 49,* **2013**, pg 4908.
[14] C. C. Cheng, W. S. Yu, P. T. Chou*, et al.*, Chem Commun, *vol 2003,* **2003**, pg 2628.
[15] D. Suresh, C. S. B. Gomes, P. T. Gomes*, et al.*, Dalton Trans, *vol 41,* **2012**, pg 8502.
[16] W. R. Browne, R. Hage, and J. G. Vos, Coord Chem Rev, *vol 250,* **2006**, pg 1653.
[17] E. Orselli, G. S. Kottas, A. E. Konradsson*, et al.*, Inorg Chem, *vol 46,* **2007**, pg 11082.
[18] R. Prins, R. A. de Graaff, J. G. Haasnoot, C. Vader, and J. Reedijk, Chem Commun, **1986**, pg 1430.
[19] S. Fanni, C. Di Pietro, S. Serroni, S. Campagna, and J. G. Vos, Inorg Chem Commun, *vol 3,* **2000**, pg 42.
[20] R. Hage, J. G. Haasnoot, H. A. Nieuwenhuis, J. Reedijk, D. J. A. D. Ridder, and J. G. Vos, J Am Chem Soc, *vol 112,* **1990**, pg 9245.
[21] B. E. Buchanan, R. Wang, J. G. Vos, R. Hage, J. G. Haasnoot, and J. Reedijk, Inorg. Chem., *vol 29,* **1990**, pg 3263.
[22] M. G. B. Drew, M. J. Hudson, P. B. Iveson, M. L. Russell, and C. Madic, J Chem Soc Dalton, **1999**, pg 2433.
[23] S. Soman, J. C. Manton, J. L. Inglis*, et al.*, Chem Commun, *vol 50,* **2014**, pg 6461.
[24] S. Chang, J. Kavitha, S. Li*, et al.*, Inorg Chem, *vol 45,* **2006**, pg 137.
[25] H. E. Gottlieb, V. Kotlyar, and A. Nudelman, J Org Chem, *vol 62,* **1997**, pg 7512.
[26] M. Montalti, A. Credi, L. Prodi, and M. T. Gandolfi, *Handbook of photochemistry* (CRC press, **2006**).
[27] Bruker. APEX2 (v2012.4-3), SAINT (Version 8.18C) and SADABS (Version 2012/1). Bruker AXS Inc., Madison, Wi, USA, **2012**,
[28] G. M. Sheldrick, Acta Crystallogr A, *vol 64,* **2008**, pg 112.
[29] P. Dijkstra, D. Angelone, E. Talnishnikh, H. J. Wortche, E. Otten, and W. R. Browne, Dalton Trans, *vol 43,* **2014**, pg 17740.
[30] M. Frisch, G. Trucks, H. B. Schlegel*, et al*, Gaussian 09, revision A. 02; Gaussian, Inc, **, 2009**
[31] E. Runge and E. K. Gross, Phys Rev Lett, *vol 52,* **1984**, pg 997.
[32] T. Yanai, D. P. Tew, and N. C. Handy, Chem Phys Lett, *vol 393,* **2004**, pg 51.

Chapter 3

RADIATION MEASUREMENTS

In this chapter the detection of nuclear radiation using the INCAS³ triazole scintillator (ITS), synthesized as described in chapter 2, is reported. The response of the scintillator is compared to a commonly used commercial scintillator, EJ-309:5B. The difference in performance between EJ-309:5B and ITS is investigated in regard to the characteristics of individual traces and the spectrum generated. The aim of the study described in this chapter is to establish the efficiency of ITS cocktail for radiation detection purposes.

1. Introduction

As discussed in chapter 1, liquid scintillation is an important approach in the development of large-scale neutron detectors. An important liquid organic scintillator (LOS) in radiation detection is EJ-309, a commercially available liquid scintillator (produced by ELJEN Technology), which is used because of its sensitivity in the detection of neutrons and gamma rays. Furthermore this LOS has been investigated extensively.[1-11] For these reasons, EJ-309 has been chosen to be the standard to which the performance of a new LOS such as ITS (INCAS³ triazole solution) is compared. As shown in chapter 2, ITS is comprised of the common scintillator solvent DIN (di-isopropylnapthalene, also used in EJ-309) and a fluorophore, a boron triazole complex (figure 3.1).

Other commercial scintillators used include; NE-213*, BC-523 A2† and EJ-339:A2. NE-213 has a slightly better neutron/gamma discrimination capability than EJ-309 due to the use of a different solvent (xylene vs DIN).[12-14] However, the xylene used in NE-213 is flammable and toxic and is inappropriate for large-scale detector applications (> 1 m³). EJ-309, on the other hand, which is based on DIN is considered safer during handling due to its higher flashpoint and vapor pressure, lower toxicity and lower reactivity towards plastics when compared to NE-213. EJ-309 is manufactured in two versions, an undoped, and a boron-doped version, EJ-309:5B, which includes 5% (w/w) boron (of natural isotope abundance). Boron is added to scintillators to enhance the probability of thermal neutron capture, since the boron-10 isotope has a large neutron capture cross section. For detailed information as to the characteristics and components of EJ-309 and EJ-309:5B see section 2.1.4 and reference [14].

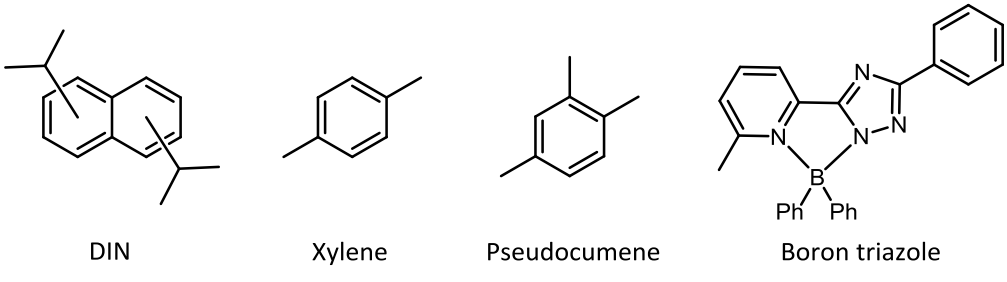

Figure 3.1. Three solvents used frequently in liquid scintillators; DIN, xylene, pseudocumene together with boron triazole, the fluorophore used in ITS.

Other commercially available liquid scintillators (including BC-523 A2, or the equivalent EJ-339:A2) have 2% (w/w) boron-10 enriched boron added to the original cocktail. As EJ-309:5B contains natural boron, it's boron-10 content is only 1%, meaning that BC-523 A2 and EJ-339:A2 perform better regarding more frequent thermal neutron capture and

* Nuclear Enterprises LTD, Winnipeg Canada

† Saint Gobain Crystals, Nemours France

subsequent detection, however enriched boron is of only limited availability.[10, 15-17] A further drawback of BC-523 and EJ-339:A2 is that they employ a solvent, pseudocumene (figure 3.1) for which the flash point is only -8 °C whereas the flash point of EJ-309:5B is 144 °C. Their low flash point renders these scintillators inappropriate for applications involving large volume (> 1 m^3) liquid organic scintillators; which is the focus of the present study.

In this chapter, the properties of ITS are investigated regarding the response of the scintillator when exposed to radiation sources. First the experimental setup is described, the characteristics of EJ-309:5B are determined and then compared with data obtained with ITS.

2. Experimental

The performance of any liquid scintillator is reliant on conversion of the energy, deposited by high energy photons originating from nuclear reactions, being scattered on electrons (Compton effect), ultimately leading to detectable light pulses. The overall efficiency relies on the integration of scintillator, photodetector, readout electronics and the data processing algorithms used. Hence, all experiments were performed with as minimal a difference in the measurement conditions as possible. The measurement setup consisted of a photomultiplier (PMT), an interchangeable cell for holding the liquid scintillator, a high voltage power supply, a dedicated signal acquisition and processing unit (PHASE), a laptop, and radioactive sources (^{137}Cs and ^{22}Na, figure 3.2).

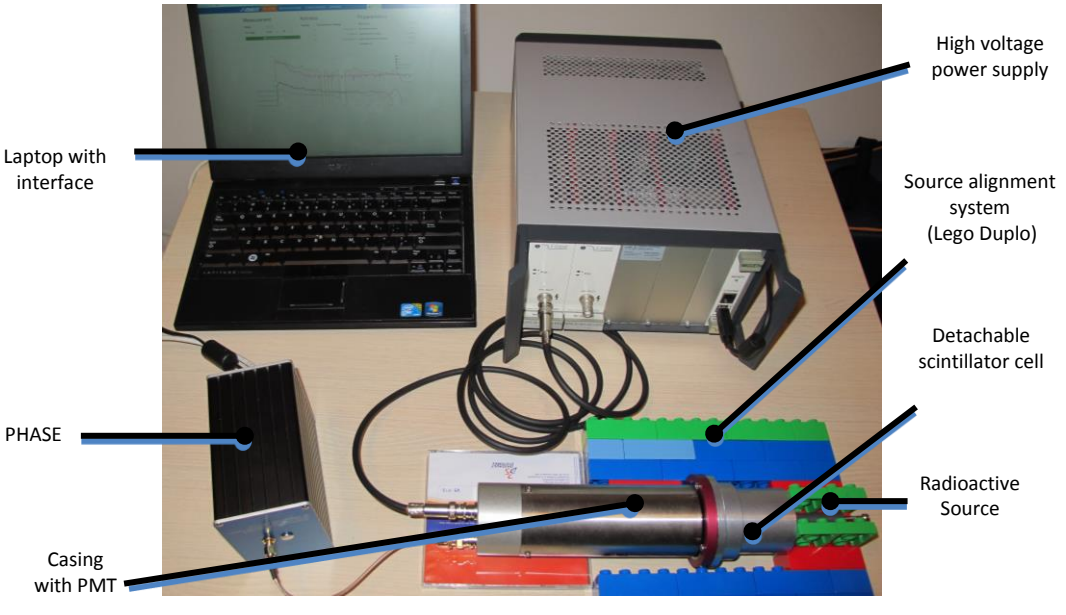

Figure 3.2. Measurement system. The detector assembly is placed horizontally and the radioactive source is placed against the scintillator cell wall in the middle of the symmetry axis of the detector.

In order to minimize systematic errors, all measurements with EJ-309:5B and ITS were obtained with an identical hardware configuration. Thus, the only variable in the setup was the liquid scintillator (EJ-309:5B or ITS), which was contained in identical hermetically sealed interchangeable scintillator cells.

2.1. Detector assembly

The liquid scintillator detector, manufactured by Scionix, consists of a PMT housed together with a voltage divider in an aluminium casing and is coupled to an interchangeable scintillator cell (figure 3.3). A SHV connector on the housing enables input of the high voltage power supply (HVPS) and a BNC connector allows signal output. The PMT is a 10-stage Hamamatsu R7724 with peak sensitivity at 420 nm (with a quantum efficiency of 26 % at 420 nm), a rise time of 2.1 ns and a 1.2 ns transit time spread.[18]

The liquid scintillator, either EJ-309:5B or ITS, is contained in a cylindrical scintillator cell (figure 3.3) and has an inner diameter of 51 mm with a length of 51 mm. The active volume of the cell is approximate 100 mL (gross volume less expansion volume). The inside of the cell is coated with a reflective coating except for the window, which is made of optical glass (borosilicate BK7). The optical window contacts the liquid to maximize light throughput. One cell was prefilled by the supplier with EJ-309:5B, the other cell containing the ITS scintillator was filled at the institute in a nitrogen-purged glovebox after degassing of the scintillator cocktail. The cell is filled to 97 % volume with liquid and 3 % of the volume is gas (N_2) to allow for thermal expansion of the scintillator liquid. The cell is bolted onto the PMT casing with the optical window of the cell in contact with the PMT window.

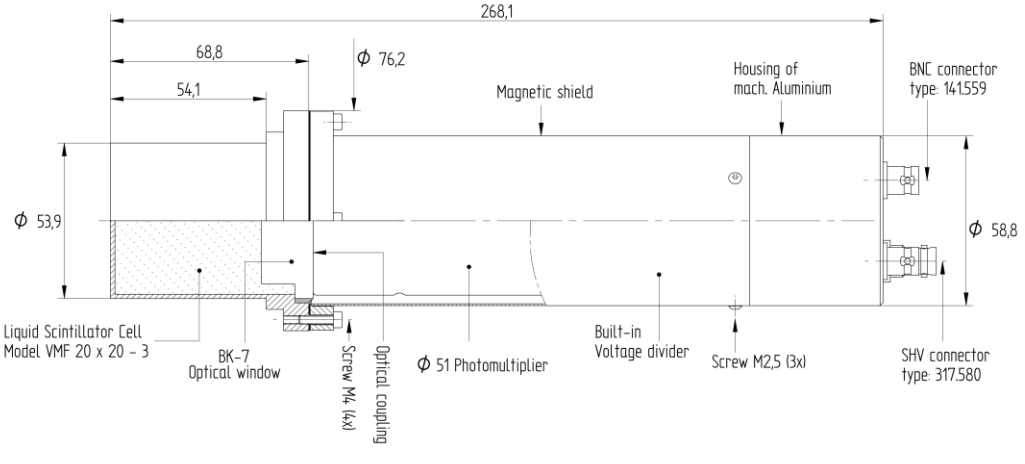

Figure 3.3. Mechanical layout of the detachable scintillator cell and PMT housing (dimensions in mm), reproduced from Scionix technical files.

2.1.1. PMT amplification

The response of the detector was characterized to determine a driving voltage that provides an optimum in the signal to noise ratio by variation in the high voltage differentials set over the PMT. A change in the high voltage power supply results in a change to the gain of electron multiplication (table 3.1), see appendix A for further details. The gain increases exponentially with a linear increase in the applied voltage from the power supply as is expected for PMTs.[18, 19]

Table 3.1. High voltage power supply settings during experiments and corresponding amplification factor by the PMT (relative to 1.3 kV). For specific details of PMT and PMT characterization see appendix A and reference [18].

High voltage power supply setting (kV)	1.3	1.6	1.7	1.8	1.9	1.95
Amplification factor (relative to 1.3 kV)	1	3 ⅓	4 ⅔	6 ⅔	9	10.5

2.1.2. PHASE; read-out system

Figure 3.4. PHASE, signal acquisition and processing unit.

The PHASE is an INCAS³ custom built device for signal acquisition and processing (figure 3.4). It is a compact modular system consisting of four functional modules. The PHASE performs analogue conditioning and signal digitalization, dead-time-free real-time signal processing and embedded high-level analysis of the processed signal.[20, 21] The version used in these experiments is capable of running at either 250 MHz with 10-bit resolution or at 1 GHz with 12-bit resolution; the latter setting was used during experiments. Incoming signals were sampled and processed using the onboard FPGA (field-programmable gate array). The processed result is a histogram of the signal amplitudes abstracted from the single traces; i.e.

a pulse height spectrum of the measured radiation, comparable with an energy spectrum (figure 3.5). For this purpose, the amplitude of the pulse is determined via moving-window-decomposition and moving average filter, for full description see [21].

For further offline analysis raw data was stored in the form of a trace; a recording of the digitized energy output as a function of time. Due to software architecture, raw traces are stored with a sample speed of only three signals per second, unconnected to the actual incoming signal rate. Offline analysis can be either visual inspection of the traces or processing of the traces to generate the pulse height spectrum as is normally performed online using the PHASE.

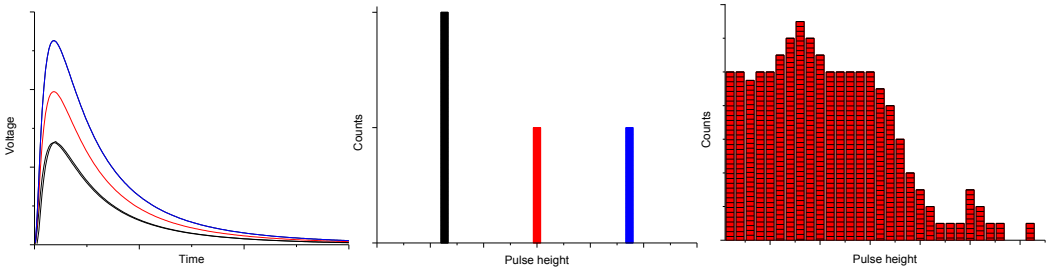

Figure 3.5. Spectrum processing. Left: 4 signals amplitudes of detected events. Traces are digitized and every specific signal amplitude is binned into a histogram (middle), the trace with lowest amplitude appears twice thus is counted twice for the histogram. After processing of 200+ individual traces, an amplitude spectrum emerges (right).

2.1.3. PHASE parameters

Unless stated otherwise the parameters for the PHASE were set as shown in table 3.2. Incoming signals were digitized by the 12 bit ADC over 4096 channels. The trigger was set to trigger after a positive threshold level of 1608 (12 bit) at 600 ns, while the baseline of the signal fluctuates around a level of 1560 (± 14).* The energy difference between the baseline and level 1608 equals an analogue output of about 40 mV from the PMT. Filters to calculate the amplitude of the measured pulse were used as following; the energy of the pulse is determined by moving window decomposition (which is set via the moving window discriminator coefficient and the moving window discriminator width), this transforms the incoming pulse into a square signal. A moving average filter (set via moving average width and moving average time) then estimates the amplitude of the square signal. The histogram conversion factor is used to set the scale for the measured spectrum and compresses or stretches the displayed spectrum accordingly.

* The baseline is offset from the centre position (channel 2048) to allow for maximum range in the positive region and is therefore situated at channel 1560.

Table 3.2. Configuration settings of the PHASE employed during measurements.

Trigger polarity	Positive	Histogram conversion factor	100
Trigger level (channel)*	1608	Moving average width	80
Trigger horizontal position (ns)	600	Maximum amplitude time	180
Trigger configuration	Level	Moving window discriminator coefficient	4000
Baseline time	0	Moving window discriminator width	250

* baseline is positioned at channel 1560 ± 14

2.1.4. Commercial scintillators: EJ-309 and EJ-309:5B

EJ-309 exhibits a fast decay component of 3.5 ns and should, according to theory*, show a second longer decay component, with a much lower amplitude than the fast component.[22, 23]

Table 2.3. Decay time constants and intensities of liquid scintillators EJ-309 and EJ-309:5B under exposure to nuclear radiation (© 2010, IEEE. Reprinted with permission [11]).

Scintillator	Particle	Fast component		Medium component		Long component		Background component	
		Decay const (ns)	(%)	Decay const (ns)	(%)	Decay const (ns)	(%)	Decay const (ns)	(%)
EJ-309	Gamma	3.7 ± 0.4	80	31 ± 3	10	140 ± 10	7	790 ± 80	3
	Fast N	4.8 ± 0.5	46	32 ± 3	24	140 ± 10	20	620 ± 60	11
EJ-309:5B	Gamma	4.2 ± 0.4	73	35 ± 4	12	160 ± 20	10	880 ± 90	6
	Thermal N	4.9 ± 0.5	49	35 ± 3	26	160 ± 20	18	890 ± 90	7
	Fast N	4.9 ± 0.4	42	35 ± 3	22	160 ± 20	19	770 ± 90	17

Experiments with EJ-309 by Szczęśniak *et al.* show that EJ-309 exhibits this second longer decay component and that even a third component can be identified.[11] From table 2.3 it can be seen that the difference in composition between EJ-309 and EJ-309:5B leads to different decay components. The reason for this is that the addition of boron containing compounds displaces the original scintillator cocktail, thus decreasing the amount of energy capturing solvent and light emitting fluorophore present in the scintillator. All decay time components of EJ-309:5B show a longer decay time than that of undoped EJ-309, regardless of the specific type of radiation. As can be seen there is no entry for thermal neutrons with the undoped version of EJ-309, since thermal neutrons are not absorbed very well by this undoped cocktail, i.e. boron needs to be added for successful thermal neutron capture (see chapter 1).

The elongation of the decay time is caused by the lower concentration of fluorophore in EJ-309:5B which decreases the energy transfer rate between solvent and fluorophore, and consequently results in longer decay times.[24] The decrease in the concentration of active

* The slower component arises from the presence of slower mechanisms causes by the energy deposition e.g. ion-recombination effects and merger of triplet states.

compounds will also result in a decrease in emission yield (70% decrease according to ELJEN Technology).[22] In neutron detection experiments, EJ-309:5B is used as a scintillator instead of EJ-309, which is less suited for neutron detection.

2.1.5. Radioactive sources

The response to exposure to radiation was tested with two radioactive sources; ^{137}Cs and ^{22}Na. The ^{137}Cs source decays 95% of the time via beta minus decay to ^{137m}Ba, a metastable isotope, which emits a gamma ray with an energy of 662 keV (figure 3.6). The activity of the ^{137}Cs source which was used in the experiments was 10 kBq at time of use.

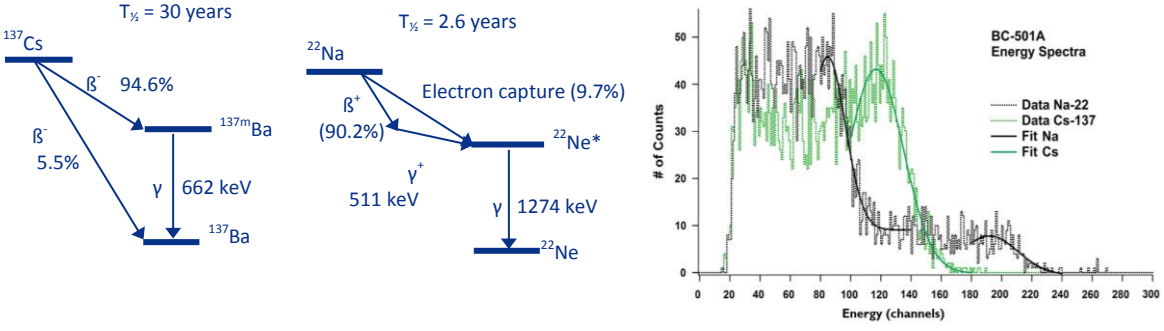

Figure 3.6. Decay scheme for ^{137}Cs (left) and ^{22}Na (middle), energy spectra of ^{137}Cs and ^{22}Na obtained with liquid scintillator BC501 (right), adapted with permission, copyright Elsevier (2014) [25].

The second source used is ^{22}Na, which decays via beta plus decay. The beta particle (a positron) is annihilated upon encountering its antiparticle, the electron. This generates two 511 keV gamma rays which move back to back from each other. The resulting daughter nucleus is a ^{22}Ne atom in the excited state. Relaxation of the ^{22}Ne atom produces a gamma ray with an energy of 1274 keV. The activity of the ^{22}Na source which was used in the experiments was 1.5 kBq at time of use.

In a solid state scintillator a photon can deposit all its energy in the detector by means of the photoelectric effect. For ^{22}Na this results in a measurable peak at 662 keV. The photoelectric effect only is possible in the presence of atoms with high atomic mass on which the photon can be absorbed. Liquid scintillators in general only possess light atoms (C, H, N) preventing occurrence of the photoelectric effect. Therefor in liquid scintillators energy can only be deposited via Compton scatter were a photon collides with an electron. The energy deposition of this process is a continuum falling off at the Compton edge where the deposited energy is at its maximum (when a photon is deflected 180°). The energy of such an effect can be calculated via equation **3.1,** where $E_{Compton\ edge}$ is the energy of the Compton edge, E_0 the energy of the incoming photon and m_e the mass of the electron. This provides the maximum Compton edge energy for ^{137}Cs to be determined at 478 keV and of ^{22}Na at 341 and 1062 keV.

$$E_{Compton\ edge} = E_0\left(1 - \frac{1}{1+\frac{2\,E_0}{m_e\,c^2}}\right) \qquad \textbf{3.1}$$

3. Results and discussion

3.1. High voltage power supply settings for EJ-309:5B and ITS

For the experiments with ITS the measurement setup and all parameters were initially kept identical to those used with EJ-309:5B. However early indicative tests showed that ITS exhibits a lower count rate under similar testing conditions. As can be seen in figure 3.7 (left side) the count rate (rate of signals exceeding the threshold) of ITS is a factor 10 lower than EJ-309:5B at 1.3 kV, this difference decreases with increasing voltage, however this is due to an overall increase in count rate (including background), not by an improved performance of ITS relative to EJ-309:5B. The most probable reason for the lower count rate of ITS is a much lower emission output compared to EJ-309:5B, see section 3.4.1 for more details. For both scintillator cocktails the signal to background ratio drops off fast above 1.6 kV (figure 3.7, right side). The reason for the increased count rate from the background signal arises from dark currents and other factors at high voltages, which are discussed in section 3.4.3.

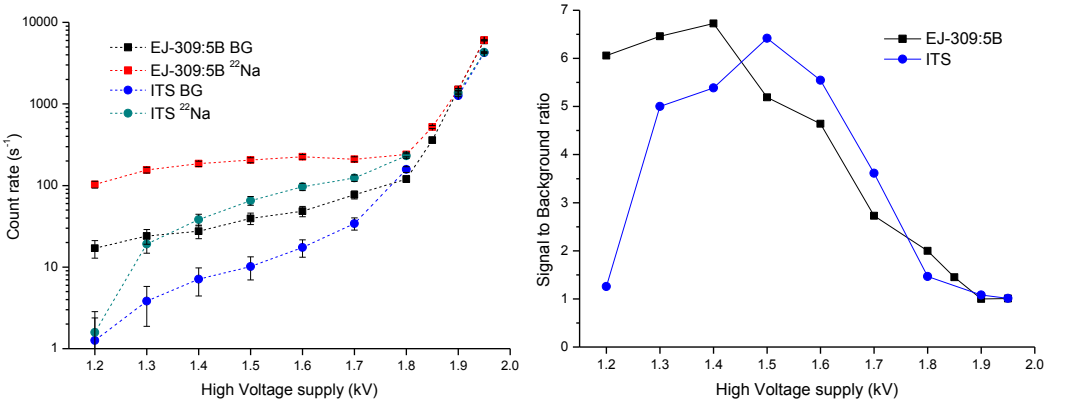

Figure 3.7. Left: Count rate vs high voltage settings measured with and without a ^{22}Na source for EJ-309:5B and ITS, (margin of error is the square root of the count rate). Right: signal to background ratio of EJ-309:5B and ITS.

Besides the lower count rate of ITS compared to EJ-309:5B it also displays a more compressed spectrum than previously seen with EJ-309:5B. Therefore it was decided to test ITS with high voltage power supply settings of 1.7, 1.8 and 1.9 kV and not at 1.6 kV as was used with EJ-309:5B. This higher setting of the high voltage power supply is a balance between higher count rates and acceptable signal to background ratios. It should be noted that working at 1.9 kV is at the practical limit of the PMT as can be seen from figure 3.7 as the background count rate has an extensive influence on the total counts and the linear response of the system may be compromised.

3.2. Decay patterns of EJ-309:5B and ITS

3.2.1. Traces, decay patterns and decay times of EJ-309:5B

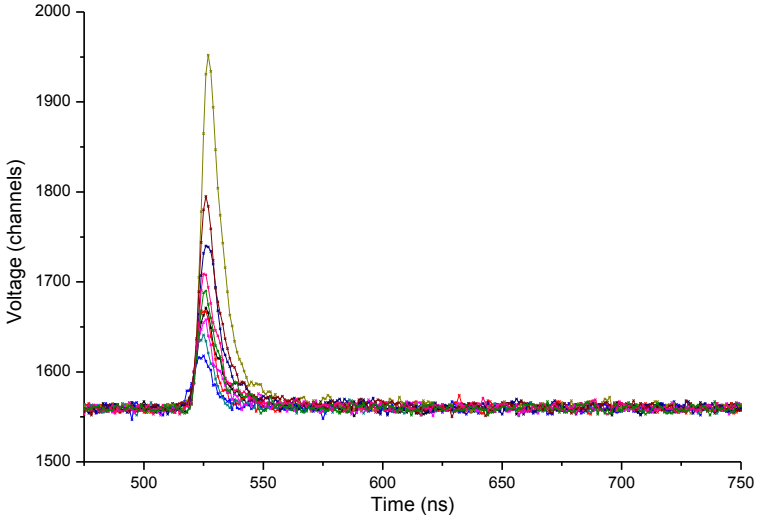

Figure 3.8. Sample of traces obtained from exposure of EJ-309:5B to radiation emitted by the ^{22}Na source. (PMT power supply set at 1.3kV, trigger level on channel 1608 at 521 ns)

An EJ-309:5B filled scintillator cell was exposed to radiation emitted by the ^{137}Cs and ^{22}Na sources, and both raw traces and spectra were acquired with the PHASE. Figure 3.8 shows traces (raw signal) recorded with EJ-309:5B exposed to the ^{22}Na source. As mentioned in section 2.1.3 the PHASE is set to measure both positive and negative signals reducing the 12 bit resolution from 4096 to 2048 channels. To increase the resolution the baseline was offset from the center (channel 2048) to channel 1560.

As stated above, up to three decay components have been identified by Szczęśniak in the decay profile of the EJ-309:5B cocktail: a high intensity fast component, a medium component, and a slow component.[11] To establish the decay profile of our specific setup all obtained traces were normalized and subsequently averaged to one curve, which allowed for fitting of a decay profile to that curve.[26] Attempts to fit a three-component exponential decay profile to the obtained trace did not lead to stable, consistent solutions. Fitting two exponentials to the decay profile resulted in a short component of 5.0 ns and a long component of 32 ns with an intensity of 8% relative to the fast component (see figure 3.9 on page 60). These values are in the range of those reported by Szczęśniak of 4.2 and 35 ns and an intensity of 12.5% of the slow component compared to the fast component. Attempts at fitting a single exponential decay curve to the data were unsuccessful. It is interesting to note that the decay time of the systems excited with nuclear radiation is longer than when excited with light as shown in chapter 2 of this thesis, where a single decay time of 2.6 ns was obtained with excitation at 255 nm. An explanation for the discrepancy between excitation with light and with radiation is that the former were performed within a thin film arrangement; minimizing self-absorption. In

contrast, the nuclear radiation excitation experiments which were performed with a large volume, give rise to self-absorption and subsequent delays in the energy transfer processes. An indication that self-absorption plays a role can be found in the fact that the rise time of EJ-309 when excited with light is 1.1 ns whereas excitation with nuclear radiation increases this to 2.9 ns.[14] Chapter 4 and 5 of this thesis will discuss this in more detail as this effect is most likely due to self-absorption.

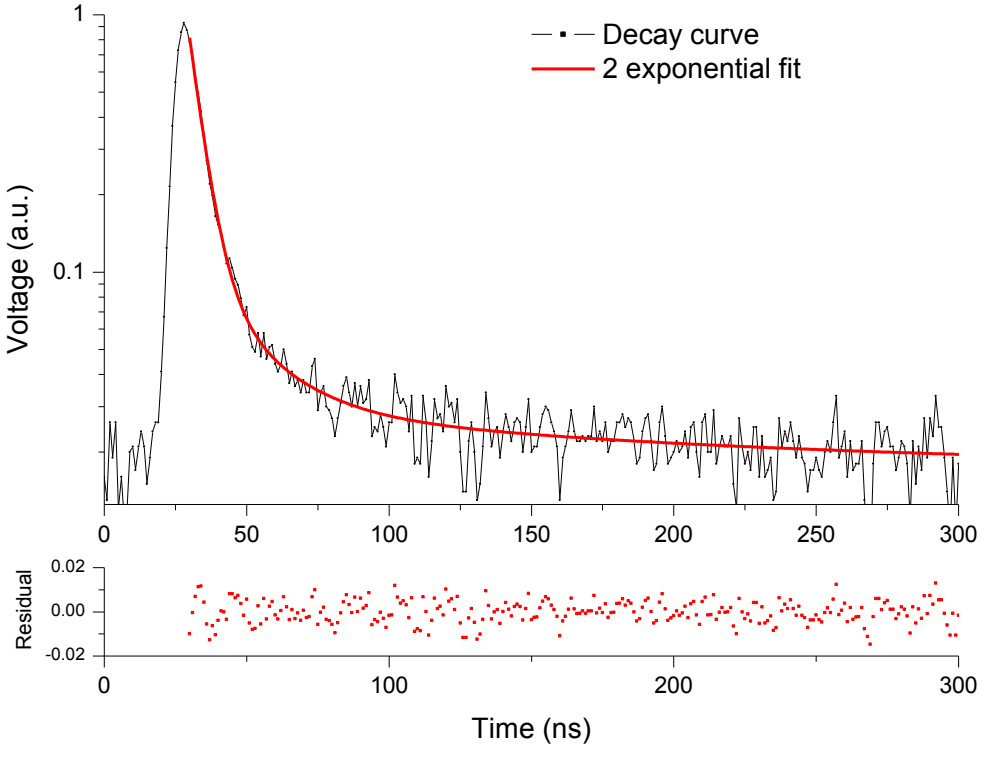

Figure 3.9. Top: 200 traces of EJ-309:5B, normalized and averaged (black line), and bi-exponential fit (red line, τ_1 = 5.0 ns and τ_2 = 32 ns, 8% intensity) Bottom: residuals of the fit.

The actual values of the decay constants are of importance when trying to separate the signals arising from neutron and (background) gamma radiation by means of pulse shape discrimination (PSD). As PSD involves determining the differences between the decay profile of gamma and neutron signals, it is important that there is a clear difference in the decay profiles between neutron and gamma signals, which will be the subject of future research. In this study only gamma ray emitting sources were used so pulse shape discrimination is not possible.

For the present tests, with only gamma sources, the actual value of the decay constants is not of importance as establishing an energy spectra is the primary goal, and not PSD; provided that the decay constants fit with the timing characteristics needed for a correct functioning of

the PMT and for the PHASE generation of an energy spectrum.* Of importance when producing energy spectra is the total amount of energy which is deposited per pulse, not the time over which the energy is deposited (with the condition that the (normalized) pulse shape is constant for different intensities).

3.2.2. Traces and decay patterns of ITS

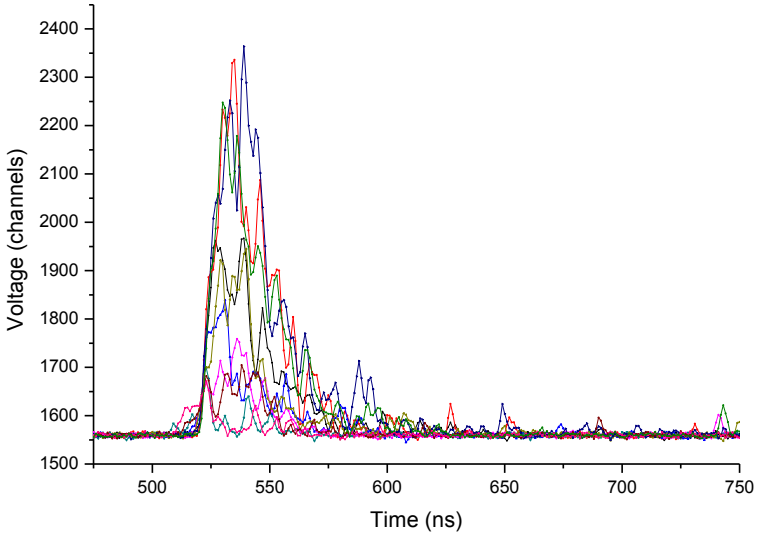

Figure 3.10. Sample of traces from ITS while exposed to the ^{22}Na source. An irregular decay pattern is visible (PMT power supply set at 1.9 kV, trigger level on channel 1650, at 521 ns).

As for the experiments with EJ-309:5B the ITS filled scintillator cell was exposed to radiation emitted by ^{137}Cs and ^{22}Na sources. Both raw traces and spectra were acquired with the PHASE. As noted above, figure 3.8, EJ-309:5B has a "textbook" decay profile following a two component exponential decay. From figure 3.10 it can be seen that ITS does not possess such a clean decay profile. It consists of more irregularity, especially at higher voltages. Due to the use of a higher amplification factor (the HVSP was set at 1.3 kV when measuring the dataset for figure 3.8, while it was set to 1.9 kV for figure 3.10, leading to a PMT multiplication factor of 9), the measured signal is as strong as with EJ-309:5B, but without the "textbook" smoothness; there are large fluctuations superimposed on the signal. The most plausible cause for this effect is noise; the high amplification causes the noise to increase and distort the peak shape. A second factor is that the intensity of scintillation light produced by ITS is less compared to EJ-309:5B (at identical HVPS setting), thereby making the actual physical processes become visible in the decay pattern (see section 3.4.1 for an estimate of the amount of photons generated). With the greater flux of photons generated by EJ-309:5B, this decay profile has a statistically relevant sample size such that the decay profile fits the mathematical

* A signal with a decay time ranging from 1 to 20 ns will work with the current PMT and PHASE. Slower systems might also work; at least until the point when pulse pile-up will influence proper data processing.

prediction well; individual interactions are averaged out by the large sample size. With the low flux of photons generated by ITS individual physical processes, e.g., slightly delayed ion recombination, have such an impact on the timing of the population of states that the result is an irregular decay curve. The consequence of this is that due to diverse excitation pathways initiated by ionizing particles, scintillating compounds are excited by different routes, for example ionization or excitation by Coulomb interactions, which after process specific decay times ultimately generate the scintillation light.[27] Each of these excitation and relaxation processes takes (a different) time and where there are a limited number of excited molecules, these time differences becomes apparent.* Integration of the total charge of a pulse will however provide the total charge of the pulse and the presence of irregular decay patterns is not of substantial influence on data processing. For further discussion of the decay profiles of ITS see section 3.4. The most probable origin of the distortion in the traces is a combination of high levels of noise and low levels of light.

3.3. EJ-309:5B

3.3.1. Pulse height spectra of ^{137}Cs and ^{22}Na radiation obtained with EJ-309:5B

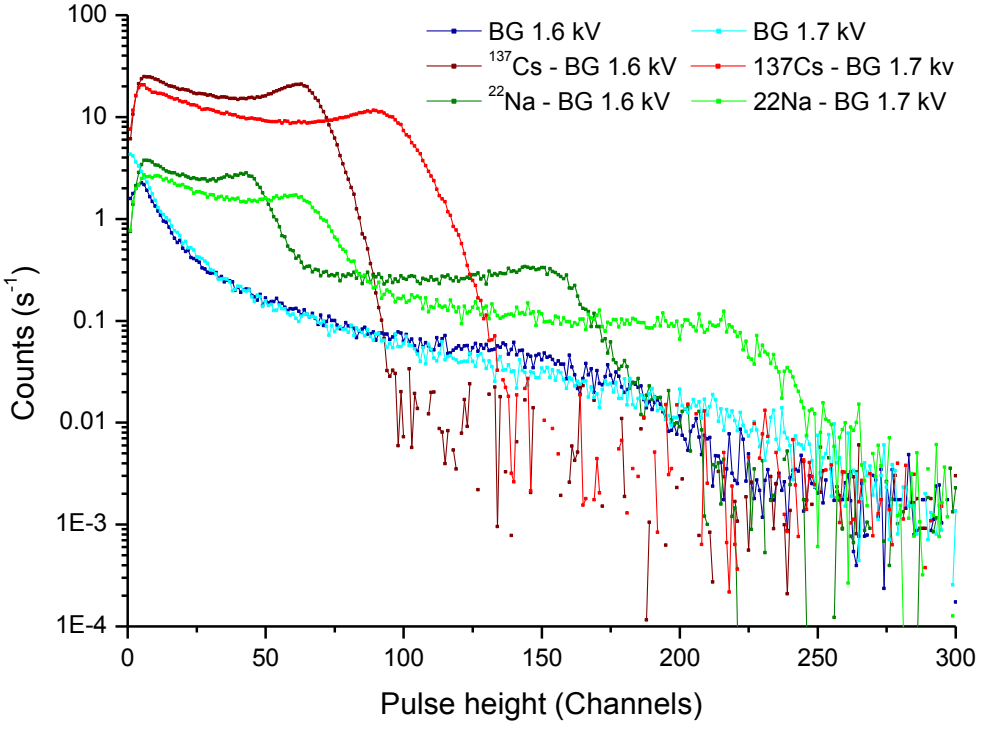

Figure 3.11. Pulse height spectra obtained with EJ-309:5B at 1.6 and 1.7 kV.
Blue line: background signal; red line: ^{137}Cs – BG signal; green line: ^{22}Na - BG signal.

* One photon will give one peak, two photons will give two peaks due to timing differences. If the sample size is large enough the emission of photons will turn into one continuous smooth decay profile; as is with EJ-309:5B.

The PHASE provides a histogram of the pulse height of a pulse abstracted from single traces; this histogram displays the pulse height spectrum of the measured radiation (referred to as: raw ^{137}Cs spectrum or raw ^{22}Na spectrum, figure 3.11). Offline subtraction of the background spectrum (referred to as: BG) produces the spectrum of the radioactive source in question (referred to as: ^{137}Cs – BG or ^{22}Na – BG). The x-axis of the histogram displays pulse height in channels. The channels of the pulse height spectrum depict the pulse height of the trace against count rate. The channels are derived by the FPGA through data binning of the pulse height of the traces. The y-axis displays the counts at a specific channel.

As shown in figure 3.11 (and figure 3.12 for Gaussian fitted spectra), the spectra measured with EJ-309:5B show broad features. There is a smeared out shoulder on the Compton continuum instead of a distinct peak for ^{137}Cs and two shoulders for ^{22}Na. The single shoulder in the cesium spectrum corresponds to the Compton edge at 478 keV (arising from the 662 keV gamma ray), which is positioned at channel 61 and 89 for 1.6 and 1.7 kV, respectively (see table 3.4), with the position of the peak being established by fitting a Gaussian curve to the edge of the Compton continuum. In the spectrum of ^{22}Na the 511 keV annihilation gamma ray is visible as a Compton edge with an energy of 341 keV positioned at channel 42 and 58 (for 1.6 and 1.7 kV respectively). The ratio between Compton edge of cesium and sodium should be 1.4 (478/341 keV) but is 1.5 (channel 61/42) at 1.6 kV HVPS; this indicates that the zero energy point is not positioned at channel zero by the FPGA and that a shift of the zero energy point should be applied to the x-axis of the spectra.

Table 3.4. Characteristics of Compton edge determined with EJ-309:5B.

	Mean position	Theoretical mean	Compton edge difference	Ratio	Baseline shift	Baseline shift	1062keV Compton edge (calc)	1062 keV Compton edge (found)
	Channel [a]	keV	Channel [b]	keV /chan	Channel	keV	Channel	Channel
EJ 1.6 Cs	61	478	20	6.9	8.3	57	-	-
EJ 1.6 Na	42	341					144	146
EJ 1.7 Cs	89	478	31	4.4	19	84	-	-
EJ 1.7 Na	58	341					217	206

[a] Mean position was determined from maximum of Gaussian peak fit, see figure 3.12 for details.

[b] Compton edge difference between ^{137}Cs and ^{22}Na peak is 137 keV.

By using the separation between the ^{137}Cs Compton edge, at 478 keV, and the ^{22}Na Compton edge, at 341 keV, the amplitude spectrum can be calibrated. This enables determination of the shift of the zero energy point. At 1.6 kV the separation between the ^{137}Cs and ^{22}Na Compton edges is 137 keV or 20 channels, giving a ratio of 6.9 keV per channel. Using this ratio for the measured Compton edges shifts the zero energy to channel -8.3.[*] Using this

[*] At 1.6 kV HVPS setting the 341 keV Compton edge of ^{22}Na should be positioned at channel 60 (341/6.9) and the 478 keV Compton edge from ^{137}Cs should be positioned at channel 70 (478/6.9). This is an average difference of 8.3 channels when compared to their measured position, resulting in the zero energy shift of 8.3 channels at 1.6 kV.

calibration ratio also sets the 1062 keV Compton edge of ^{22}Na at the correct position (± 2%). This indicates that the mechanism responsible for the incorrect ratio between Compton edges is the zero point energy and not factors as non-linear scaling.

There are two possible causes for the shift in the zero energy position in the signal; a ground loop between the high voltage power supply and the PHASE or the digitized signal zero level in the processing is incorrect. Determining which of these two phenomena is responsible for the shift of zero energy falls outside the scope of this study.

As can be seen in figure 3.11, the spectra obtained with EJ-309:5B show a shift of position of the Compton edge with increasing high voltage power supply for both cesium and sodium. This shift is caused by the voltage dependent amplification factor of the PMT. Changing the HPVS from 1.6 to 1.7 kV resulted in an increase in the amplification factor of ca. 1.5 to 1.6, which corresponds with the corrected shifts of the Compton edge position indicating proper behavior of the detector system (multiplication factor of 1.5, 1.5, and 1.6 for respectively the 341, 478, and 1062 keV Compton edges).[18]

3.3.2. Compton edge positions of EJ-309:5B

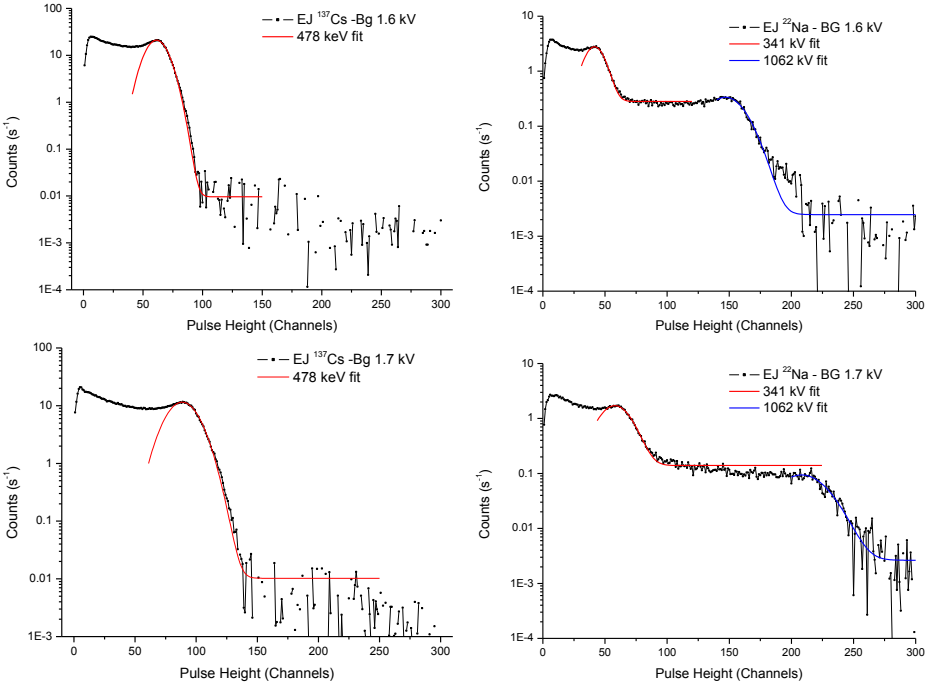

Figure 3.12. Gaussian fit of the EJ-309:5B spectrum at the 478 keV ^{137}Cs Compton edge (left side) and the ^{22}Na 341 and 1062 keV (right side) Compton edge with a power supply voltage of 1.6 (top) and 1.7 kV (bottom). Left top: ^{137}Cs - BG at 1.6 kV; left bottom: ^{137}Cs - BG at 1.7 kV; Black line measured spectrum, red line fit to 478 keV Compton edge. Right top: ^{22}Na - BG at 1.6 kV; right bottom ^{22}Na - BG at 1.7 kV; Black line measured spectrum, red line fit to 341 keV Compton edge , blue line fit to 1274 keV Compton edge . The relevant background signal was subtracted from all spectra.

To establish the position of the Compton edge the 341, 1072 and 478 keV Compton edges were fitted with a Gaussian curve (see figure 3.12). To be able to fit a Gaussian curve to the Compton edge the fit was performed to the less distorted right side of the Compton edge.

3.3.3. Count rates of EJ-309:5B

Table 3.5. Count rate for EJ-309:5B scintillator exposed to ^{137}Cs and ^{22}Na.

High voltage power supply	BG	^{137}Cs – BG		^{22}Na – BG	
	total count rate	total count rate	Adjusted count rate [a]	total count rate	Adjusted count rate [a]
(kV)	s^{-1}	s^{-1}	s^{-1}	s^{-1}	s^{-1}
1.6	44 ± 0.5	1323 ± 17	1561 ± 300	171 ± 2.3	200 ± 40
1.7	55 ± 0.6	1201 ± 16	1581 ± 300	151 ± 2.3	199 ± 40

[a] Margin of error influenced mainly by uncertainty in lost counts from zero energy shift.

The total count rate recorded using EJ-309:5B while irradiating with the cesium source at 1.6 kV HVPS setting is 1.3 kcounts per second and 1.2 kcounts per second at 1.7 kV, a decrease of 9%, see table 3.5. This decrease is in contrast to expectances; a higher driving voltage should shift the position of the Compton edge but the amount of counts should remain stable (see figure 3.6). The reason for this discrepancy is the zero energy shift, mentioned in section 3.3, which curtails a part of the low energy section of the spectrum. This cut-off is 57 keV at 1.6 kV and 84 KeV at 1.7 kV (table 3.4). When extrapolating the counts not counted in the cut-off region the count rate of both settings increases to 1.6 kcounts per second.

The total count rate of 1.6 kcount per second for ^{137}Cs at 1.6 kV is ca. 12-fold lower than the emission rate of the ^{137}Cs source (20 kBq). Allowing for a lower rate due to the 2π geometry of the measurement setup, instead of a 4π enclosure, the count rate in the detector should under ideal circumstances be halved to 10k counts per second. Other factors decreasing the rate are scintillator and PMT efficiency and the volume of the scintillator cell, which allows radiation to escape the detector enclosure before detection occurs. For a liquid scintillator the detector efficiency is expected to be ca. 10 - 20 % leading to a count rate of ca. 1 to 2 kcounts per second measured as coming from the source.[28] The total count rate of 1.6 kcount (^{137}Cs – BG), fits well within this range (16%).

This reasoning also holds for the ^{22}Na source, which has an activity of 1.5 kBq, the measured activity with the ^{22}Na source is ca. 200 counts per second, which counts for an efficiency of 12.5%, in line with expectations (again 10-20%).

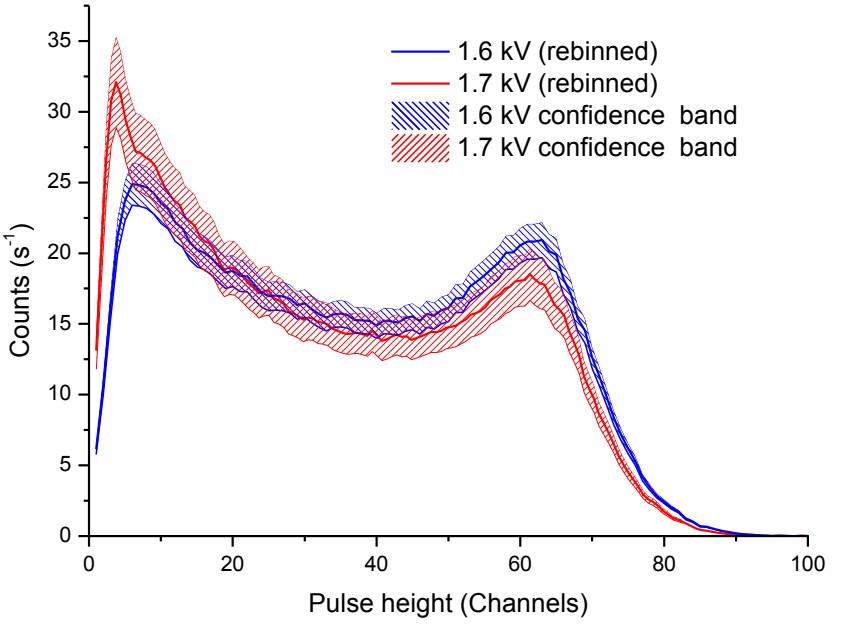

Figure 3.13. Comparison of original 1.6 kV EJ-309:5B spectrum (blue) irradiated with ^{137}Cs and re-binned 1.7 kV spectrum (red). Confidence band set at 10%.

When comparing the 1.6 and 1.7 kV spectra the latter has an appearance of lower count rate, which is a visual misrepresentation caused by broadening of the whole Compton continuum at increased HSVP settings (figure 3.11 and 3.12). This broadening causes spectrum to be spread over more channels; decreasing the intensity per channel, giving a distorted image. When re-binning the ^{137}Cs 1.7 kV spectrum to match that of the ^{137}Cs 1.6 kV spectrum it is apparent from figure 3.13 that the two spectra match well regarding overall shape. It is to be noted that the fluctuation in count rate can be up to 15%.

3.4. ITS

3.4.1. Spectra of ^{137}Cs and ^{22}Na radiation obtained with ITS

As mentioned in section 3.1, the spectra of ITS show a lower count rate and are more compressed than those obtained with EJ-309:5B (see figure 3.14), indicating a lower scintillator efficiency at similar high voltage power supply settings.

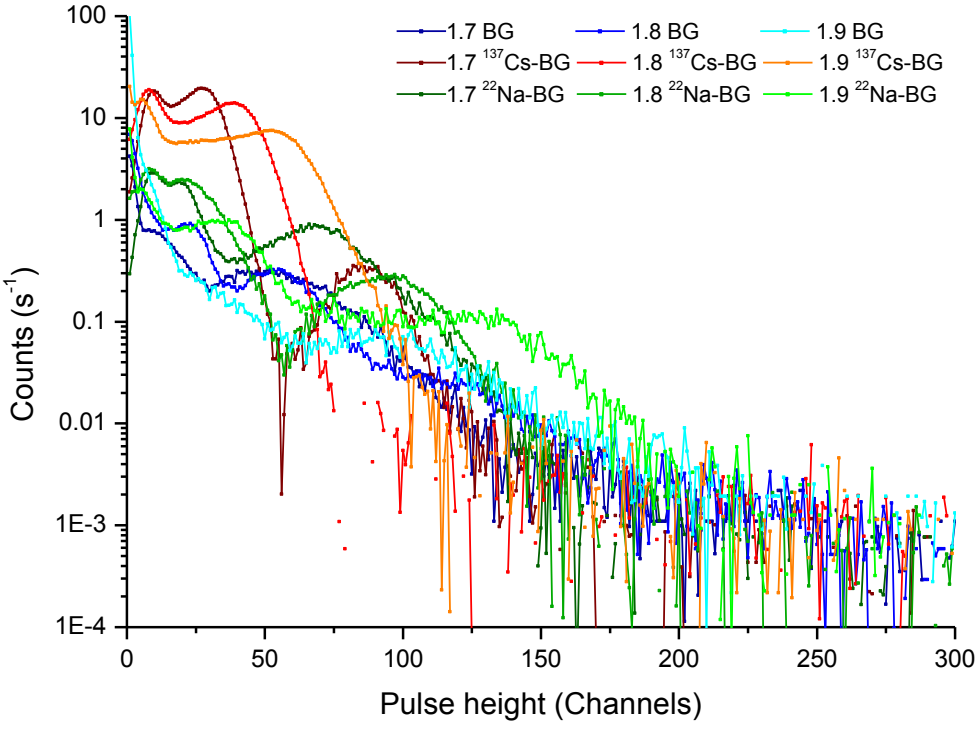

Figure 3.14. Spectra obtained with ITS at 1.7, 1.8 and 1.9 kV high voltage power supply. Blue line: background signal; red line: ^{137}Cs – BG signal; green line: ^{22}Na signal

The spectra obtained with ITS, although appearing to be of good quality, present a number of anomalies (individual Gaussian fitted spectra are shown in figure 3.15). The spectrum of ^{137}Cs at 1.7 kV has a second peak around channel 100 for which a clear explanation cannot yet be given (a 2% count rate relative to the Compton continuum).* The other two cesium spectra taken at 1.8 and 1.9 kV do not display this peak. The Compton edge at 1062 keV in the ^{22}Na spectrum at 1.7 kV might show some signs of the unidentified peak as seen in the ^{137}Cs spectrum but this is only apparent as a suboptimal fit of the tail of the Compton edge.

In the spectrum of ^{22}Na at 1.8 kV, the 341 keV Compton edge is broadened when compared to that of 1.7 kV but the position of the edge is not shifted as expected (only by half a channel). The mean at 1.8 kV is at the same position as the 341 keV Compton edge measured at 1.7 kV. The position of the mean of the 1062 keV Compton edge does shift however, indicating a change of HVPS setting and not a measurement error. The relative positions of the 341 keV Compton edge at 1.7 and 1.9 kV are placed as expected, as are all of the 1062 keV Compton edges, indicating that the 341 keV Compton edge position at 1.8 kV is

* Other radiation experiments performed at the same time in the building might have influenced our measurements, however this is mere speculation.

incorrect and not the one at 1.7 or 1.9 kV.As with EJ-309:5B the ratio between the positions of the Compton edges of ^{137}Cs and ^{22}Na is incorrect, and thus an offset has to be established (table 3.6). Because the measurement of ITS with ^{22}Na at 1.8 kV is flawed it cannot be used to establish an offset at this HVPS setting. However, as the edge position of cesium at 1.7 and 1.9 kV is known, estimating the shift of cesium at 1.8 kV by using the multiplication factor for the PMT (see appendix A) is possible; the position for the 478 keV Compton edge of cesium is estimated to be at channel 39.

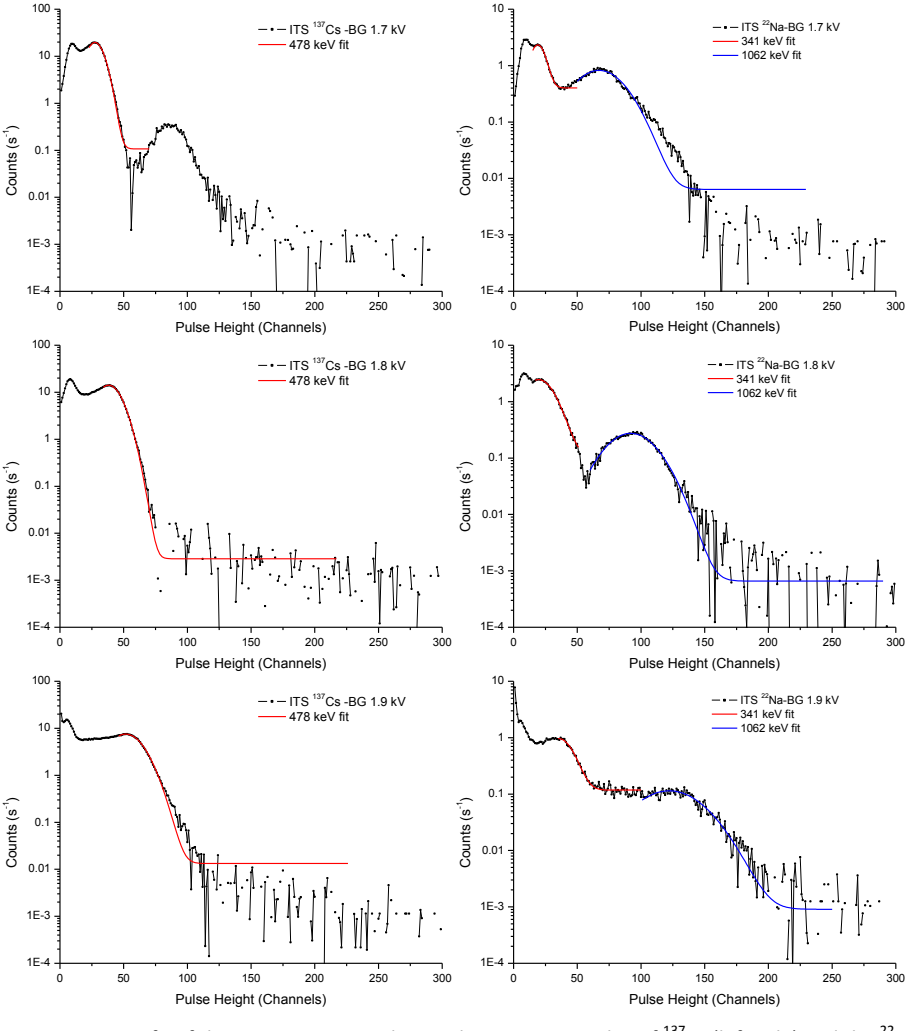

Figure 3.15. Gaussian fit of the ITS spectrum at the 478 keV Compton edge of ^{137}Cs (left side) and the ^{22}Na 341 and 1062 keV Compton edges (right side) with a power supply voltage of 1.7 (top), 1.8 kV (middle) and 1.9 kV (bottom). Left top: ^{137}Cs - BG at 1.7 kV; left middle: ^{137}Cs - BG at 1.8 kV; left bottom: ^{137}Cs - BG at 1.9 kV. Black line measured spectrum, red line fit to 478 keV Compton edge. Right top: ^{22}Na - BG at 1.7 kV; right middle ^{22}Na - BG at 1.8 kV; right bottom ^{22}Na - BG at 1.9 kV; Black line measured spectrum, red line fit to 341 keV Compton edge, blue line fit to 1062 keV Compton edge. The relevant background signal was subtracted from all spectra.

Table 3.6: Data of Compton edges measured with ITS for 1.7 and 1.9 kV.

	Mean position Channel [a]	Theoretical mean keV	Compton edge difference Channel [b]	Ratio keV /chan	Baseline shift Channel	Baseline shift keV	1062 keV Compton edge (calc) Channel	1062 keV Compton edge (found) Channel
ITS 1.7 Cs	27	478	8.2	16.1	2.6	42	-	-
ITS 1.7 Na	19	341					63	66
ITS 1.9 Cs	52	478	16	8.3	5.2	43	-	-
ITS 1.9 Na	36	341					123	122

[a] Mean position was determined from maximum of Gaussian fit, see figure 3.15 for details.
[b] Difference between ^{137}Cs and ^{22}Na Compton edge is 137 keV.

3.4.1. Count rates of ITS

The count rate of ITS is stable over the range of high voltage settings used when considering the counts lost to the zero energy shift (table 3.7), indicating a functioning scintillator. However the count rate of ITS is considerably lower compared to EJ-309:5B. It should be noted that the count rates at 1.9 kV are most probably influenced by the magnitude of the noise and how well the PHASE can handle the noise, as the background count rate at 1.9 kV is half the count rate of the actual signal.

Table 3.7: Count rate of EJ-309:5B and ITS scintillator exposed to ^{137}Cs and ^{22}Na.

Scintillator	High voltage power supply	BG total count rate	^{137}Cs – BG total count rate	^{137}Cs – BG Adjusted count rate [a]	^{22}Na – BG total count rate	^{22}Na – BG Adjusted count rate [a]
	(kV)	s^{-1}	s^{-1}	s^{-1}	s^{-1}	s^{-1}
EJ-309:5B	1.6	44 ± 0.5	1323 ± 17	1561 ± 300	171 ± 2.3	200 ± 40
EJ-309:5B	1.7	55 ± 0.6	1201 ± 16	1581 ± 300	151 ± 2.3	199 ± 40
ITS	1.7	40 ± 0.4	541 ± 6.6	681 ± 200	95 ± 1.5	118 ± 30
ITS[b]	1.8	59 ± 0.6	608	--	96	--
ITS	1.9	200 ± 2.4	522 ± 8.1	702 ± 200	73 ± 3.0	115 ± 30

[a] Margin of error influenced mainly by uncertainty in lost counts from zero energy shift.
[b] 1.8 kV ITS measurement is greyed out as it is considered invalid.

3.4.2. Photon generation

As discussed earlier (section 3.1) and in the previous paragraph, the count rate of ITS is lower than with EJ-309:5B. Furthermore, the intensity of the light generated by ITS is lower than for EJ-309:5B. The ^{137}Cs Compton edge of EJ-309:5B, at 1.6 kV lies at (corrected) channel 69, while Compton edge of the more amplified ITS scintillator at 1.9 kV lies at (corrected) channel 57 for ITS. Since the channels numbers are directly related to the pulse height of the recorded trace the pulses recorded with ITS are lower in pulse height but amplified to similar level as EJ-309:5B due to the greater amplification factor. As can be seen from table 3.1 the PMT has a multiplication factor of three when going from a power supply setting of 1.6 kV to

1.9 kV. Thus ITS needs an amplification factor of at least 3 to reach the same level of intensity as EJ-309:5B this means that more than 3 times as many photons are generated by scintillation events in a sample of EJ-309:5B than in a sample consisting of ITS.*

Based on the specifications provided by ELJEN Technology, the light yield for EJ-309 is 11,500 scintillation photons from the interaction with a 1 MeV electron.[22] For ITS this would mean that less than 4000 photons would be generated in such an event. ELJEN technology does not provide a number for the photon production of EJ-309:5B but Swiderski states that 1850 Phe/MeVee are generated when using EJ-309:5B, which would generate only ca. 600 photons for ITS at that energy level.[10] If we assume a linear response for the light yield, a 662 keV gamma ray would generate of the order of a 400 photons. As the maximum quantum efficiency of the PMT is 24%, at 420 nm, this results in only 100 photons being amplified by the PMT. It is therefore reasonable to assume that it is individual physical processes which cause the irregularities seen in the decay profiles of ITS traces.

3.4.3. Trace analysis; impact of PMT on signal output

Measurements with the PMT are done at several high voltage power supply settings of the PMT. The higher these settings the higher the multiplication factor of the PMT becomes (see table 3.1). To determine the level of noise generated by the PMT at these high settings the PMT was connected to an empty scintillator cell (i.e. containing only air). Raw data is collected by means of a positive level trigger (set at a lower level (1575) instead of the normal level of 1608) and 1000 data points were recorded. The captured data is displayed to show a trace of the voltage (and therefore energy) recorded over time (figure 3.16 left). Traces from the empty scintillator cell show that at near maximum settings of the high voltage power supply (1.95 kV) a rather consistent peak emerges with a very short low amplitude signal. The duration of the pulse is determined by taking the FWHM of each peak and plotting a histogram of incidence of each FWHM (figure 3.16 right). This histogram displays a bimodal distribution of the FWHM of each pulse. As expected, a feature with a very short duration (< 1 ns) arises due to noise in the signal; owing to the high amplification, some of the peaks in the noise set are above the level trigger level.

A second distinct peak in the histogram is wider in its FWHM and can be fitted with a Gaussian curve (mean value for the FWHM peak of 2.8 ns). Since measuring an empty scintillator cell should only give rise to signals due to noise (with a very short duration; FWHM < 1 ns), the second distinct signal, the feature with a FWHM of 2.8 ns, indicates a real source.

* Setting the HV supply higher does not increase the number of photons produced but increases the extent of amplification in the PMT. Therefore, the same results at different HV settings mean that the amplification makes it seem that there is the same number of photons, which is not the case. Besides an increase in amplification, an increase of the HV setting will also increase the possibility of spontaneous electron emission from the PMT, i.e. an increase in dark current.

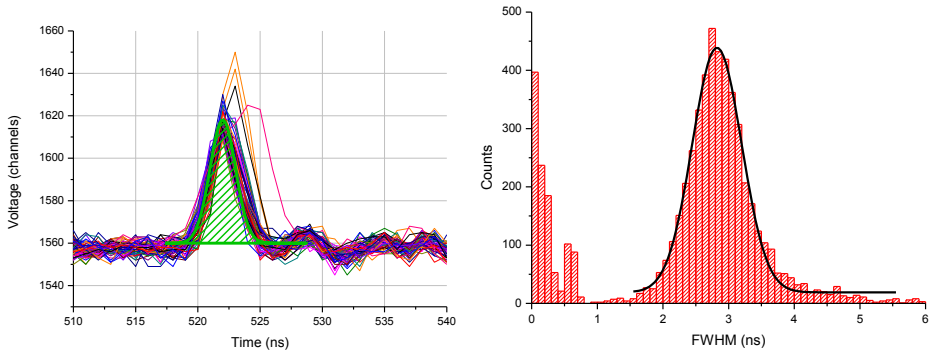

Figure 3.16. Left: Traces from an empty scintillator cell at 1.95 kV HVS setting. Green line Gaussian fit with a FWHM of 2.8 ns at 522 ns. For clarity the trigger level was set at channel 1608, equal to 40 mV thus not displaying noise. Right: FWHM distribution from 6k of traces, the signal follows a Gaussian curve (black line, mean at 2.8 ns). Trigger level was set at channel 1575, equal to 10 mV, to show short duration noise and the clear separation of the noise from the other feature.

When measuring with the commonly used level trigger setting (level 1608) the peak from the noise is no longer seen in the FWHM histogram (figure 3.17). This indicates that the noise is below the normal setting of the level trigger and is therefore of little concern. The other feature remains and is present in the data set collected at high HVPS settings.

The low intensity and rapid character of these peaks points to a possible origin of the distribution; the spontaneous emission of single electrons from the photocathode.[23] By using such a high bias over the PMT this process is amplified to such an extent that it can be measured. We can thus conclude that the fast low amplitude signals, seen in an empty cell, are the result of the emission of single electrons from the photocathode and we can expect that in further experiments these signals occur also. Furthermore, this effect will influence traces from sources with low light intensity especially.

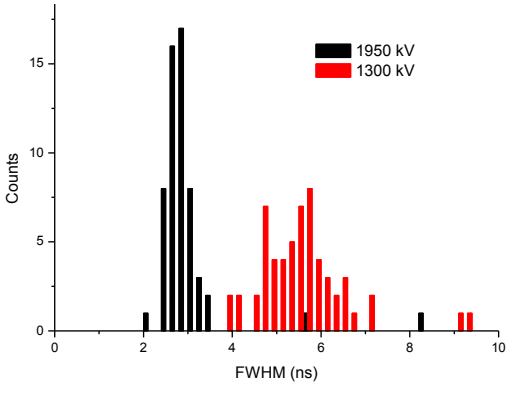

Figure 3.17. FWHM of traces obtained with empty cell at 1.3 and 1.95 kV.
Level trigger at level 1608 cuts of noise (which is apparent in figure 3.16 with a trigger level of 1575). Counts were normalized to account for count rate difference.

An effect seen when lowering the high voltage power supply from 1.95 kV to 1.3 kV is that the mean of the FWHM peaks shifts about from 2.8 to 5.4 ns, see figure 3.17. This is accompanied with an expected decrease in count rate due to a less signals passing the level trigger. The count rate for an empty cell at 1.3 kV is about 3 events min^{-1}, while at 1.95 kV the count rate is greater than 3 s^{-1}. It is therefore expected that at low HVPS settings the effect of noise will be minimal with regard to the signal input rate.

3.4.4. PMT influence on traces of ITS irradiated with ^{22}Na

When examining the traces recorded by exposing ITS to the sodium source (see figure 3.18) a comparable pattern to that of figure 3.16 is seen. When the power supply is set at 1.95 kV the majority (90%) of the raw traces obtained with the ITS filled scintillator cell display a similar signal to those determined earlier with the empty scintillator cell (see previous page). Fast low amplitude pulses of several nanoseconds and a maximum of intensity of about 50 channels (corresponding to an amplitude of around 40 mV).

The intensity of the single electron emission from the photocathode is in the same magnitude as the irregularities seen in a normal trace of ITS. This indicates that these irregularities are events of only a photon or electron in energy, strengthening the argument that physical processes are responsible.

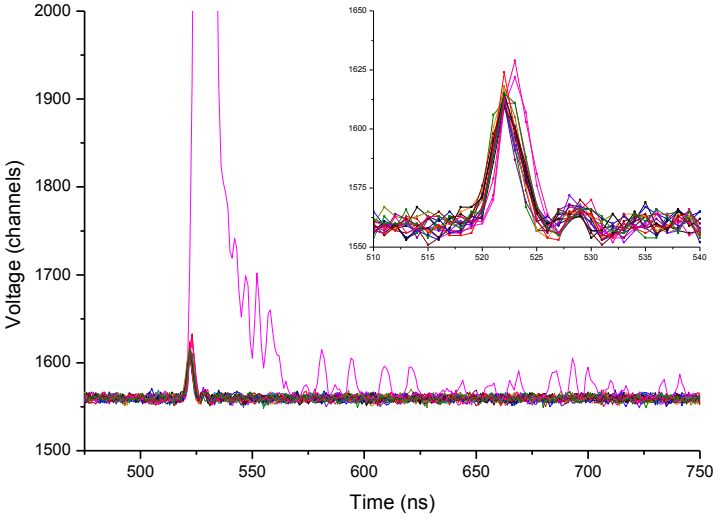

Figure 3.18. Traces of the fast low amplitude signals found in ITS traces at 1.95 kV HVPS with ^{22}Na as a radioactive source. For comparison, one normal trace, measured in the same dataset, is also depicted. Inset: details of the fast low amplitude peaks.

As discussed in section 3.4.3, measurements with an empty cell also display these fast signals arising from PMT dark current and noise and arise not from the scintillator processes. From the histogram in figure 3.19, the FWHM of the empty and ITS filled cell are of comparable value (2.8 vs 3 ns mean). This confirms that the fast low amplitude signals obtained with ITS are also the result of spontaneous emission of single electrons from the

photocathode and not, for example, from some low-level light emission effect in the scintillator. Note the high number of counts at energies with FWHM value of 10 ns or higher in the histogram of ITS, which corresponds with the width of traces from radiation. It should be noted that this phenomenon, of fast low amplitude signals is also seen with EJ-309:5B at a high voltage power supply setting of 1.95 kV but since the working conditions of EJ-309:5B lie much lower than 1.95 kV this is of minimal influence under normal measurement conditions.

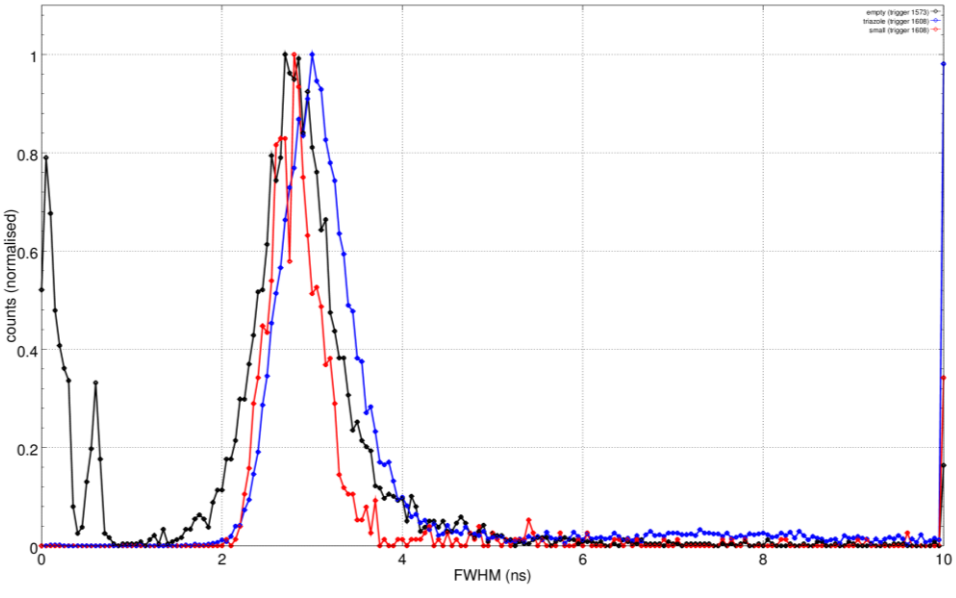

Figure 3.19. FWHM determined for peaks measured with an empty scintillator cell (black line: trigger level at 1608; red line: trigger level at 1580, 6k counts) and a scintillator cell filled with ITS (blue line: trigger level at 1608, 12k counts). High voltage power supply set at 1.95 kV in all experiments.

3.5. PHASE – raw traces comparison

While the PHASE is equipped with a series of digital filters on the FPGA, which are used to analyze the obtained traces, this system is not suited to analysis of unconventional decay profiles generated by the ITS cocktail. Therefore a sub-optimal setting was used with both scintillators; EJ-309:5B and ITS. Instead of relying on the shape of the pulse to generate a pulse height spectrum these settings have the effect that they sum the pulse height of the traces over the region of interest to produce a pulse height spectrum.[29]

A series of raw traces were recorded to estimate the accuracy of these non-standard filter settings used on the PHASE and these 30k+ traces were processed to obtain a spectrum (figure 3.20) to compare with those generated by the PHASE directly.

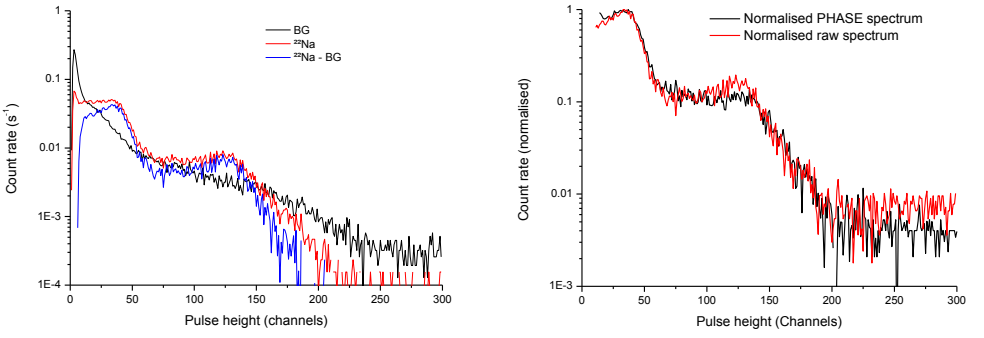

Figure 3.20. Left: Spectrum of ^{22}Na obtained with raw output traces from ITS with high voltage power supply at 1.95 kV. Red line: raw ^{22}Na spectrum; black line: background spectrum; blue line ^{22}Na – BG spectrum.
Right: overlay of normalised PHASE spectrum (black) and raw output traces (red).

Due to embedded software running on the FPGA, the rate for obtaining raw traces directly from the PHASE is only three traces per second while the actual count rate of the PHASE is unaffected. Processing the raw traces into a spectrum and overlaying this with the spectrum generated directly with the PHASE shows that spectrum obtained by means of the raw traces is similar to that obtained by means of the PHASE.

3.5.1. Background count rates

The increase in background rate going from 1.7 to 1.8 kV with ITS going from 1.6 to 1.7 kV is comparable with the increase observed with EJ-309:5B. However, as can be seen from figure 3.21 the increase in BG count rate is more than threefold when going from 1.8 to 1.9 kV with ITS. The steady increase going from 1.7 to 1.8 kV indicates that the cause of the increase in count rate at 1.9 kV stems from the rise in HVPS and that the use of ITS is not the source of this dramatic increase. Also the spectra depicted in figure 3.15 on page 67 indicates that the count rate in the low energy part of the background spectrum (channel 1-5) increases with a factor of 10 when going from 1.8 to 1.9 kV high voltage power supply. The count rate of these first 5 channels at 1.9 kV is 170 counts per second and thus strongly influences the total count rate of 200 counts per second.

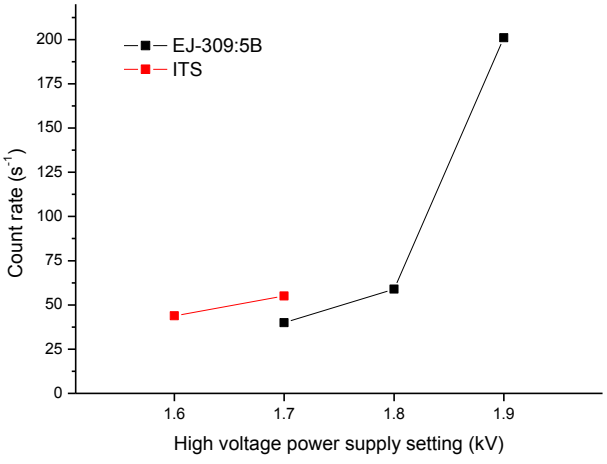

Figure 3.21. Count rate of the background signal for EJ-309:5B and ITS.

A thorough study of the background pulse height indicates that there are features in the background measurements (figure 3.11, 3.14 and 3.22). Certainly with the ITS there are features visible, with EJ-309:5B it is not conclusive if they are there or not. Moving to a different location (>25 km apart) to eliminate radiation from the sources and to change the buildings background spectrum shows that also at the other location there are shoulders in the spectrum (figure 3.22). These broad features arise either by means of processing errors due to poor signal shape or are due to radioactive contaminates introduced during fabrication of the cocktail or filling of the scintillator cell. The sharp features in the 1.8 and 1.9 kV at channel 175 and 230 are for all probability electronic artifacts only seen in the second location and did not occur in any of the previously shown spectra.

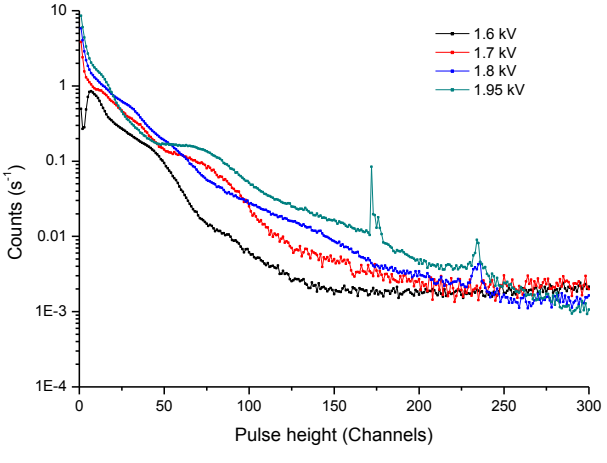

Figure 3.22. Background signals recorded with EJ-309:5B at a different location.

3.6. Discussion

There are multiple issues encountered while performing measurements of ITS and the PHASE that hinder correct data analysis. These are partly due to the low photon flux from ITS combined with working outside the optimum zone of the PHASE. Due to the low photon flux there is insufficient data to provide for a statistically sound decay profile for ITS. This deviation from “textbook” decay profile can lead to erroneous interpretation of the decay profile by the PHASE. The imperfections in the traces influences the amplitude which in turn influences the determination of the energy of the peak as the PHASE is designed to function with exponential decay profiles only. The low energy part of the spectrum is sensitive as this is near the trigger level, resulting in the generation of electronic artefacts and high background rates.

The low light flux from ITS compared to EJ-309:5B leads to data sets of different quality. While EJ-309:5B produces statistically sound data sets ITS does not provide enough light at 1.7 kV and too many artefacts are present at 1.9 kV. The high setting of 1.9 kV leads to artefacts due to operation near the limits of the PMT working conditions, increasing spontaneous emission of electrons.

4. Conclusion

At most points EJ-309:5B outperforms ITS, this mainly stems from the low light output by ITS when compared with EJ-309:5B. To achieve the same energy output ITS has to be amplified 3 times indicating that ITS in this composition provides a poor light yield. This low light yield results in statistically poor distributions for the excited states, which produce decay profiles that deviate from expected signals.

Furthermore not all experiments with EJ-309:5B were flawless; the zero energy shift and the features in the background. Hence, more extensive testing of EJ-309:5B and ITS is required to reveal the origin of these anomalies.

While the more erratic behavior of the decay profile might have a negative impact on signal processing it is shown that with this hardware configuration automatic processing did not deviate substantially from offline processing, enabling higher data acquisition rates by direct FPGA processing.

Overall it can be stated that EJ-309:5B is a better scintillator than ITS under these test conditions. As stated in chapter 2 the low solubility of the boron triazole limits the concentration of the boron triazole compared with those achieved with the fluorophores in EJ-309:5B. Enhancing solubility of the boron triazole might increase light yield thus decreasing many of the problems encountered due to the low light emission and the complications associated with it.

5. References

[1] A. Tomanin, J. Paepen, P. Schillebeeckx, R. Wynants, R. Nolte, and A. Lavietes, Nucl Instrum Meth A, *vol 756,* **2014**, pg 45.

[2] A. C. Kaplan, M. Flaska, A. Enqvist, J. L. Dolan, and S. A. Pozzi, Nucl Instrum Meth A, *vol 729,* **2013**, pg 463.

[3] M. M. Bourne, S. D. Clarke, E. C. Miller, M. Flaska, and S. A. Pozzi, Nucl Sci Symp Conf Rec (NSS/MIC), **2010**, pg 981.

[4] L. Stevanato, D. Cester, G. Nebbia, and G. Viesti, Nucl Instrum Meth A, *vol 690,* **2012**, pg 96.

[5] S. F. Naeem, S. D. Clarke, M. Flaska, and S. A. Pozzi, Proc INMM Annual Meeting, **2013**

[6] S. F. Naeem, S. D. Clarke, and S. A. Pozzi, Nucl Instrum Meth A, *vol 726,* **2013**, pg 120.

[7] F. Pino, L. Stevanato, D. Cester, G. Nebbia, L. Sajo-Bohus, and G. Viesti, Appl Radiat Isotopes, *vol 89,* **2014**, pg 79.

[8] S. F. Naeem, S. D. Clarke, and S. A. Pozzi, Nucl Instrum Meth A, *vol 714,* **2013**, pg 98.

[9] C. C. Lawrence, A. Enqvist, M. Flaska, S. A. Pozzi, and F. D. Becchetti, Nucl Instrum Meth A, *vol 729,* **2013**, pg 924.

[10] L. Swiderski, M. Moszynski, D. Wolski*, et al.*, IEEE T Nucl Sci, *vol 57,* **2010**, pg 375.

[11] T. Szczesniak, M. Moszynski, A. Syntfeld-Kazuch*, et al.*, IEEE T Nucl Sci, *vol 57,* **2010**, pg 3846.

[12] T. Kögler, A. R. Junghans, R. Beyer*, et al.*, J Instrum, *vol 7,* **2012**, pg C03047.

[13] ELJEN TECHNOLOGY, *Material safety data sheet on EJ-309*

[14] Eljen technologies *EJ-309 Liquid scintillator pulse-shaped discrimination properties*

[15] Saint Gobain *BC-523A specifications sheet*http://www.crystals.saint-gobain.com/uploadedFiles/SG-Crystals/Documents/SGC BC523A Data Sheet.pdf

[16] Eljen technology, *EJ-339A specification sheet*, 2014

[17] *Neutron Detectors: Alternatives to Using Helium-3* (U. S. Government Accountability Office, **2011**), GAO-11-753.

[18] Hamamatsu, *R7724 specification sheet*

[19] *Photomultipliers: data handbook. PC04* (Philips Components, **1990**).

[20] E. Talnishnikh, L. Paganini, J. Stegenga*, et al*, in Anima 2013 conf proc, 2013), p. 1

[21] J. Stegenga *INCAS³ Solutions | PHASE-250-10 Technical specifications* http://www.incas3-solutions.com/custom-product-solutions/phase-250-10/

[22] Eljen technologies, *Boron loaded EJ-309 liquid scintillator scintillator properties sheet*

[23] G. F. Knoll, *Radiation detection and measurement* (John Wiley & Sons USA, **1989**).

[24] P. Dijkstra, in preparation,

[25] P. Blanc, M. Hamel, C. Dehé-Pittance, L. Rocha, R. B. Pansu, and S. Normand, Nuclear Instruments and Methods in Physics Research Section A: Accelerators, Spectrometers, Detectors and Associated Equipment, *vol 750,* **2014**, pg 1.

[26] PicoQuant, FluoFit Pro Software,

[27] F. Brooks, Nucl Instrum Methods, *vol 162,* **1979**, pg 477.

[28] D. L. Horrocks, *Application of Liquid scintillation counting* (Academic Press, Inc, **1974**).

[29] J. Stegenga (private communication)

Chapter 4

SCINTILLATOR COCKTAIL COMPOSITION AND COMPARISONS

As discussed in chapters 2 and 3 the efficiency of the scintillator cocktail ITS (INCAS³ triazole scintillator) in radiation detection experiments is below that of commercial radiation detection cocktails. In this chapter a comparison between a commercial scintillator (EJ-309) and ITS is made to attempt to understand the origins of the differences in efficiencies.

The main differences investigated are in regard to photophysical aspects of the cocktails, including transmission of light through the solutions and subsequent emission. Furthermore the overall efficiency for light emission and the fluorescence decay times of these cocktails are determined.

1. Introduction

Compatibility with the electronical components of current radiation detection systems necessitates that a new scintillator cocktail should function similarly to existing scintillators. Therefore the composition and characteristics of newly developed scintillator cocktails should resemble the composition and characteristics of known scintillators.[1, 2] General guidelines on composition and characteristics are available in textbooks but specifications of current scintillation technologies are proprietary information and not readily available, with legally required material safety datasheets (MSDS) providing little by way of useful information.[3] As discussed in chapter 1 of this thesis, there are general guidelines for the composition of liquid organic scintillators (LOS); An LOS will comprise of a solvent, a fluorophore and typically a wavelength shifter (WLS) also; their individual characteristics are discussed below.

1.1. Solvent

The solvent in an LOS must contain a component containing conjugated π-bonds; in order to absorb the energy deposited by charged particles, and be able to re-emit that energy as UV or visible light.[4] In general these conjugated systems are aromatic, with either one or two aromatic rings. At present solvents are chosen from a pool of only four candidates: pseudocumene, linear alkyl benzene (LAB), phenyl xylyl ethane (PXE) and di-isopropylnapthalene (DIN) (figure 4.1).

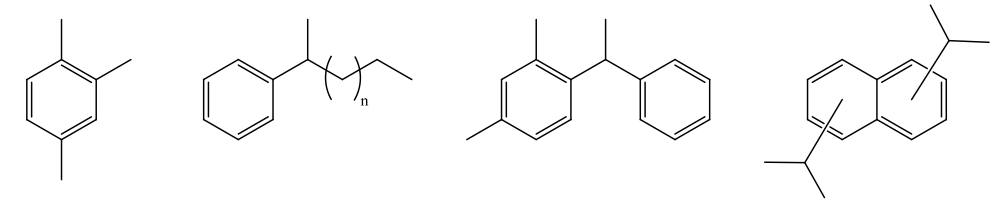

1,2,4-trimethylbenzene
Pseudocumene
PS

-
Linear alkyl benzene
LAB

2,4-dimethyl-1-(1-phenylethyl)benzene
Phenyl Xylyl Ethane
PXE

-
Di-isopropylnaphthalene
DIN

Figure 4.1. Liquid organic scintillator solvents
(systematic name, trivial name and abbreviation).

Initially toluene and xylene were used as scintillator solvents but for environmental reasons they have since been phased out. Similarly, pseudocumene is currently being phased out and replaced by LAB, PXE or DIN. The actual choice between these three solvents depends on several factors specific to the desired scintillator, such as safety (flash point, vapour pressure), cost, efficiency and availability.[5, 6] PXE, LAB and DIN exhibit similar photophysical properties; the solvents all absorb energy in the UV-A/B region populating electronically excited states and then relaxing by emitting that energy as light with energy in the UV-A region. The emission of light by the solvent in the UV region presents two drawbacks (in regard to efficient use in radiation detectors); the PMTs (photomultiplier tubes) used in

radiation detection are not optimised to absorb light over this wavelength range, and the solvent will re-absorb the light it emits, lowering the total photon emission efficiency and elongating emission decay lifetimes.[7, 8]

1.2. Fluorophore and Wavelength shifter

A fluorophore is added to the solvent in order to circumvent the limitations encountered when using a solvent only. This fluorophore accepts the excitation energy from the solvent and emits this at a longer wavelength (with an emission maximum in the range 370 - 390 nm, for currently used fluorophores).[4] In order to ensure efficient energy transfer from the solvent to the fluorophore, its concentration is relatively high: 1 - 4% (w/w). It should be noted that this concentration is much higher compared to those typically used in fluorescence studies (« 0.1% fluorescent compound) and self-absorption and solubility are limitations that are encountered. The fluorophores currently used in scintillator cocktails still emit UV light, which is not absorbed optimally by the PMT photocathode. Thus a second fluorophore, called a wavelength shifter (WLS), is added to ensure matching of the emitted light with the optimum responsivity of the PMT (420 nm).[8] Addition of the WLS also ensures a decrease in re-absorption of emitted light by the other components (solvent and fluorophore) in the scintillator cocktail. This wavelength shifter is present at much lower concentrations than that of the fluorophore.

As the development of liquid organic scintillators and PMTs has proceeded concurrently since the 1950s, both have been optimised towards each other in a self-reinforcing process (regarding emission and absorption characteristics). Engineering a liquid scintillator that does not confirm with the input characteristics of a PMT will therefore be hindered by a technology vacuum. Current output characteristics of commercial scintillators should be used as a starting point to be able to use existing off-the-shelf detector technology. This applies to the emission wavelength but also the timing characteristics of the cocktail. For this reason, in this chapter, the properties of EJ-309, a widely used commercial scintillator are investigated and compared with a new cocktail.[3, 9-11]

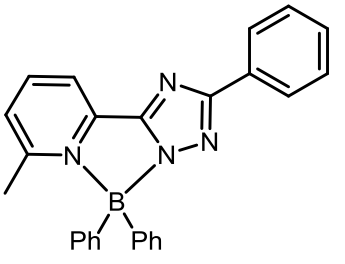

Figure 4.2. Structure of the boron triazole used in ITS.

In order to reduce the amount of fluorophore and WLS needed in a scintillator cocktail a previously described boron triazole [see chapter 2 and figure 4.2] was selected.[12] The boron triazole was chosen because of its high quantum yield and absorbance (resp. 0.75 and 34.000

M^{-1} cm^{-1}), close matching to PMT absorbance optimum (λ_{em} = 424 nm) and ease of synthesis. The boron triazole produces a novel scintillator cocktail when dissolved in a common scintillator solvent (DIN); the INCAS³ Triazole Scintillator (ITS). The relatively low concentration, at which the boron triazole needs to be added to yield a working scintillator, is due to the high molar absorptivity and quantum yield of the boron triazole complex enabling high efficiency of energy absorption and emission. Furthermore the wavelength of emission (424 nm) by the boron triazole ensures good correspondence with the maximum of the PMT photocathode sensitivity (420 nm), see chapter 2 and appendix A for further details. This close matching of boron triazole emission and PMT sensitivity obviates the requirement for a distinct WLS. The solvent of choice was DIN, which, as will be discussed in section 3.1, is also used in EJ-309, to allow for a direct comparison between EJ-309 and ITS.

The efficiency of ITS in a radiation detection test is 40% lower than that of EJ-309. The primary goal of the work described in this chapter is to gain insight into the differences in behaviour and efficiencies between EJ-309 and ITS. Photophysical measurements were performed to establish the similarities and dissimilarities between these two cocktails. These insights can provide a basis for further development of more efficient cocktails.

2. Experimental

DIN was a gift from PerkinElmer Groningen, EJ-309 was purchased from Scionix; both were used without further purification. Boron triazole was prepared according to previously reported method.[12] FT-Infrared spectra were recorded as neat liquids using a PerkinElmer Spectrum400 FTIR spectrometer equipped with an ATR accessory. UV/vis absorption spectra were recorded on a Specord600 UV/vis absorption spectrometer (AnalytikJena) as neat liquids in a 50 µm pathlength FTIR liquid cell or diluted in heptane in a 1 cm quartz cuvette. Emission and excitation spectra were recorded using a JASCO FP7200 spectrofluorimeter, and were corrected for instrument response. Emission spectra were recorded with excitation provided by a 75 W Xe lamp coupled to a Quantum Northwest QPOD2e temperature controlled cell holder via a Zolix Omni150 monochromator, 300 l/mm grating and 500 nm blaze. Emitted light was collected at 90° with a suitable long pass filter (Thorlabs) via an SMA coupled 200 micron core fibre to a Shamrock 163 spectrograph (Andor Technology) and iDus-420-OE CCD (Andor Technology). Spectra were typically recorded as 10 accumulations of 0.1 s duration. Spectra were calibrated with the emission of TL rooms lights. Quantum yields were determined relative to a diphenylanthracene in ethanol.[13] Fluorescence decay lifetimes were measured using a PicoQuant PicoHarp 300 TCSPC, equipped with τ-SPAD detector and LDH pulsed diodes, in a Quantum Northwest QPOD2e temperature controlled cell holder. GC-MS analysis was performed on a HP 6890 GC Series equipped with HP 5973 Mass Selective Detector and dimethylpolysiloxane column.

3. Results and discussion

As mentioned in section 1.1 one of the possible solvent for use in scintillator cocktails, is DIN. This solvent is a mixture of di-isopropylnapthalene isomers, and increasingly used in contemporary scintillation cocktails. It has good spectral characteristics and high flashpoint, low vapour pressure and is regarded as non-toxic.[14, 15] GC-MS analysis of EJ-309 shows the presence of DIN in EJ-309. The identification of the specific fluorophore and WLS in EJ-309 by GC-MS was unsuccessful due to the relatively low concentration of the fluorophore and WLS in EJ-309, their detection by gas chromatography was precluded by the limit of detection of the apparatus.

3.1. IR spectra of DIN, EJ-309 and ITS

The FTIR transmission spectra of DIN, EJ-309, and ITS are essentially identical (figure 4.3) which indicates that the major component of these samples, i.e. the solvent, is the same in each case. From the bands at 2960 cm^{-1} ($-CH_3$) and 2870 cm^{-1} (-CH) it is apparent that there is a substantial proportion of methyl and isopropyl groups as is expected from the sample of di-isopropyl napthalene (DIN).

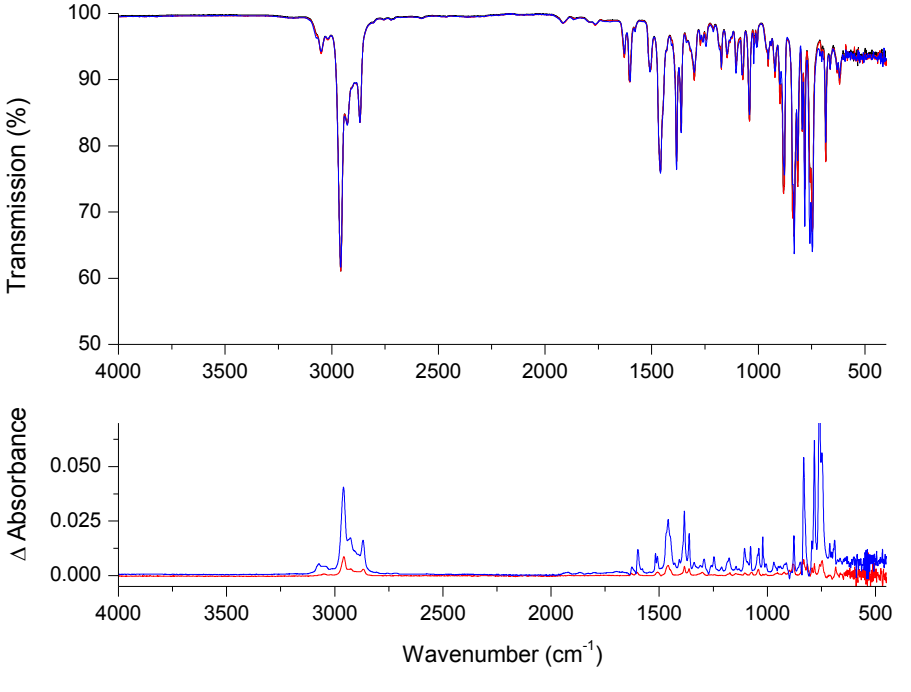

Figure 4.3. Top: FTIR transmission spectra of DIN (black), ITS (blue) and EJ-309 (red), recorded as neat liquids on an ATR. Bottom: FTIR difference absorption spectra of ITS (red) and EJ-309 (blue) after subtraction of the spectrum of DIN.

Close examination of the difference in absorption of EJ-309 and ITS compared to DIN shows subtle differences. Minor shifts in wavenumber indicate that there are only small differences between the DIN sample (provided by PerkinElmer) and EJ-309. These small differences combined with the similarity of the GC-MS data indicate that the difference between EJ-309 and DIN arises from differences in specific isomeric composition, e.g. arising from differences in suppliers or manufacturing process.

3.2. UV/vis absorbance and emission spectra

The high absorbance of the liquids (DIN, EJ-309 and ITS) precluded the use of standard cuvettes (1.5 mm pathlength) in determining absorption spectra and instead a liquid IR cell with a pathlength of 50 µm was employed. Dilution in heptane (Uvasol grade) was used where absorbance needed to be decreased further.

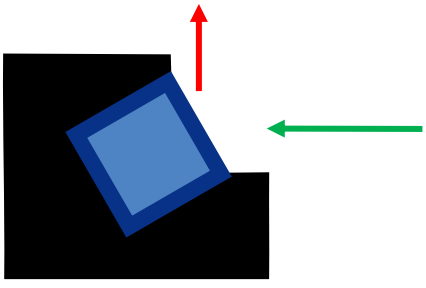

Figure 4.4.: Top view of 60° front face excitation / emission measurement arrangement. Black: holder for cuvette holds cuvette in 60° angle relative to incoming light (green arrow). Blue square: 1.5 mm cuvette with liquid inside (light blue). Red arrow: light emitted towards detector.

Fluorescence spectra where obtained using a custom cell holder which places the cell in such a manner that the front face of the cuvette is at an angle of 60° with respect to the excitation source (see figure 4.4). The 60° front face arrangement enables the measurements of neat liquids despite low transmission of the solvent. Emitted light only has to travel a short length through the solution to excite the cuvette, limiting re-absorption (see paragraph 3.6). Decay lifetimes of the fluorophore were measured with a customised PicoQuant instrument with the 60° arrangement also in place.

3.3. Electronic absorption spectrum of DIN

The absorption of DIN in the UV hinders acquisition of an absorption spectrum in a 1 cm cuvette and even with a 50 µm pathlength liquid FTIR cell the absorbance is still greater than 2.5. Diluting the sample in heptane (to 90 µM) allows for the absorption spectrum of DIN to be recorded, which shows absorption maxima at ca. 225 nm and 278 nm (see figure 4.5). A third weaker absorption band is observed at 321 nm. Further dilution of this sample (to 2 µM) reveals the absorption maximum at 229 nm (ε is $13 * 10^4$ M^{-1} cm^{-1} at 229 nm and $6.5 * 10^3$ M^{-1} cm^{-1} at 278 nm, table 4.1).

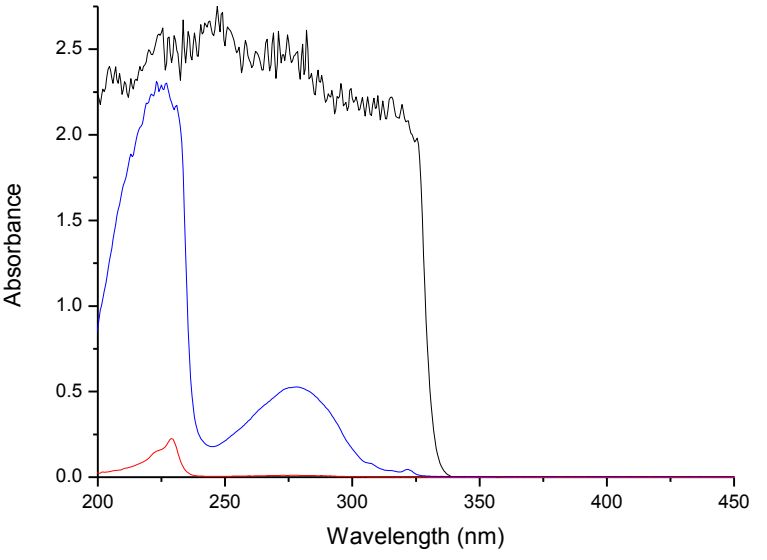

Figure 4.5. UV/Vis absorption spectrum of neat DIN in a 50 µm pathlength cell (black line). Absorption spectrum of DIN (90 µM in heptane, blue line). Absorption spectrum DIN (2 µM in heptane, red line).

Table 4.1. Overview of photophysical properties of DIN in heptane.

λ_{max} (nm)	Absorbance	ε (* 1000 M^{-1} cm^{-1})	Penetration depth [a] (µm)
229	0.226	130	0.017
278	0.527	5.9	0.37

[a] penetration depth is defined as the distance over which 90% of the light is absorbed.

The molar absorptivity of DIN is highest at 229 nm and high at 255 and 278 nm, and hence the penetration depth of light through DIN at 229 and 278 nm is less than a micron (table 4.1, figure 4.6). For light at 229 nm, the penetration depth is only 17 nm i.e. a few monolayers, and it can be assumed that all light at this wavelength will be absorbed in the scintillator regardless of the dimensions or geometry of the container. At 278 nm, the absorbance is less and the penetration depth is ca. 370 nm. At 255 nm, a wavelength used for excitation in the present studies (see paragraph 3.12), the penetration depth is around 700 nm. As can be seen from figure 4.5 the absorption measured with the 50 µm pathlength cell is greater than 1 at < 325 nm, i.e. a penetration depth in DIN of 50 µm or less.

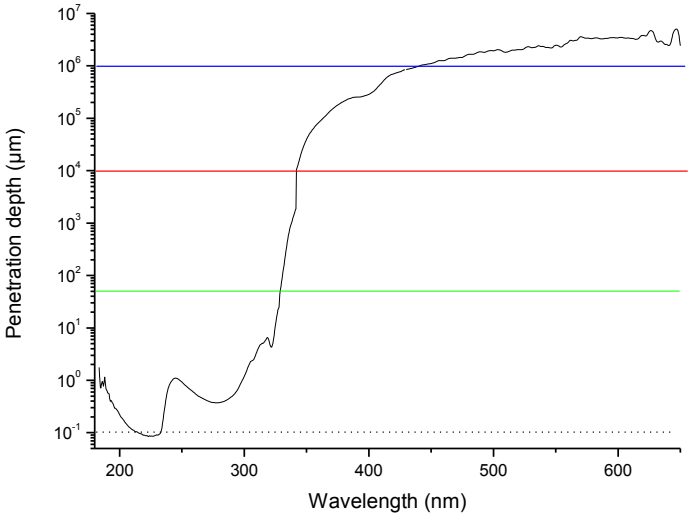

Figure 4.6. Penetration depth of light in neat DIN. Blue line: 1 meter mark; expected size of full scale detector. Red line: 1 cm; pathlength of standard optical cuvette. Green line: 50 µm IR cell. Black dotted line: region of upper limit of Dexter energy transfer. Graph is a combination of diluted DIN, 50 µm and 1 cm pathlength measurements.

3.4. Electronic absorption spectrum of EJ-309

EJ-309 shows absorption from 200 to about 400 nm (figure 4.7, right), with the region of greatest absorption due to DIN. The absorption bands with lower intensity, not present in DIN, are due to the addition of the fluorophore and a wavelength shifter. Comparison of EJ-309 to DIN shows that there are three additional absorption bands in the spectrum; a shoulder to the DIN band around 330 nm, a maximum at 358 nm and a less intense band at 378 nm.

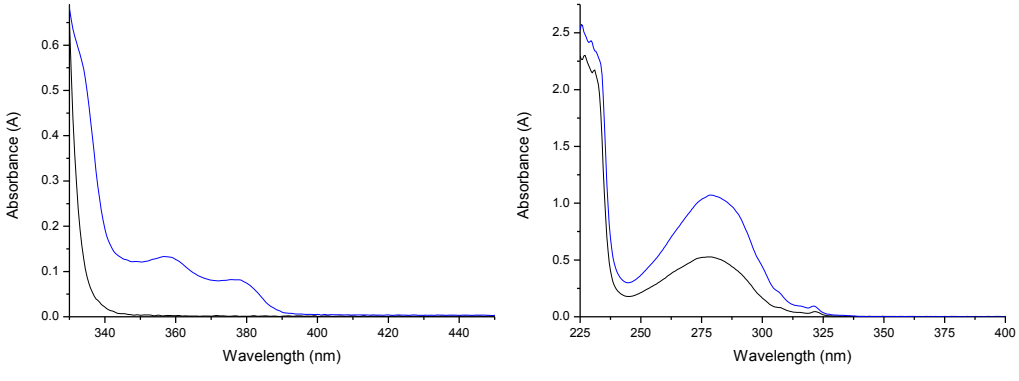

Figure 4.7. UV/vis absorption spectra of EJ-309 (blue) and DIN (black) in heptane. Left: 1,000 times dilution; 40 µM. Right 50.000 times dilution; ca. 1 µM.

As can be seen from the right side of figure 4.7 further dilution of EJ-309 with heptane (to 50.000 times dilution) shows the correspondence of the solvent bands in EJ-309 with those observed for in DIN.

3.5. Electronic absorption spectrum of ITS

EJ-309 was diluted a 1000 fold in heptane, to achieve an absorbance of 0.1 at 370 nm. ITS had to be diluted around 300 times to achieve that same absorbance at 370 nm (see figure 4.8), showing that the absorption by the fluorophore (and wavelength shifter) is only moderately higher in EJ-309 than in ITS.

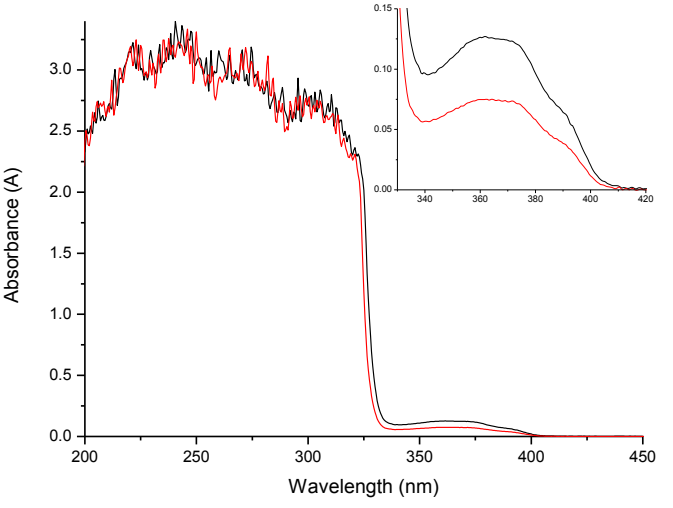

Figure 4.80 UV/vis Absorption spectrum of ITS in heptane
(Black: 332 times dilution; 18µM. Red: 1000 times dilution; 5.8 µM)

Table 4.2. Data for EJ-309 and ITS solutions in heptane.

Compound	Dilution (times)	Absorbance maximum (nm)	Absorbance	Fluorophore concentration (µM)	E (* 1000 M^{-1} cm^{-1})
EJ 309	1000	357	0.133	40 [a]	3.4
EJ 309	1000	376	0.082	40 [a]	2.1
ITS	1000	362	0.075	5.8	13

[a] Concentration of EJ-309 was set arbitrarily assuming a 1% (w/w) of fluorophore concentration with a mass of 230 Da.

The absorbance at 325 nm of EJ-309 is greater than that of ITS at the same dilution factor (table 4.2). The molecular structures of the fluorophores used in EJ-309 are not publicly available, nor are their concentrations. It is expected, based on the literature, that the

concentration of these fluorophores will be in the range of 1 - 4% (w/w) and will have a molar mass of 200 - 400 g mol^{-1}; it was assumed that the lowest concentration of fluorophore, which would allow proper energy transfer, is in the order of 40 mM (1% of fluorophore with a mass of 230 Da, e.g., terphenyl or diphenyloxazole). This concentration corresponds in a molar absorptivity of ca. of 3 * 10^3 M^{-1} cm^{-1}. It is interesting to note that the actual molar absorptivity of ITS is almost double that, which means that, at the same concentration, ITS absorbs more light than EJ-309. However, due to the lower solubility of the ITS fluorophore in DIN the achievable absorption for ITS is less than that of EJ-309.

3.6. Emission and excitation spectroscopy

Fluorescence excitation and emission spectra were obtained for neat undiluted DIN, EJ-309 and ITS in order to investigate the absorption and emission of energy in the scintillator cocktails. Spectra were obtained with a 60° front face arrangement to minimise the impact of inner filter effect, thereby using only a thin film at the surface of the wall of the cuvette for photophysical measurements and not the bulk of the sample.[7] As discussed in section 3.2 the penetration depth of UV light in DIN is less than a micrometer ensuring total absorption at the surface of the cuvette. Light emitted towards the detector therefore only has to travel this short distance before leaving the solution limiting self-absorption.

3.7. Emission and excitation spectrum of DIN

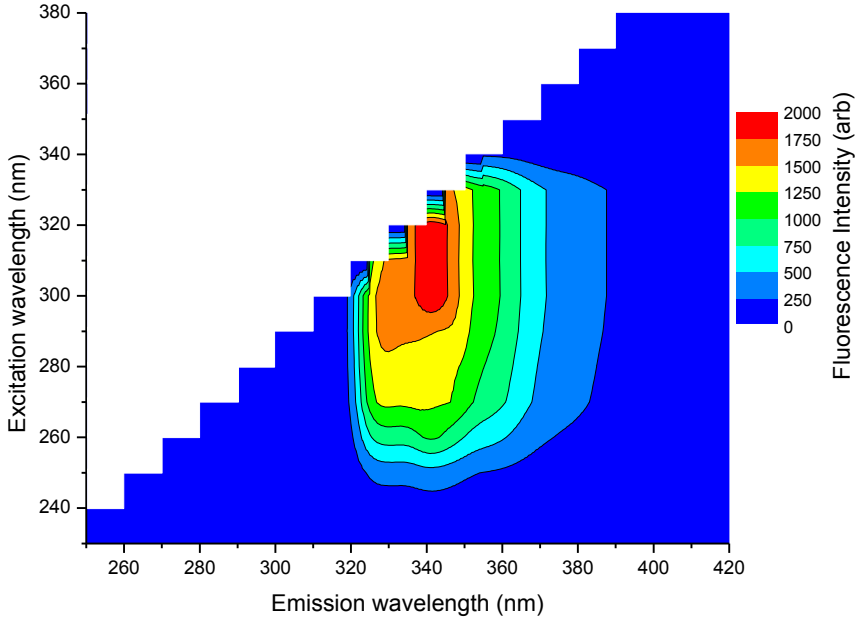

Figure 4.9. Contour plot of emission/excitation spectra of neat DIN (60° front face configuration). Recorded with 10 nm steps in excitation wavelength.

As is evident from figure 4.9 and figure 4.10, DIN emits light between 320 to 390 nm and absorbs between 250 to 340 nm. Since the emission and absorption spectra of DIN (λ_{em} < 320 nm and λ_{ex} > 320 nm) overlap, the emitted light can be re-absorbed by the solvent. This re-absorption will result in an elongation of the measured excited state as light will undergo the absorption/emission process multiple times before reaching the detector. Furthermore not all the light absorbed will be re-emitted due to non-radiative de-activation processes, lowering the total efficiency of the system. From the emission spectra it can be seen that the emission spectrum of DIN retains its shape when excitation is varied from 250 nm to 310 nm.*

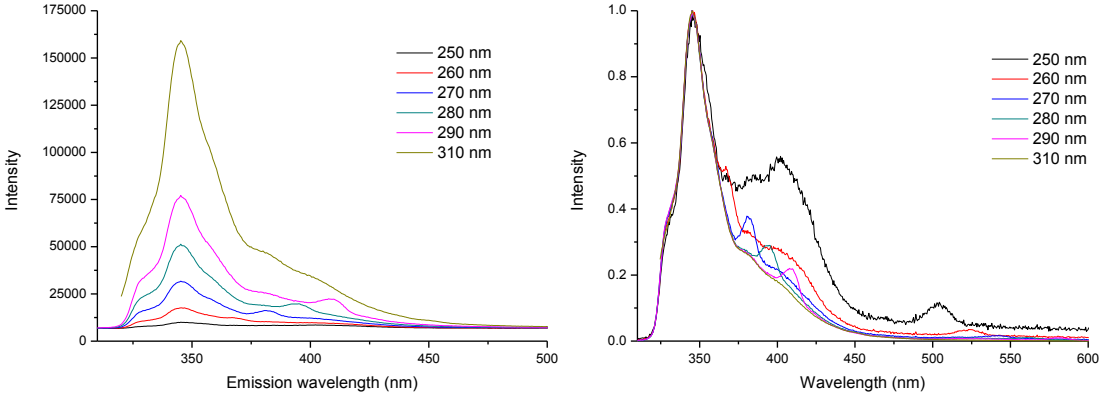

Figure 4.10. Left: Emission spectra of neat DIN using excitation between 250 and 310 nm (60° setup configuration). Right: normalised emission spectra (Raman scatter at 370, 380, 395 and 410 nm, and double of emission at 500 and 520 nm)

3.8. Emission and excitation spectrum of EJ-309

The emission / excitation contour plot of EJ-309 (figure 4.11) shows little emission in the wavelength range associated with direct emission of DIN (340 nm). Three distinct bands are apparent in the emission spectrum of EJ-309. The most intense emission band lies at 421 nm, with a second band at 399 nm and the third at 366 nm. It is thus clear that the excitation energy from DIN is transferred from DIN to the fluorescent compounds of EJ-309, which serve as acceptors, which then emit that energy as blue light. It should be noted that a large part of this emission still lies in the UV region of the spectrum and is not well matched to commonly used PMT photocathode coatings thereby reducing energy capture efficiency. Furthermore EJ-309 emission at wavelengths shorter than 400 nm is reabsorbed as the absorption band of EJ-309 extends to 400 nm. Thus as with DIN the EJ-309 cocktail can reabsorb the light it emits, lowering total efficiency and stretching the decay lifetime.

* Extra features arising from Raman signals and 2th order diffraction of the excitation light are also observed.

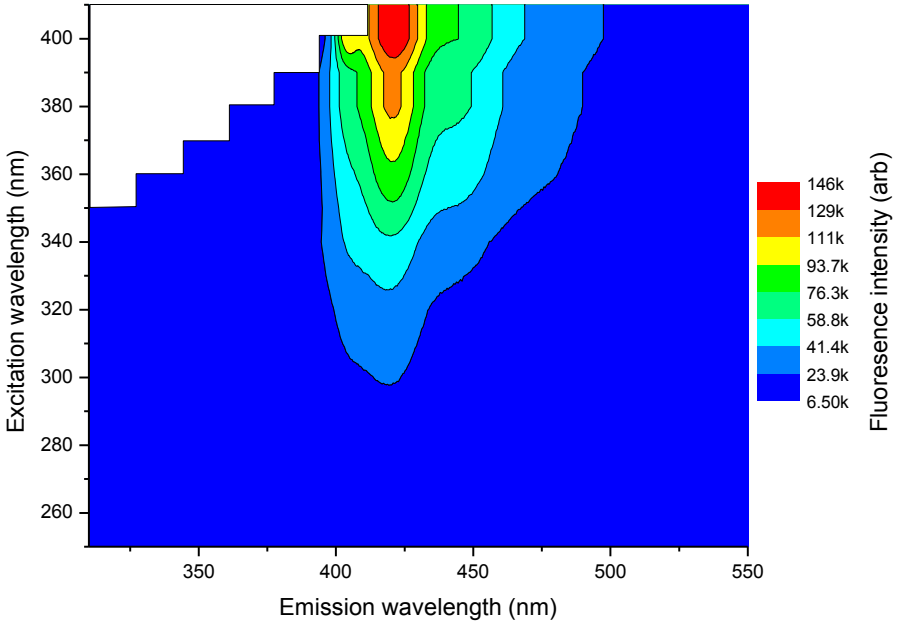

Figure 4.11. Contour plot of emission/excitation spectra of neat EJ-309 (60° front face configuration). Recorded with 10 nm excitation wavelength steps.

Figure 4.11 does not show a clear indication of emission in the DIN region (340 nm), but upon closer inspection of the emission spectra in figure 4.12, the shape of the emission bands does change slightly as the excitation wavelength is varied. At all excitation wavelengths, the emission maximum lies at 420 nm, however at excitation wavelengths < 350 nm there is some emission (<9% of total emission) around 350 nm. The source of this could be direct emission from DIN itself, indicating that energy transfer to the solutes is incomplete.

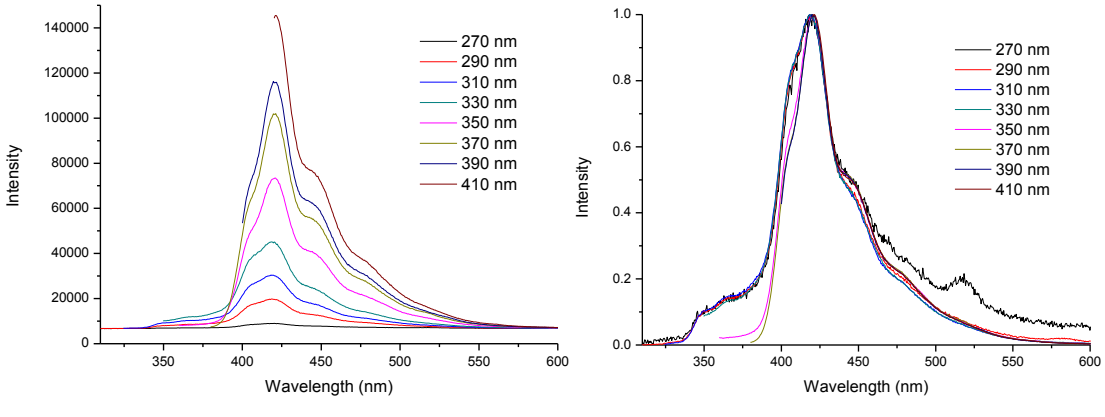

Figure 4.12. Left: Emission spectra of neat EJ-309 using excitation between 270 and 410 nm (60° front face configuration). Right: normalised emission spectra.

3.9. Emission and excitation spectrum of ITS

The excitation / emission contour plot of ITS (Figure 4.13) shows that there is an emission in the region of 340 nm, arising from emission from DIN, indicating that energy transfer from DIN to ITS is incomplete. The direct emission from DIN accounts for 12% of the total emission of the cocktail; slightly higher than seen in EJ-309. The emission of ITS is at a slightly longer wavelength than the maximum sensitivity of the PMT (444 nm vs 420 nm) [8] and shifted from the original boron triazole emission maximum of 424 nm, measured at lower concentrations (figure 4.14). This shift in emission maximum is due to the inner filter effect caused by the high concentration of fluorophore in the cocktail.

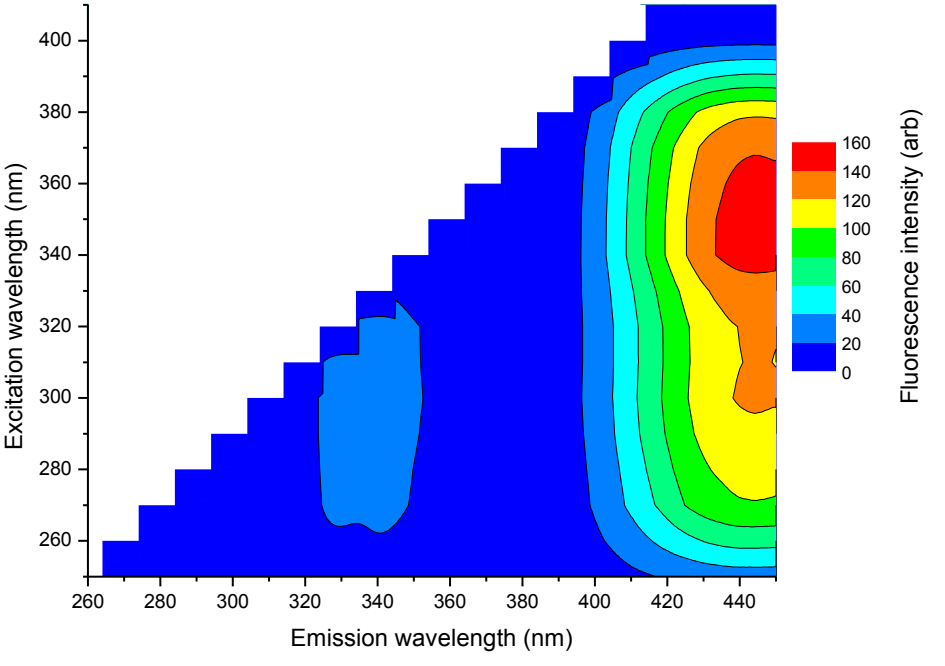

Figure 4.13. Contour plot of emission / excitation spectra of neat ITS. An emission peak from DIN is visible at 340 nm, indicating incomplete energy transfer of DIN to fluorophore (60° front face configuration). Recorded with 10 nm excitation wavelength steps.

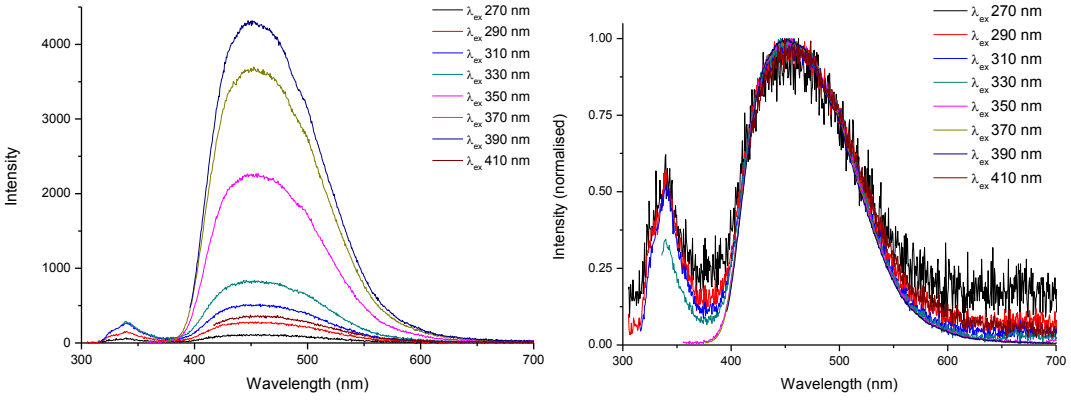

Figure 4.14. Left: Emission spectra of neat ITS using excitation between 270 and 410 nm (60° front face configuration). Right: normalised emission spectra.

3.10. EJ-309 and ITS comparison

A comparison of emission spectra shows that EJ-309 has more intense emission than ITS when excited at 270 nm (21% more, table 4.3). The emission intensity of ITS at an excitation of 370 nm is however more intense than EJ-309. The quantum yield at 370 nm excitation was determined for diluted cocktails of ITS and EJ-309 and is similar at resp. 0.63 and 0.64. At dilute concentrations there is no energy transfer from DIN to the fluorophores so comparison of dilute samples around 250-290 nm (excitation of DIN) is not possible as DIN does not transfer energy to the fluorophores but undergoes direct emission (section 3.11). Therefore standard quantum yield determination cannot be employed at these shorter wavelengths. Comparing neat samples of the fluorophores shows lower efficiency of ITS (80%) compared to EJ-309.

The emission maximum of ITS is red-shifted compared to that of EJ-309 (figure 4.15). Where the emission maximum of EJ-309 overlaps with the maximum efficiency of the PMT photocathode coating, the emission maximum of ITS is ca. 24 nm off. Examination of the emission spectra of dilute solution of the boron triazole in chapter 2 shows that the emission maximum was at 424 nm. The cause of this shift is the inner filter effect due to the high concentration of fluorophore. The broader emission band of ITS results in a lower efficiency regarding detection by the PMT as the decrease in PMT efficiency is 25% from optimum to 500 nm. As the emission band of EJ-309 is much sharper and at the most efficient point. Calculations indicate that due to this ITS has a 70% lower efficiency of than EJ-309.

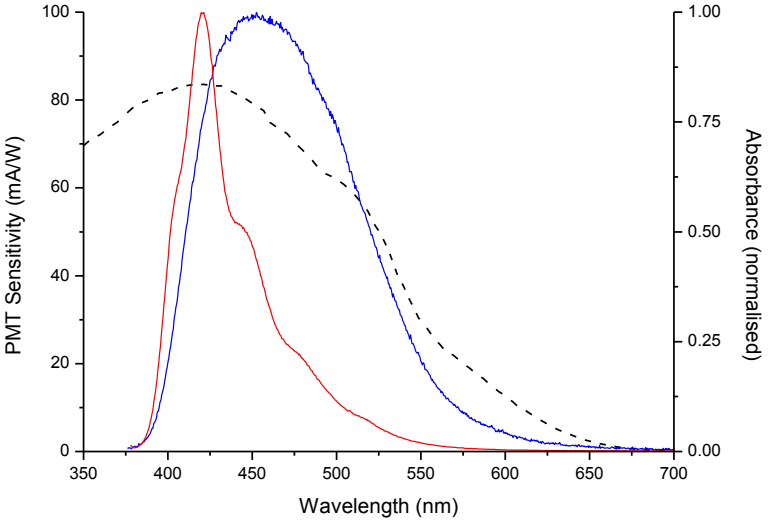

Figure 4.15. PMT sensitivity (black dotted line, Hamamatsu R7724) and (normalised) emission spectra from ITS (blue) and EJ-309 (red) (λ_{em} = 270 nm). PMT data redrawn from ref [8].

Table 4.3. Optical properties of EJ-309 and ITS

	$\lambda_{em\ max}$ (nm)	Fluorescence intensity [a] λ_{ex} 270 nm	Fluorescence intensity [a] λ_{ex} 370 nm	Φ 270 nm [b]	Φ 370 nm [c]
ITS	444	30732	659040	0.79	0.63
EJ-309	421	38792	813522	1	0.64

[a] neat sample. [b] neat samples, quantum yield relative to EJ-309.

[c] 1000 fold dilution in heptane, quantum yield relative to 9,10-diphenyl anthracene.

The efficiency of ITS might be improved by dissolving more fluorophore in the cocktail. However solubility is at maximum for this specific compound. Increasing the solvability of the boron triazole in DIN might be achievable, e.g. by introducing more aromatic character to allow for better dissolution in the aromatic solvent or decrease the possibility of aggregation by using bulky substituent as iso-amyl or tert-butyl groups (figure 4.16). However changing substituents on the triazole ligand or substituting the phenyl groups on the boron by naphthalene groups can alter the photophysical properties of the compound drastically.[12]

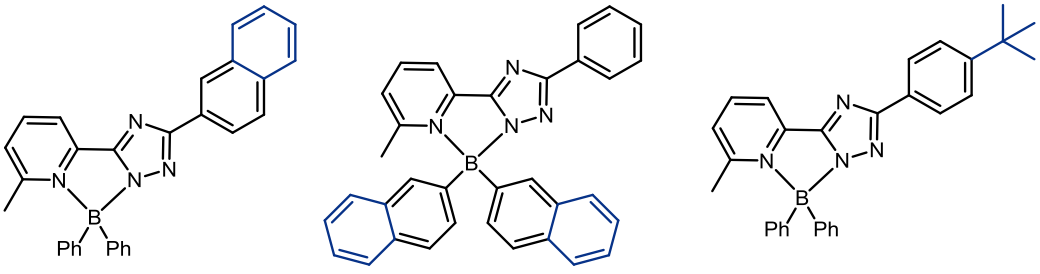

Figure 4.16. Possible options for more soluble boron triazoles. Left and middle complex introduce more aromaticity for dissolution improved interaction with the aromatic solvent. Right introduces more steric hinder preventing stacking and has favourable interaction with the isopropyl groups present in DIN.

3.11. Diluting EJ-309

The presence of 3 components (solvent, fluorophore and WLS) in the EJ-309 cocktail causes difficulties in unravelling of individual contributions and interplay in the emission spectra of neat EJ-309. Diluting EJ-309 in heptane (ca. 8 µM) can however enable distinction of the different components contributions. At this low concentration efficient energy transfer from DIN to fluorophore and from fluorophore to WLS is hindered because the intermolecular distance is so long that direct emission of light will be favoured over energy transfer (see chapter 1). At a concentration of ca. 8 µM the interatomic distance between two fluorophore molecules is around 600 nm, beyond the range of Föster energy transfer (an upper limit of ca. 100 nm).

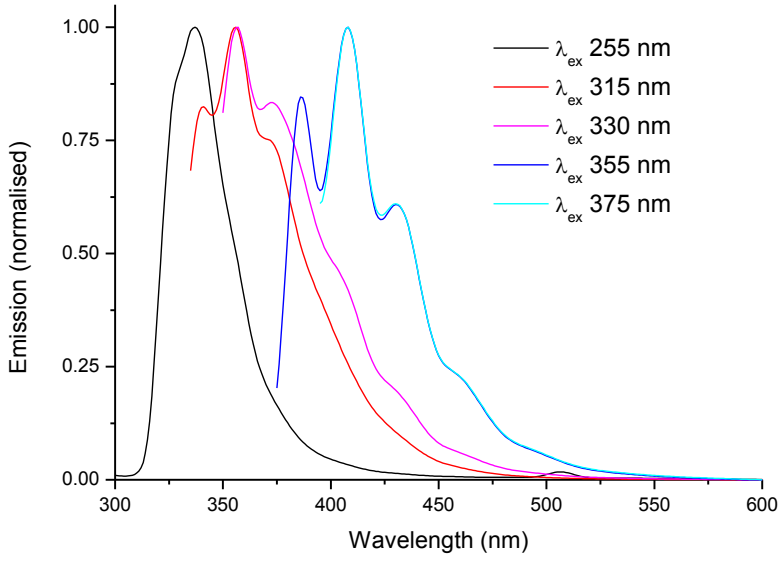

Figure 4.17. Normalised emission spectra EJ-309 diluted in heptane (ca. 8 µM) at various excitation wavelengths.

In order to clarify the contributions of the individual components (solvent, fluorophore and WLS) the diluted cocktail was irradiated at several wavelengths (figure 4.17) showing three distinct emission bands. When the sample is excited at 255 nm only a single emission band with a maximum at 340 nm is observed; the emission spectrum is similar to that of undiluted DIN (figure 4.10). Excitation at 315 and 335 nm the emission spectrum shows a different shape; three maxima at 340, 356 and 374 nm. The emission band at 340 nm arises from DIN, but the emission bands at 356 and 374 nm were not present in the 255 nm excitation spectrum indicating that these bands arise from solutes and not the solvent. The emission spectra upon excitation at 355 and 375 nm are different again; there are 3 maxima, at 386, 408 and 430 nm. These emission bands are not observed in either the emission spectrum of DIN nor upon excitation at 315 nm, and these bands are only weakly distinguishable as small shoulders upon excitation at 335 nm. It is therefore concluded that these emissions are due to emission from the WLS.

As can be seen from figure 4.18, the shape of the spectra of undiluted EJ-309 and the spectra obtained with diluted EJ-309 do not overlap. The cause for this inconsistency may be twofold; the spectrum of neat EJ-309 is a combination of the 315 and 355 spectra and / or there is self-absorption in the undiluted sample which decreases the peak intensity and cause an apparent peak shift. Linear combinations of the emission spectrum of λ_{ex} 315 nm excitation with that of at λ_{ex} 355 nm do not result in a good function of neat EJ-309. For that reason we assume the emission spectrum seen with EJ-309 is a, by self-absorption, modified version of the WLS spectrum. Self-absorption is possible since neat undiluted EJ-309 absorbs light up to 400 nm, thereby able to decrease the peak maximum, see figures 5 and 4. Self-absorption will absorb light of a certain wavelength and re-emit this at longer wavelengths causing a red shift in the emission spectrum.

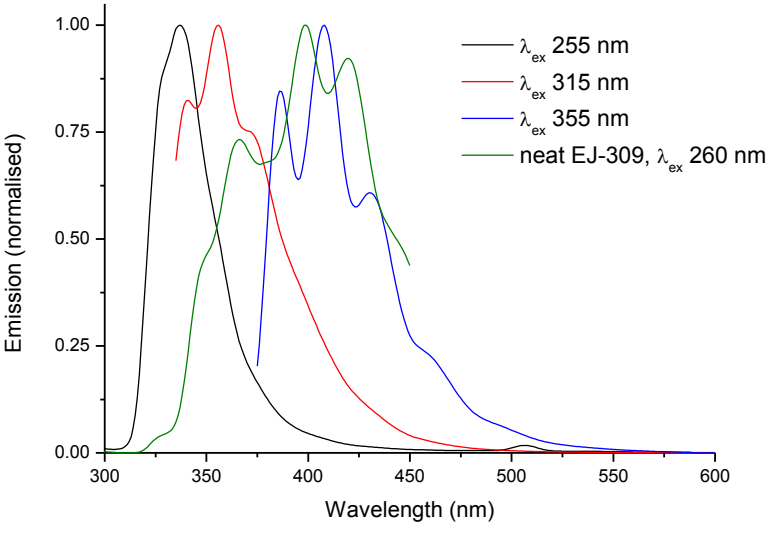

Figure 4.18. Normalised emission spectra of EJ-309 (diluted 5000 fold) in heptane at various excitation wavelengths and neat EJ-309 (λ_{ex} = 260 nm).

The excitation spectra (λ_{em} = 430 nm) of diluted EJ-309 (figure 4.19, black dash) shows the maximum of excitation at 310 nm, which, as seen in figure 4.9 and figure 4.11, is the excitation region of DIN and EJ-309. It is clear from the emission spectra that excitation at 315 nm does not cause energy transfer to the WLS (which would produce a spectrum as λ_{ex} 355 nm).

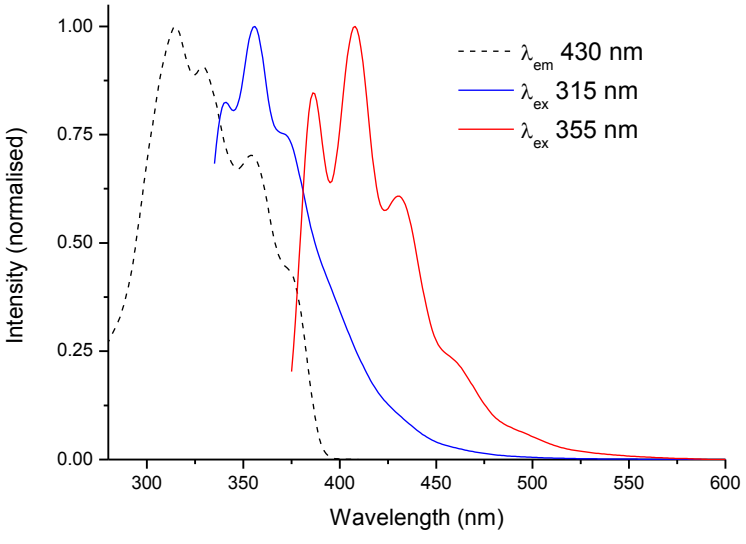

Figure 4.19. Emission and excitation spectra of EJ-309(diluted 5000 fold in heptane). Excitation spectrum recorded at λ_{em} 430 nm (black dash), emission spectra recorded at λ_{ex} 315 (blue line) and 355 nm (red line).

The absorption of a molecule does not have to correspond with the excitation spectrum, i.e. a non-fluorescent compound does have an absorbance spectrum but not an excitation spectrum. Comparing the excitation and emission spectrum of EJ-309 shows that there is a good overlap between excitation and the absorption spectrum as can be seen in figure 4.20.

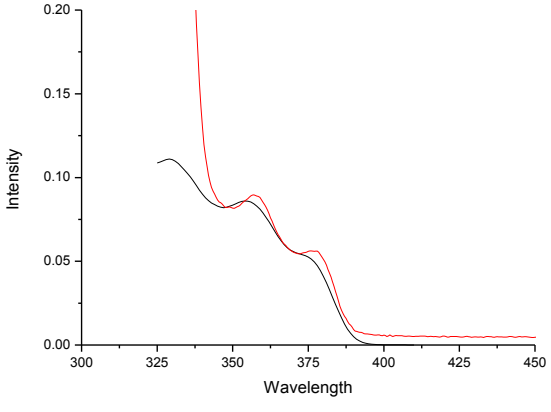

Figure 4.20. Excitation (red) and absorbance (black) spectra of EJ-309

3.12. Simulating the effects of radiation with light

Light with a wavelength of 255 nm possesses similar energy levels as the energies associated with the processes that deposit energy in a solvent by means of nuclear interactions.[16] This makes light of 255 nm a fast and safe substitute for experiments with radioactive sources. When irradiating the 3 solutions (DIN, EJ-309 and ITS) with 255 nm light their emission spectra differ to a large extent (figure 4.21). DIN only emits in the UV region; most intensely around 325-350 nm (vide supra). EJ-309 has a broad emission spectrum ranging from 350 nm to 490 nm, with a small indication of direct emission from DIN. The emission spectrum of ITS however clearly shows an emission band resulting from direct DIN emission. The bulk of ITS cocktail emission is, however, in the visible range, indicating that while the energy transfer from solvent to solute is not complet, it is still efficient.

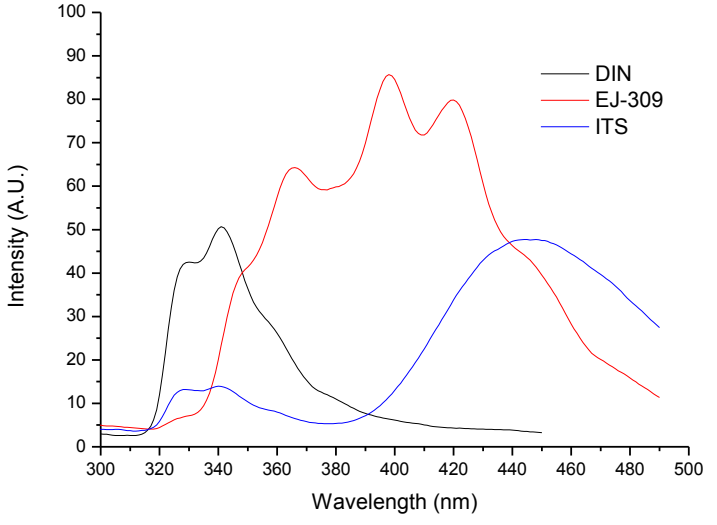

Figure 4.21. Emission spectra of DIN (black), EJ-309 (red) and ITS (blue). Wavelength of light used for excitation was 255 nm.

Table 4.4. Relative quantum yield of DIN, EJ-309 and ITS

	Intensity	Relative QY
DIN	2292	1.0
EJ	7791	3.4
ITS	4123	1.8

Due to the large overlap of the absorption and emission spectra of DIN there will be losses in the energy output by means of the inner filter effect. As stated in the introduction this is overcome by addition of the fluorophores which have relative low self-absorption due to its lower concentration. To quantify this effect the quantum yield of the EJ-309 and ITS

cocktails were calculated relative to that of DIN. It is apparent from table 4.4 that providing the pathway for energy transfer from solvent to fluorophore increases the overall light output efficiency. The emission intensity of EJ-309 is more than 3 times higher than that of DIN on its own. Or to phrase it differently; relying on direct emission from undoped DIN will cause 70% of the excitation to be lost for detection. When using ITS as scintillator cocktail the emission efficiency also increases compared to DIN, albeit with a factor of less than 2.

3.13. Fluorescence lifetimes

The emission decay lifetimes from the scintillator cocktails and the solvent (DIN) where determined by time correlated single photon counting (TC-SPC). In aerated solutions in a 60° front face arrangement to minimise inner filter effects.

Table 4.5. Fluorescent lifetimes of DIN and scintillator cocktails EJ-309 and ITS.

	λ_{ex}	short decay component	rise time	long decay component	Intensity rise/short	Intensity short/long
	(nm)	(ns)	(ns)	(ns)	(%)	(%)
DIN	255	7.2	-	22	-	33
EJ-309	255	2.6	1.1	-	82	-
ITS	255	11	5.0	-	91	-

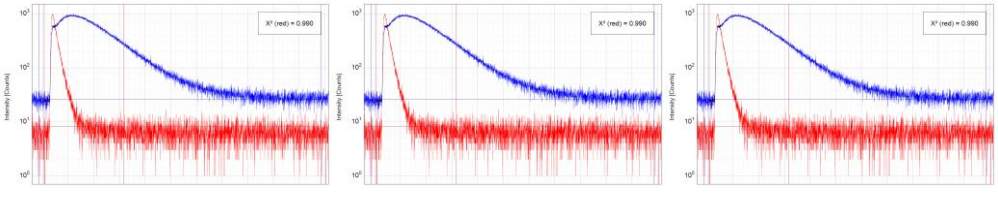

Figure 4.22. Fluorescent decay curves of EJ-309 (left), DIN (middle)and ITS (right).

As can be seen from table 4.5 the emission decay profile of DIN has a long component of 22 ns and a shorter, less intense component of 7.3 ns. The excited state of DIN has a reasonable long lifetime when compared to compounds used for fluorescence and scintillator experiments (less than 10 ns).[13] When doping DIN with a fluorophore the excited state of DIN is effectively quenched by the fluorophore and emission from DIN is not observed. The excitation energy is transferred to the fluorophore which can emit the energy as visible light. The transfer of energy takes a finite amount of time and hence a rise time component is observed (see chapter 5 for more details on energy transfer in scintillators). Although the fluorescence lifetime of the cocktail compromises of components from DIN (long) and the fluorophore (short) the total lifetime is shorter than of neat DIN and not a simple summation of the lifetimes of DIN and the fluorophore. There is, however, a large difference between the decay lifetime in EJ-309 and ITS, where the decay lifetime of the EJ-309 cocktail is only 10% of

that of DIN, ITS reduces the decay lifetime by 50%. Also the rise time in ITS is almost 5 times longer than with EJ-309. This is probably caused by the higher fluorophore concentration in EJ-309, which is around a factor 10 higher than the fluorophore concentration in the ITS cocktail. As the energy transfer rate is dependent on the distance between donor and acceptor a higher concentration enables faster energy transfer in EJ-309 due to shorter solvent solute distances.[7]

4. Conclusions

The desire to further investigate the performance of ITS, our scintillator cocktail, prompted a detailed study of the photophysical characteristics of ITS. The addition of the boron triazole to DIN shows a remarkable increase in light emission and a significant decrease in fluorescence decay lifetimes, greatly enhancing the scintillation abilities of the liquid.

Compared with EJ-309 the quantum yield of ITS is identical at λ_{ex} 370 nm. By slight adjustments to the triazole ligand it should be possible to tune the solvation of the complex and to decrease the amount of self-absorption so that all properties of ITS match or even surplus that of EJ-309.

5. Reference

[1] J. B. Birks, *The theory and practice of scintillation counting* (Macmillan, New York, **1964**).
[2] D. L. Horrocks, *Application of Liquid scintillation counting* (Academic Press, Inc, New York, **1974**).
[3] Eljen technologies *EJ-309 Liquid scintillator pulse-shaped discrimination properties*
[4] G. F. Knoll, *Radiation detection and measurement* (John Wiley & Sons USA **1989**).
[5] C. Buck, *Development of metal loaded liquid scintillators for future detectors to investigate neutrino properties* (Ruperto-Carola University of Heidelberg, **2004**), p. 123
[6] Borexino Collaboration, Nucl Instrum Meth A, *vol 585,* **2008**, pg 48.
[7] J. R. Lakowicz, *Principles of Fluorescence Spectroscopy* (Springer US **2006**).
[8] Hamamatsu, *R7724 specification sheet*
[9] A. C. Kaplan, M. Flaska, A. Enqvist, J. L. Dolan, and S. A. Pozzi, Nucl Instrum Meth A, *vol 729,* **2013**, pg 463.
[10] S. F. Naeem, S. D. Clarke, and S. A. Pozzi, Nucl Instrum Meth A, *vol 726,* **2013**, pg 120.
[11] L. Stevanato, D. Cester, G. Nebbia, and G. Viesti, Nucl Instrum Meth A, *vol 690,* **2012**, pg 96.
[12] P. Dijkstra, D. Angelone, E. Talnishnikh, H. J. Wortche, E. Otten, and W. R. Browne, Dalton Trans, *vol 43,* **2014**, pg 17740.
[13] M. Montalti, A. Credi, L. Prodi, and M. T. Gandolfi, *Handbook of photochemistry* (CRC press **2006**).
[14] S. H. Song, K. K. Joo, S. H. So, and I. S. Yeo, J Korean Phys Soc, *vol 63,* **2013**, pg 970.
[15] L. He, L. Zhang, X. Luo*, et al.*, J Lumin, *vol 148,* **2014**, pg 256.
[16] Pin Yang, C. D. Harmon, F. P. Doty, and J. A. Ohlhausen, IEEE T Nucl Sci, *vol 61,* **2014**, pg 1024.

Chapter 5

ENERGY TRANSFER IN LIQUID SCINTILLATORS

In this chapter energy transfer in an organic liquid scintillator is explored using a model system comprised of only a solvent and one fluorophore. In particular emission decay lifetime studies are employed to understand the influence of fluorophore concentration and temperature variations on energy transfer dynamics.

1. Introduction

Since the outset of the nuclear era, liquid organic scintillators (LOS) have played an important role in the detection of radiation.[1, 2] Although scintillator cocktails have been used for many years, the details of the mechanisms by which energy transfer occurs and the rates of internal energy transfer are still not well understood and subject to debate (with focus of the discussion mainly on if energy transfer is via Dexter or Förster pathways).[3-11]

1.1. Current research focus

Current research into liquid organic scintillators is limited to increase the quality of (existing) scintillator cocktails and interest into the mechanism of energy transfer in scintillators has waned since the end of the 1960s. At the beginning of the nuclear age interest in how scintillators functioned was at a peak and studied with then state-of-the-art technology. Attention to liquid scintillators and the fundamentals of energy transfer diminished in the mid-1970s, but interest in liquid scintillators was revived at the end of the 1980s with detectors situated at nuclear power reactors and beamlines; e.g., the LSND scintillator and Bugey detector (respectively filled with commercial BC-517P and NE-320).[12-14] However the focus of these studies was on detector technology and understanding of fundamental physics, rather than on energy transfer in scintillators.

Current research projects employing and investigating liquid organic scintillators, e.g. SNO+, Borexino, Daya Bay, Juno and Reno, focus their attention on attenuation of light and accompanied purification of scintillators.[15-20] Less focus is on gaining fundamental knowledge of scintillator photochemistry and energy transfer; for example, one of the most used wavelength shifters (bis-MSB) was only recently characterised under scintillator conditions, prior to these studies emission quantum yield and extent of re-absorption were unknown, demonstrating the limited fundamental knowledge available in the field.[21] Indeed improvements in scintillator efficiency and the study of energy transfer has been done mainly with nuclear radiation sources, whereby the individual steps in the energy transfer process are not investigated; only the final emission is recorded, providing insight into the characteristics of the specific scintillator under investigation.[22-27]

1.2. Challenges and simplification of a model scintillator

A principle reason for the limited knowledge regarding energy transfer in liquid scintillators, besides a lack of active research, is the difficulty in studying the energy transfer processes in a system as complex as a liquid organic scintillator cocktails. These scintillator cocktails are comprised of several components (solvent, fluorophore and wavelength shifter and sometimes neutron capture agents) whose absorption and emission spectra show strong overlap with each other. This overlap makes it difficult to separate the individual contributions of these components in the energy transfer process (figure 5.1). A detailed study of their behaviour individually in the cocktail is all the more challenging as absorption, quenching, trivial energy transfer, Dexter energy transfer, Förster energy transfer and emission all play a

part. Furthermore the concentrations of the solutes is remarkably high compared to those used in conventional photophysical experiments (1-5% w/w vs µM concentrations) therefore knowledge gained under conventional photophysical situations is not directly relevant to scintillator technology.

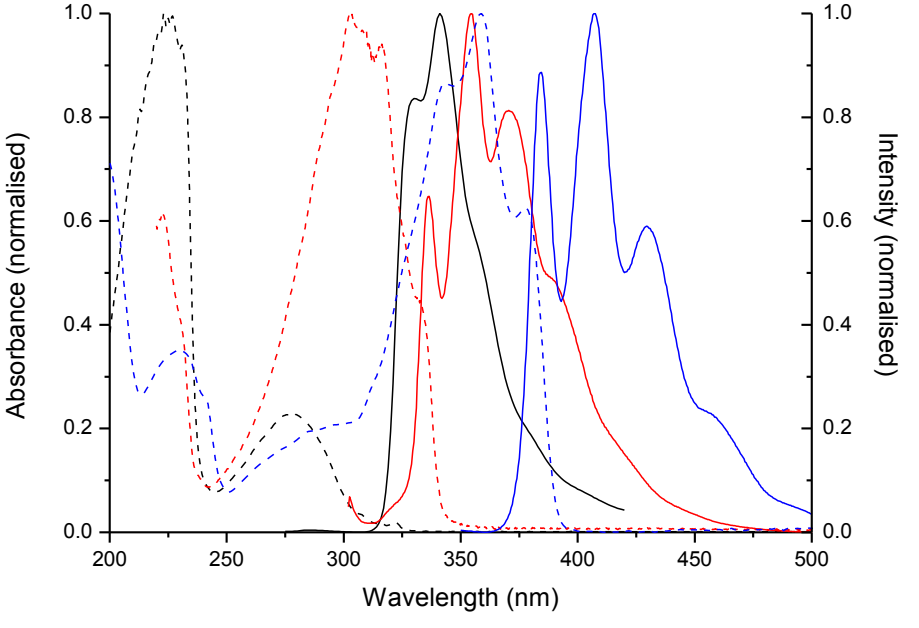

Figure 5.1. Emission (line) and absorption spectra (dash) of the components of a typical scintillator cocktail, consisting of DIN (black), PPO (red) and POPOP (blue). Data for PPO and POPOP from Du *et al*.[28]

Simplification of the scintillator cocktail's composition was expected to facilitate the study of energy transfer and in the present chapter this is achieved by using solvent and only one fluorophore in the model cocktail, i.e. a wavelength shifter (WLS) is not employed. It must be stressed that the concentrations of the fluorophore will be far from standard photophysically relevant conditions, with free pathlengths in the µm range or shorter (see chapter 4). The single solute model cocktail is used to develop a detailed understanding of the processes involved with regard to energy transfer in the detector, and consists of the solvent (LAB or DIN, which are both widely used in LOS) and a fluorophore, bodipy (figure 5.2).[29, 30] The advantage of using only bodipy as fluorophore instead of the more commonly used fluorophores and WLS combinations is that the solvent has less of a spectral overlap with the longest wavelength absorption bands of bodipy. The large separation of solvent emission (ca. 350 nm) and bodipy emission (ca. 500 nm) enables monitoring of emission from the individual components. Furthermore the quantum yield of bodipy is near unity and its molar absorptivity is > 50.000 M^{-1} cm^{-1} making it an excellent compound for photophysical studies.

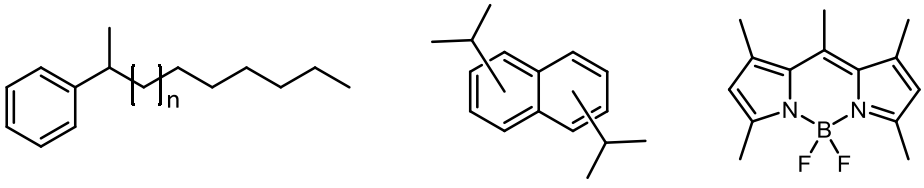

Figure 5.2. Compounds used in the model scintillator cocktail. Left: Linear alkyl benzene (LAB). Middle: Di-isopropylnaphthalene. Right: 1,3,5,7,8-pentamethyl-difluorobodipy. (The solvents used contain a mixture of isomers).

1.3. Excitation and energy transfer in liquid scintillators

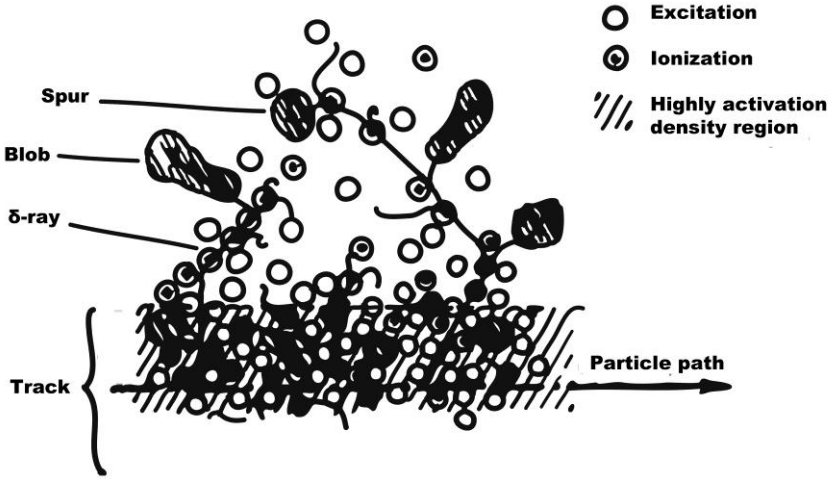

Figure 5.3. Schematic representation of the excitation induced by a charged particle in a liquid organic scintillator (redrawn from ref [31])

When a nuclear particle or gamma-ray interacts with a liquid organic scintillator a myriad of reactions and particles come into play; ionisation, secondary electrons and other species (figure 5.3).[31] The overall effect is that energy is absorbed by the scintillator cocktail and molecules are excited to higher electronic energy states. As the concentration of solute is relatively low compared to the total fluid volume it can be assumed that all deposited energy is absorbed by the solvent molecules of the scintillator cocktail. Excited solvent molecules can relax to the ground state either; radiatively, non-radiatively through thermal relaxation, or by energy transfer (figure 5.4 and section 1.4).

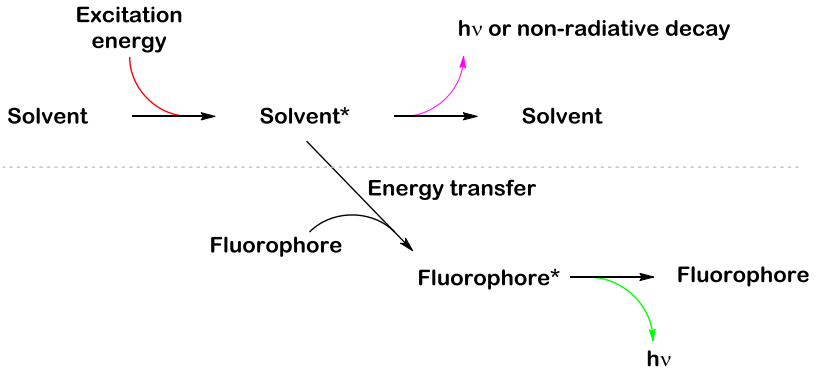

Figure 5.4. Possible pathways for excitation and relaxation of a solvent molecule and possible subsequent emission by the fluorophore. A solvent molecule gains energy from a source of excitation energy and can emit a photon, decay by non-radiative means, e.g. heat or energy transfer to a fluorophore. The fluorophore in the excited state can than emit a photon.

When an excited solvent molecule undergoes non-radiative decay the excitation energy is lost. Dissipation via vibrational relaxation to the matrix, i.e., heat, means that this energy is not registered by photomultiplier detectors (PMTs).[32] With radiative decay the solvent molecule emits a photon, this emission will, due to the nature of the solvents used, be in the UV-A range. Therefore it will not be registered by standard PMTs, due to their low photon absorption efficiency at these wavelengths. For detection purposes this energy must therefore also be considered as lost. Energy transfer from the solvent to a solute molecule is achieved through several pathways, including trivial energy transfer, Förster dipolar coupling, and Dexter electron exchange (see chapter 1).

After transfer of the energy from the donor molecule to the acceptor molecule the latter is in an excited state. In the case of bodipy the excited molecule will emit its energy as visible light (> 500 nm). Bodipy can undergo non-radiative decay but with a quantum yield of (near) unity this pathway can be disregarded.[29]

Under standard conditions for emission spectroscopy the interaction between excitation energy and solvent is undesirable and the wavelength of excitation is longer than that of the short pass cut-off wavelength of the solvent.[33] However, since in liquid scintillator technology excitation of the solvent is an intrinsic part of the detection method, detailed investigation of solvent emission has to be carried out; leading to conditions and processes that are alien to standard photophysical studies. Thus, to obtain a good understanding of the energy transfer processes in the liquid scintillator energy transfer chain, the solvent must be excited directly, as occurs when a liquid scintillator detector is deployed in the field.

1.4. Means of excitation; nuclear radiation or light

There are two approaches to excite solvent molecules when studying LOS behaviour; with nuclear radiation or irradiation with light, simulating nuclear radiation. As nuclear radiation sources are cumbersome to handle due to health and safety requirements excitation by light becomes the preferred choice. Furthermore, as can be seen from figure 5.3, a multitude of processes occur during interaction of radiation with matter. These processes result in elongation of the duration of the excitation pulse as different processes have different durations. Due to this effect a radiation event is not an instantaneous event but rather occurs over an extended time range, in contrast to excitation by light, for which the pulse duration can be controlled precisely, e.g. picoseconds (figure 5.5). This leads to shorter rise times and shorter overall pulse duration. Consistent timing is essential in energy transfer experiments as emission of a photon from an excited molecule is a statistical process and can happen between 0 and ∞ after excitation. Fluorescence lifetimes (τ defined as I_0/e) can only be correctly determined if the start of excitation is determined at significantly shorter time scales than the subsequent processes.*

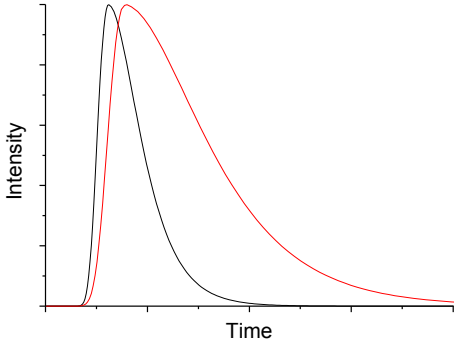

Figure 5.5. Expected shape of fluorescence decay curve with excitation by means of light pulse (black line) or an elongated fluorescence decay curve with excitation by means of nuclear radiation (red line).

Once the molecule has reached the excited state it will undergo fast relaxation processes (internal conversions and vibrational relaxation in under a picosecond) to the S_1 excited state, from which it can engage in energy transfer (figure 5.6).[34] Excitation by means of radiation or light will thus result in the same S_1 energy level and thereby justifies the choice for safer and easier to handle optical excitation in the present study.

* There is a difference between the decay times defined in photophysics (τ_{fluor}) and those in nuclear science ($\tau_{radiation}$), τ_{fluor} is defined to be the time when the emission intensity has decreased to $1/e$ of the maximum while $\tau_{radiation}$ is defined as time when the intensity is equal to 1/10 of the maximum. $\tau_{radiation}$ is about a factor 2.3 longer and confusion between the two should be avoided, in this chapter when τ is written τ_{fluor} is intended.

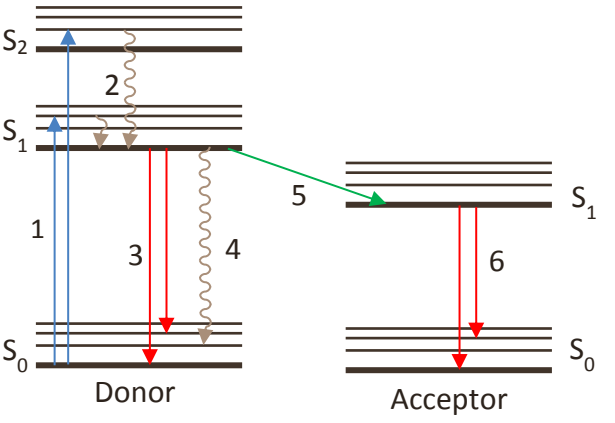

Figure 5.6. Jablonski diagram showing; Step 1: A molecule is excited to an exited state (S_1 or higher) from the ground state (S_0). Step 2: Vibrational relaxation and internal conversion brings the molecule to the lowest thermally equilibrated excited state (Kasha's rule) after which it emits as fluorescence (step 3), is quenched by other means (step 4) or the excitation energy is transferred from the donor to the acceptor (5), which then emits a photon (6)

1.5. Photophysical model

As discussed in this thesis, at high fluorophore concentrations energy transfer can occur from solvent to fluorophore. The most common mode of energy transfer in normal photophysical systems is trivial energy transfer; whereby light is emitted by the solvent molecule and re-absorbed by the fluorophore. At higher concentrations dipolar interactions or electron transfer can occur. In liquid scintillators trivial energy transfer is of low importance for energy transfer from solvent to fluorophore as emission efficiency of the solvent is relatively low (quantum yield < 0.05).[35] Furthermore the concentration of fluorophore in liquid scintillators is high enough to enable other means of (faster) energy transfer.*

The focus of this chapter is on the emission characteristics of the concerted process and individual steps thereof; this includes spectral shape and intensity, and fluorescence decay times of the emitted light. The reason to investigate fluorescence decay lifetimes is that they are important factors for pulse shape discrimination (PSD), a technique used in radiation detection to distinguish between different radiation types e.g. neutrons, gamma rays and protons. PSD works by examining the difference in ratios in the prompt part of the pulse and the delay part of the pulse (figure 5.7, left side). Particles with high dE/dx (neutrons) have a longer decay time than those with lower dE/dx ratios (gamma-ray) and thus the ratios between prompt and delayed part will be different. At high energies identification of different sources is obtainable (figure 5.7, right side), but with low energy signals a clear separation between the different sources is more difficult to obtain.

* At the concentrations employed in this study (10 µM and 5 mM) the intermolecular distance between fluorophore molecules is in the range of 60 and 7 nm respectively.

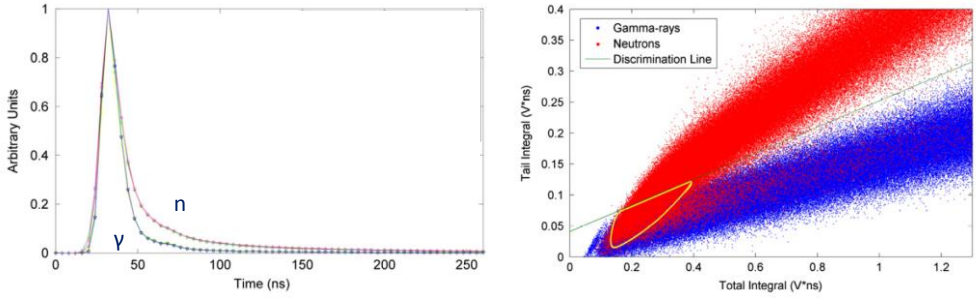

Figure 5.7. Left: Neutron and gamma-ray pulses from ^{252}Cf (normalized). Right: Tail vs. total integral of measured pulses from ^{252}Cf source. Neutron pulses (in red) and gamma-ray pulses (in blue) separated at high energies but overlapping at low energies (yellow region). Reproduced with permission, copyright Elsevier (2011) [36]

Fluorescence lifetimes are influenced by temperature changes and thus changes in temperature will cause changes in the characteristics essential for correct PSD. As temperatures can vary widely depending on where and when the detector is deployed this should be taken into account (as working conditions might be sub-zero in artic to +50 °C in tropical/desert regions).

1.6. Goal

In this chapter, the factors that influence the modes and decay rates of energy transfer in liquid organic scintillators (LOS) are investigated. A better insight into the processes concerning the scintillator cocktail might allow for improvement of scintillator composition or for improvement of the algorithms used in PSD. The study was performed at two different concentrations; at photophysical levels, where absorbance is relatively low albeit that it is not representative of real scintillator conditions, and at scintillator composition levels, where the concentration of fluorophore is near maximum solubility but scintillator efficiency is also at a maximum, these characteristics are compared with those of EJ-309, a commercial LOS.[37] To the best of our knowledge no such investigation has been reported in literature recently, and never by means of disentangling the characteristics of all the individual components.

2. Results and discussion

Before developing a model for the energy transfer processes that take place in a scintillator cocktail, the photophysical properties of the individual components must be ascertained. Hence, several experiments were performed to obtain this information (figure 5.8).

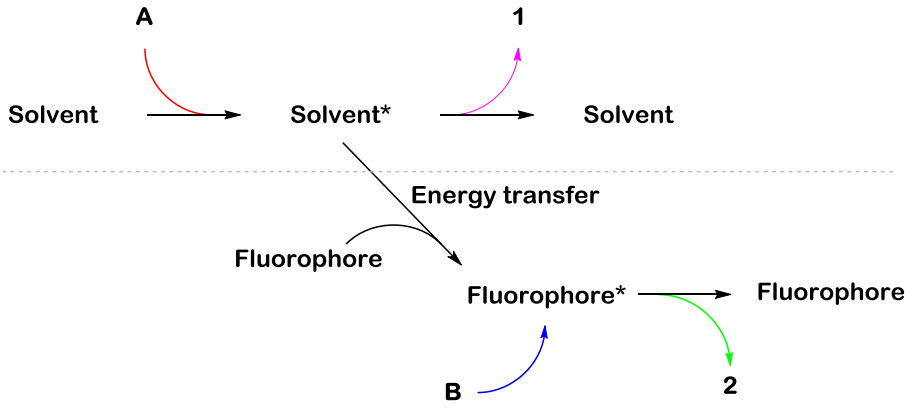

Figure 5.8. Excitation and emission possibilities in the energy transfer scheme. **A** is excitation by 255 nm light, **B** is excitation at 355 nm or 450 nm. **1** is emission around 340 nm, **2** is emission > 500 nm.

- The photophysical properties of the non-doped fluorescent solvent (LAB) were determined to establish the "pure" response of the solvent (excitation **A**, emission **1**)
- The photophysical properties of bodipy in a non-fluorescent solvent (ethanol) were determined so to establish the "pure" response of bodipy (excitation **B** emission **2** in ethanol).
- The photophysical properties of bodipy in the fluorescent solvent were determined; bodipy is excited directly to avoid influence from energy transfer and determine the influence of the solvent properties (e.g., viscosity) on its photophysical properties (excitation **B** emission **2** in LAB).
- The photophysical properties of the doped solvent were determined by measuring the UV light emitted from the solution, to establish the quenched response of the solvent (excitation **A** emission **1** in LAB).
- The photophysical properties of bodipy when excitation is resonant with the solvent to establish the total energy transfer cascade system (excitation **A** emission **2** in LAB).
- The photophysical properties of bodipy under non-standard photophysical conditions, i.e. at the high concentrations used to perform radiation testing and comparison with EJ-309 (excitation **A** emission **2** in DIN).

2.1. Characteristics of pure LAB

2.1.1. Absorption and emission spectra of LAB

The emission of neat LAB is ca. 325 – 375 nm is at a maximum at 340 nm, the range of excitation is from 225 to 300 nm with maxima at 247 and 288 nm (figure 5.9). Excitation of LAB at 255 nm* will therefore excite the solvent molecule, which subsequently can transfer its excitation energy to bodipy. Comparing the excitation and absorbance spectra shows that most absorbed energy does not cause the molecule to attain the excited state (as indicated by the low quantum yield of 0.03).

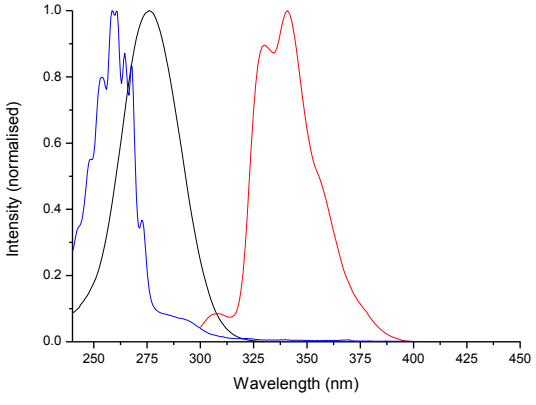

Figure 5.9. Absorbance (blue), excitation (black) and emission spectra (red) of LAB. Even by employing an epi-fluorescence arrangement the inner filter effect could not be avoided and causes an apparent dip in the maximum of the emission peak.

2.1.2. Fluorescence lifetimes of LAB

An increase in temperature results in a shortening of the fluorescence lifetime of pure LAB (figure 5.10), which is caused by a decrease in viscosity which enables faster quenching of the excited state. The decrease in fluorescence lifetime with increasing temperature follows the Arrhenius equation (inverse temperature versus rate constant), indicating that LAB responds to quenching factors, i.e. temperature and viscosity, as expected from the literature.[33] The extent of lifetime decrease is significant; going from -10 °C to 80 °C the decay lifetime (Δt is 24 ns) decreases by half.

The effect of increased quenching at higher temperatures is also apparent in a plot of temperature versus emission count rate (figure 5.11). As the pulse rate of the irradiating LED is held constant the observed emission count rate should also remain constant, if there is no influence of temperature. However, the emission count rate decreases with an increase in temperature, indicating that with an increase in temperature the quenching rate increase.

* 255 nm is a wavelength which resembles the energies associated with excitation by radiation.[38]

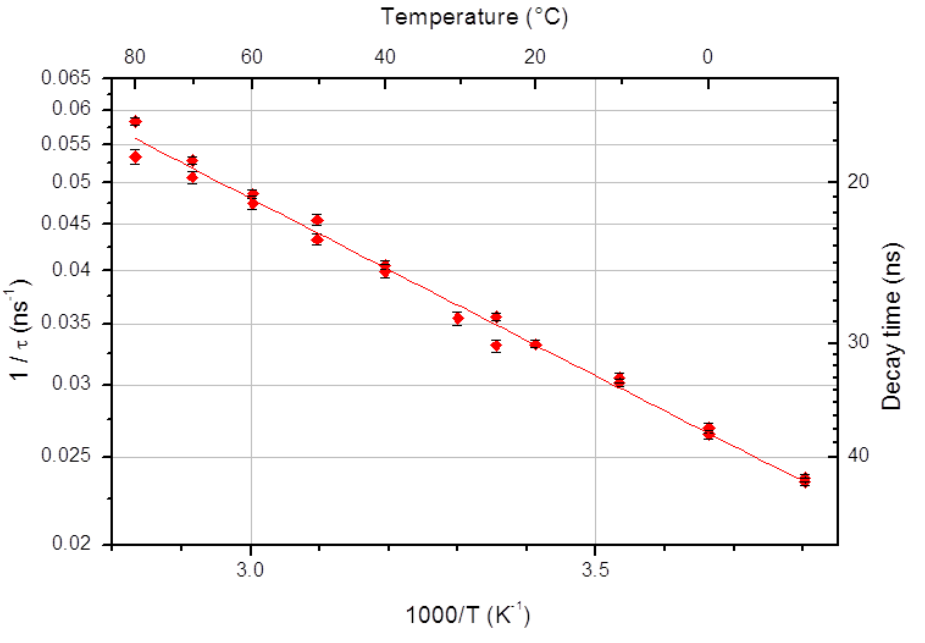

Figure 5.10. Arrhenius plot showing the relation between the fluorescence lifetime of undoped LAB and temperature (note $\log_{10}$ scale of y-axis).

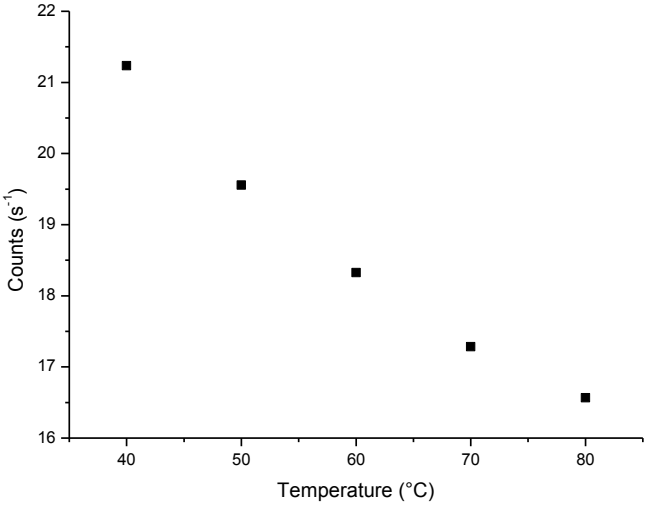

Figure 5.11. Fluorescence at various temperatures after subtraction of background count rate.

2.2. Characteristics of bodipy

Bodipy dissolved in a non-luminescent solvent, e.g. ethanol, can only be excited by direct absorption of excitation energy and not by energy transfer from the solvent. The excitation spectrum of bodipy in ethanol (figure 5.12) shows a maximum at 501 nm, and a second excitation band, assigned to the $S_0 \rightarrow S_2$ transition, is at 360 nm.[39] The emission spectrum shows a single emission band with a Stokes shift of only 6 nm. Absorbance and excitation spectra can be considered to overlap, as a mismatch of just 4 nm is within experimental error.

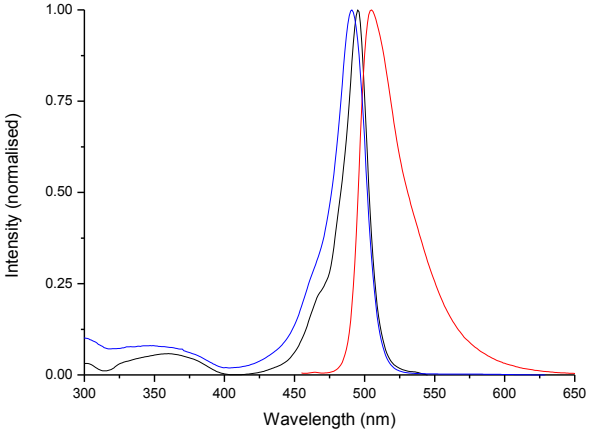

Figure 5.12. Absorbance (blue), excitation (black) and emission (red) spectra of bodipy in ethanol.

The 6 ns fluorescence lifetime of bodipy in ethanol differs slightly under the various circumstances employed in the studies described in this chapter.[30] * Regarding solvents there are two major factors that can influence the fluorescence lifetime; viscosity and polarity. Lower viscosity will enable higher collision rates (interaction between molecules) and internal rotations, both are important for (non-radiative) deactivation of excited states and an increase in these rates shortens the lifetime of the fluorophore in its excited state, also resulting in a decrease in the total emission intensity (figure 5.13).[33] Differences in solvent polarity will also change the environment around the excited molecule altering the lifetime of the excited state.[33] A favourable environment will stabilise the excited state, resulting in an increase of fluorescence lifetime. Another factor possibly influencing the fluorescence lifetime is the presence of oxygen, which can quench the excited state and thereby reduce emission intensity and shorten emission lifetime.[33]

* The fluorescence lifetime of bodipy is dependent on temperatures also, but since it is a more rigid molecule than LAB the effect is less pronounced, and of no significant influence.[40]

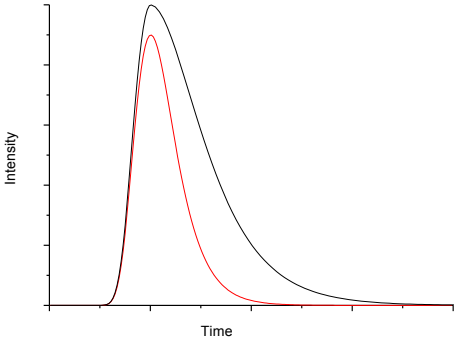

Figure 5.13. Expected shape of fluorescence decay with standard conditions (black) and quenching conditions (red). Quenching of the excited stated reduces both fluorescence lifetime and emission intensity as the long lifetime states are quenched and result in no observable emission.

2.2.1. Fluorescence lifetime of bodipy

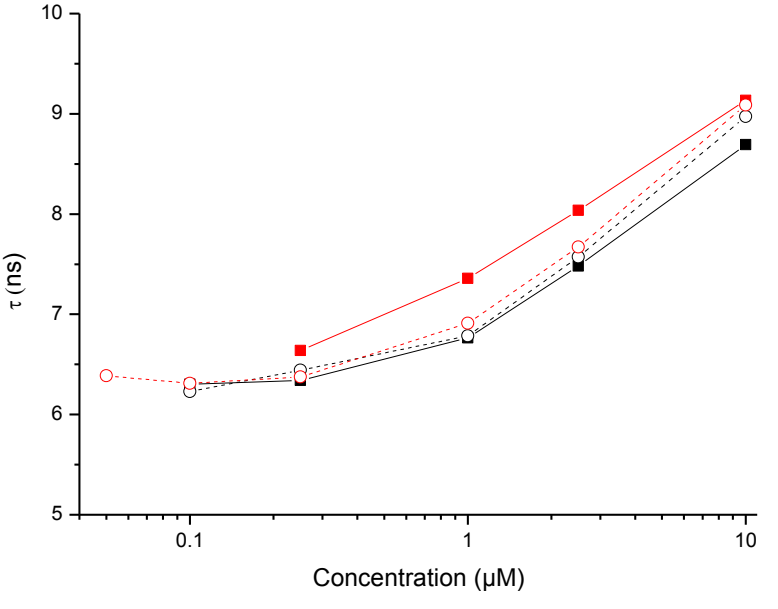

Figure 5.14. Fluorescence lifetime of bodipy in ethanol at various concentrations air equilibrated solvent (black) or under an argon atmosphere (red). λ_{ex} 350 nm (solid square) or λ_{ex} 450 nm (open circle).

Increasing the concentration of bodipy in solution influences the measured fluorescence decay lifetime. As the bodipy concentration is increased the observed fluorescence lifetime is increased (figure 5.14). The fluorescence lifetime of the bodipy molecule itself is not intrinsically influenced by the change in concentration but there is a subsequent effect; at

higher concentrations re-absorption of the light (trivial energy transfer) causes the apparent increase of the fluorescence lifetime. This re-absorption creates a delay between the photon emission from the first molecule and detection. The impact of increasing bodipy concentration from 0.05 µM to 10 µM (a 200 fold increase) is a ca. 40% longer decay lifetime.

The presence of oxygen in the solution does not lead to significant quenching and thus a change in emission lifetime and is not further investigated in this work. Also the influence on the fluorescence lifetime by changing the of excitation light (λ_{ex} = 350 nm or 450 nm) is minimal.* Thus demonstrating that excitation is not dependent on the wavelength of excitation and therefor validates our method, which by means of different excitation wavelengths allows for different energy transfer pathways to be probed.

2.2.2. Influence of concentration on spectral shape

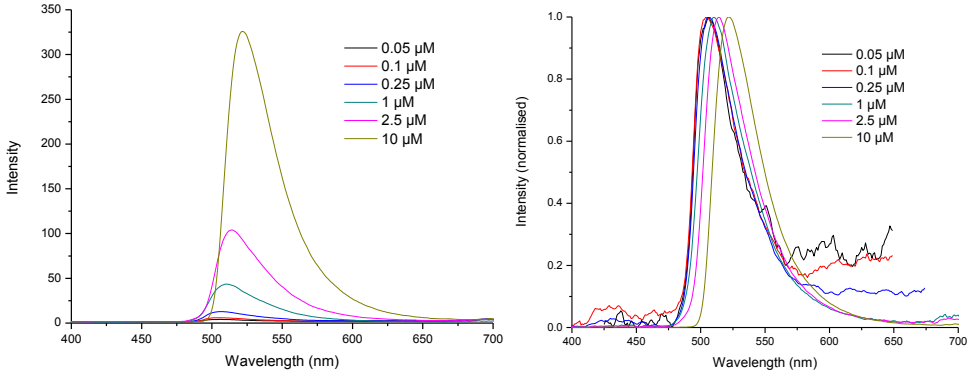

Figure 5.15. Left: Emission spectrum of bodipy in ethanol with increasing bodipy concentration. Right: Normalised emission spectra of bodipy in ethanol with increasing bodipy concentration.

With an increase of bodipy concentration the emission intensity will also increase (figure 5.15, left side). However with higher concentrations of bodipy comes an increase in inner filter effect. An increase in bodipy concentration will, in addition to influencing the fluorescence lifetimes (section 2.2.1), influence the shape of the emission spectrum of bodipy, figure 5.15 (right), as a red-shift of the emission maximum. The absorbance of the solution is so high that the emitted light cannot penetrate through the solution and light is re-absorbed and emitted at a longer wavelength. Whereas the 0.05 and 0.10 µM solutions have an emission maximum at 506 nm the maximum is shifted by 17 nm to 523 nm in the 10 µM solution.

These high concentrations of fluorophores clearly produce an unwanted effect regarding photophysical properties and are therefore avoided in typical photophysical experiments, where, as rule of thumb, a maximum absorbance of 0.1 is used. It should therefore be

* It should be noted that the intensity of fluorescence emission is dependent on the wavelength of excitation, as the absorbance at 450 nm is much larger than at 350 nm.

emphasised that in the concentration dependant measurements which are performed here the absorption is much higher than that and there is a substantial inner filter effects in the cocktails used.

2.3. Characteristics of bodipy in LAB

Bodipy dissolved in LAB offers several pathways to excite the molecules with light and several pathways to measure the emission from the excited molecules (figure 5.16). The solvent can be excited directly at 255 nm, which is representative for excitation by nuclear radiation.[38] Bodipy can be excited in the $S_0 \rightarrow S_2$ band at 350 nm or in the $S_0 \rightarrow S_1$ band at 450 nm. Emission from the cocktail can be monitored at two wavelengths, either around 340 nm to monitor the emission from LAB (with a 325 – 375 nm bandpass filter in place), or with a long pass filter in place (> 500 nm) by allowing only emission from bodipy to be monitored.

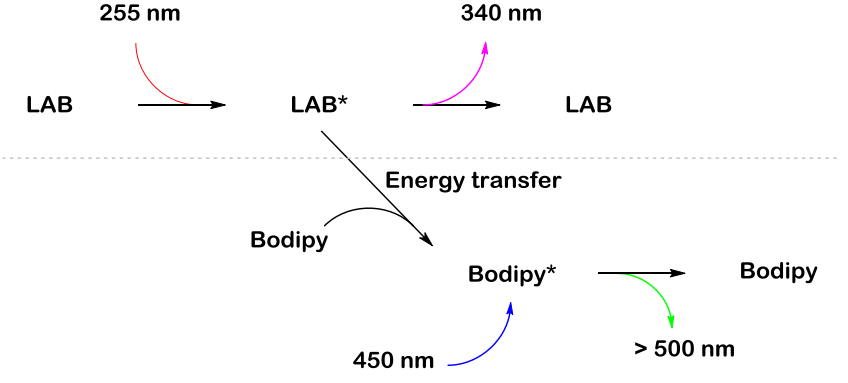

Figure 5.16. Possible absorbance, emission and energy transfer pathways with bodipy in LAB cocktail.

When the solution is excited at 450 nm energy transfer from the solvent to bodipy is by-passed and bodipy is excited directly. In this case only the effect of LAB as solvent on the environment of bodipy is of influence, e.g. viscosity and polarity. When LAB is excited at 255 nm and the emission is monitored at 340 nm the quenching effect of bodipy on the excited state of LAB is observed and the emission from bodipy is filtered out. When the solution is excited with 255 nm and emission is observed > 500 nm the fluorescence lifetime is a combination of the interaction of LAB and bodipy photophysics in which the intermolecular energy transfer under investigation is involved.

2.3.1. Direct excitation and emission of bodipy

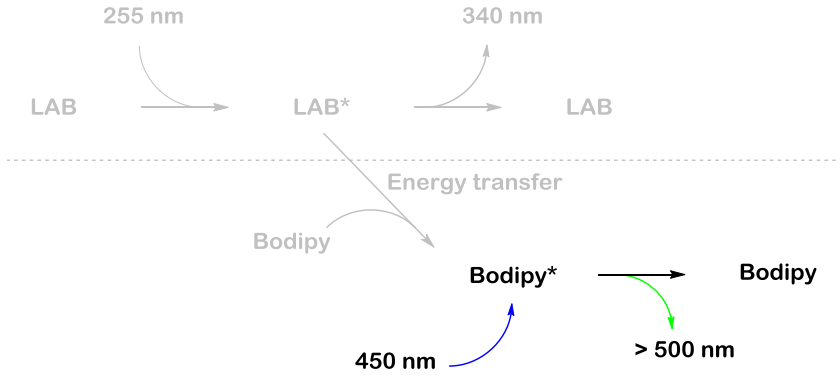

Figure 5.17. Direct excitation and emission of bodipy. (For this section non-relevant portion is greyed out.)

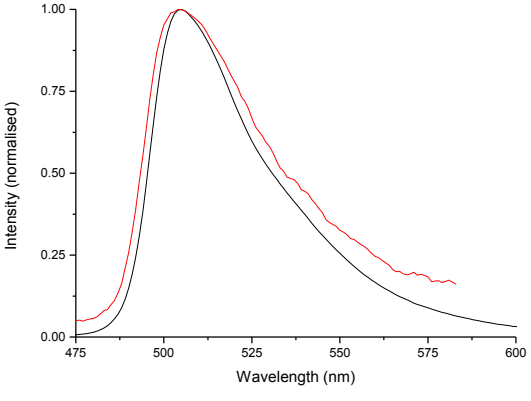

Figure 5.18. Emission spectra of bodipy in ethanol (black) and LAB (red), 0.1 µM and λ_{ex} 450 nm.

Bodipy is rather insensitive to its environment with largely constant photophysical properties (e.g. emission maximum and fluorescence lifetimes, figure 5.18).[41] A negligible change in emission maxima of 1 nm is due to a change in refractive index.[33]

When bodipy is dissolved in LAB and excited at 450 nm the fluorescence lifetime increases with concentration, as seen in ethanol (figure 5.19). The fluorescence lifetime of bodipy in LAB is comparable with bodipy in other solvents (including ethanol) again indicating that the interacting of bodipy with LAB is weak. The minor increase in fluorescence lifetime of bodipy in LAB compared to ethanol is ascribed to the increased viscosity of LAB which increases fluorescence lifetime, similar to the temperature dependence of LABs fluorescence lifetime (section 2.1.2). As the viscosity of the solvent increases, when moving from ethanol to LAB, internal rotation and collisions become more restricted, leading to less quenching of the long lived portion of the excited states, leading to a longer fluorescence lifetime.

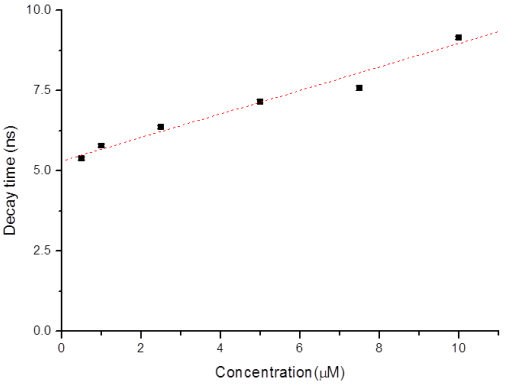

Figure 5.19. Fluorescence lifetimes with various bodipy concentrations in LAB, λ_{ex} 450 nm.

2.3.2. Quenched LAB emission

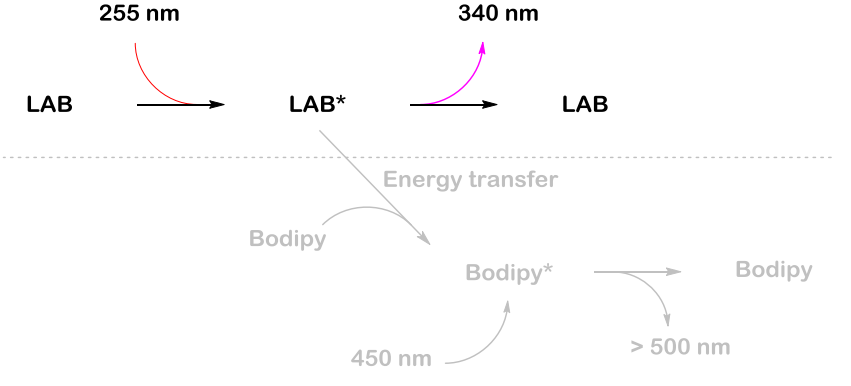

Figure 5.20. Direct excitation and emission of LAB. (For this section non-relevant portion is greyed out.)

Monitoring the fluorescence emission from the bodipy / LAB mixture with a 325 - 375 nm bandpass filter in place allows for the fluorescence emission of LAB to be studied, without interference of bodipy emission (figure 5.20). Energy transfer to bodipy quenches the excited state of LAB and the emission intensity of LAB decreases significantly with increasing bodipy concentration (figure 5.21, left), at a concentration of 10 µM bodipy quenches 90% of the emitted light compared to neat LAB. This indicates that the excited state of LAB is quenched very effectively by energy transfer to bodipy.

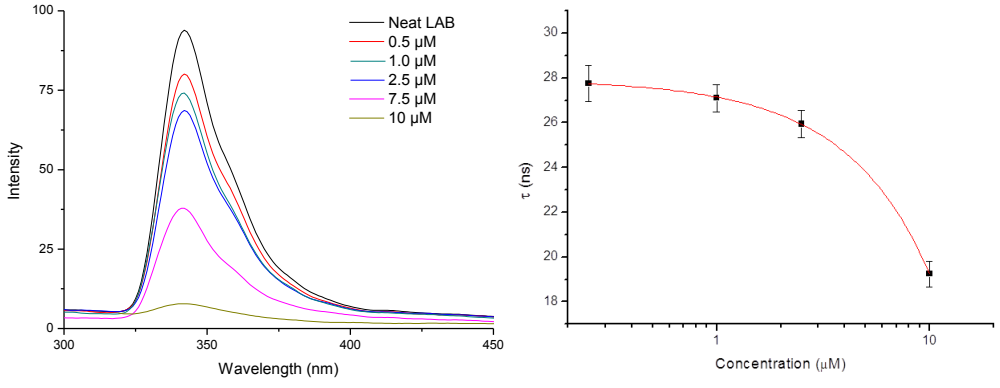

Figure 5.21. Left: Emission spectra (left) and LAB fluorescence lifetimes (right) of LAB with various bodipy concentrations. λ_{ex} 255 nm, λ_{em} 275-375 nm

An increase of bodipy concentration decreases the fluorescence lifetime of LAB (figure 5.21). As long lived excited states have more time to undergo energy transfer these will be quenched more effectively showing no emission, resulting in registration of the short lifetime population; causing an overall shorter fluorescence decay time. Combined with the data from the decrease in emission intensity leads to the conclusion that the long lived excited states of LAB are quenched effectively by bodipy and that therefore the average fluorescence lifetime of LAB shortens and the emission intensity is reduced. This effect is not linear as can be seen from the decrease of intensity and lifetime, a sharp decrease is observed at concentrations > 2.5 µM, caused by moving from trivial energy transfer to Dexter and Föster region. This corresponds to Stern-Volmer model; a higher quencher concentration shortens the excited state lifetime and decreases the emission intensity.[33] However, in the present case the quencher is not the end station for the excitation energy but merely a detour to emission as visible light.

2.3.3. Energy transfer from LAB to bodipy

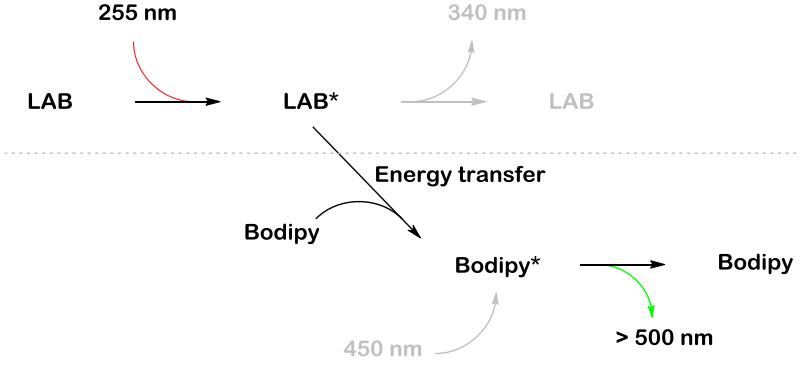

Figure 5.22. Direct excitation of LAB, energy transfer to bodipy and emission from bodipy. (for this section non-relevant portion is greyed out)

Studying the energy transfer from LAB to bodipy is possible by exciting the solution of bodipy in LAB at 255 nm and, by means of a 400 nm long pass filter, filtering LAB out from the measured emission. By using this setup only the emission from bodipy is monitored by the detector. A clear increase in bodipy emission is visible with increasing bodipy concentrations (figure 5.23, left side). Furthermore the aforementioned redshift of the bodipy emission maximum is visible again (as in ethanol; section 2.2.2). When the bodipy concentration increases the fluorescence lifetime decreases; as a higher concentration of bodipy enables faster energy transfer due to the shorter interatomic distance between donor and acceptor molecules. As can be seen from figure 5.23 (right side) the lifetime at low bodipy concentrations is longer than the original LAB emission times. The reason for this is that this multicomponent system effectively adds the 2 emission times. Before a photon is emitted by bodipy it must receive its excitation energy from LAB, and as is know from section 2.1 this process has a lifetime of 30 ns. At low bodipy concentrations Dexter and Förster energy transfer are almost non-existent and the only means of energy transfer to bodipy from LAB is via trivial energy transfer over greater distances. The higher the concentration of bodipy the faster the energy transfer from LAB to bodipy can occur as Föster and Dexter energy transfer take over. The self-absorption of light at higher concentrations also plays a role as was seen in bodipy ethanol mixtures in section 2.2; at high bodipy concentrations this caused an elongation of the measured fluorescence lifetime. This phenomenon will also be present in the LAB bodipy mixture; and therefore cause an increase in fluorescence lifetime counteracting the decrease in fluorescence lifetime due to improved energy transfer.

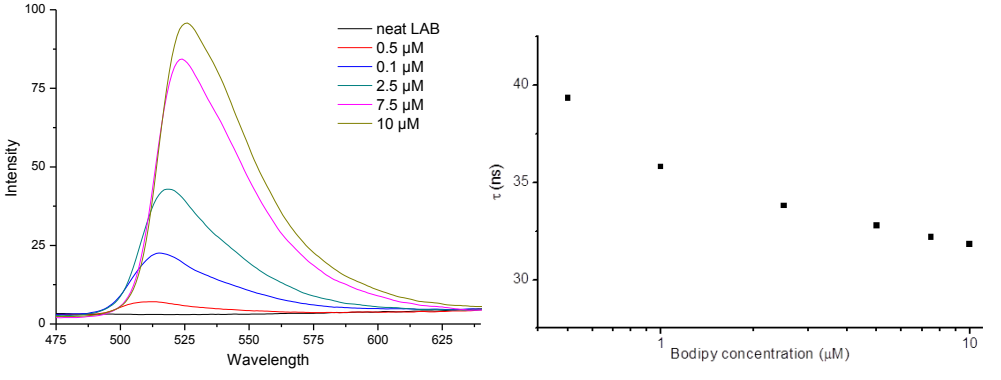

Figure 5.23. Left: Emission spectra (left) and bodipy fluorescence lifetimes (right) of bodipy in LAB at various bodipy concentrations, λ_{ex} 255 nm, λ_{em} > 450 nm.

The increase in emission lifetime (when comparing bodipy in ethanol and LAB) indicates that absorbance of the 255 nm light is via LAB and not directly via bodipy as this would result in lifetimes < 10 ns. At a concentration of 10 µM fluorescence lifetime is still significantly higher for the LAB / bodipy mixture than for ethanol / bodipy mixture while 90% of the LAB excitation is quenched. These data confirm the photophysical behaviour of the model compound; i.e. energy is absorbed by the solvent and transferred to the fluorophore.

2.3.4. Temperature effects

As with pure LAB, there is a temperature dependence on the fluorescence lifetime when using bodipy doped LAB. Between -10 to 60 °C a difference of ca. 20 ns is observed in the fluorescence lifetime of LAB emission (figure 5.24). The relative difference between lifetimes at high and low temperature is similar to that for LAB without bodipy (Δt = 20 ns) but the absolute values are decreased (from 40 to 20 with undoped LAB).

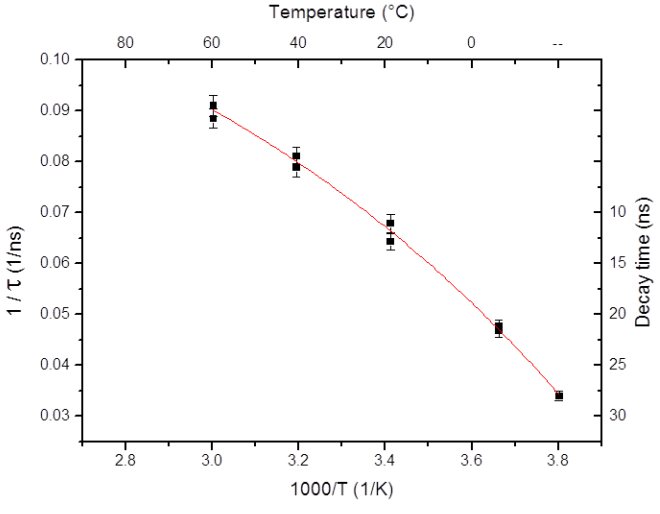

Figure 5.24. Temperature dependence of 10 µM scintillator solution, λ_{ex} 255 nm, λ_{em} > 500 nm.

2.4. High scintillator concentrations.

2.4.1. Fluorescence lifetimes

During radiation testing (chapter 2 and 3 of this thesis) it was found that low fluorophore concentration in the scintillator cocktail leads to an inefficient scintillator.[42] Furthermore, there is a trend in liquid organic scintillators, moving away from LAB as a solvent and instead going towards DIN (di-isopropylnaphthalene) (figure 5.2). Therefore it was decided to load DIN with a very high concentration of fluorophore (bodipy) to simulate, more realistically, the workings of an applied scintillator. Although 5 mM bodipy in DIN can be achieved, extensive stirring and ultrasonic cycles were required and it is likely that this is the maximal solubility. In addition to the bodipy-DIN cocktail, the fluorescence lifetimes of EJ-309 are investigated. EJ-309 is a commercial radiation detection scintillator, the composition of which is proprietary, from chapter 3 of this thesis it is known that the solvent used in this cocktail is DIN.[37]

The decay times of DIN (**1**), EJ-309 (**2**) and bodipy in DIN (**3**) were measured for 3 different pathways (figure 5.25). Excitation and emission of the solvent (left; red and magenta arrow), excitation and emission from the fluorophore (middle; blue and green arrow) and excitation of the solvent with energy transfer to the fluorophore and emission by the fluorophore (right; red and green arrow).

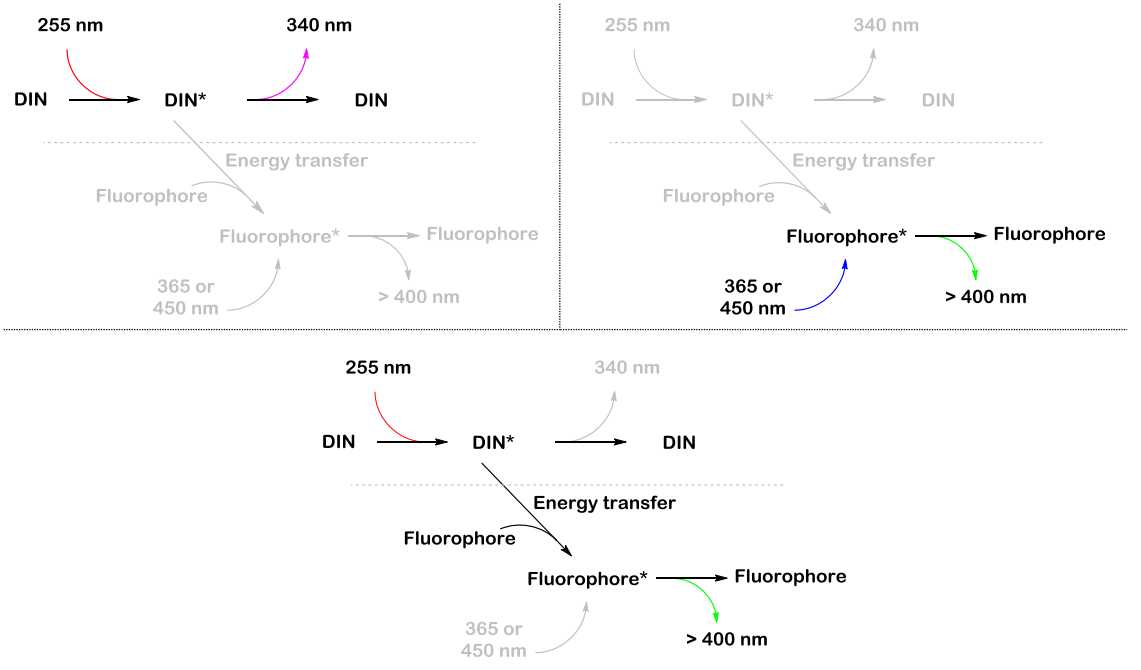

Figure 5.25. Different possible excitation and emission pathways. Left: Excitation and emission of solvent. Middle: Excitation and emission of fluorophore. Right: Excitation of solvent and emission from fluorophore.

5

Table 5.1. Fluorescence lifetimes of different scintillator cocktails
1: neat DIN, **2**: EJ-309, **3**: 5 mm bodipy in DIN.

Entry	Cocktail	Emitter	λ_{ex} (nm)	λ_{em} (nm)	τ_1 (ns)	τ_{rise} (ns)	τ_2 (ns)	Count rate intensity ratio τ_1 : τ_{rise} : τ_2
A	**1**	DIN	255	>280	22	-	7.2	100 : - : 1
B	**2**	DIN	255	325-385	2.6	0.9	*	100 : 100 : 1
C	**3**	DIN	255	325-385	5.0	-	*	100 : - : 1
D	**2**	EJ-309	365	>400	1.3	-	*	100 : - : 1
E	**3**	Bodipy	450	>500	9.5	-	*	100 : - : 1
F	**2**	EJ-309	255	>400	2.6	1.4	*	100 : 100 : 1
G	**3**	Bodipy	255	>500	10	4.0	*	100 : 80 : 1

* a second fluorescence lifetime (50 ns) is observed but with a low intensity.

Emission from neat DIN (entry **A,** table 5.1) with a major decay time of 22 ns and a second component (10% intensity) of 7 ns is slow in regard to fluorescence lifetimes of fluorophores in solution (<10 ns).[34] The direct excitation of the fluorophores (entry **D** and **E**) shows that the resulting fluorescence lifetimes are much shorter compared to DIN (and in line with normal fluorescent solutions). The quenching effect by means of addition of the fluorophores to DIN is considerable; the fluorescence lifetimes of the excited DIN state is reduced down to 2.6 and 5 ns for respectively EJ-309 and the bodipy cocktail (entry **B** and **C**).

Direct excitation of the fluorophore shows that the fluorophores used in EJ-309 display a fluorescence lifetime almost an order of magnitude shorter than that of the bodipy DIN cocktail (entries **D** and **E**). The fluorescence lifetime of bodipy in DIN is 9.5 ns, longer than for bodipy at lower concentrations, this indicates that there is re-absorption of the emitted light by bodipy at the high concentrations of fluorophore (5 mM) used.

From measuring the energy transfer over the whole pathway of the scintillator it is apparent that EJ-309 is a faster scintillator than bodipy in DIN with lifetimes of 2.6 and 10 ns respectively (entries **F** and **G**). It should be noted that the fluorescence lifetime at 5 mM is much shorter compared to previously used lower bodipy concentrations (20 ns and longer at concentrations of 10 µM and lower, section 2.3).

For optimal fitting of the fluorescence decay curves it is necessary to model cocktails **2** and **3** with a second decay time (entries **B** to **G**). The amplitude of this long component (around 50 ns) is however negligible compared to that of the main fluorescence decay time (only 1% intensity). Whenever there is a rise time component in the fit it is about equal in intensity to that of the main decay intensity. This indicates that this stems from energy transfer whereby the energy is transferred from the solvent to the fluorophore before final decay occurs.

2.4.2. Temperature dependence

As shown in sections 2.1.2 and 2.3.4 an increase in temperature has an influence on the fluorescence lifetime of a sample by means of an increase of the diffusion rate. As the rate of diffusion is dependent on the viscosity and therefore the temperature of the sample, changing the temperature of 5 mM bodipy in DIN from -10 to 80 °C again shows this influence. Excitation of bodipy in DIN via the solvent (λ_{ex} 255 nm) shows a linear response to temperature for the fluorescence lifetime (figure 5.26). Again the decrease in fluorescence lifetime is significant with almost a halving of the decay time.

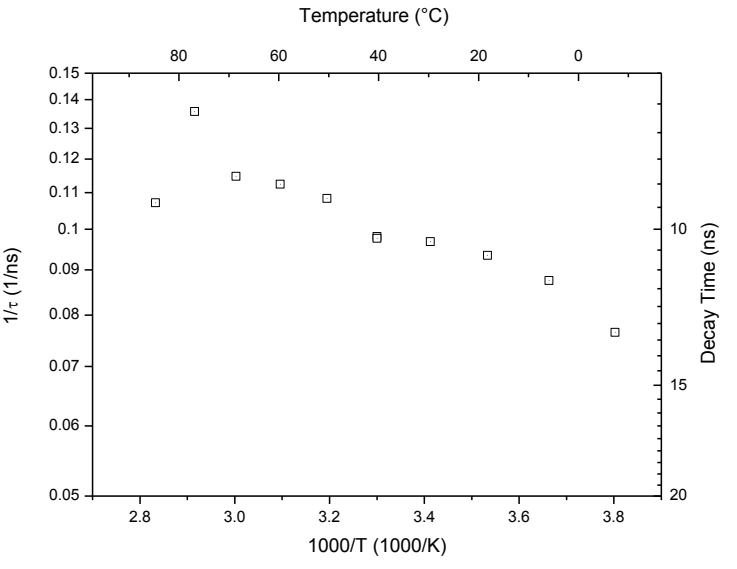

Figure 5.26. Plot showing the relation between the fluorescence lifetime and temperature of 10 mM bodipy in DIN. Temperature from 80 to -10 °C, λ_{ex} 255 nm λ_{em} > 500 nm. (Note $\log_{10}$ scale of y-axis)

3. Conclusions

The aim of this chapter, to find a model scintillator cocktail to probe the workings of a scintillator has been fully fulfilled. Bodipy in DIN functions as is expected from a scintillator. There is no impact on the good photophysical properties of bodipy itself in the solvents used; providing a fast and efficient fluorophore to be used in a scintillator. The quenching of the solvent by bodipy is very efficient, at a concentration of just 10 µM 90% of the excitation energy from the solvent is transferred to bodipy. There are drawbacks to using bodipy as a scintillator fluorophore; self-absorption is high due to overlap of emission and absorption spectra, leading to a decrease in efficiency. Self-absorption can be overcome by using fluorophores with larger Stoke's shift, widening the "space" between emission and absorption, but this will come with the price of lower quantum yield. If perfect overlap of fluorophore emission and PMT sensitivity is needed the red shift due to high fluorophore concentrations should be taken into account, as this can shift the emission maximum by at least 17 nm.

Temperature has a significant effect on the fluorescence lifetime of the cocktail with a difference of 100% over the relevant temperature range, a change of 40% in temperature. As the differences between different types of radiation in pulse shape discrimination at low energies are very small it may be that inaccuracies due to temperature fluctuation play an important role in the possible energy resolution. It might be that resolution of the different types of radiation at low energy levels will prove to be impossible as small temperature

gradients over large detectors might prove to be difficult to control.* Concentration is of much less importance for changes in lifetime; a 200 fold increase in concentration only leads to a 40% change in fluorescence lifetime.

At concentrations which are near photophysical relevant concentrations (≤ 10 µM) energy transfer is considerably slower than at concentrations used in scintillator technology (≥5 mM). The increase of decay time by means of self-absorption is lower than the decrease caused by increased energy transfer. Thus doping of LAB with a fluorophore has a positive effect on timing.

At scintillator concentrations (5 mM) the energy transfer from DIN to LAB cuts fluorescence lifetimes in half, where the commercial EJ-309 reduces lifetimes to 10% of the original value. For specific applications, such as with silicon photomultipliers, whose absorbance is optimal > 500 nm, the bodipy cocktail might show good results due to the long emission wavelength.

4. Experimental section

4.1. Materials and instrumentation

Bodipy was synthesised according to ref [30]. DIN and LAB were kindly donated by Perkin Elmer Groningen, EJ-309 was purchased from Scionix, and other solvents were Uvasol grade purchased at Sigma Aldrich. All solvents were used without further purification. Bodipy was readily dissolved in LAB at all concentrations. Bodipy in DIN was dissolved after several sequences of heating to 100 °C and sonication to achieve a 5 mM concentration, precipitation was not observed over time.

UV/vis absorption spectra were recorded on a Specord600 UV/vis absorption spectrometer (AnalytikJena) as neat liquids in 1.5 mm quartz cuvette. Emission and excitation spectra were recorded using a JASCO FP7200 spectrofluorimeter, and were corrected for instrument response. Fluorescence decay lifetimes were measured using a PicoQuant PicoHarp 300 TCSPC, equipped with τ-SPAD detector and LDH pulsed diodes, in a Quantum Northwest QPOD2e temperature controlled cell holder.

5. Reference

[1] J. B. Birks, *The theory and practice of scintillation counting* (Macmillan, **1964**).
[2] D. L. Horrocks, *Application of Liquid scintillation counting* (Academic Press, Inc, **1974**).
[3] S. G. Cohen and A. Weinreb, P Phys Soc Lond B, *vol 69,* **1956**, pg 593.
[4] I. B. Berlman, J Chem Phys, *vol 33,* **1960**, pg 1124.
[5] J. B. Birks and K. N. Kuchela, Proc Phys Soc, *vol 77,* **1961**, pg 1083.

* A detector might be a sea container sized unit, standing in the blazing sun.

[6] J. Nafisimo, J. B. Birks, and K. R. Naqvi, P Phys Soc Lond, *vol 91,* **1967**, pg 449.
[7] J. B. Birks, S. Georghiou, and I. H. Munro, J Phys Pt B Atom M P, *vol 1,* **1968**, pg 266.
[8] A. Hallam and J. B. Birks, J Phys B, *vol 11,* **1978**, pg 3273.
[9] N. U. R D Mathad and, J. Phys. D, *vol 19,* **1986**, pg 1381.
[10] D. L. Andrews, Chem. Phys., *vol 135,* **1989**, pg 195.
[11] R. Sasson and A. Weinreb, J Lumin, *vol 48-9,* **1991**, pg 239.
[12] J. J. Napolitano, S. J. Freedman, G. T. Garvey*, et al.*, Nucl Instrum Meth A, *vol 274,* **1989**, pg 152.
[13] M. Abbes, B. Achkar, S. AitBoubker*, et al.*, Nucl Instrum Meth A, *vol 374,* **1996**, pg 164.
[14] M. Avenier, Nucl Instrum Meth A, *vol 284,* **1989**, pg 29.
[15] C. Kraus and S. J. M. Peeters, Prog Part Nucl Phys, *vol 64,* **2010**, pg 273.
[16] J. B. Benziger, M. Johnson, F. P. Calaprice*, et al.*, Nucl Instrum Meth A, *vol 417,* **1998**, pg 278.
[17] Borexino Collaboration, Astropart Phys, *vol 16,* **2002**, pg 205.
[18] F. An, Q. An, J. Bai*, et al.*, Nucl Instrum Meth A, *vol 685,* **2012**, pg 78.
[19] J. S. Park, J. Lee, I. S. Yeo*, et al.*, Nucl Instrum Meth A, *vol 707,* **2013**, pg 45.
[20] J. K. Ahn, S. Chebotaryov, J. Choi*, et al.*, Phys Rev Lett, *vol 108,* **2012**, pg 191802.
[21] D. Xue-Feng, W. Liang-Jian, Z. Xiang*, et al.*, Chinese Phys, *vol 39,* **2015**, pg 126001.
[22] X. Hua-Lin, D. Jing-Shan, and W. Nai-Yan, Chinese Phys C, *vol 34,* **2010**, pg 571.
[23] H. O'Keeffe, E. O'sullivan, and M. Chen, Nucl Instrum Meth A, *vol 640,* **2011**, pg 119.
[24] P. Lombardi, F. Ortica, G. Ranucci, and A. Romani, Nucl Instrum Meth A, *vol 701,* **2013**, pg 133.
[25] C. Aberle, C. Buck, F. X. Hartmann, and S. Schönert, Chem Phys Lett, *vol 516,* **2011**, pg 257.
[26] M. Wurm, F. von Feilitzsch, M. Goger-Neff*, et al.*, Rev Sci Instrum, *vol 81,* **2010**, pg 053301.
[27] T. M. Undagoitia, thesis on "Measurement of light emission in organic liquid scintillators and studies towards the search for proton decay in the future large-scale detector LENA" (Technische Universität München, **2008).**
[28] H. Du, R. A. Fuh, J. Li, L. A. Corkan, and J. S. Lindsey, Photochem Photobiol, *vol 68,* **1998**, pg 141.
[29] G. Ulrich, R. Ziessel, and A. Harriman, Angew Chem Int Ed, *vol 47,* **2008**, pg 1184.
[30] M. Shah, K. Thangaraj, M. Soong*, et al.*, Heteroat Chem, *vol 1,* **1990**, pg 389.
[31] F. Brooks, Nucl Instrum Methods, *vol 162,* **1979**, pg 477.
[32] *Photomultipliers: data handbook. PC04* (Philips Components, **1990**).
[33] J. R. Lakowicz, *Principles of Fluorescence Spectroscopy* (Springer US, **2006**).
[34] N. J. Turro, V. Ramamurthy, and J. Scaiano, *Modern molecular photochemistry of organic molecules* (Univ. Sciece Books, **2010**).
[35] C. Buck, thesis on "Development of metal loaded liquid scintillators for future detectors to investigate neutrino properties" (Ruperto-Carola University of Heidelberg, **2004).**
[36] S. D. Ambers, M. Flaska, and S. A. Pozzi, Nucl Instrum Meth A, *vol 638,* **2011**, pg 116.
[37] Eljen technologies *EJ-309 Liquid scintillator pulse-shaped discrimination properties*
[38] F. H. Brown, M. Furst, and H. Kallamann, Discuss Faraday Soc, *vol 27,* **1959**, pg 43.
[39] R. Ziessel and A. Harriman, Chem Commun, *vol 47,* **2011**, pg 611.
[40] I. López-Duarte, T. T. Vu, M. A. Izquierdo, J. A. Bull, and M. K. Kuimova, Chem Commun, *vol 50,* **2014**, pg 5282.
[41] A. C. Benniston and G. Copley, Phys Chem Chem Phys, *vol 11,* **2009**, pg 4124.
[42] P. Dijkstra, D. Angelone, E. Talnishnikh, H. J. Wortche, E. Otten, and W. R. Browne, Dalton Trans, *vol 43,* **2014**, pg 17740.

Chapter 6

LANTHANIDE TRIAZOLE COMPLEXES

The triazole ligands described in chapter 2 of this thesis are applied here as static sensitizers of lanthanide ions. Combining the high molar absorption of triazoles with the lanthanide emission opens opportunities for the use of lanthanide emission biological applications. In this chapter the characteristics of triazole based lanthanide complexes are described, which provide a basis for sensitized lanthanide emission in water. Furthermore the optimal denticity of the ligands' binding to lanthanide ions is studied.

1. Introduction

1.1. Lanthanide sensitisation by internal energy transfer

In the previous chapters of this thesis attention was directed to energy transfer between molecules in solution (and the solvent itself). Intramolecular energy transfer between individual components of a molecule is the focus of this chapter, in particular with regard to lanthanide emission.[1-3] Lanthanide ions show UV to NIR emission with narrow linewidths (< 10 nm FWHM), and for this reason are used in many fields requiring emission e.g. Nd:YAG lasers, cathode ray tubes. However excitation with intense UV light or by electrons is needed, as direct excitation by UV or visible light is inefficient (ε = 0.1 M^{-1} cm^{-1}). The poor (parity forbidden) absorption by the heavily shielded f-orbitals of the lanthanide ions necessitates the use of other approaches to populate the lanthanide ions' exited states, i.e. the use of ligands which can function as antennas, to harvest UV/Vis light and transfer energy to the lanthanide ions.

Absorbance of light by the ligand populates a singlet excited state, but proximity of the heavy lanthanide facilitates intersystem crossing to triplet states. By this pathway the excited state of the ligand can be converted to an excited metal centred state of the lanthanide(III) ion. Overlap between the energies levels of the ligand and metal excited states allows for the transfer of excitation energy from the ligand to the lanthanide ion.

Apart from narrowness of the emission bands of lanthanides, long lived phosphorescence decay lifetimes are characteristic (millisecond timescale). This long emission lifetime enables discrimination from the short lived biological auto-fluorescence (nanosecond timescale) and the emission arising from the lanthanides in in vivo experiments.

One of the requirements of imaging probes in biological systems is their ability to function in aqueous media, which presents a challenge as although lanthanide emission is insensitive to solvent polarity changes and oxygen quenching due to the shielding of the f-orbitals, the excited states of the lanthanide complexes are quenched by NH and OH oscillators, including water. Hence the use of lanthanides in water based media, is limited to the timescale of lanthanide emission (milliseconds), which enables quenching by water to be a major relaxation pathway. Shielding the lanthanide ion from solvent interactions by means of a ligand scaffold will decrease the effect of OH oscillators, however, even if a large part of the lanthanide is shielded from OH oscillators the excited state will still be quenched considerably.[4, 5]

The environment of the lanthanide is influenced by the surrounding ligand with an increase in the number of ligands around the metal changing its electric dipole, resulting in "hypersensitive" transitions.[6] Lanthanides have two transition types; magnetic dipole (MD) and electric dipole (ED). MD transitions originate only from internal $4f^n$ configurations, and are in-sensitive to the coordination sphere, while ED transitions, which extend outside of the $4f^n$

configuration (thus more in contact with the ligand), are sensitive to the environment, and thereby provide information about the inner coordination sphere of the lanthanide ion.[7]

Lanthanide complexes to date have focused on nitrogen binding ligands motif; including pyridyls, tetrazoles and pyrazoles,[8-12] especially tridentate and tetra dentate ligands, which show good characteristics in regard to emission properties. However, most focus has been on solid state emission rather than in water or other biologically relevant media.

1.2. Chapter outline

Pyridyl 1,2,4-triazole ligands were applied in boron complexation as reported in chapter 2 of this thesis and for separation purposes, an important field in lanthanide chemistry where triazole ligands were successfully employed, although the photophysics of these complexes were not explored.[13] As triazoles absorb in the UV and bind to lanthanides, the effects of these ligands on the photophysical properties of the lanthanide ions are of interest. The influence of coordination number is investigated with three ligands (figure 6.1), differing in size and denticity, either bidentate, tridentate or pentadentate. Increasing shielding, from water by the ligand, is expected to decrease quenching of excited Ln(III) states and increase emission intensity.

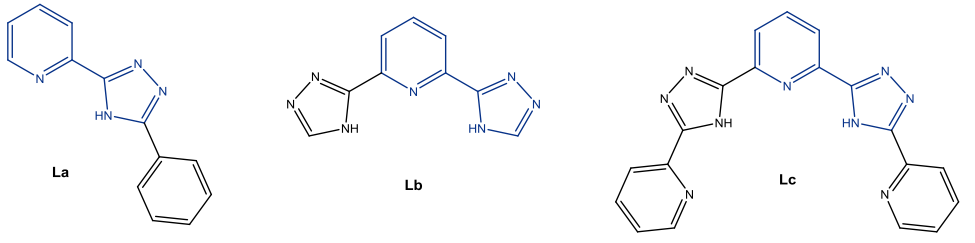

Figure 6.1.1. Structure of ligands (with common triazole pyridine structure in blue) **La**: bidentate pyridyl triazole, **Lb**; tridentate pyridyl bi-triazole and **Lc**; pentadentate trispyridyl bi-triazole.

The emission spectra of the lanthanide complexes provides direct information regarding the efficiency of internal energy transfer and shielding from OH oscillators provided by the ligands. A key factor is the number of ligands that bind to the lanthanide ions. Due to the coordination numbers typical of lanthanide ions (8-12) this can vary considerable. The more sterically demanding ligand **Lc** is expected to be more hindered than the smaller ligand **La**. As sensitised lanthanide ion emission is of most relevance to biological systems, experiments were performed in water as well as in methanol.

2. Results

2.1. Synthesis

The synthesis of ligand **La** is described in chapter 2 of this thesis, ligand **Lb** and **Lc** were provided by T.C. Canrinus.[14, 15] Complexation of ligands to lanthanide ions in methanol was achieved by deprotonation of the ligand with NaOMe followed by addition to the respective lanthanide(III) salt in methanol (set to a pH similar the ligand containing solution). Complexation in water was achieved by using micromolar solutions of the ligand with addition of the respective lanthanide (III) salt in water.

2.2. Photophysical properties of ligands and complexes in methanol

2.2.1. UV/vis absorption spectra of lanthanide complexes in methanol

Slow addition of a solution of the relevant lanthanide salt to a solution of deprotonated ligand in methanol results in a significant change in the shape and intensity of the spectrum (figure 6.2). Subtraction of the initial absorption spectrum of the ligand (with correction for the decrease in ligand concentration) shows the emergence of a band at ca 305 nm. After an initial increase in absorbance the bands decrease again with further addition of terbium(III). This change in intensity of one band at different metal to ligand ratios points to the formation of at least one lanthanide triazole complex in solution. The ligand/metal ratio can cover a wide range, i.e. from 2:1, 1:1, 1:2, to 1:3 and higher.

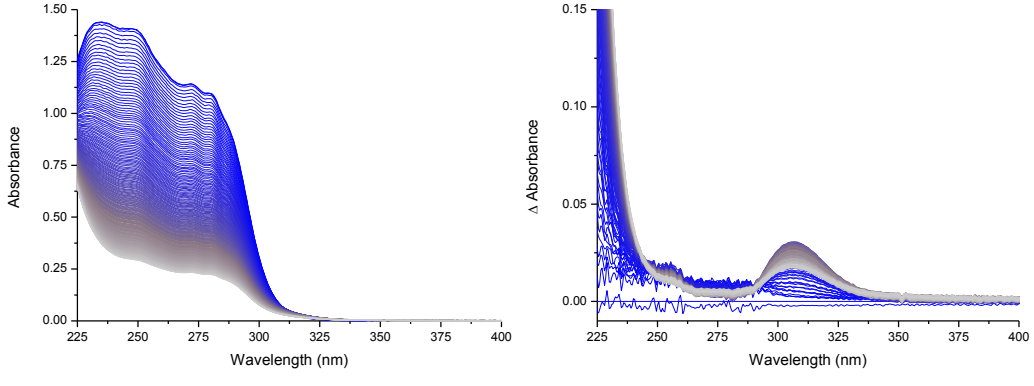

Figure 6.2. Left: UV/vis absorbance spectra upon addition of up to 3 equivalents of Tb(III) to **La** in methanol (dark blue line; **La** only, white line; with 3 equivalents of Tb(III)). Right: Difference absorption spectra. Spectra were corrected for the decrease in ligand concentration.

The Job's plot method was used to determine the dominant ligand/Ln(III) ratio, by variation of M:L ratios.[16] The application of the Job's plot acquires four conditions to be met: the total concentration of the solution must be constant, optical attenuation follows the Lambert-Beer law, pH remains constant and only one complex is dominant.[16] When these

conditions are met a Job's plot should provide a maximum at a stoichiometric point, i.e. 0.5, 0.66 or 0.75 (respectively 1:1, 2:1 or 3:1 ligand to metal ratio). The Job's plot, figure 6.3, shows that the maximum lies at χ_{La} = 0.5 when adding a solution of terbium(III) salt to triazole **La,** indicating that a terbium triazole complex with a ratio of 1:1 (Tb:**La**) dominates in solution.

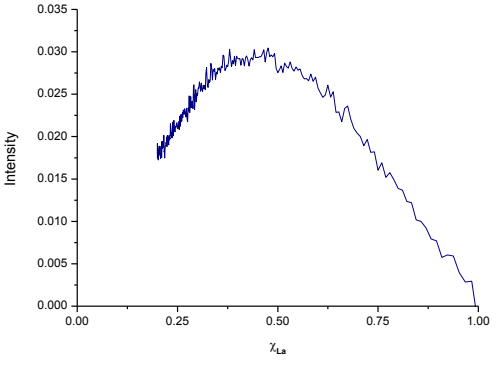

Figure 6.3. Job's plot of addition of Tb to **La**.

In case of **Lb** addition of terbium(III) results in the appearance of two bands and a decrease in absorbance at ca 290 and 321 nm (figure 6.4).* This change in intensity is accompanied by a bathochromic shift of 10 nm.

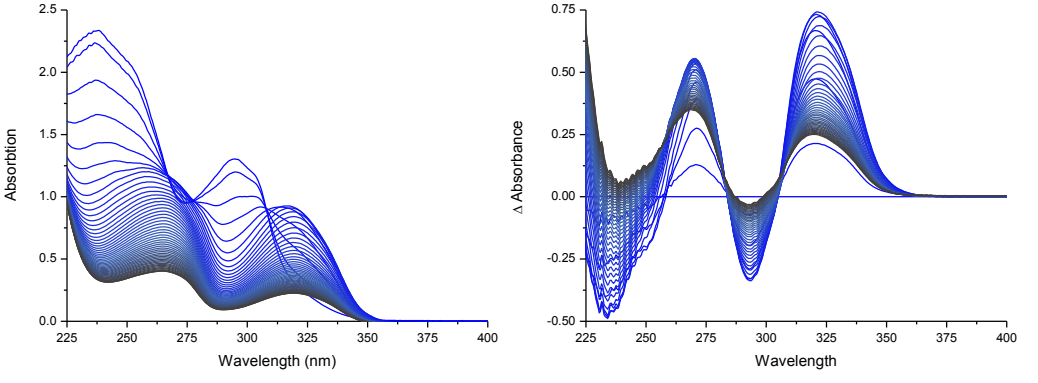

Figure 6.4. Left: UV/vis absorbance spectra upon addition of up to 3 equivalents of Tb(III) to **Lb** in methanol (dark blue line; **Lb** only, white line; with 3 equivalents of Tb(III)). Right: Difference absorption spectra. Spectra were corrected for decrease in ligand concentration.

The maximum of the Job's plot (figure 6.5) lies at χ_{b} = 0.7 when adding a solution of terbium(III) salt to triazole **Lb**. However the Job's plot is only valid when there is one static dominant species. These data indicate that there is a mixture of 2:1 and 3:1 complexes present in solution. The reasons why more than one distinct complex forms can be twofold: there is no

* The increase of the band at 250 nm is due to the addition of NO_3^- (present as counterion to Tb(III)).

preference for bis or tris ligand complexes or one of the species is kinetically stable and prevents the system reaching a minimum energy state during the timescale of the experiment.[17]

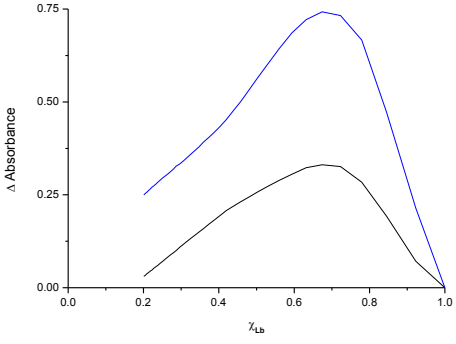

Figure 6.5. Job's plot of addition of Tb to **Lb**, λ_{abs} 292 (black) and 321 nm (blue).

Gradual addition of terbium(III) to ligand **Lc** results in a change in absorbance at 290, 315 and 344 nm (figure 6.6), again accompanied by a bathochromic shift.

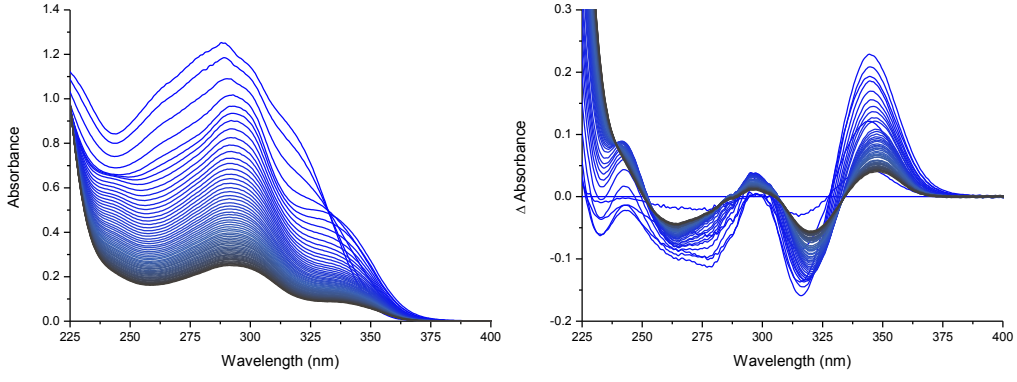

Figure 6.6. Left: UV/vis absorbance spectrum upon addition of up to 3 equivalents of Tb (II) to **Lc** in methanol (dark blue line; **Lc** only, white line; with 3 equivalents of Tb(III)). Right: Difference absorption spectra. Spectra were corrected for decrease in ligand concentration.

A Job's plot of the addition of Tb(III) to **Lc** shows that the absorbance at 315 and 344 nm lies at a χ_b 0.85, again in between stoichiometric points (figure 6.7). This indicates that a single species is not dominant, which is supported by the mismatch of the maximum of the 296 nm band with the 315 and 344 bands maxima.

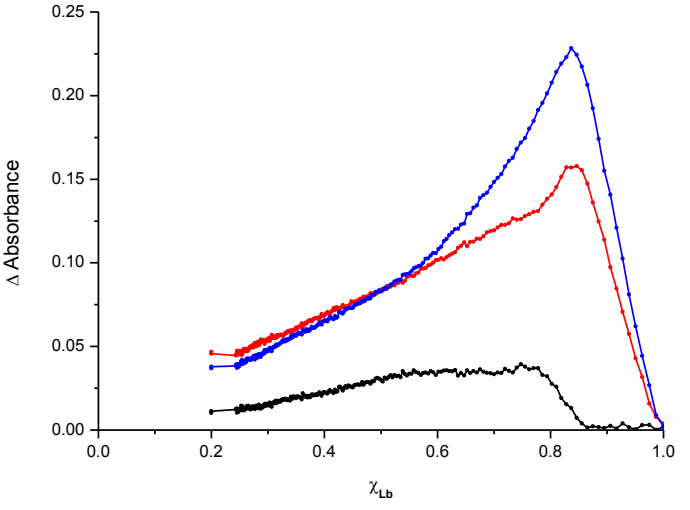

Figure 6.7. Job's plot of addition of Tb(III) to **Lc**, λ_{abs} = 296 (black), 315 (red) and 344 nm (blue).

Comparing the spectra of Tb-**La**, Tb-**Lb** and Tb-**Lc** complexes shows the effect of the increase in conjugation in the series. Ligand **La** absorbs at ca. 315 nm and a shift is seen at 320 nm. Ligand **Lb** absorbs at ca. 350 nm and ligand **c** till ca 375 nm, the most change when complexation is seen around 321 nm and 344 nm respectively.

2.2.2. Emission spectra of lanthanide complexes in methanol

The emission spectrum of ligand **La** is a broad band ranging from < 400 to 600 nm. Addition of terbium(III) salt results in the appearance of lanthanide emission bands (figure 6.8), confirming that the triazole transfers excitation energy to the lanthanide(III) ion.

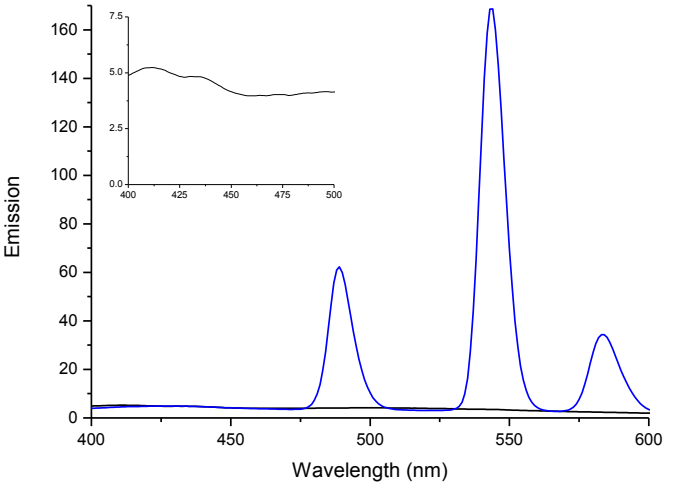

Figure 6.8. Emission spectra of ligand **La** (black) and Tb(III) - **La** complex (blue), λ_{ex} = 310 nm, detail of ligand emission in inset.

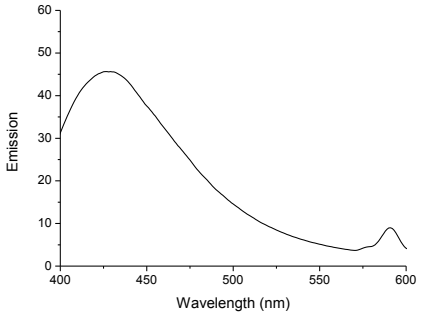

Figure 6.9. Emission spectrum of Eu(III)-**La** complex, λ_{ex} 310 nm.

With Eu(III) salts energy transfer from the ligand to the europium ion is less efficient, with a mixed emission spectrum consisting of triazole fluorescence and Eu (III) phosphorescence (figure 6.9).

The broad emission spectrum of ligand **Lb** in solution decreases upon addition of Tb (III) salt, with a concomitant increase in Tb (III) phosphorescence (figure 6.10). The emission spectra of Eu (III) and Tb (III) complexes show negligible emission from the triazole ligand and thus energy transfer is efficient (figure 6.11). With addition of dysprosium (III) to **Lb** minor signs of triazole emission are visible underneath lanthanide emissions while with samarium(III) triazole emission is a significant part of the emission spectrum, indicating that energy transfer is less efficient in these complexes. Neodymium(III) and Holmium(III) show no clear lanthanide emission in the visible region. For holmium a possible mismatch in the excitation level energies between the excited states of **Lb** and Ho (III) prevents energy transfer. For neodymium visible emission is not expected as neodymium(III) emits in the NIR (figure 6.12, page 137). [2]

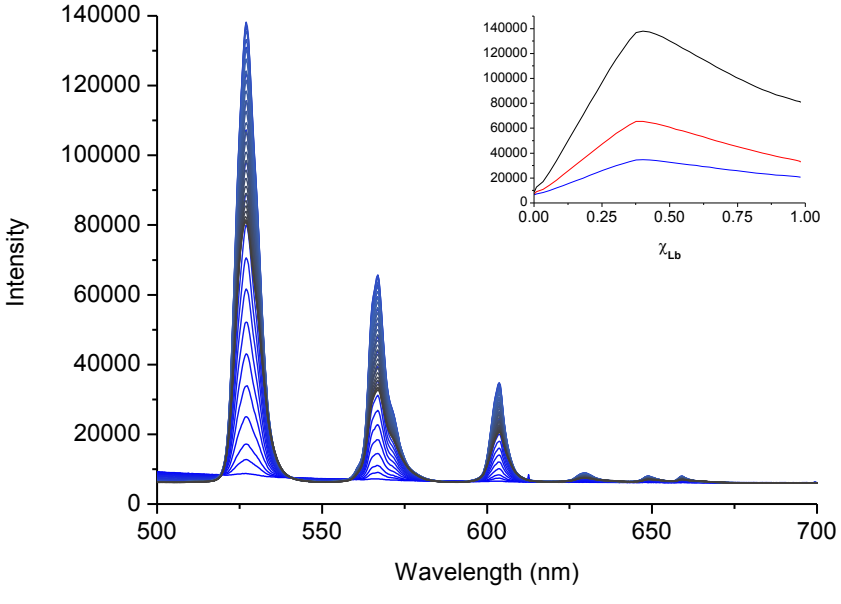

Figure 6.10. Emission spectrum as a function of molar fraction of Tb (III) to **Lb**. Inset: Job's plot

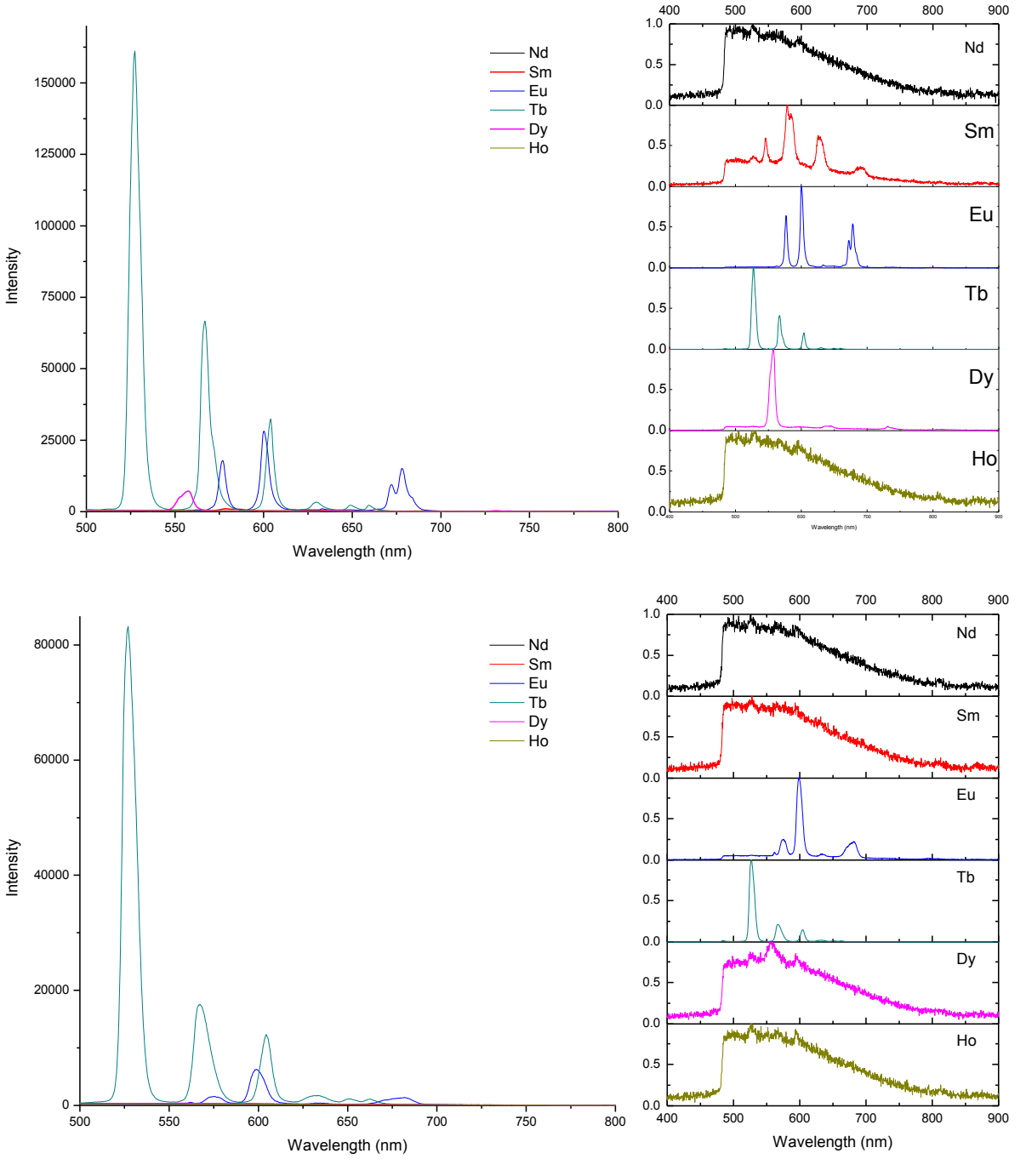

Figure 6.11. Top left: Emission spectra of Ln (III) complexes of **Lb** formed in situ, with a 2:1 ratio, λ_{ex} 309 nm. Top right: normalised emission spectra. Bottom left: Emission spectra of Ln (III) complexes of **Lc** formed in situ with a 2:1 L:M ratio, λ_{ex} 309 nm. Bottom right normalised emission spectra.

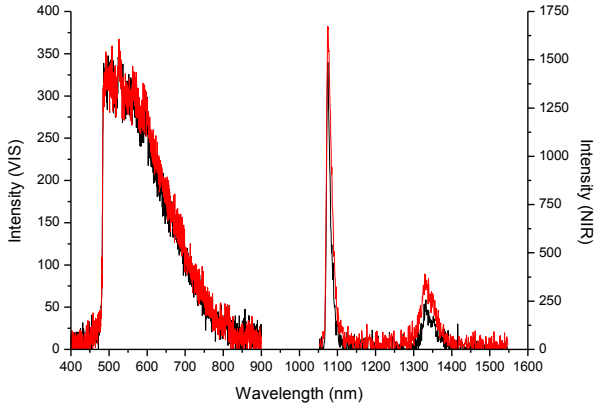

Figure 6.12. VIS and NIR emission spectrum of **Lb** (black) and **Lc** (red) with Nd (III), 2:1 L:M ratio *

A Job's plot based on the emission data of terbium (III) with **Lb** is consistent with data obtained from absorption spectra; i.e. the maxima of the emission based Job's plot are at a stoichiometric ratio of 0.7 (figure 6.10, inset and section 2.2.1).

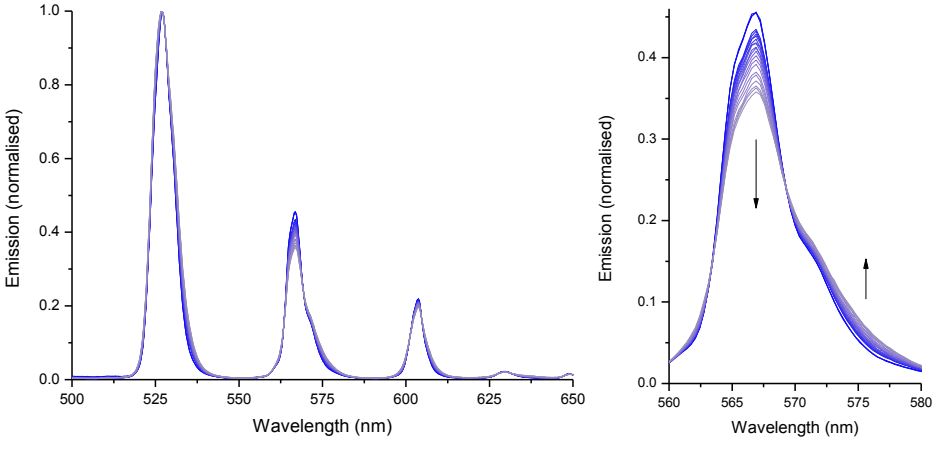

Figure 6.13. Left: Emission spectra of Tb (III) titrated to **Lb**. Normalised to (Tb)$^5D_4 \rightarrow {}^7F_5$ (527 nm) Right: expansion of 567 nm band. A long pass filter (> 500 nm) removes the (Tb)$^5D_4 \rightarrow {}^7F_6$ band (490 nm).

As terbium (III) is added to the ligand the coordination ratio (Tb:L) varies, which is apparent from the hypersensitive transitions (figure 6.13 and section 1.1). The (Tb)$^5D_4 \rightarrow {}^7F_5$ transition (527 nm) is a magnetic dipole transition; which is insensitive to the coordinating environment and thus can be used as reference for normalisation. The $^5D_4 \rightarrow {}^7F_4$ transition

* Absorption of NIR by the solvent (methanol) decreases the intensity of the recorder signal and reduces the quality of the spectrum.

(567 nm) is an electric dipole transition, which is sensitive to the environment [18], and the change in the type of ligands (**Lb** or H_2O) coordinated to the metal ion results the spectral shape of the $^5D_4 \rightarrow {}^7F_4$ transition to undergo subtle changes, while the $^5D_4 \rightarrow {}^7F_5$ transition remains unperturbed. This data demonstrate that there is a change in the coordination sphere of the metal ions as the M:L ratio is varied.

Addition of lanthanide salts to ligand **Lc** shows a similar trend as with ligand **Lb** (figure 6.11, bottom page 136), however, energy transfer from the ligand to the lanthanide (III) ion is less efficient compared to Ln (III) **Lb** complexes. Lanthanide emission is strong with terbium (III) and europium (III) and weak emission from dysprosium (III) is superimposed over the ligand emission. In all cases lanthanide (III) emission is less intense compared to when using ligand **Lb**, in fact samarium (III) displays no lanthanide emission. These data indicate that energy transfer from ligand **Lc** to the lanthanide (III) ions is less efficient then for **Lb**.

2.2.3. Quantum yield emission of lanthanide complexes

Table 6.1 shows that the quantum yield of emission of the terbium (III) complexes is greater for both **Lb** and **Lc** compared to the corresponding europium (III) complexes. The lower efficiency of europium compared to terbium lies in line with literature, were a difference of 50% is no exception. [19, 20] The quantum yield of both **Lb** complexes is greater than with **Lc** complexes, indicating that **Lb** shows better energy transfer characteristics. The absolute values for quantum yields of the terbium (III) complexes lie in the range expected, while those of the europium (III) complexes is lower than expected from literature (5 - 67% quantum yield).[19, 20]

Table 6.1. Quantum yield of Tb (III) and Eu (III) complexes in methanol with ligand **Lb** and **Lc**.

	Terbium Quantum yield (%)	Europium Quantum yield (%)
Ligand **Lb**	35	5
Ligand **Lc**	24	1.5

2:1 ligand to metal ratio was employed, $[Ru(bpy)_3]^{2+}$ was used as quantum yield reference.

The quantum yield of complexes of **La** were not determined but were clearly much lower than those with **Lb** and **Lc**. In contrast to Eu (III) and Tb (III) complexes of **Lb** and **Lc** which show almost no triazole fluorescence, **La** ligand emission was apparent. It is therefore concluded that the efficiency of ligand **La** complexes is less than that of ligands **Lb** and **Lc**.

2.2.4. Emission lifetime data

As mentioned in section 1.1, the emission lifetime of lanthanides (III) ions lies in the millisecond range; and the emission lifetimes that were recorded correspond with this, confirming ligand binding to terbium (III) and europium (III) (figure 6.14, table 6.2 and 6), in solution at room temperature and in the glassy state at 77 K. In the glassy state diffusion is stopped and dissociation of the complex is prevented during the lifetime of the excited state. Four metal to ligand ratios were employed; 1:2, 1:1, 1:2 and 1:3. Within experimental error, emission lifetimes for all emission bands are similar per complex.

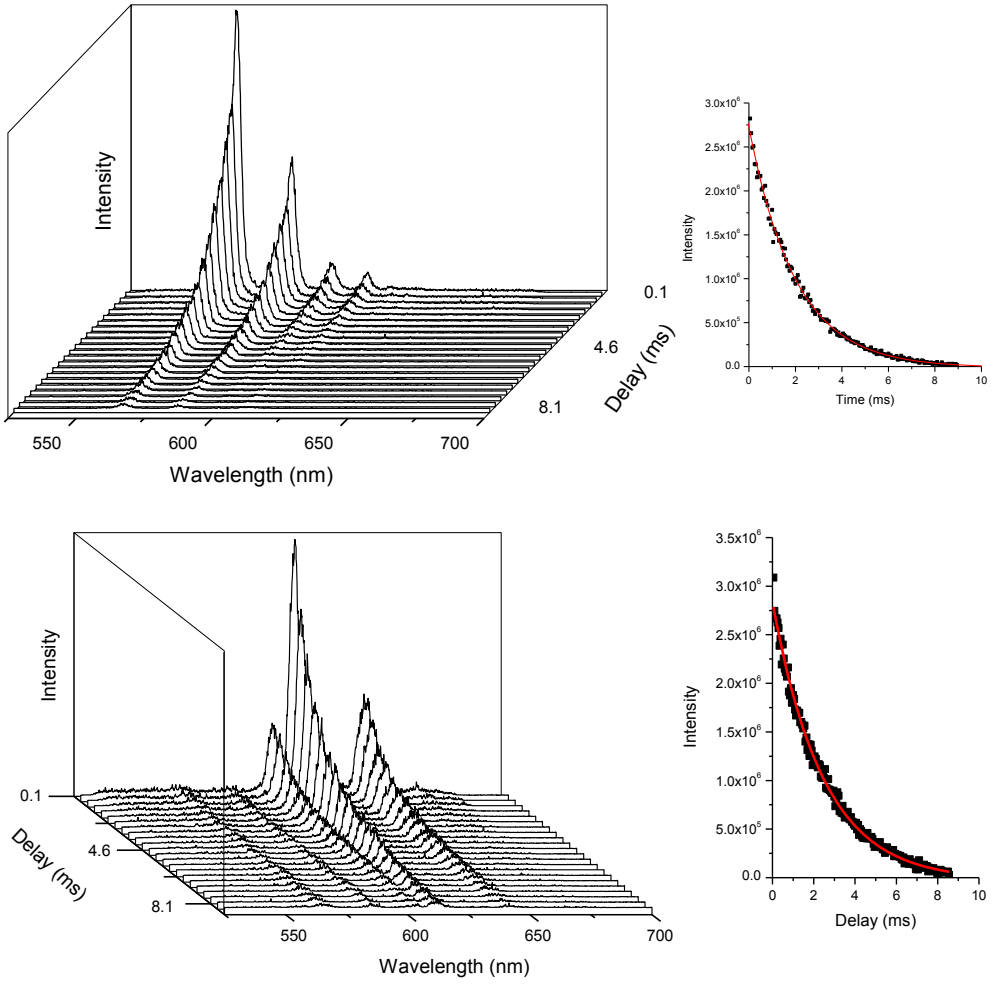

Figure 6.14. Top Left: Time resolved emission spectra of Tb (III) complexed to **Lb**.
Top Right: Fitting of exponential decay curve to 580 nm band.
Bottom left: Time resolved emission spectra of europium (III) complexed to **Lc**.
Bottom right: fitting of exponential decay curve to 580 nm band.

Table 6.2. Emission lifetimes of terbium (III) complexes with ligand **Lb** (left) and ligand **Lc** (right) at different ligand ratios. Lifetimes are an average of 4 emission bands.

b:Tb	τ (ms) RT		τ (ms) 77K	
1:2	0.78	±0.004	1.55	±0.015
1:1	1.11	±0.013	1.70	±0.008
1:2	1.99	±0.007	1.59	±0.008
1:3	1.99	±0.018	1.87	±0.021

c:Tb	τ (ms) RT		τ (ms) 77K	
1:2	0.92	±0.004	1.34	±0.045
1:1	1.64	±0.009	1.66	±0.011
1:2	1.58	±0.035	1.43	±0.042
1:3	1.45	±0.040	1.49	±0.072

Emission lifetimes of the ligand lie in the nanosecond range (chapter 2 of this thesis), the measured emission lifetimes, which lie in the millisecond range clearly indicate that measured emission is from the lanthanide (III) ion and not from ligand emission. Also the long timescale of emission lifetimes shows that diffusion dynamic quenching is not at play.

At lower temperatures the decay lifetime should increase as diffusion limited quenching processes are hindered, thus allowing the excited state to be longer. With increasing ligand ratio the lifetime of terbium complexes at RT increases more than that at 77K (resp 0.78 to 2.0 ms and 1.55 to 1.87 ms). More shielding of the lanthanide from the (quenching) environment by the ligand decreases quenching pathways and increases the lifetime at room temperature. Due to the influence on ligand exchange at 77 K this effect is less pronounced at lower temperatures. Complex Tb-**Lc** shows a significant increase in emission lifetime going from 1:2 to 1:1 L:M ratio, at higher ligand ratios the lifetime is constant or even less. From this data it is apparent that binding of at least one ligand to the terbium (III) ion has a significant impact on emission lifetime.

The lifetimes of europium (III) complexes with ligand **Lc** in solution are significantly shorter than those of the terbium (III) complexes, however the Eu-**Lb** complexes show similar trends to the Tb (III) complexes, indicating binding of the ligand increases emission lifetime.

Table 6.3. Emission lifetimes of europium (III) complexes with ligand **Lb** (left) and **Lc** (right) at different ligand ratios. Lifetimes are an average of 3 emission bands.

Eu:**Lb**	τ (ms) RT		τ (ms) 77K	
1:2	0.52	±0.012	0.73	±0.005
1:1	0.63	±0.012	0.92	±0.014
1:2	1.52	±0.086	1.46	±0.108
1:3	2.58	±0.096	1.90	±0.246

Eu:**Lc**	τ (ms) RT		τ (ms) 77K	
1:2	0.64	±0.008	0.77	±0.005
1:1	0.73	±0.012	0.74	±0.005
1:2	0.79	±0.017	0.81	±0.008
1:3	0.76	±0.021	1.49	±0.012

The lifetime of the Eu(III) **Lc** complex has a similar lifetime as tris coordinate Eu(III) tri-pyridine complexes reported in literature (0.7 ms).**[9, 12]** The long lifetime of Eu(III) Lb complexes at high ligand ratios is more than double, combined with the high quantum yield this indicates good shielding by **Lb** compared to **Lc** from OH oscillators, preventing quenching from long lived states. The lifetimes of the Tb(III) complexes lies in line with those reported (1.5 ms).[12]

2.3. Photophysical properties of ligands and complexes in water

2.3.1. UV/vis absorption spectra

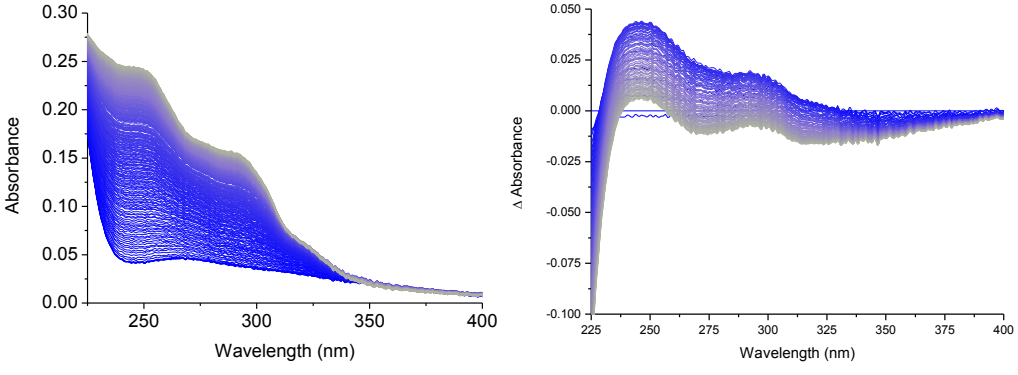

Figure 6.15. Left: UV/Vis Absorbance spectrum upon addition of 5 equivalents **Lb** to Tb(III) in water (dark blue line; Tb(III) only, white line; with 5 equivalents of **Lb**). Right: Difference absorbance spectra. Spectra were corrected for decrease in ligand concentration.

Addition of terbium (III) to ligand **Lb** in water results in substantial change in the absorbance spectrum, at 250, 292 and 321 nm (figure 6.15).

A Job's plot of each band shows a stoichiometric ratio of 0.6 (figure 6.16) and is therefore again indecisive as to which specific complex has formed; as with lanthanide complexes in methanol. However, the maximum of the Job's plot is shifted from 0.7 in methanol to 0.6 in water, indicating that the most probable species present in solution are the 1:1 and 1:2 complexes instead of the 1:2 and 1:3 complexes as found in methanol. The cause of this lower binding ratio is most probably the stronger coordination of water to the metal ion as opposed to methanol.

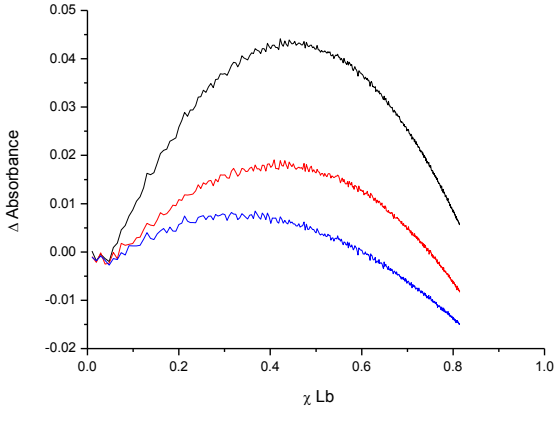

Figure 6.16. Jobs plot of Tb(III) and ligand **Lb** in water at 250 (black), 290 (red) and 310 nm (blue).

2.3.2. Emission spectra of lanthanide complexes in water.

The emission spectra of the Tb(III) **Lb** complex, figure 6.17, shows distinct terbium emission upon addition of terbium to **Lb**. When considering the decrease in Tb(III) concentration at the different ratios the intensity of emission keeps increasing.

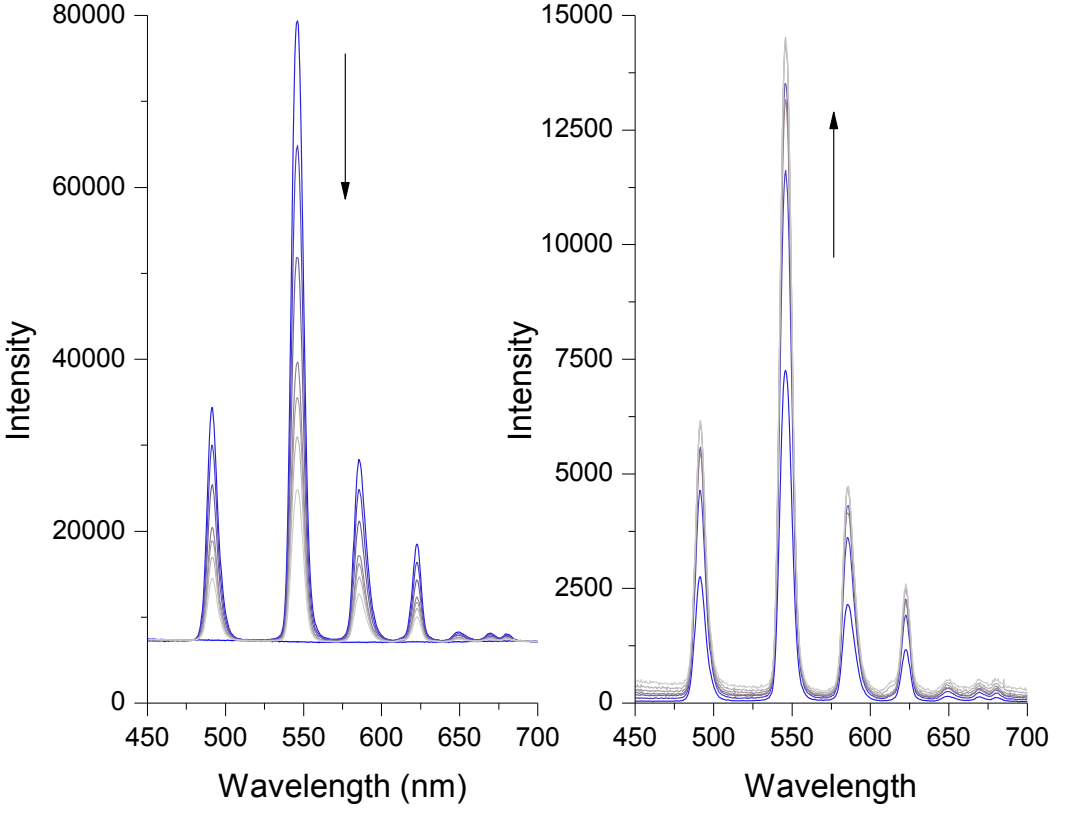

Figure 6.17. Left: Emission spectrum of Tb(III) **Lb** complex in water with increasing **Lb** concentration (M:L from 1:1 to 1:7), λ_{ex} 310 nm. Right: left spectrum corrected for dilution.

At pH 7.6 deprotonation is enough to allow for complex formation and lanthanide emission. However, at pH 9.9, figure 6.18, emission from the lanthanide is considerably stronger than compared to the emission at pH 7.6. The relative quantum yield going from pH 7.6 to 9.9 increases a factor of 4, indicating that the binding efficiency near biological relevant pH is not optimal.

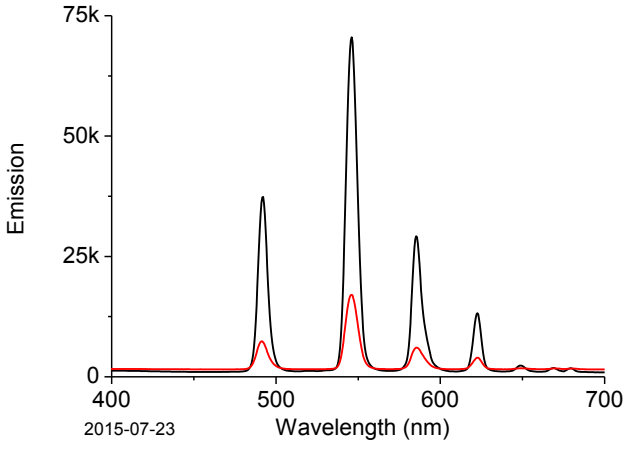

Figure 6.18: Emission of Tb (III) **Lb** complex (M:L 1:1) at pH 7.6 (red) and pH 9.9 (black), luminescence intensity was corrected by the absorbance at excitation wavelength 310 nm.

3. Conclusion

A series of triazole lanthanide complexes has been characterized by means of photophysical studies in this chapter. The terbium based complexes show very promising lanthanide emission, while other lanthanides are somewhat hindered. The bi-triazole pyridine ligand (**Lb**) shows best performance regarding light emission. Apparently there is a Goldilocks effect, a too small ligand (**La**) does not protect the metal ion enough from OH oscillators, while a bigger ligand (**Lc**) might be too bulky to bind in an optimal way.[21, 22]

Furthermore lanthanide emission in water was shown, indicating that the Tb-**Lb** complex can even function in water based media making this a potential candidate for biological studies in water based media. The emission of light by lanthanides in water is difficult to achieve due to the overwhelming presence of quenching OH oscillators, making the emission even more important.

The use of the Job's plot method provides a clear ratio for complexes formed with **La** of 1:1. Complexes of Tb (III) and Eu (III) with **Lb** and **Lc** in methanol and terbium and **Lb** in water show no clear stoichiometric point, indicating that the binding is either dynamic or more than one species are present.

4. Experimental

4.1. Materials and instrumentation

All chemicals were purchased from Sigma-Aldrich and used without further purification. Technical grade solvents were used for reactions and recrystallizations. NMR spectra were obtained using a Varian Mercury Plus (400MHz), a VXR-S (300MHz) or a Varian Mercury Plus (200MHz). Δ

In the synthesis of ligands precautions have to be taken to avoid any contact with metal as it results in formation of complexes, manifested in the compounds turning yellow and solutions turning purple when touched with a metal spatula. No metal needles or spatulas could be used so syringes were used without needle and custom made glass spatulas were used.

4.1.1. Synthesis of Lb

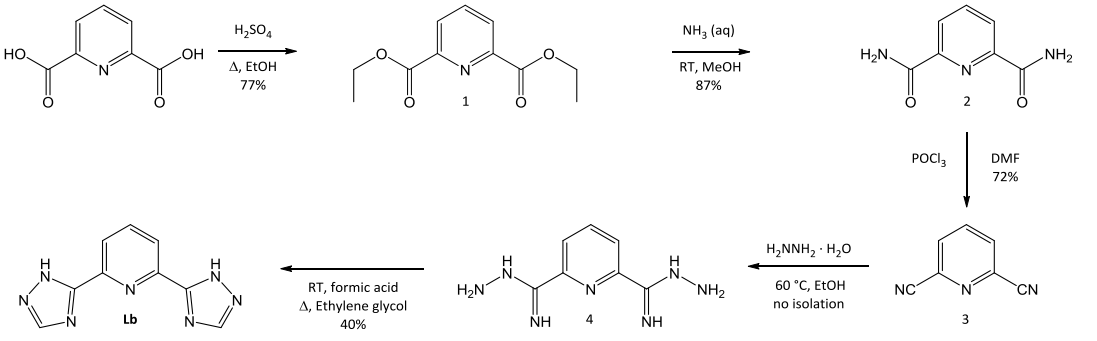

Figure 19: Synthesis of **Lb**

Diethyl pyridine-2,6-dicarboxylate (1)

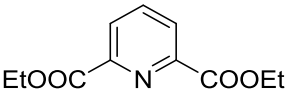

20.0 g (0.12mol) of pyridine-2,6-dicarboxylic acid was suspended in 140 mL of ethanol. 3 mL of concentrated sulfuric acid was added and the milky white solution was heated at reflux overnight. The resulting clear mixture was allowed to cool to room temperature and the ethanol was removed in vacuo. The resulting oil was neutralized with a saturated $NaHCO_3$ aqueous solution and extracted with 2 x 100 mL of dichloromethane. The combined organic layers were washed with 2 x 100 ml of brine and the solvent was removed in vacuo. The resulting oil solidified upon standing, yielding 20.63 g (92.41 mmol, 77.2%) of solid white product. ^{1}H NMR (300 MHz, $CDCL_3$) δ 8.42 – 8.16 (d, *J* = 7.8, 2H), 7.97 (t, *J* = 7.8, 1H), 4.46 (q, *J* = 7.1, 4H), 1.43 (t, *J* = 7.1, 6H). ^{13}C NMR (101 MHz, $CDCl_3$) δ 165, 149, 138, 128, 62, 14.

Pyridine-2,6-dicarboxamide (2)

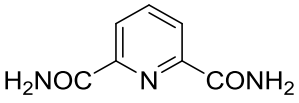

10.0 g (44.80 mmol) of **1** was dissolved in 9 mL of methanol. The solution was added slowly to 45 mL of stirring ice cooled 25% aqueous ammonia. A precipitation occurred after a half hour and 21 mL of methanol was added. The solution was stirred at room temperature overnight. The product was collected by filtration and washed with cold methanol, yielding 6.47 g (39.17 mmol, 87%) of white product. ^{1}H NMR (300 MHz, DMSO-D_6) δ 8.85 (s, 2H), 8.21 – 8.06 (m, 3H), 7.67 (s, 2H). ^{13}C NMR (75 MHz, DMSO-D_6) δ 166, 150, 140, 125.

Pyridine-2,6-dicarbonitrile (3)

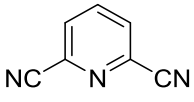

4.00 g (24.22 mmol) of **2** was dissolved in 100 mL of DMF and warmed (90 °C) until clarification. The solution was cooled to 0 °C and 4 mL of $POCl_3$ was added drop wise. The resulting clear, yellow solution was stirred at room temperature (20 °C) for 3 h. 100 mL of dichloromethane were added and the combined organic layers were washed with 2 x 100 mL of water. The organic layer was reduced in volume in vacuo until a thick mixture was obtained. The product was crashed out by addition of a small amount of ice, filtered, washed with water and dried, yielding 2.32 g (17.97 mmol, 72%) of white crystals. ^{1}H NMR (300 MHz, DMSO-D_6) δ 8.40 – 8.26 (m, 3H). ^{13}C NMR (50 MHz, DMSO- D_6) δ 141, 134, 133, 117.

Pyridine-2,6-bis(carboximidhydrazide) (4)

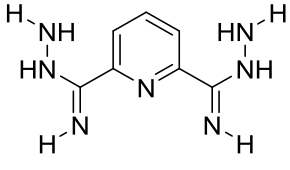

2.2 g (17.04 mmol) of **3** was dissolved in 40 mL of ethanol. 16 mL of hydrazine monohydrate was added and the solution was stirred at 60 °C for 2 h. The solution was allowed to cool to room temperature. The product was obtained by filtering, washed with cold methanol (-4 °C) and air dried. The product was used immediately in the next reaction.

2,6-di(1H-1,2,4-triazol-5-yl)pyridine (Lb)

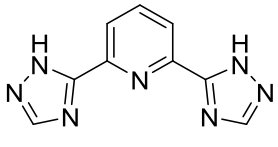

30 mL of formic acid was cooled to 0 °C and **4** was added in small portions. After **4** was dissolved the mixture was stirred for 3 h at room temperature (20 °C). The acid was removed in vacuo. The resulting thick mixture was heated at reflux with 2 mL of ethylene glycol for 70 min. The mixture was allowed to cool to room temperature. 20 mL of methanol were added and the mixture was heated at reflux for 20 min. After cooling to room temperature the product was filtered, washed with diethyl ether and air dried. 1.46 g (6.86 mmol, 40% in two steps) of product was obtained as white powder. ^{1}H-NMR (300 MHz, DMSO-D_6) δ 14.39 (s, 2H) δ 8.31 (s, 1H), 8.09 (s, 2H). M.P. > 335 °C. DART MS spectrum: M+ 213.10 Da (100) and Da 214.20 (22%) and Da 214.13 (6) Calculated: m/z: 213.08 (100%), 214.08 (9.7%), 214.07 (29.3%)

4.1.2. Synthesis of Lc

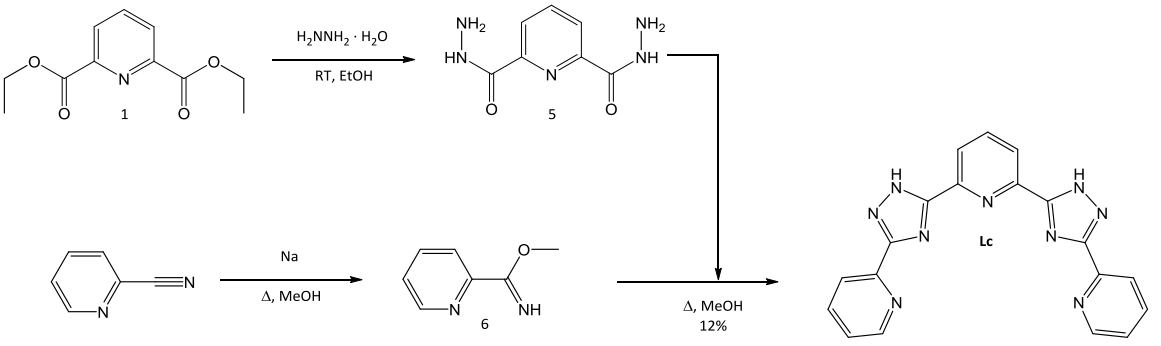

Figure 20: Synthesis of **Lc**

1,3-bis(3-(pyridin-2-yl)-1H-1,2,4-triazol-5-yl)pyridine (Lc)

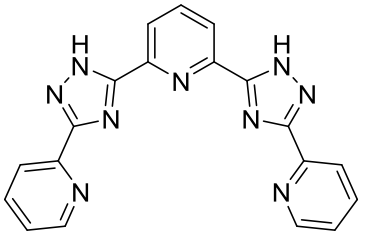

0.5 g of sodium was added slowly to 100 mL of ice cooled methanol and 10 g (96.05 mmol) of cyanopyridine (**14**) was added , the mixture was heated to reflux for 3 h, resulting in a solution of methyl benzimidate **15**. Concurrently 10 g of **6** was dissolved in 100 mL of ethanol and 25 mL (10 equivalents) of hydrazine monohydrate was added. The mixture was stirred at room temperature for 1 h. The precipitate was filtered and washed with cold ethanol (0 °C), yielding the pyridine-2,6-dicarbohydrazide **13**. The precipitate (**13**) was added slowly to the methyl benzimidate solution (**15**) at room temperature. The resulting mixture was heated at reflux for 2 h. The solution was allowed to cool to room temperature and the precipitate was collected by filtration and washed with cold ethanol (0 °C). The resulting solid was heated to reflux in 20 mL of ethylene glycol. The cooled solution was filtered and the solids were recrystallized from ethanol. ^{1}H-NMR (400 MHz, DMSO-d_6) δ 15.06 (s, 2H), 8.75 (s, 2H), 8.25 (m, 5H), 8.01 (s, 2H), 7.54 (s, 2H). M.P. 208.4-209.1 °C. DART MS spectrum: M+ 365.03Da (100%) and 366.11 Da (23%) and 367.12 Da (3%) Calculated: m/z: 365.14 (100%), 366.14 (24.8%), 367.15 (2.5%)

4.1.3. Methanol solutions

The formation of the lanthanide complexes was investigated using stock solutions of known molarity for all ligands and lanthanide salts in methanol. Micro pipettes (Gilson) were used to mix the stock solutions and dilute them to a molarity, which is measurable by all spectrometers used. The pOH of the methanol used for the measurements was adjusted by using a sodium methoxide methanol solution.

4.1.4. Aqueous solutions

Dissolution of ligand **b** in water can be troublesome, when using high concentrations of ligand addition of base is needed for successful deprotonation of the ligand. Under presence of air the high pH of the solution causes formation of insoluble lanthanide carbonates making

this route unsuccessful. Degassing the solution is an option for spectroscopic measurements but is not possible when using in vivo techniques. However deprotonation by base addition is not needed when working at low concentrations but due to the low concentration this will result in lower light yield.

4.1.5. UV/Vis absorption spectroscopy

All absorption spectra were recorded using a Specord S600 spectrometer, with a 73.4 µM solution of ligand in methanol in quartz or plastic cuvettes. All titrations were performed by using a NE-4000 syringe pump. A quartz cuvette equipped with a stirring bar was used for the titrations.

4.1.6. Vis and NIR emission spectroscopy

All emission spectra were measured in a 90° configuration between the excitation source and the detector. A 150 Watt Xe arc lamp coupled to a Zolix 150 mm monochromator was used as excitation source to provide monochromatic excitation, filtered with a 530 nm short pass filter (Semrock). A Thorlabs fiber coupled cuvette holder was used. A 450 nm long pass filter was used before the collection optics. A Newton EMCCD (Andor Technology) coupled with a Shamrock SR-303i spectrograph was used to record emission spectra. The detector was calibrated using fluorescent room lights. Complexation was analyzed using solutions of ligand in methanol in a quartz or plastic cuvette. All titrations were performed using a NE-4000 syringe pump, together with a 1 cm path length quartz cuvette fitted with a stirring bar. Quantum yields were determined relative to that of $[Ru(bpy)_3]^{2+}$ in air equilibrated water.[23]

For NIR emission a glass cuvette was used to reduce absorption by the cuvette in the NIR region. A 355 nm laser was used and the emission was detected by an Idus InGaAs-detector.

4.1.7. Time resolved emission spectroscopy

The time resolved emission spectra of the complexes were recorded in methanol in 5 mm glass NMR tubes. The complexes were excited using a Nd:YAG pulsed laser (355 nm, 6 ns FWHM). Detection by an Andor ICCD-Gen2 with a Zolix 300 spectrograph. A digital delay generator (DG535) was used to relay the trigger from the detector to the laser. By increasing the delay time between exciting and detection of the emission (gate opening) a lifetime decay curve could be build up. Lifetime decays were fitted with mono exponential decay functions to obtain emission lifetimes.

4.1.8. Preparation Lb solution in water

The solubility of **Lb** in water is much lower than in methanol, therefor 4.26 mg (20 µM) **Lb** was dissolved in 2 liter of water, stirring 2 days at room temperature resulted in the desired solution.

4.1.9. Job's plot

Job's method was used to determine the composition of the complexes in solution.[2,3] Here, the titration of Tb^{3+} (10 µM in water) with solution of L1 (10 µM in water) was conducted by the syringe pump. Specifically, 11.0 ml of L1 (10 µM in water) was adding to 2.5 ml of Tb^{3+}

solution (10 µM in water) by syringe pump (rate, 15 ml/hour), the process was followed by UV/vis spectroscopy (the solution was kept stirring).

5. Reference

[1] G. A. Crosby, R. M. Alire, and R. E. Whan, J Chem Phys, *vol 34,* **1961**, pg 743.
[2] J. R. Lakowicz, *Principles of Fluorescence Spectroscopy* (Springer US, **2006**).
[3] R. v. Eldik and Grazyna Stochel, *Inorganic Photochemistry, Volume 63 (Advances in Inorganic Chemistry)* (Academic Press,).
[4] W. D. Horrocks Jr and D. R. Sudnick, J Am Chem Soc, *vol 101,* **1979**, pg 334.
[5] A. Beeby, I. M. Clarkson, R. S. Dickins*, et al.*, J Chem Soc Perk T 2, **1999**, pg 493.
[6] J. G. Buenzli, Chem. Rev., *vol 110,* **2010**, pg 2729.
[7] M. F. Reid and F. Richardson, J Phys Chem, *vol 88,* **1984**, pg 3579.
[8] M. Albrecht, O. Osetska, J. Klankermayer, R. Froehlich, F. Gumy, and J. G. Buenzli, Chemical Communications, **2007**, pg 1834.
[9] P. Coppo, M. Duati, V. N. Kozhevnikov, J. W. Hofstraat, and L. De Cola, Angewandte Chemie-International Edition, *vol 44,* **2005**, pg 1806.
[10] V. M. Mukkala, M. Kwiatkowski, J. Kankare, and H. Takalo, Helv. Chim. Acta, *vol 76,* **1993**, pg 893.
[11] V. M. Mukkala and J. J. Kankare, Helv. Chim. Acta, *vol 75,* **1992**, pg 1578.
[12] A. Dossing, European Journal of Inorganic Chemistry, **2005**, pg 1425.
[13] M. G. B. Drew, M. J. Hudson, P. B. Iveson, M. L. Russell, and C. Madic, J Chem Soc Dalton, **1999**, pg 2433.
[14] T. R. Canrinus, thesis on "New anionic ligands for lanthanide emission" (Stratingh Institute for chemistry, **2014).**
[15] P. Dijkstra, D. Angelone, E. Talnishnikh, H. J. Wortche, E. Otten, and W. R. Browne, Dalton Trans, *vol 43,* **2014**, pg 17740.
[16] P. Job, Ann Chim, *vol 9,* **1928**, pg 113.
[17] E. S. Andreiadis, R. Demadrille, D. Imbert, J. Pecaut, and M. Mazzanti, Chemistry–A European Journal, *vol 15,* **2009**, pg 9458.
[18] M. Nazarov, *New Generation of Europium-and Terbium-Activated Phosphors: From Syntheses to Applications* (CRC Press, **2011**).
[19] A. Chauvin, F. Gumy, D. Imbert, and J. G. Bünzli, Spectroscopy letters, *vol 37,* **2004**, pg 517.
[20] S. Comby, D. Imbert, A. Chauvin, J. G. Bünzli, L. J. Charbonnière, and R. F. Ziessel, Inorg. Chem., *vol 43,* **2004**, pg 7369.
[21] R. Southey, *Goldilocks and the Three Bears* (Longman, London, 1837)
[22] P. Davies, *The Goldilocks enigma: why is the universe just right for life?* (Houghton Mifflin Harcourt, **2008**).
[23] M. Montalti, A. Credi, L. Prodi, and M. T. Gandolfi, *Handbook of photochemistry* (CRC press, **2006**).

Chapter 7

Perspective

In this last chapter an overview of the progress as described in this thesis and a perspective is given. Future challenges and directions will be discussed to aid future efforts towards novel liquid scintillator technologies.

Overview

The work described in this thesis is built on decades of research into radiation detection, and focused on the central question as to whether a new generation of scintillators could be produced. The final answer to this question was that this is indeed possible as was shown with the scintillator cocktail described in this thesis. There were however some hurdles which needed to be taken to come to this final result. The research performed in this thesis addresses therefore a broad range of scientific methods; organic synthesis, chemical and physical characterization, radiation measurements, and lead to comparisons and photophysical model development.

Chapter 1 describes the field under investigation, or more correctly the fields under investigation as the work in this thesis requires knowledge of radiation detection, fluorescence and the use of scintillators. The focal point of the foreseen application is large scale detectors where the most appropriate detector type, i.e. liquid scintillator, is the main focus with specific attention to energy transfer in liquid scintillators.

Chapter 2 describes the synthesis of triazoles and subsequent formation of a new class of compounds; boron triazole complexes. By modifying the ligand system surrounding the boron diphenyl core the luminescence properties of the system can be tuned to different absorption and emission wavelengths. The high quantum yield and molar absorption coefficient of the boron triazoles were indicators that these compounds showed promise to be used successfully in liquid scintillators technology.

In the chapter 3 the full potential of boron triazoles as liquid scintillators was investigated. By exposing the ITS cocktail to gamma radiation a spectrum of the source could successfully be reproduced. The low light yield of the scintillator cocktail limited the rate of data acquisition and subsequent analysis, encumbering precise and speedy determination of radioactivity. The current boron cocktail can certainly be used to detected radiation; however, modification of the ligands to enhance solubility must be balance with other factors to see increased performance. An advantage of the complexes is the flexibility provided by the convergent synthetic route to 1,2,4-triazoles.

The fluorophores developed in chapter 3 were applied in chapter 4. Chapter 4 reports the comparison between EJ-309 and the boron triazole cocktail using photophysical methods. Absorption and emission spectra probed the overall efficiency of the system and show that boron triazoles suffer from low solubility and relative high self-absorption (inner filter effects).

Improvement in the efficiency of the boron triazole cocktail was pursued through gaining insight into the energy transfer processes as described in chapter 5. By using a model scintillator several pathways for energy transfer were investigated. By caring out experiments on different components of the scintillator systems under relevant conditions, it is now clear that the standard approach to photophysical studies and expectations are not directly applicable to scintillator photophysics.

In chapter 6 an alternative use of triazole based ligands is explored in their use in lanthanide complexation and the study of their photophysical properties. In methanol and in water these complexes show promise as luminescent probes, however, the precise composition of the complexes formed remain to be elucidated. An important finding is that an increase in denticity does not necessarily translate to an increase in ligation efficiency.

Future

The key aspect that emerged as most important during the execution of the research described in this thesis is the interplay/mutual dependence of the various components in the scintillator. From a photophysical perspective the boron-triazole compounds possess all requirements to function as a scintillator; high molar absorption and high quantum yield. Under scintillator conditions several challenges were encountered; solubility - which is not normally a problem in photophysics! - is low compared to existing scintillators and furthermore high self-absorption diminishes the yield of emission detected. For future applications increased solubility by use of “solvating groups” is an important objective as well as decreasing the spectral overlap of absorption and emission bands of the fluorophore. On the positive side, however, the use of a single fluorophore is promising as was shown in this thesis, and further modifications could even lead to the necessary improvements needed to the application. Permutations of the robust triazole backbone, which as was shown to be easily modified, is therefore the most prospectful approach.

The energy transfer pathways in liquid organic scintillators have been elaborated by the work in this thesis; a possibility which allows further exploration of the method as a model scintillator cocktail. The approach facilitates the search for different (or even better) model scintillator cocktails but also opens the field to actually improve energy transfer pathways in the scintillator device. Coupled with our clarification of scintillator behavior under high concentration conditions, enables the search for improved scintillator cocktails.

Although the work presented in this thesis is somewhat off the beaten track in terms of molecular photophysics research, advances in understanding of scintillator technology are urgently needed. An improvement of liquid scintillator technology enables/improves the world of radiation physics to start many new large scale experiments. It would enable the mapping of radionuclides in the Earth, monitoring of nuclear power reactors for non-proliferation, provide suitable targets for long beam line experiments and might even provide an answer why the universe is comprised of matter (and not antimatter).

Appendix A

PMT CHARACTERISATION

A.1. Introduction

Photomultipliers (PMTs) are a commonly used for radiation detection.[1] In this thesis PMTs have been used for characterization of scintillator cocktails and to test the PHASE. The final goal is to use PMTs in combination with liquid scintillators in radiation detectors.

A complete setup consisting of photomultiplier with integrated voltage divider and removable scintillator cell was provided by Scionix (figure B.1). After initial testing it was noted that measurements done with this PMT displayed traces going through zero (also known as ringing). Since this artefact was caused by faulty hardware Scionix modified the PMT assembly so it was able to cope with the fast signals (nanosecond timescale) generated by our scintillators.

Figure B.1. Scintillator cell with PMT housing connected to 100 MHz PHASE.
(Picture Deborah Roffel, INCAS[3])

In order to assure correct response of the PMTs to incoming signals, tests were performed to verify the response of the PMT to different light intensity, driving voltage, and wavelength of incoming light.

A.2. Experimental

A calibrated white light source (avantes avalight-hal-cal) was connected via a fiber optic cable to a Zolix-λ 3007 monochromator. Light coming out of the monochromator was directly shone on the PMT window (figure b.**2**). The PMT was connected to a ISEG high voltage supply and a Tektronix DPO 4032 350 MHz oscilloscope. The setup was controlled by a custom written LabVIEW program. Light intensity was controlled by varying the width of the monochromator entrance from 3 to 0.1 mm. A 1-120-500 grating was used in the monochromator.

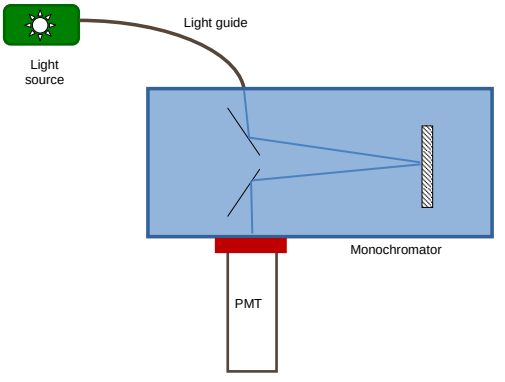

Figure B.2. PMT measurement setup

A.3. Results

A.3.1. Varying intensity of the light

With fixed wavelength (420) and two fixed driving voltage (1.35 and 1.8 kV) the intensity of the incoming light was varied by changing the width of the slit through which the light passes into the monochromator.

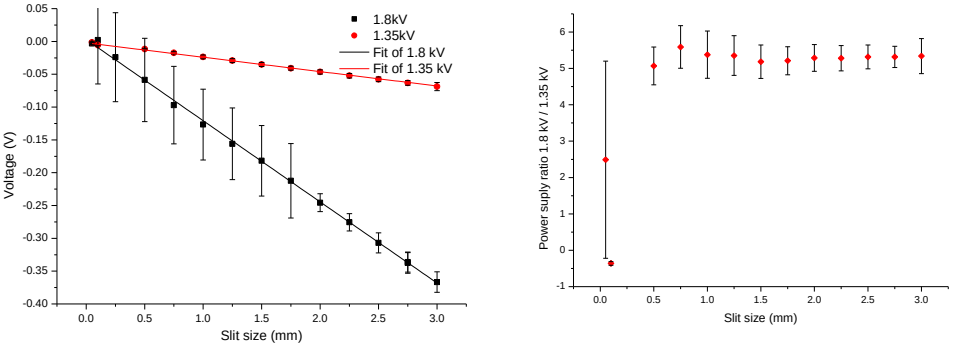

Figure B.3: Response of PMT at different light intensities with 420 nm excitation (left). Ratio of different driving voltages at different light intensities (right).

Figure B.3 shows the response of the PMT to have a linear character for both low intensity and high intensity. A linear fit (y = a + b * x) to the 1.8 kV is represented by y = 0.00293 – 0.1237 * x and the fit of the 1.35 kV measurement is represented by a line of y = 0.00213 – 0.02191 * x.

Figure 3 (right) shows that there is a constant ratio between the two intensities. With the slit opening ranging from 0.5 mm to full open the ratio 1.8 kV / 1.35 kV has a fixed value of around 5.3 ± 0.3. This value is close to the ratio of the two fitted functions of 5.65, the deviation arises from the difference in intercept of the two functions. With smaller slit size the error of measurement is too high to get reliable results.

A.3.2. Varying driving voltage

With fixed wavelength (420 nm) and two different slit widths (0.25 and 3 mm) the driving voltage of the PMT was varied, ranging from 1.3 to 1.95 kV.

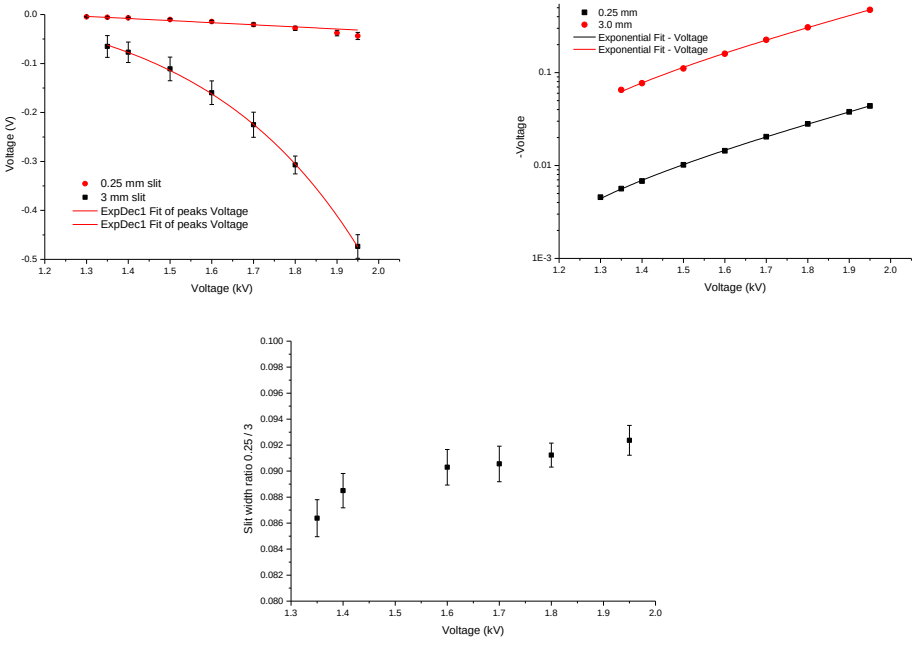

Figure B.4. Response of PMT at different driving voltages with 420 nm excitation. Top left: linear y-axis, top right: logarithmic y-axis, bottom: ratio between 0.25 and 3 mm slit width.

Figure B.4 (top right) displays an exponential response to driving voltage with low and high light intensity as is expected with PMTs.[2] The absolute results of measurements can be fitted with the function $y = y_0 + A * \exp(R_0 * x)$. For the 0.25 mm slit this results in the function y = -0.00358 + 2.26553 * 10-4 * exp(2.74031 * x) and for the 3.0 mm slit the function is y = -0.04358 + 2.98 * 10-4 * exp(2.64564 * x). As figure 4 (bottom) indicates there is a minimal difference in ratios between 3.0 and 0.25 mm slit width.

A.3.3. Varying Wavelength

With fixed driving voltage (1.35 kV and 1.8 kV) and two fixed light intensities (3.0 and 0.25 mm slit width) the response of the PMT to different wavelengths was measured.

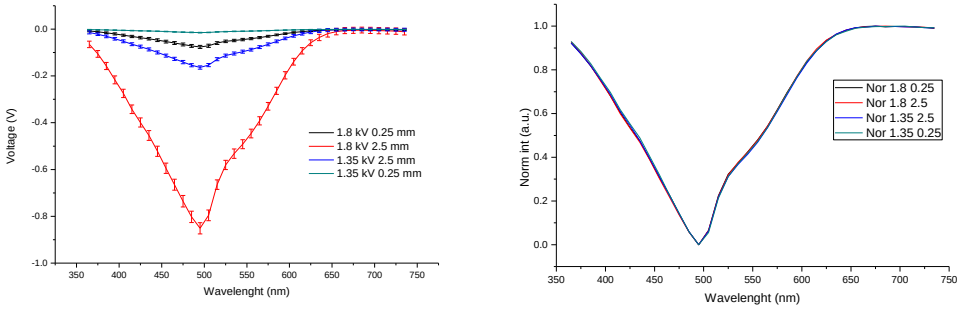

Figure B.5. PMT response at different wavelengths (left) and normalized PMT response (right)

As can be seen from figure B.5 the response with high light intensity and high driving voltage gives the highest response, as is expected. The form of all responses is identical, which becomes clear from the normalized response where all traces overlay nearly perfect. This shows that changing light intensity or driving voltage only influences the intensity of the trace.

A.3.4. Optimal wavelength

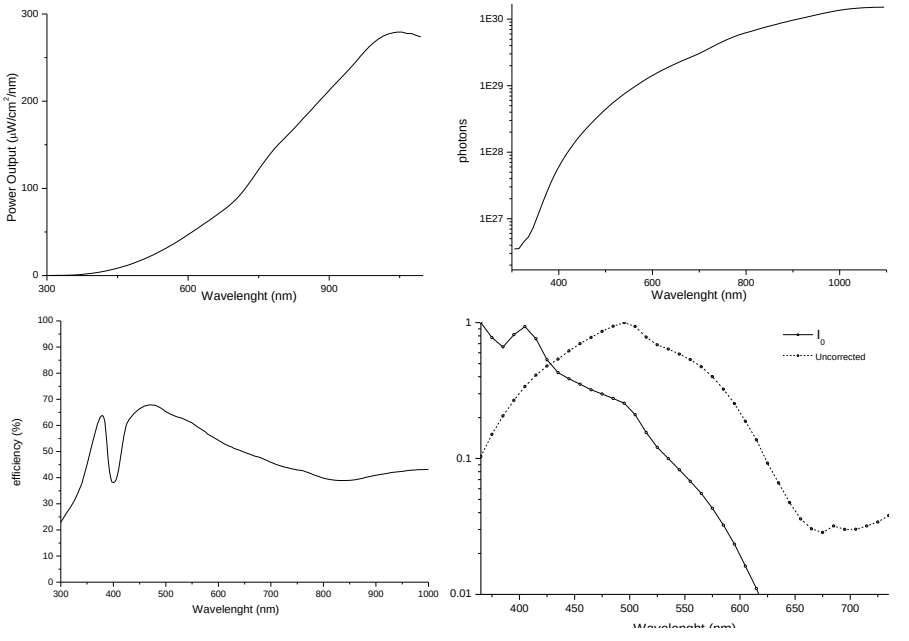

Figure B.6. Output of light source at different wavelengths (top left), output of photons per wavelength (top right), efficiency of monochromator grating at different wavelengths (bottom left), corrected and uncorrected response of PMT (bottom right).

Figure B.6 shows that the PMT is most sensitive for light with a wavelength of 500 nm. However the light source does not provide a constant output over all wavelengths. Figure B.6 shows that in the UV range the power output is minimal while the maximum is reached in the IR range. Since a PMT does not count power but photons the lamp output is divided by the Planck constant to yield the amount of photons at each wavelength (figure B.6 top left).

Another factor influencing the light intensity at a specific wavelength is the efficiency of the grating in the monochromator. Figure B.6 (left bottom) shows this efficiency and as can be seen there is a large dip in grating efficiency around 400 nm. The measured intensity of the PMT is related to the number of photons and grating efficiency by the formula

$$I_{meas} = I_0 * hv * Gr_{eff} \quad \textbf{1}$$

Where I_{meas} is the uncorrected measured intensity, I_0 the real intensity, hv the photon count and Gr_{eff} the efficiency of the grating. Obtaining the corrected original intensity can be done by using formula 2.

$$I_0 = I_{meas} / (hv * Gr_{eff}) \quad \textbf{2}$$

This yields graph B.6 (bottom right) which shows that the maximum response of the PMT is shifted to the blue. The real position of the maximum is hard to pinpoint. The low values for light intensities at low wavelengths introduce a large error in this region.

A more elaborate setup to obtain a well-defined corrected spectrum was unsuccessful due to the low intensity of the light source.

A.4. Conclusions

The PMT responds as expected. Changing light intensity, driving voltage or wavelengths results in the expected intensity change. A well-defined point for maximum efficiency concerning wavelength cannot be given.

Appendix B

TIME CORRELATED SINGLE PHOTON COUNTING (TC-SPC)

B.1. Experimental

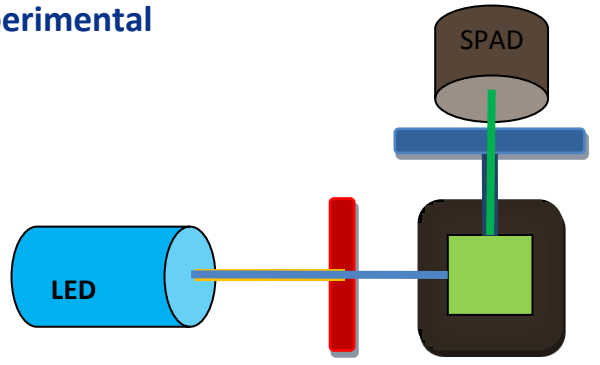

Figure B.1. TC-SPC set-up: light emitted by an LED (blue cylinder) is passed through a filter (red) and is absorbed in the cuvette (green square). Emitted light passes through a high pass filter (blue) and is absorbed by a single photon avalanche diode (SPAD, grey cylinder).

For time correlated single photon counting (TC-SPC) the sample, a cuvette filled with the scintillator cocktail, is excited by means of a pulsed light source of very low intensity, therefore exciting only a few molecules per pulse (figure B.1). The light is passed through a band pass filter, removing all unwanted wavelengths and is absorbed in the cuvette. The light emitted by the excited molecules is measured at a 90° angle, with respect to the incoming beam. The emitted light is passed through a high pass filter to eliminate scatter light and remaining light is measured by means of a single photon avalanche diode (SPAD). By choosing light sources with different emission wavelengths the sample can be excited at those different wavelengths (255, 350 and 450 nm) and therefore each compound in the mixture can be excited selectively. Inserting a filter, (bandpass or cut-off type) between the cuvette and the detector determines which specific wavelengths can be measured by the detector. This ensures the monitoring of the emission of only one component from the total mixture. Temperature control ranging from -10 to 80 °C allows investigation of temperature dependence of the fluorescence lifetime.

B.2. Fluorescence lifetime measurements; a short intro

The fluorescence lifetime of a liquid sample can be determined by means of TC-SPC. With this technique a photon is sent into the fluorescent solution and the time required to arrive at the detector is measured. This spread of arrival times is converted into a histogram of time versus intensity. Over time a fluorescence decay profile is built up (figure B.2, blue line). The fluorescence lifetime is defined as $\tau = \frac{I_0}{e}$, but simply determining this value from the graph

ignores the characteristics of the measurement setup.[1] What should be taken into consideration is that the generated light pulse is not of instantaneous character but possesses a certain width and the travel time of the light pulse needs to be taken into consideration. Measuring diffuse reflections of the pulsed source provides the instrument response function (IRF, figure B.2, red line). By means of reconvolution the IRF signal from the measured signal the pure signal from the fluorescent sample can be determined (black line, overlaid over the blue line).

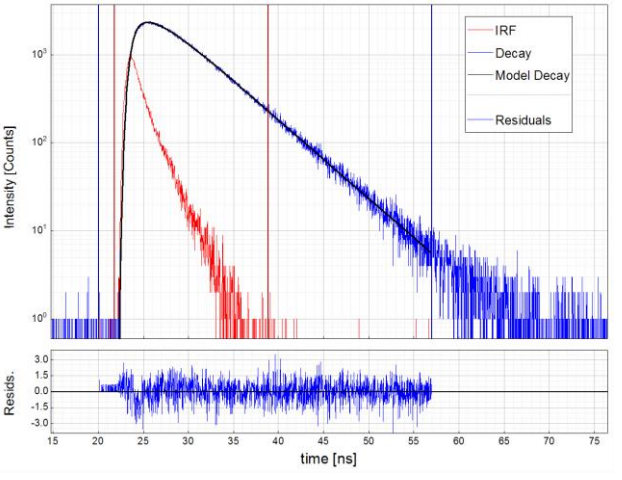

Figure B. 2. Histogram of the fluorescence lifetime of LAB (blue line), the instrument response function (IRF, red line) and the fitted function (black line).

B.3. Justifying TC-SPC as excitation of the scintillator instead of nuclear radiation

Precise timing in experiments when using a radioactive source are difficult, either using a ^{22}Na source or more elaborate setups.[2] Furthermore the use of radioactive sources falls under strict guidelines. As excited state of a molecule is not dependent on the origin of excitation energy light can be used instead of nuclear radiation.[2] TC-SPC is a simple, nuclear radiation free setup, with its very low level light output, it mimics the burst of energy associated with that of a gamma ray.

The energy of the pulsed LED from the TC-SPC setup has a very low power of only 1 pJ, this amounts to about 100.000 photons per pulse, which is comparable with the amount of light generated by a 511 gamma ray from ^{22}Na (around 50.000 photons).

References

[1] J. R. Lakowicz, *Principles of Fluorescence Spectroscopy* (Springer US **2006**).
[2] G. F. Knoll, *Radiation detection and measurement* (John Wiley & Sons USA **1989**).

GLOSSARY

λ_{abs}	wavelength of absorption
λ_{em}	wavelength of emission
τ	fluorescence lifetime
Φ	quantum yield
ADC	analog to digital converter
DIN	di-isopropylnaphthalene
ED	electronic dipole
FPGA	field programmable gate array
HOMO	highest occupied molecular orbital
HVPS	high voltage power supply
IAEA	international atomic energy agency
IRF	instrument response function
ITS	INCAS³ triazole scintillator
keV	kilo electron volt
keVee	kilo electron volt electron equivalent
kV	kilovolt
LAB	linear alkyl benzene
LOS	liquid organic scintillator
LSC	liquid scintillator cocktail
LUMO	lowest unoccupied molecular orbital
MD	magnetic dipole
MeVee	mega electron volt electron equivalent
NCA	neutron capture agent
PMT	photomultiplier
POPOP	1,4-bis(2-phenyloxazole-5-yl)benzene
PPO	2,5-diphenyloxazole
PS	pseudocumene
PSD	pulse shape discrimination
PXE	phenyl xylyl ethane
tSIE	transformed spectral index of the external standard
WLS	wavelength shifter

SUMMARY

Fluorescence

The focus of the studies in this thesis is the absorption and emission of light by small molecules. Fluorescence is the process in which light is absorbed by a substance (called a chromophore) and if it is also a fluorophore then the energy is re-emitted as light with a longer wavelength (figure 1). The color of light depends on the wavelength of the light; with blue light (400 nm) each photon contains more energy than red light (700 nm). One of the applications of fluorophores is in scintillators, liquids which emit light when they are exposed to radiation.

Figure 1. Fluorescence in dilute solution; UV light (known as black light in dance clubs) irradiating various fluorescent solutions. Every solution emits a specific color of light. From left to right: 2 different boron triazoles, bodipy, fluorescein and rhodamine G6.

Radiation

The radiation that scintillators absorb comes from everywhere and from many different sources (outer space, soil, and even bananas[*]) and types (alpha particles, gamma rays, visible light). A few of these sources are readily detected; such as visible light and the heat (infrared radiation), however some forms of radiation are more difficult to detect; neutrinos for example. A neutrino is a particle so light, and neutral in charge, that it has (almost) no interaction with matter.[†] At any given moment billions of neutrinos go through every human being, but, on average, only one reacts every 30 years. So if this particle is so difficult to detect, does it actually make sense to try and detect it?

[*] The B.E.D (banana equivalent dose) is a measure for how much radiation a banana contains (equivalent to 0.1 μSv). The received dose per day for a human being is around 100 B.E.D.

[†] The mass of a neutrino is estimated to be about a 10 millionth of that of the electron.

A neutrino is formed through nuclear reactions, e.g. in the sun, space or in a nuclear power plant. Information about the source from which it originated is contained in the neutrino. This provides insight into the nuclear reactions inside the sun or the precise state of a nuclear power reactor. Insight into the specific reactions occurring inside a nuclear power reactor is important as one the products of the reactor is plutonium. Plutonium is a controlled substance and is strictly controlled by the IAEA to limit the proliferation of nuclear weapons. Due to the harsh conditions inside a reactor direct monitoring is difficult as sensors are blasted by large amounts of radiation. Indirect monitoring comes with much lower levels of accuracy and thus wiggle room for foul play. A neutrino cannot be manipulated and therefore provides an independent means to establish the amount of plutonium produced in a reactor.

The primary reaction, if a large liquid filled neutrino detector is situated next to a nuclear power reactor, will be the reaction of a neutrino (specifically an electron antineutrino, $\bar{\nu}$) with a hydrogen atom (p) of the organic liquid. This reaction will produce a positron (e^+) and a neutron (n, equation 1). The positron is antimatter; as soon as this encounters its antiparticle (the electron) it will annihilate releasing energy. This energy becomes visible by generating a burst of light, which can be measured by light detectors.

$$\bar{\nu}_e + p \rightarrow e^+ + n \quad \textbf{(1)}$$

$$n + NCA \rightarrow \alpha \text{ or } \gamma \text{ (and byproducts)} \quad \textbf{(2)}$$

The neutron that is produced by the reaction can be captured by a neutron capture agent (NCA, which can absorb a neutron in its nucleus). This atom, now unstable due to the extra neutron will undergo nuclear decay and emit a gamma ray (γ) or alpha particle (α). This subsequent radiation will also result in a burst of light which can be detected by photodetectors. The step from radiation absorbed in the detector to visible light which can be detected by photodetectors can be performed by liquid scintillators.

Scintillators

The combination of fluorescence and radiation results in a scintillator, a substance which will emit light if there is radiation present. Scintillators come in many varieties; crystals of several centimeters in size, plastic strips or wires several meters long, or as a liquid. Liquid scintillators, comprised of a solvent and fluorophores, have the advantage that their size is governed by the size of their container, enabling the fabrication of detectors of several cubic meters of volume, which are well suited to detect low levels of radiation.

In a scintillator the solvent will absorb the energy of the incoming radiation and transfer this to the fluorophore which is dissolved in the scintillator. The solvent in a liquid scintillator is a so called aromatic solvent as these can readily absorb and emit the energy deposited by nuclear radiation. The downside of these aromatic solvents is their ready flammability, leading to safety risks. A second downside is that common scintillator cocktails use two or more fluorophores which reduces the efficiency of the energy transfer processes.

New scintillator cocktails

The development of a new fluorophore, dissolved in a solvent with reduced flammability would produce a new safe scintillator cocktail with good radiation detection properties.

Boron triazoles

Fluorescent compounds are often complex organic molecule or contain exotic metals, pushing up the cost of production. By combining a simple organic molecule with the non-exotic element boron it is possible to fabricate a fluorescent compound; a boron triazole complex (figure 1; left 2 bottles and figure 2 right side). The synthesis and characterization of this complex is the subject of chapter 2 of this thesis.

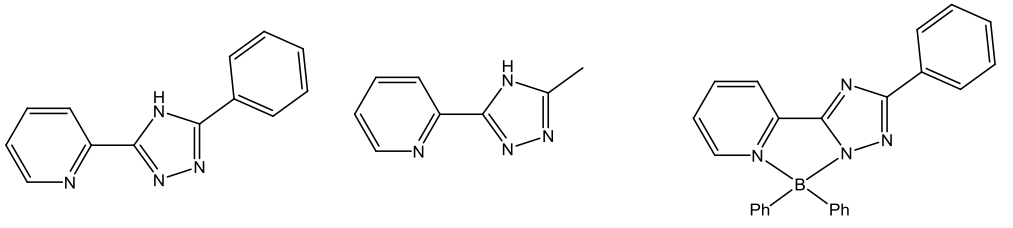

Figure 2. Examples of two triazole ligands used in this thesis (left and middle) and a boron triazole complex (right). By changing the structure of the triazole ligand the color of the emitted light can be tuned.

A boron triazole complex is made up of a boron atom surrounded by a triazole ligand and two phenyl groups. The ligand has as core structure a triazole and pyridyl group, with at the 3 position of the triazole ring the ability to employ different substituent. Depending on the type of substituents the system can change the amount of polar character, influencing the color of light emitted.

If light (of correct color) is passed through a solution of boron triazole it will be absorbed and emitted again. The emission color is dependent on the specific type of ligand used, enabling emission from deep purple (<400 nm) to green (> 500 nm, figure 3). A preliminary test with boron triazole dissolved in an aromatic solvent (di-isopropylnapthalene, DIN) showed that this scintillator can actually detect nuclear radiation.

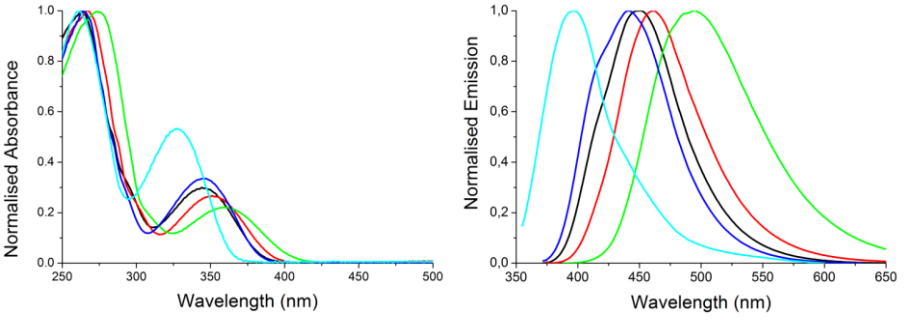

Figure 3. Absorbance spectra of several boron triazoles (left).
Emission spectra of several boron triazoles (right).

Radiation measurements

In chapter 3 the measurement of nuclear radiation by means of a dedicated setup are described (figure 4). This setup consists of a radiation source, light detector, coupled to a measuring cell containing the scintillator cocktail, a high voltage power supply, PHASE and laptop. The PHASE is a by INCAS³ designed signal detector and processor which produces a spectrum of the measured radiation.

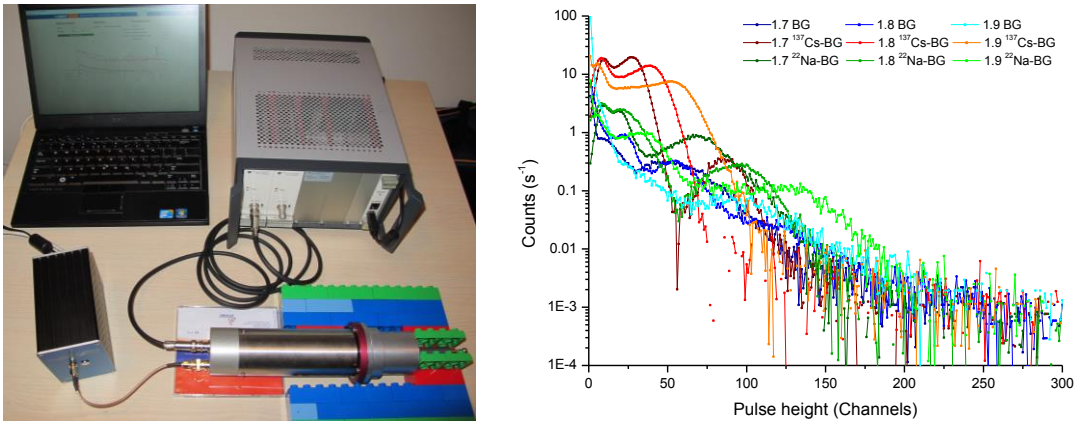

Figure 4. Measurement setup for the detection of radiation (left). Radiation spectra measured with ITS exposed to ^{22}Na and 137 Cs radiation sources at different bias voltages (right).

Two measuring cells, one equipped with EJ-309:5B, a commercial scintillator and the other with ITS, INCAS³ triazole scintillator, our in house scintillator are used to detect the radiation. The radiation which is absorbed will result in a light flash which can be detected by light detectors. By determining the energy of the light pulse it is possible to generate a spectrum of the radiation source.

Comparison between ITS and EJ-309:5B

Chapter 4 delves deeper into the properties of the ITS cocktail to better understand its characteristics. Dissolving the boron triazole in the tested solvents greatly enhances the efficiency of the scintillating function. It was further apparent that an increase in solvability of the boron triazole complex would enhance the efficiency of the scintillator.

Energy transfer in scintillators

A clear model of the energy transfer processes that proceed in liquid scintillators was obtained using a scintillator cocktail using one solvent and a bodipy dye, a fluorophore that emits green light (figure 1, middle bottle). Since the absorption spectrum of the solvent and the bodipy did not overlap, it was possible to study individual processes in the overall energy transfer scheme. It became clear that temperature played an important role in determining the properties of a liquid scintillator.

Lanthanides

Lanthanides, also called rare earth elements,[*] are typically phosphors; i.e. they remit some of the energy they absorb from light as light. However, the ability of lanthanides to absorb light is low in contrast to organic chromophores and are therefore not suitable. However, coordination of an organic ligand such as a pyridyl-triazole to lanthanide ions allows for an increase in the efficiency of light absorption by transfer of the absorbed energy by the ligand to the lanthanide ion. The specific patterns of the emission spectra of lanthanides make them interesting in applications such as labels in in vivo studies, as it is easy to distinguish their emission from other sources of fluorescence. These complexes are shown to form in methanol and in water and in both cases are emissive, which is essential for applications in biomedical science.

Conclusions

The work described in this thesis demonstrates that 1,2,4-triazole based ligands are useful in both boron and lanthanide complexation. The boron triazole complexes investigated are applicable in the detection of radioactivity. It should be noted that improved solubility is in part necessary to reach applicable levels. The lanthanide complexes, although at an early stage, are certainly interesting for biomedical applications given that the form in water readily, however further insight into the coordination chemistry of the triazole based ligands is necessary.

[*] The term rare is a misnomer from ancient times when it was assumed that lanthanides were hard to find. The fact is that they are hard to isolate but are actually rather abundant in the earth's crust and are more common than gold and even, in this thesis also used, boron.

SAMENVATTING

Fluorescentie

Dit proefschrift gaat over hoe sommige stoffen door middel van fluorescentie licht uitstralen. Fluorescentie is het proces waarbij licht door een stof (de fluorofoor) wordt opgenomen, waarna deze energie weer als licht met een iets langere golflengte wordt uitgestraald (figuur 1).[*] De kleur van licht hangt samen met de golflengte van dat licht, blauw licht (400 nm) heeft veel energie terwijl rood licht (700 nm) minder energie heeft. Een van de toepassingen van fluoroforen is in scintillatoren; vloeistoffen die licht geven indien ze worden blootgesteld aan radioactieve straling.

Figuur 1. Verschillende fluorescente oplossingen beschenen met UV licht (blacklight, bekend van de discotheek). Elke oplossing straalt zijn eigen specifieke kleur licht uit. Oplossingen van links naar rechts: twee verschillende boortriazolen, bodipy, fluoresceïne en Rhodamine G6.

Straling

De straling die scintillatoren kunnen opnemen is overal om ons heen, komend uit verschillende bronnen (de ruimte, grond, of zelfs bananen[†]) en in verschillende types (alpha deeltjes, gamma stralen, zichtbaar licht). Sommige straling is eenvoudig te detecteren; zoals zichtbaar licht of warmte (infrarood straling). Sommige vormen van straling zijn problematischer om te detecteren; bijvoorbeeld neutrino's, dit zijn neutrale deeltjes die zo licht zijn, dat ze (haast) niet met iets reageren.[‡] Zo gaan er op elk moment miljarden neutrino's door elk mens, maar reageert er gemiddeld slechts 1 neutrino per 30 jaar. Waarom dan toch de wens om een dergelijk moeilijk te detecteren deeltje te meten?

[*] Fluorescentie kan alleen plaatsvinden van een kortere golflengte (energie rijk) naar een langere golflengte (lager in energie) omdat er altijd enige energie verloren gaat tijdens het proces van energieoverdracht.

[†] De B.E.D (banaan equivalente dosis) is een maat voor de hoeveelheid straling die van een banaan komt (gelijk met 0.1 µSv). Per dag is de ontvangen dosis voor een mens nabij de 100 B.E.D.

[‡] De massa van het neutrino wordt geschat op 10 miljoenste van een electron.

Een neutrino wordt gevormd door kernreacties, o.a. in de zon, de ruimte en in kerncentrales. Uit het neutrino is informatie te halen over uit welke bron hij is ontstaan. Dit levert kennis op over de samenstelling van de zon of de precieze toestand van een kernreactor. Normaliter produceert een kernreactor een kleine hoeveelheid plutonium maar dit kan worden bijgesteld om een grotere hoeveelheid te produceren. Door verdere manipulatie van de kernenergiecentrale is het mogelijk dit extra plutonium uit het toezicht van de IEAE (International atomic energy agency) te onttrekken,* bijvoorbeeld met als doel productie van kernwapens. Echter, de neutrino's geproduceerd door reacties in de kernreactor zijn niet te beïnvloeden; door deze te meten is onafhankelijk vast te stellen hoeveel plutonium er wordt geproduceerd. Doordat de neutrino's door de reactorwand vliegen kan veilig gemeten worden, sensoren die zich binnen de reactor bevinden begeven het snel door de grote hoeveelheid destructieve straling in een dergelijke reactor.

Indien een grote, vloeistof gevulde neutrino detector naast een kernreactor staat zal de voornaamste reactie zijn dat een neutrino (specifiek een electron antineutrino, $\bar{\nu}$) reageert met een waterstof atoom (p) van de vloeistof. Deze reactie levert een positron (e^+) en neutron (n) op (vergelijking 1). Het positron is antimaterie; zodra dit zijn antideeltje tegenkomt (het electron) zullen deze twee elkaar vernietigen onder vrijmaken van energie. Deze energie wordt zichtbaar als lichtflits en kan worden gemeten met lichtdetectoren.

$$\bar{\nu} + p \rightarrow e^+ + n \qquad \textbf{(1)}$$

$$n + NCA \rightarrow \gamma \text{ of } \alpha \text{ (+ bijproducten)} \qquad \textbf{(2)}$$

Het eveneens ontstane neutron kan worden gevangen door een neutron capture agent (NCA, een atoom welke een neutron kan absorberen in zijn kern). Dit atoom, nu onstabiel door het extra neutron in zijn kern, ondergaat nucleair verval waarbij gamma straling (γ) of een alpha deeltje (α) wordt uitgezonden. Ook deze straling veroorzaakt een lichtflits welke weer kan worden gedetecteerd met lichtdetectoren. De stap van straling die wordt geabsorbeerd in de detector tot zichtbaar licht welke door een lichtdetector kan worden waargenomen kan worden gedaan door vloeibare scintillatoren.

Scintillatoren

De combinatie van straling en fluorescentie levert een scintillator, een stof die licht geeft als straling aanwezig is. Scintillatoren komen in verschillende vormen en types: kristallen van enkele tientallen centimeters groot, meters lange plastic stroken of draadjes, of als een vloeistof. Vloeibare scintillatoren, een samenstelling van een oplosmiddel en fluoroforen, hebben als voordeel dat hun grootte beperkt wordt door de container waarin ze zich bevinden, dit maakt het mogelijk om detectoren van vele kubieke meters groot te maken, welke zeer geschikt zijn voor de detectie van kleine hoeveelheden straling.

* Een van de taken van de IAEA is het voorkomen van verspreiding van kernwapens, waarvoor plutonium een grondstof is.

Het oplosmiddel in een scintillator zal de energie van radioactive straling absorberen, de vloeistof zal daarna die energie doorgeven aan de in de vloeistof opgeloste fluoroforen. De vloeistof in een scintillator is een zogenaamde aromatisch oplosmiddel, aangezien deze goed de energie kan opnemen en doorgeven naar een fluorofoor. Het nadeel van deze aromatische oplosmiddelen is echter dat in veel gevallen ze licht ontvlambaar zijn en daardoor zorgen voor een veiligheidsgevaar. Een ander nadeel is dat er in scintillatie cocktails gebruik wordt gemaakt van 2 of meer fluoroforen welke de efficiëntie van de energie overdracht nadelig beïnvloedt.

Nieuwe scintillator cocktails

De ontwikkeling van een nieuwe fluorofoor opgelost in oplosmiddel met verminderde ontvlambaarheid zou leiden tot een nieuwe scintillator cocktail met goede eigenschappen voor stralingsdetectie.

Boortriazolen

Fluorescerende stoffen bestaan vaak uit complexe organische moleculen of bevatten exotische metalen, welke de fabricage ervan prijzig maakt. Door een combinatie van een eenvoudig organische molecuul met het niet-exotische element boor, is het mogelijk een fluorescerende stof te maken; een boortriazool complex (figuur 1; twee linker oplossingen en figuur 2 rechts), de synthese en karakterisering van dit molecuul is onderwerp van hoofdstuk 2.

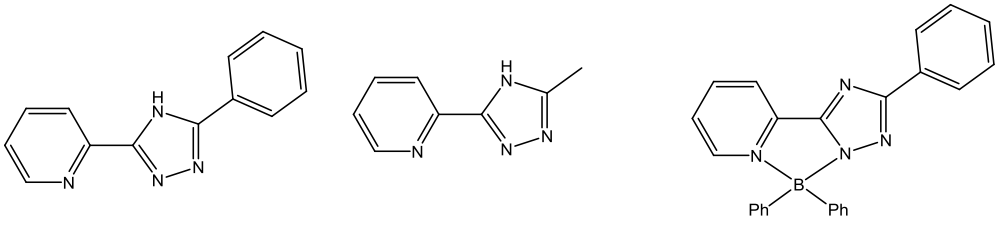

Figuur 2. Enkele triazool liganden gebruikt in dit proefschrift (links en midden) en een boor triazool complex (rechts). Door de structuur van het ligand te veranderen verandert de kleur van het uitgezonden licht.

Een boortriazool complex, als beschreven in dit proefschrift, bestaat uit een boor atoom omringt door een triazool ligand en twee phenyl groepen. Het ligand heeft als hoofdstructuur een triazool en pyridyl groep. Afhankelijk van het type substituenten gekoppeld aan het ligand veranderen de eigenschappen, wat de kleur van het uitgezonden licht verandert.

Indien er licht (van een geschikte kleur) door een oplossing van boor triazool wordt gestuurd, zal deze een gedeelte van het licht opnemen en weer uitzenden. Afhankelijk het specifieke ligand wat wordt gebruikt kan de uitgezonden kleur variëren van diep paars (< 400 nm) tot groen (500 nm, figuur 3). Tests wezen uit dat een boortriazool opgelost in een aromatisch oplosmiddel (di-isopropylnapthaleen, DIN) daadwerkelijk nucleaire straling kan detecteren.

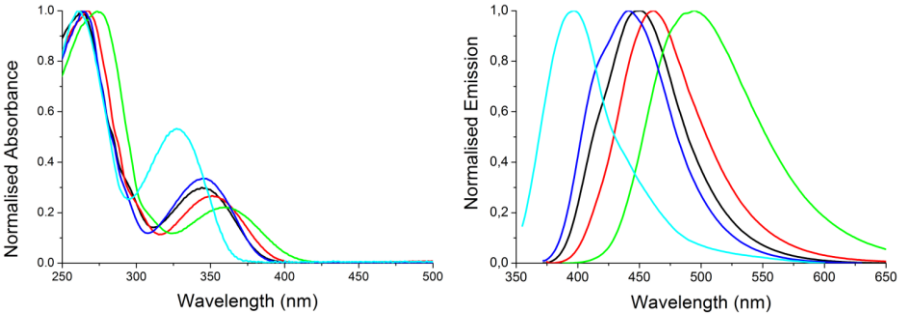

Figuur 3: Absorptie spectra van verschillende boortriazolen (links).
Emissie spectra van verschillende boortriazolen (rechts).

Stralingsmetingen

In hoofdstuk 3 wordt beschreven hoe het meten van straling plaats vindt; een vaste opstelling (figuur 4), bestaande uit een stralingsbron, een lichtdetector gekoppeld aan een meetcel gevuld met scintillator cocktail, een voedingskast, een PHASE en een laptop wordt hiervoor gebruikt. De PHASE is een door INCAS³ gebouwde signaal detector en rekeneenheid, deze genereert automatisch een spectrum van de gedetecteerde straling.

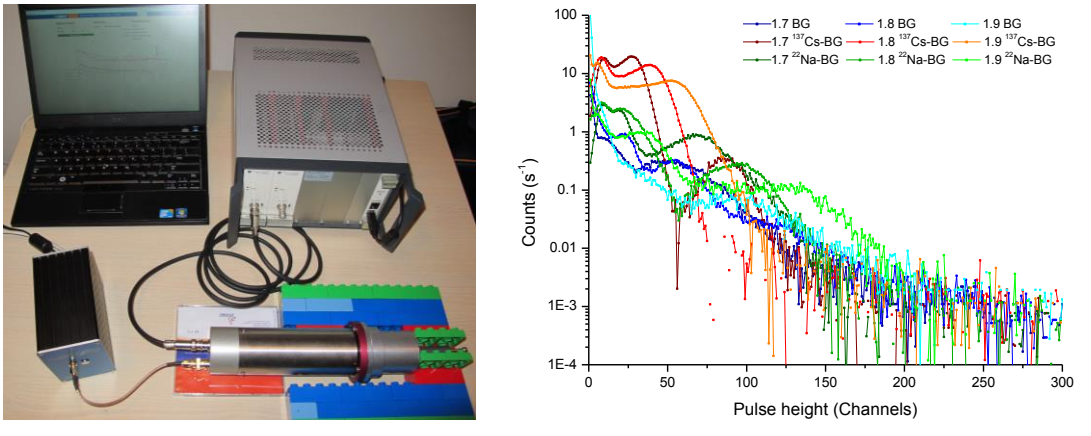

Figuur 4: Meetopstelling voor detectie van straling (links). Stralingsspectra gemeten met ITS, bestraald met ^{22}Na of ^{137}Cs stralingsbronnen bij verschillende spanningen (rechts).

Twee meetcellen, een gevuld met ITS (INCAS³ triazool scintillator, de zelf ontwikkelde scintillator cocktail), de ander gevuld met EJ-309:5B (een commerciële scintillator) zijn gebruikt voor het detecteren van straling. De straling die geabsorbeerd wordt door de scintillator, zal een lichtpuls generen, welke kan worden gemeten door lichtdetectoren. Door de sterkte van de lichtpuls te bepalen kan een spectrum van de radioactieve bron worden opgebouwd.

Vergelijking tussen ITS en EJ-309:5B

Om beter de eigenschappen van ITS te doorgronden is in hoofdstuk 4 dieper op de eigenschappen van deze cocktail ingegaan. Het oplossen van een boortriazool in de geteste oplosmiddelen heeft een sterk verbeterende invloed op de scintillerende werking. Verder is vast komen te staan dat door het verhogen van de oplosbaarheid van het boortriazool de efficiëntie van de scintillator zal verbeteren.

Energieoverdracht in scintillatoren

Om een duidelijk beeld te scheppen van de energieoverdracht in scintillatoren is een versimpeld model scintillator cocktail gemaakt, bestaande uit één oplosmiddel één fluorophore; bodipy, een fluorofoor die fel groen licht uitzend (figuur 1; middelste flesje). Doordat de licht-absorptie van het oplosmiddel en bodipy onderling goed te scheiden zijn was het mogelijk om de afzonderlijke energie overdracht processen te bestuderen. Het is duidelijk geworden dat temperatuur schommelingen van grote invloed zijn op de eigenschappen van de scintillator.

Lanthanides

Lanthanides, ook wel zeldzame aardmetalen[*] genoemd, zijn fosforen; ze zijn in staat om energie welke ze opnemen weer uit te zenden als licht.[†] Echter de mate van licht absorptie is erg laag vergeleken met organische moleculen en dus zijn pure lanthanides niet erg geschikt in lichtgevende toepassingen. Door echter een ligand als een pyridyl-triazool te koppelen aan een lanthanide is het mogelijk om de door het ligand opgenomen energie door te sturen naar het lanthanide, welke het dan uitzendt als licht. Door hun zeer specifieke uitzendpatroon zijn lanthanides erg interessant om te gebruiken als tracer in levende systemen doordat ze goed zijn te onderscheiden van andere bronnen van fluorescentie. De triazool lanthanide complexen kunnen zowel in methanol als in water worden gevormd en zijn in beide gevallen instaat licht uit te zenden, en bieden dus kansen voor toepassingen in de biomedische wetenschap.

Conclusies

Het werk beschreven in dit proefschrift toont aan dat op 1,2,4-triazool gebaseerde liganden goed zijn te gebruiken in complexen met boor en lanthanides. De onderzochte boortriazool complexen kunnen worden gebruikt om radioactieve straling te detecteren. Hierbij moet worden opgemerkt dat verbeterde oplosbaarheid de efficiëntie nog kan verhogen. De onderzochte lanthanide complexen bieden een eerste blik op hun interessante mogelijkheden om gebruikt te worden in de biomedische sector, echter verder onderzoek naar de precieze vorm van coördinatie chemie is noodzakelijk.

[*] De term zeldzaam is een misbenoeming uit vroegere tijd, tegenwoordig is bekend dat veel van de lanthanides meer voorkomend zijn dan het eerder gebruikte boor en zelfs goud.

[†] Het verschil tussen fluoroforen en fosforen is kort door de bocht het tijdsbestek waarin het licht wordt uitgezonden. Fluorescentie is vrijwel direct, fosforescentie kan langere tijd beslaan (bekend van het “glow in the dark” effect).

DANK AAN U ALLEN

De reis was lang en soms moeizaam en ik wil dan ook iedereen bedanken die aan dit goede einde heeft meegeholpen. Door de vele werkplekken leer je veel mensen kennen, maar op mijn leeftijd begint al het verval, dus kan het voorkomen dat ik mensen vergeet, daarvoor mijn welgemeende excuses.

Wesley, bedankt. Voor je geduld en begeleiding, het heeft even geduurd, maar het is dan toch zover. Het was af en toe moeilijk, qua chemie, qua experimenten, qua tijd, qua planning, qua communicatie, maar het is gelukt en het was het waard.

Heinrich, bedankt voor de kans om als eerste PhD te beginnen bij INCAS³. Toen ik begon was INCAS³ nog maar klein, in de tussentijd is er veel gebeurd. Ik heb veel plezier gehad aan onze discussies over stralingsdetectie en heb er meer over geleerd dan ik had durven dromen. Elena, zonder jou was hoofdstuk 3 niet geworden wat het is, mijn grote dank ervoor.

Iedereen bij INCAS³ wil ik graag verder bedanken; Engineers voor alle support met de PHASE, PhD's voor steun en discussie, alle anderen voor hun hulp en ondersteuning.

Professor Buffler, Professor Feringa and Professor Vos, thank you for reading my manuscript and providing valuable suggestions. Professor de Meijer and professor Rangacharyulu: thank you for your patience in helping a chemist understand nuclear physics.

Ook PerkinElmer Groningen hartelijk bedankt; voor het beschikbaar stellen van de oplosmiddelen en jullie hulp met de metingen. Ik weet niet wat ik zonder had moeten doen.

Brownies: bedankt voor de gezelligheid. Ik ben hierdoor altijd met plezier naar het lab gegaan. Dank voor steun en inspiratie. Tjalling en Juan; dank voor je werk aan de lanthanides.

C-wing: Woorden kunnen (en mogen) niet beschrijven wat ik gezien en gehoord heb bij jullie maar het was een goede tijd. Arjen: we hadden die bodipy dus toch gewoon aan die porfyrine moeten knoppen.

Iedereen van het Stratingh instituut hartelijk bedankt, vooral de supporting staff. Zonder jullie hulp was alle apparatuur voor altijd een mysterie gebleven.

Bente: papa heeft nu eindelijk meer tijd voor je. Sorry voor alle keren dat ik aan mijn proefschrift moest werken.

Esther, bedankt dat je in me geloofde en me steunde en voortdreef. Zonder jou was dit nooit gelukt. Ik hou van je.

And now my watch has ended